Investigating Interaction of Methanol with Various Surfaces by Employing Periodic Density Functional Theory

by

Shweta Mehta

10CC16A26016

A thesis submitted to the
Academy of Scientific & Innovative Research
For the Award of the Degree of
DOCTOR OF PHILOSOPHY
in
SCIENCE

Under the supervision of

Dr. Kavita Joshi

CSIR-National Chemical Laboratory, Pune

Academy of Scientific and Innovative Research
AcSIR Headquarters, CSIR-HRDC campus
Sector 19, Kamla Nehru Nagar,
Ghaziabad, U.P.–201 002, India

January-2023

Certificate

This is to certify that the work incorporated in this Ph.D. thesis entitled, "*Investigating Interaction of Methanol with Various Surfaces by Employing Periodic Density Functional Theory*", submitted by Shweta Mehta to the Academy of Scientific and Innovative Research (AcSIR), in partial fulfillment of the requirements for the award of the Degree of *Doctor of Philosophy in Science*, embodies original research work carried-out by the student. We, further certify that this work has not been submitted to any other University or Institution in part or full for the award of any degree or diploma. Research material(s) obtained from other source(s) and used in this research work has/have been duly acknowledged in the thesis. Image(s), illustration(s), figure(s), table(s) etc., used in the thesis from other source(s), have also been duly cited and acknowledged.

(Signature of Student)
Shweta Mehta
Date: 10-01-2023

(Signature of Supervisor)
Dr. Kavita Joshi
Date: 10-01-2023

STATEMENTS OF ACADEMIC INTEGRITY

I, Shweta Mehta, a Ph.D. student of the Academy of Scientific and Innovative Research (AcSIR) with Registration No. 10CC16A26016 hereby undertake that, the thesis entitled "Investigating Interaction of Methanol with Various Surfaces by Employing Periodic Density Functional Theory" has been prepared by me and that the document reports original work carried out by me and is free of any plagiarism in compliance with the UGC Regulations on "*Promotion of Academic Integrity and Prevention of Plagiarism in Higher Educational Institutions (2018)*" and the CSIR Guidelines for "*Ethics in Research and in Governance (2020)*".

Signature of the Student
Date : 10-01-2023
Place : CSIR-NCL, Pune

It is hereby certified that the work done by the student, under my/~~our~~ supervision, is plagiarism-free in accordance with the UGC Regulations on "*Promotion of Academic Integrity and Prevention of Plagiarism in Higher Educational Institutions (2018)*" and the CSIR Guidelines for "*Ethics in Research and in Governance (2020)*".

NA

Signature of the Co-supervisor (if any)
Name :
Date :
Place :

Signature of the Supervisor
Name : Dr. Kavita Joshi
Date : 10-01-2023
Place : CSIR-NCL, Pune

Dedicated to

MY PARENTS, VARUN and GORIK

Acknowledgements

"It always seems impossible until it is done."

First and foremost, I want to thank my PhD supervisor, Dr Kavita Joshi, for her continuous support from the first day of NCL until today. Her rational thinking, timely advice and 'chai pe charcha' has been remarkable in my research and life journey. There was a time I was afraid that I would never be able to finish this. Her belief in me could make it possible to gear up and chase my dreams. So, a big thank you to **Kavita** for going many miles away and making it possible for me.

I am thankful to my Doctoral Advisory Committee members, Dr Shubhangi Umbarkar, Dr C.P. Vinod and Dr T. Raja, for their valuable suggestions during all the DAC meetings. I would also like to thank the present and past directors of CSIR-NCL and HoDs of the Physical and Material Chemistry Division. I am also thankful to the AcSIR for managing my academic profiles, CSIR for providing the infrastructure and UGC for financial assistance during this journey.

I want to thank my former labmates, Anju, Vaibhav, Medhaj, and Saurabh, for being around in my initial days. Many thanks to Sheena, Kavita, Aathira, Meema, and Ashwini, for all the fun times and conversations from science to moral science. They were always refreshing. I am fortunate to have worked with such caring and helping lab members. I am also thankful to the new members of my group, Nikhil, Ameeya, Dipak, and Harshita, with whom I enjoyed many frolic moments. I would also like to thank all my friends Aishwarya, Shalmali, Madhura, Siddhanta, Aadil, Amit, and Hrushikesh, made this journey more enjoyable. I am thankful to Vipin for helping with lots of paperwork and procedures.

Unreservedly, I also want to mention special thanks to all the collaborators: Dr Carita, Dr Sushant, Dr Shreekumar, Dr Shubhangi, Sachin, Mira, Geeta, Abhinav. A special thanks to Mira, who gave me hands-on training to do experiments and analyze the experimental results.

Words cannot express my gratitude to my parents. They always stood up for me even though situations were not in my favour. Thanks for everything. I am also thankful to all my family members, who were always helpful and supportive at every stage of this journey.

Finally, but by no means least, I lack words to express my appreciation to my loving husband, Varun, for his incredible patience, dedication, confidence and support throughout my pursuits. His never-ending love, understanding and care against all odds gave me the courage to complete this work successfully. A special thanks to my newborn son Gorik who have directly and indirectly

inspired and energized me daily for work. Thank you for your inspiration, son. You made every day a new beginning for me.

Contents

List of Figures

List of Tables

Chapter 1

Introduction

As the world's population increases, so the energy required for daily activities. To date, the primary energy source on a global scale is non-renewable fossil fuels, particularly coal, natural gas, and oil. These organic resources, which have been around for thousands of years, are depleting rapidly. The Energy Information Administration (EIA) reports that in 2021, demand for all fossil fuels has increased dramatically.[7] According to the predictions of EIA, energy consumption rate will increase by more than 50% in the coming decades, with Asia accounting for most of the increase.

The environmental problem associated with the usage of fossil fuels and their finite supply has sparked a broad, intense quest for alternative energy sources that can meet global energy demands without harming the environment. Various renewable sources are emerging as alternate energy sources, such as solar, wind, geothermal, hydrothermal, biomass energy, hydrogen, and methanol. Hydrogen energy is one such energy source being discussed recently and considered the cleanest form of energy as its byproduct is only water. Although hydrogen is the cleanest form of energy, its application on a larger scale is limited. Currently to date, hydrogen production is very energy-consuming and its transportation and storage are two major hurdles in realizing hydrogen economy. The other renewable energy source is methanol.

1.1 Methanol

Methanol, also known as wood alcohol, is the simplest aliphatic alcohol. It is a light (molecular weight 32.04), volatile, colourless liquid. Robert Boyle first isolated pure methanol in 1661 via the distillation of buxus (boxwood).[8] Methanol can be produced from several carbon-containing feed-stocks, such as natural gas, coal, biomass, and CO_2. Steam reforming of natural gas produces syn gas (H_2, CO and CO_2), which is further converted to methanol via reverse water gas shift reaction (eq. 1.1) or hydrogenation of carbon monoxide (eq. 1.2). Industrially, methanol is produced from the hydrogenation of CO_2 (eq. 1.3) in the presence of the catalyst, Cu-ZnO/Al_2O_3 at 473-573K and

100 MPa pressure.

$$CO_2 + 3H_2 \rightarrow CH_3OH + H_2 \tag{1.1}$$

$$CO + 2H_2 \rightarrow CH_3OH \tag{1.2}$$

$$CO_2 + 3H_2 \rightarrow CH_3OH + H_2O \tag{1.3}$$

As proposed by Olah, the production of methanol from CO_2 is an environmentally benign way of avoiding CO_2 sequestration (which is a costly process) and also provides a reduction of greenhouse gas by productive reprocessing of CO_2.[9]

1.1.1 Applications of methanol

Methanol is a potential hydrogen carrier. Methanol is liquid at room temperature, unlike hydrogen, which is volatile (B.P.: -253^{o}C) and explosive gas at ambient conditions. It can be easily handled, stored, and transported at the point of utilization. The reformation of methanol produces hydrogen at the point of use and is thus exempted from the expensive methods of hydrogen storage and transportation. This way, hydrogen can be produced in situ in the fuel cell.

Methanol is also blended with gasoline and used in transportation fuel without changing the existing vehicular infrastructure. M85 is mainly used for methanol-fueled vehicles, a mixture of 85% methanol and 15% unleaded gasoline.[10] The experimental study suggests that the thermal brake efficiency considerably improves with the addition of methanol and the NO_x and CO emission reduces.[11] Apart from transportation fuel, MeOH is also used as a cooking fuel which does not produce soot on burning because of pre-oxygenated carbon. Recently, Niti-Aayog has launched the first canister-based methanol cooking fuel program in India.[12]

As shown in Fig.1.1, 30% of methanol is consumed worldwide for the production of formaldehyde only. Remaining 70% is used for the production of various hydrocarbons such as methyl ter butyl ether (MTBE), acetic acid, dimethyl ether (DME), methyl methacrylate, methylamines, gasoline/fuel, and other chemicals.[1]

Methanol to formaldehyde:

Formaldehyde is commercially the most important aldehyde because of its application in various sectors such as in the production of resins, automotive, textile, and aviation. Methanol is the primary source of the production of formaldehyde. Industrially, three different methods are

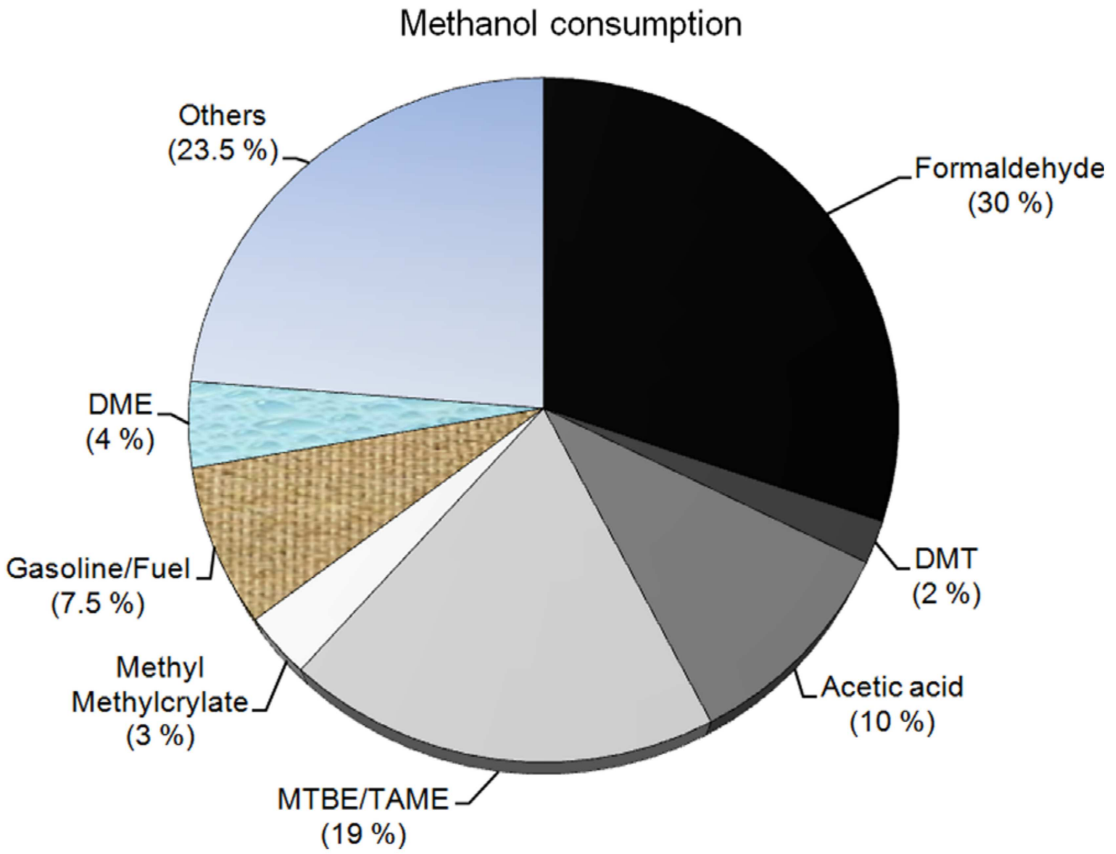

Figure 1.1: *Application of methanol in production of various hydrocarbons*[1]

used to produce formaldehyde from methanol: the silver process, the BASF process, and the Formox process. The first two methods use silver as a catalyst, while the Formox process uses iron-molybdenum oxide for formaldehyde production.[13] The conversion of methanol to formaldehyde occurs in two ways:

1. Dehydrogenation of methanol: This is an endothermic process with reaction energy as high as 84 kJ/mol (refer to eq. 1.4). For the silver and BASF process, the production of formaldehyde from methanol occurs via dehydrogenation. The operating temperature for this method is more than 600^{o}C.

2. Oxidative dehydrogenation of methanol: This is an exothermic process with reaction energy as -159 kJ/mol (refer to eq. 1.5). In the Formox process, the methanol-to-formaldehyde conversion occurs by oxidative dehydrogenation of methanol. The operating temperature for this process is 250-400^{o}C.

$$CH_3OH\ (g) \rightleftharpoons CH_2O\ (g) + H_2\ (g)\ ;\ \Delta\ H = 84\ kJ/mol \tag{1.4}$$

$$CH_3OH\ (g) + 1/2\ O_2\ (g) \rightleftharpoons CH_2O\ (g) + H_2O\ (g)\ ;\ \Delta\ H = -159\ kJ/mol \tag{1.5}$$

Apart from the industrial catalyst, vanadium-based catalysts are also extensively explored for the conversion of methanol to formaldehyde.[14–17] Vanadium oxides supported on various metal oxides exhibits different conversion and selectivity for methanol to formaldehyde formation. Apart from the two methods mentioned above, other methods have also been suggested, such as photocatalytic oxidation of methanol,[18] partial oxidation of methanol in supercritical CO_2,[19] hydroboration of CO_2 to formaldehyde,[20] oxidation of methane to MeOH and formaldehyde.[21]

One of the major application of methanol is the production of DME. The heating characteristics of DME are similar to liquified petroleum gas, making it an alternate energy source in both domestic and industrial applications. DME can be synthesized either from natural gas or by methanol dehydration; however, the later is thermodynamically the most favourable and controlled synthesis route. Methanol is also emerging as a convenient hydrogen and can be easily transported to the place of utilization. Methanol is also used in the direct methanol fuel cell, where it is oxidized to produce protons and electrons.

1.1.2 Role of DFT in catalysis

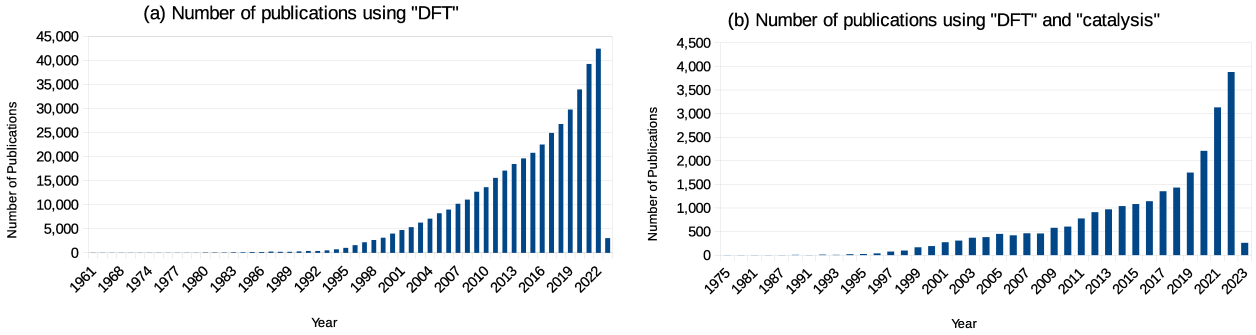

Figure 1.2: *(a) The number of publications using the keyword "DFT" from the SciFinder since 1964.*[2] *The research in DFT exponentially increased in the 21st century. (b) The number of publications using the keyword "DFT" and "catalysis" from the SciFinder.*[3] *The application of DFT in the catalysis field is increasing linearly and has attracted significant attention over the last decade.*

Density functional theory is an incredibly successful method for determining solutions to the Schrödinger equation, which describes the ground-state of electrons. It is derived from theoretical concepts without relying on experimental data, resulting in accurate and reliable theoretical results at a modest computational cost. This approach has rapidly evolved to be used as a tool in various domains of science, such as chemistry, physics, materials science, chemical engineering, geology,

etc., as shown in Fig.1.2-(a). The application of DFT has exponentially increased since 21^{st} century.

Advances in DFT allow us to describe catalytic reactions at surfaces with the detail and accuracy required for computational results to be meaningfully compared to experiment. Theoretical studies also describe chemical reactions in detail and comprehend differences in catalytic activity from one catalyst to the next. Such comprehension enables screening of chemical space for designing better catalysts. As shown in Fig.1.2-(b), there has been a tremendous increase in the use of DFT for catalysis in the last decade.

One of the most classic examples of the application of DFT in understanding the reaction mechanism is by Honkala et al. for the synthesis of ammonia.[22] The Haber-Bosch process for ammonia synthesis is $N_2 + 3H_2 \rightarrow 2NH_3$. The reaction proceeds in the presence of iron or ruthenium catalyst at greater than 500^oC temperature and more than 100 atmospheric pressure. Although the reaction was proposed by Haber and Bosch around a hundred years ago its mechanism is still not clear due to the complexity of the reaction. DFT played a vital role in deducing the mechanism of the ammonia synthesis process. Honkala et al. used DFT calculations to investigate flat and stepped facets of Ru nanoparticles to synthesize ammonia from nitrogen and hydrogen. They predicted that there are 12 elementary steps involved in the net chemical reaction on the catalyst surface. The reaction rate of these elementary steps depends on the environment of the catalyst surface. Moreover, the most important reaction is the dissociation of the N_2 bond, which has less energy barrier at the stepped facet than at the flat facet. They also predicted the nanoparticle's shape as a particle size function. They observed a correlation between the diameter of the nanoparticle and the number of the active site for N_2 bond dissociation. The results obtained by DFT were compared with the experimental measurements at an industrial scale, and the predicted results were in excellent agreement with the experimental measurements.

The example mentioned above shows the impact of DFT calculations in understanding the thermodynamics of the reactions. Also, the predicted results of DFT could be validated by experimentation, demonstrating the accuracy and reliability of the DFT results.

1.1.3 Methanol dissociation: literature studies

Methanol is the simplest aliphatic alcohol and is treated as one of the standard molecules in surface science for investigating its interaction with surfaces.[23] Several methanol applications in biosensors, devices, organic dielectrics, and nanolithography makes it a vital molecule for investigation.

It has been observed that the conversion of methanol to any other value-added product requires breaking its O-H and C-H bonds with substantial bond dissociation energies, viz. 96.1 kcal/mol and 104.6 kcal/mol, respectively.[24] Due to the immense importance of methanol as feedstock in various industries, extensive studies of the activation and decomposition of methanol on various systems

have been carried out. The optimum catalyst should be active enough to dissociate the methanol molecule and favour the desorption of desired products. As discussed above, there are various applications of methanol and depending upon the desired product, the adsorption/dissociation of methanol is required.

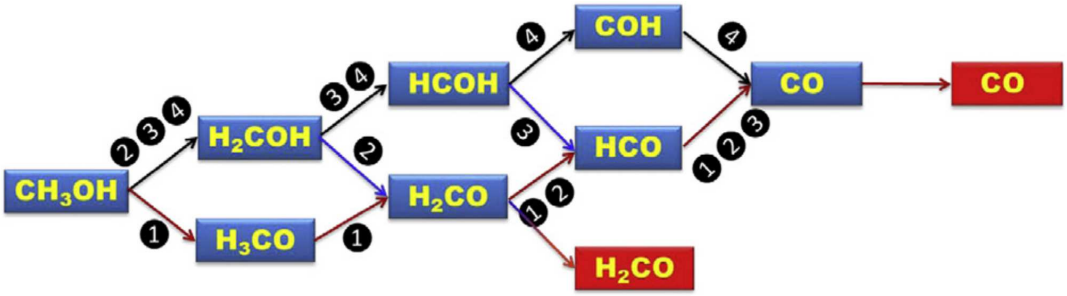

Figure 1.3: *The figure represents four possible pathways of methanol decomposition.*[4] *The boxes in blue and red show the intermediates and products formed during the methanol decomposition.*

Partial decomposition of methanol leads to the formation of formaldehyde, whereas complete decomposition produces CO. Both these reactions are endothermic. Four possible pathways are proposed for the conversion of methanol to CO[4] as shown in Fig.1.3. The blue boxes represent the intermediates, and the red boxes show the products formed during methanol decomposition.

Various catalysts like metal surfaces,[25–39] metal alloys,[40–44] metal clusters,[45–48] metal oxides,[49–55] mixed metal oxides,[56] and zeolites[57–59] have been explored in great detail for the conversion of methanol to value-added products. It has been observed that generally, methanol dissociates to methoxy and hydrogen at coinage metal surfaces which upon increasing temperature, recombine to produce methanol and desorb from the surface. The rate-determining step on the coinage metal surfaces is the dissociation of the O-H bond, and formaldehyde formation is the major outcome.[60–62] Contrarily, for precious metal surfaces such as Pt, Pd, and Rh, the complete decomposition of methanol takes place with the dissociation of C-H bond as the primary step. The major product of methanol decomposition on these surfaces is CO and H_2. Oxygen-adsorption on the metal surfaces leads to the variation in geometric and electronic properties of the surfaces, consequently altering their catalytic activity. The activation barrier for O-H bond dissociation substantially reduces on oxygen-preadsorbed metal surfaces.[27,63,64]

Metal oxides show better catalytic activity due to various acidic and basic sites on the oxide surface. However, the basicity of oxides favours the dehydrogenation of methanol. Both oxygen anion and metal cation operate synergistically. Surface oxygen atoms favour dehydrogenation by abstracting the hydrogen from the MeOH and forms surface hydroxide, whereas metal cations stabilize the intermediates formed during the decomposition of MeOH. ZnO has been explored for the decomposition of methanol. In a DFT study, Pala and Metiu studied methanol adsorption with

$(10\bar{1}0)$ facet of pristine and cationic atom doped ZnO.[65] They report that molecular adsorption of methanol is most favoured on the pristine ZnO $(10\bar{1}0)$ surface. Vo et al. investigated the ZnO for adsorption and decomposition of methanol using periodic DFT study.[66] The decomposition mechanism on $(10\bar{1}0)$ surface of ZnO follows the order as $CH_3OH \rightarrow CH_3O + H \rightarrow CH_2O + H$. The activation barrier for methanol to formaldehyde on the $(10\bar{1}0)$ surface is 1.20 eV. In another study, Deng et al. demonstrated the conversion of methanol to formaldehyde on the ultrathin layers of ZnO supported on Au (111) using temperature-programmed reaction spectroscopy and DFT.[67] They report that the partial oxidation of methanol to produce formaldehyde occurs at T = 580K. Their DFT studies predict that methanol dehydrogenation initiates with the dissociation of the O-H bond followed by C-H bond dissociation with an overall activation barrier for the reaction is 19.0 kcal/mol.

Here, we have presented a short summary of few literature studies, however, for thorough literature on methanol decomposition catalysts, readers are recommended a few comprehensive review articles.[4,68,69]

1.2 Motivation

So far we have discussed importance of MeOH as fuel, hydrogen carrier or a raw material for other value added chemicals. We have also briefly discussed role of DFT in understanding reaction mechanism. However, there are several catalysts explored for the conversion of methanol to value-added products. For rational designing of a catalyst, it is crucial to understand the interaction of a molecule with different facets and distill out the essential factors leading to desired products. The ultimate goal of any DFT-based computation is to deduce trends and gain predictive power by understanding the results in terms of underlying electronic structure. We aim to understand the interaction of methanol with a series of Zn-based catalysts by employing DFT. We want to investigate the correlation between the electronic structure of a bare facet and the outcome of methanol's interaction with a facet. Most of the reactions are carried out with polycrystalline catalysts with several facets exposed to the adsorbate species. As has been discussed, surface reactions are sensitive to the structural arrangement of atoms. Thus it becomes imperative to analyze the interaction of various catalyst surfaces with the adsorbate for the rational designing of the catalyst. DFT offers an efficient and accurate tool to investigate elementary reactions at the surface, which could be reasonably compared with the experimental measurements. In this thesis, we investigated the interaction of methanol with several facets of Zn-based catalysts using DFT, which is discussed in the following chapters.

1.3 Plan of thesis

The aim of this thesis is to understand the interaction of methanol with different Zn-based systems using periodic density functional theory. Based on the underlying electronic structure, we tried to understand the variation in nature of Zn and O in different environments like pure metallic state, oxygen preadsorbed metal, metal oxide and mixed metal oxide.

Chapter 2: We present the theoretical framework which forms the base of DFT and standard operating procedures. We begin by discussing the Schrödinger equation, Born-Oppenheimer approximation as implemented in density functional theory. Following this, we discuss Hohenberg-Kohn's theorem and the Kohn-sham equation for mapping the one many-body interacting electrons problem to many one-body non-interacting electron problems. Next, we discuss the pseudopotential and plane wave basis set employed in VASP. The last section discusses setting up the system as per our calculations.

Chapter 3: In this chapter, we inspect the systematic interaction of methanol with zinc surfaces and oxygen-preadsorbed zinc surfaces. $(10\overline{1}0)$, $(10\overline{1}1)$, $(10\overline{1}3)$ are explored in this study. We report that the MeOH physisorbs all the facets of the pristine Zn. MeOH adsorption triggers significant reconstruction on the $(10\overline{1}0)$ facet, whereas the extent of reconstruction substantially reduces for the other two facets. Further, oxygen adsorption on the metallic Zn surfaces significantly reduce the activation barrier for the O-H bond from the flat facets and becomes negligible at the step facet. Interestingly, upon oxygen adsorption, the decomposition of the O-H bond of methanol becomes exothermic at all facets compared to the metallic surfaces.

Chapter 4: Exposure of oxygen to metal surfaces leads to oxide formation. In this chapter, we have carried out a systematic study of methanol adsorption on various facets of ZnO, which includes two flat [$(10\overline{1}0)$ and $(11\overline{2}0)$] and two stepped [$(10\overline{1}3)$ and $(11\overline{2}2)$] surfaces. O-H bond dissociation is thermodynamically the most favourable outcome on stepped facets, whereas chemisorption of MeOH with 7-10% O-H bond activation is observed on the flat facets. We also report considerable surface reconstruction upon MeOH adsorption. However, the reconstruction is less on the stepped surfaces than on the flat facets. Further, partial oxidation of MeOH is favoured on ZnO facets. Our detailed electronic structure analysis brings out the rationale behind the surface-dependent interaction of MeOH. Analysis of the underlying electronic structure of the bare surfaces explains the facet-dependent reactivity observed in the case of ZnO. Facets with available empty states near Fermi lead to O-H bond dissociation, whereas the absence of empty states near Fermi leads to O-H bond activation.

Chapter 5: In this chapter, we proposed a new mixed metal oxide ($ZnAl_2O_4$) as a catalyst for the activation of methanol. It is interesting to note that the proposed catalyst is a derivative of two commonly used industrial catalysts, Al_2O_3 and ZnO towards MeOH synthesis. We discuss two

prominent facets, (311) and (220) facets of $ZnAl_2O_4$, which are the most prominent peaks in XRD of the spinel structure. These two surfaces offer significant O-H bond activation and exhibit one case for each spontaneous dissociation of the O-H bond. Also, the (311) surface undergoes subsequent dissociation of one of the C-H bonds. The produced formaldehyde remains strongly adsorbed on the Al site of the surface due to the higher affinity of Al for oxygen. Careful investigation of the underlying electronic structure of bare surfaces explains that the availability of surface oxygen in the vicinity of adsorbing methanol is essential for the decomposition of methanol. The structural arrangement of atoms on the surface turned out to be another essential factor in understanding the adsorption energy trends. We also propose that the (311) surface offers better catalytic activity than (220) due to its stepped geometry and availability of inequivalent adsorption sites for interaction with an incoming MeOH.

Chapter 6: In this chapter, we investigated the interaction of methanol with ZnO by theoretical and experimental approaches. We observed spontaneous conversion of methanol to formaldehyde on $(10\bar{1}1)$ facet. Not only does formaldehyde form, but it also desorbs from the surface. Formaldehyde formation is thermodynamically the most favourable outcome at $(10\bar{1}1)$ facet. The presence of non-zero states at the Fermi level explains the greater reactivity of this facet. By carefully understanding our theoretical results, we designed an experiment to study the interaction of methanol with ZnO at RT and atmospheric pressure. The FTIR and HPLC both evident the formation of formaldehyde as a product of this reaction. Also, there is no peak other than formaldehyde in the reaction mixture, indicates towards 100% selectivity of formaldehyde with 3% conversion in 1h at ambient conditions. Further tuning of the catalyst may enhance the conversion rate of methanol. The theoretical investigation followed by experimental validation paves a very efficient way towards designing of catalyst.

Chapter 7: Methanol decomposition is essential for its conversion to value-added products. Understanding the interaction of methanol with different Zn-based systems is vital for the rational design of catalysts for methanol decomposition. In this last chapter, we compared the electronic structures of all Zn-based systems investigated in this thesis work. By carefully investigating the density of states of these different systems, we could establish a correlation between the electronic signature and the outcome of the interaction of methanol with these systems. These findings will pave the way toward the rational design of catalysts.

Chapter 8: A summary of the thesis work has been reported in this chapter. Future scope for the current studies using different theoretical approaches are discussed in this chapter.

DFT results are widely accepted but limited by their experimental validation due to differences in reaction conditions. Interestingly, we could validate our theoretical results by experimental methods, as discussed in detail in chapter 6.

Chapter 2

Theoretical formalism

The evolution of quantum mechanics in the early 1900s enabled the computation of the properties of atoms, molecules, and solids in principle. However, no mathematical tools were available to solve these complex equations. Paul Dirac, in 1929 mentioned that "The underlying physical laws necessary for the mathematical theory of the large part of physics and whole of chemistry are thus completely known, and the difficulty is only that the exact application of these laws leads to equation much too complicated to be soluble." The development of approximate methods and better computers for solving these complex equations played a critical role in shaping the fields of quantum chemistry as they are today. In quantum mechanics, the state of a system is described by a wavefunction, Ψ, that is a function of the time and particle's coordinates. This wavefunction is not observable and has no physical significance. However, it contains all the information about a system. This information can be extracted using a suitable quantum mechanical operators. In the last two decades, density functional theory (DFT) has emerged as the utility player of computational chemistry. The popularity of DFT stems primarily from simplicity that it offers and low computational cost. Enhanced computational power over last few decades has allowed us to study complex and large systems compared to other wavefunction based methods.

In this chapter, we present the theoretical framework and standard operating procedures used for the calculations presented in this thesis. We begin by discussing the Schrödinger equation, and Born-Oppenheimer approximation. Following this, we discuss Hohenberg-Kohn theorems and the Kohn-sham equation for mapping the many-body interacting electrons problem to many one-body non-interacting electron problems. Next, we discuss the concept of pseudopotentials and plane-wave basis set. The last section discusses setting up the system as per our calculations.

The Schrödinger Equation

Erwin Schrödinger in 1926 proposed for the first time the wavefunction and equation govern-

ing its change with time known as time-dependent Schrödinger equation ($H\Psi(x,t) = E\Psi(x,t)$). The time-independent, nonrelativistic form of Schrödinger equation is $H\psi(x) = E\psi(x)$. In this equation, H is the Hamiltonian operator, and ψ is a wavefunction which depends only on the spatial coordinates of the particles. For simple systems like a particle in a box or harmonic oscillator, the Hamiltonian has a simple form, and the schrödinger equation can be solved exactly. However, for a system with 'N' ions and 'n' electrons, the Hamiltonian is expressed as:

$$\hat{H}_t = \left(\frac{-\hbar^2}{2}\right)\sum_{I=1}^{N}\frac{\nabla_I^2}{M_I} + \left(\frac{-\hbar^2}{2}\right)\sum_{i=1}^{n}\frac{\nabla_i^2}{m_e} + \sum_{I}^{N-1}\sum_{J>I}^{N}\frac{Z_I Z_J e^2}{|R_I - R_J|} + \sum_{I}^{N}\sum_{j}^{n}\frac{Z_I e}{|R_I - r_j|} + \sum_{i}^{n-1}\sum_{j>i}^{n}\frac{e^2}{|r_i - r_j|} \tag{2.1}$$

where, the terms are kinetic energy of ions, the kinetic energy of electrons, ion-ion interaction, ion-electron interaction, and electron-electron interaction respectively. The solution of this schrödinger equation contains all the information of the system. The eigenvalues of the Hamiltonian correspond to the system's energy states, and the lowest eigenvalue will be the ground state energy. However, finding the solution of the Schrödinger equation is challenging and needs further simplification. The first step towards this is separating ionic degrees of freedom from that of electronic.

The ions are much heavier than the electrons (each proton/neutron in an atom is 1800 times heavier than an individual electron). Hence the response to the surrounding change is much faster in the case of electrons than ions. Consequently, the ionic motion can be separated from the electronic motion. This is the Born-Oppenheimer approximation or adiabatic approximation.[70] After applying the Born-Oppenheimer approximation for a fixed ionic configuration the Hamiltonian can be written as:

$$\hat{H}_{ele} = \left(\frac{-\hbar^2}{2}\right)\sum_{i=1}^{n}\frac{\nabla_i^2}{m_e} + \sum_{I}^{N-1}\sum_{J>I}^{N}\frac{Z_I Z_J e^2}{|R_I - R_J|} + \sum_{I}^{N}\sum_{j}^{n}\frac{Z_I e}{|R_I - r_j|} + \sum_{i}^{n-1}\sum_{j>i}^{n}\frac{e^2}{|r_i - r_j|} \tag{2.2}$$

The terms represent the kinetic energy of electrons, ion-ion interaction, ion-electron interaction, and electron-electron interaction. However, the ion-ion interaction is constant for a given structure.

Since electrons are fermions, the electronic wavefunction must be antisymmetric to exchange of electrons. Despite the implementation of the Born-Oppenheimer approximation, the solution of Schrödinger equation for an 'n' interacting electrons is complex. The wavefunction of an electron in time-independent Schrödinger equation is a function of three spatial coordinates. For an 'n' electron system, the wavefunction is a '3n' dimensional function which makes the solution of Schrödinger equation as an impossible task. For example, in the case of a Zn system with 100

atoms, the wavefunction is a 9000-dimensional function (every atom with 30 electrons having 3 dimensions each), which indeed is an impossible task. All the wavefunction based methods have limitations in terms of the system size that could be handled. The readers are directed to some nicely written books for detailed discussion of the same.[71–73]

2.1 Density functional theory

This theory uses electron density, instead of the wavefunction, as a fundamental variable for the calculation of the energy of the system. The electron density, ρ(r), is a '3' dimensional variable which reduces the computational expenses. Density functional theory is based on two theorems proposed by Hohenberg and Kohn.[74] The first theorem of Hohenberg-Kohn states, *For any system of interacting particles in an external potential $V_{ext}(r)$ the potential $V_{ext}(r)$ is determined uniquely, except for a constant, by the ground state particle density $\rho(r)$.*[75] Thus, the total energy of an interacting electron system is a functional of electronic density, and there is a one-to-one correspondence between the electron density and external potential. The corollary to the theorem says that since the Hamiltonian is thus fully determined, except for a constant shift of the energy, it follows that the many-body wavefunctions for all states (ground and excited) are determined. Therefore, all system properties are completely determined given only the ground state density ρ(r). The first theorem of Hohenberg-Kohn states that an electron density functional exists to solve the Schrödinger equation but says nothing about what the functional is.

The second theorem defines an important property of the functional. It states that the *universal functional for the energy E[ρ] in terms of the density $\rho(r)$ can be defined, valid for any external potential $V_{ext}(r)$. For any particular $V_{ext}(r)$, the exact ground state energy of the system is the global minimum value of this functional, and the density $\rho(r)$ that minimizes the functional is the exact ground state density $\rho_0(r)$.*[75] The density that can minimize the functional of energy with respect to the electron density E[ρ_0(r)] is exactly the ground state electron density. This is the variational principle. For any electron density (ρ_{trial}), such that $\int \rho_{trial}(\mathrm{r})\delta(\mathrm{r}) = \mathrm{N}$ then, E[ρ_{trial}] $\geq$ E_0, where E_0 is the ground state energy. The Hohenberg-Kohn theorems are existential because they proposed the existence of a functional which relates the electron density and ground state energy but could not provide any strategy to find this functional or the ground state electron density. Kohn and Sham in 1965, provided the mathematical expression to use these theorems.[76] Kohn-Sham mapped one many-body the problem of interacting electrons to many one-body problems of non-interacting electrons. The electron-electron interaction is approximated by an auxiliary system. In this system, the electrons do not directly interact with each other, instead the presence of all other electrons is approximated by an effective potential, and each electron interacts with this effective potential. All the differences because of Kohn-Sham assumptions are incorporated in the exchange-correlation

term. The total energy functional with Kohn-Sham formalism is,

$$E_{tot}[\rho(r)] = E_{known}[\rho(r)] + E_{XC}[\rho(r)] \tag{2.3}$$

where the functional is split into a collection of terms which can be written in simple mathematical expressions are included in E_{known} and rest everything in E_{XC}. The E_{known} is,

$$\begin{aligned} E_{known}[\rho(r)] = \tfrac{\hbar^2}{m} \textstyle\sum_i^{N_e} \int \psi_i^* \nabla^2 \psi_i dr + \int V(r)\rho(r) dr \\ + \frac{e^2}{2} \int\int \frac{\rho(r)\rho(r')}{|r-r'|} dr dr' + \sum_{I>J} \frac{Z_I Z_J}{|R_I - R_J|} \end{aligned} \tag{2.4}$$

On RHS, the terms in order are kinetic energy of the electrons, Coulomb interactions between electrons and the nuclei, Coulomb interaction between pairs of electrons and the Coulomb interactions between pairs of nuclei and ρ is expressed as

$$\rho(\mathrm{r}) = 2\textstyle\sum_i \Psi_i{}^*(\mathrm{r})\Psi_i(\mathrm{r}) \; . \tag{2.5}$$

and the exchange-correlation energy is expressed as,

$$E_{XC}[\rho(r)] = \int \rho(r)\epsilon_{xc}\rho(r) dr \tag{2.6}$$

The new Kohn-Sham equation for a non-interacting electron system can be expressed as,

$$\left[\tfrac{\hbar^2}{2m}\nabla^2 + V_{ext}(r) + V_H(r) + V_{xc}(r)\right]\psi_i(r) = \epsilon_i \psi_i(r) \tag{2.7}$$

The first term is kinetic energy of electron, V_{ext} is interaction of electron and nuclei, V_H is Hartree potential, and is defined as,

$$V_H(r) = e^2 \textstyle\int \frac{\rho(r')}{|r-r'|} dr \tag{2.8}$$

The Hartree potential is the coulomb repulsion between the electron considered in one of the Kohn-Sham equations, and all electrons in the system define the total electron density. While considering all electrons, the interaction from the electron which is considered in the Kohn-Sham equation is also included, thus self-interaction is also part of V_H. The corrections due to self-interactions are incorporated into the exchange-correlation potential. The exchange correlation potential is the functional derivative of exchange-correlation energy,

$$V_{xc}(r) = \tfrac{\delta E_{xc}[\rho]}{\delta \rho(r)} \tag{2.9}$$

To solve the Kohn-Sham equation, we need to know the V_H potential, which is derived from

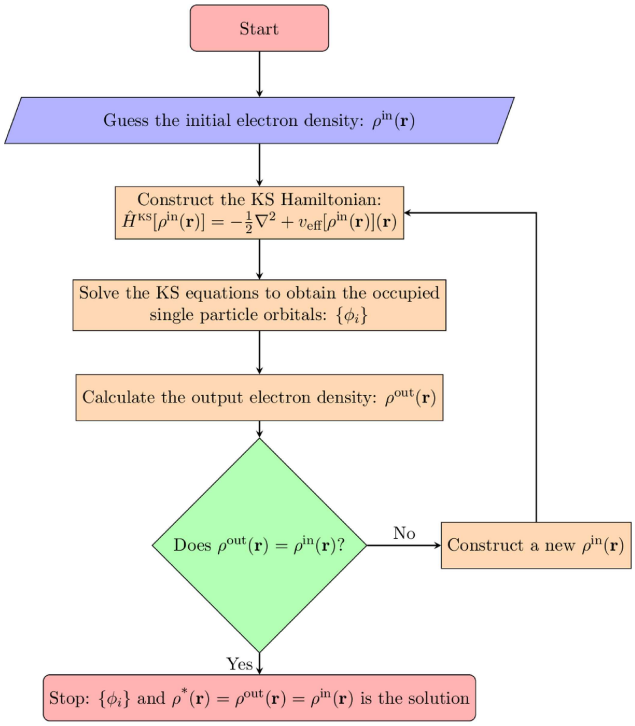

Figure 2.1: *Self consistency cycle for solving Kohn-Sham equation.*[5]

the electron density and to find the density, the single electron wavefunction must be known, which is obtained by solving the Kohn-Sham equation, this makes a vicious circle. Hence, Kohn-Sham equations must be solved selfconsistently. We start with random wavefunctions and initial charge density (in our case, superposition of atomic charge density) to solve the Kohn-Sham equation, which gives us improved wavefunction and new charge density which is now used for solving the Kohn-Sham equation. The schematic representation is shown in the Fig. 2.1.

2.2 Essentials of DFT calculations

Let us briefly summarize the discussion so far. We want to find out the ground state energy of a system by solving the time-independent Schrödinger equation. By implementing Born-Oppenheimer approximations, we could separate the ionic and electronic degrees of freedom. With the help of Hohenberg-Kohn theorems and the Kohn and Sham formalism, the many-body interacting electrons problem could be mapped to many one-body non-interacting electrons. Now, the exchange-correlation part in the eq.2.7 is the most tricky part.

2.2.1 Exchange-Correlation functional

The computation of exchange-correlation energy is the most complicated part of solving the Kohn-Sham equation. The exact form of the exchange-correlation functional is not known. There is just one case where this functional can be exactly derived: uniform electron gas. In uniform electron gas, the electron density is constant at all points in space (the ideal situation). Taking a suggestion from here, the exchange-correlation energy at each position in the real system is calculated as exchange-correlation energy from uniform electron gas at electron density observed at that point.

Local density approximation: The most widely used framework for exchange-correlation functional is local density approximation (LDA). As the name suggests, this framework uses local density to define the exchange-correlation functional. This framework assumes that the density, which is generally nonuniform, is uniform locally. This approach does not consider the corrections to exchange-correlation at a point due to inhomogeneity in the neighbouring charge density. The exchange-correlation potential using LDA is given by,

$$V_{xc}^{LDA}(r) = V_{xc}^{electrongas}\left[\rho(r)\right] \tag{2.10}$$

This approach is best applied to solids similar to uniform gas and nicely predicts bond lengths. However, the energies are overestimated in the weakly bonded structure. Numerous efforts have been put in to improve the LDA. One such approximation is generalized gradient approximation.

Generalized gradient approximation: The GGA includes information from the electron density and gradient of the density. It is expressed as,

$$V_{xc}^{GGA}(r) = V_{xc}^{electrongas}\left[\rho(r)\ , \nabla\rho(r)\right] \tag{2.11}$$

As clear from the eq.2.11, the GGA approach takes into account the spatial variation of electron density. GGA includes more physical information as compared to the LDA, hence GGA could improve the calculated bond energies and bond lengths. It works reasonably well with weakly bonded systems. Various functionals within GGA frameworks are available such as BP, BLYP, PE, etc. The two most commonly used functionals for solid systems are Perdew-Wang functional (PW91) and Perdew-Burke-Ernzerhof (PBE) functional. Several hybrid functionals are also used such as B3LYP, PBE0, B98, etc. Hybrid functionals are a combination of a portion of exact exchange from Hartree-Fock theory and exchange and correlation from other sources. We have used GGA-PBE in our calculations of periodic solids which provides reasonable accuracy with optimal computational expenses.

As discussed in the preceding section, with the help of Kohn-Sham formalism, the many-body

complex problem reduces to the single-body problem. It could successfully model simple systems with many electrons in a finite space, however, computation for large systems still remains formidable. Another approximation implemented in DFT is pseudopotential.

2.2.2 Pseudopotentials

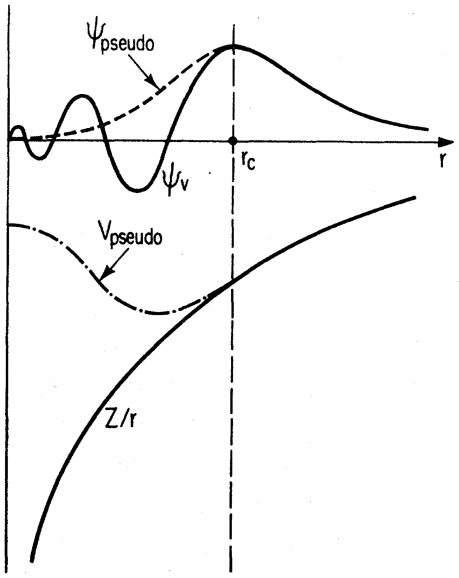

Figure 2.2: *Comparison of all electron wavefunction and potential (solid black curve) with pseudo wavefunction and potential (dotted black curve) respectively.*[6]

The DFT computation for larger system is still computationally expensive due to a large number of core electrons. For example, in our case, a 100-atom Zn system will have 3000 electrons (a total of 30 electrons in each Zn atom). Physically, the valence electrons participate in the chemical bonding, not the core electrons. Pseudopotential approximation reduces the expense of computation by replacing the core electrons with the strong ionic potential by a weaker and smoother pseudopotential within the core region. This is known as frozen-core approximation method. The pseudopotential and pseudofunction are generated in such a way that beyond the cutoff radius, they are identical to the true potential and true wavefunction, respectively, as shown in Fig.2.2. All the radial nodes of the wavefunction inside the core radius are removed, but the charge is conserved. Due to the removal of radial nodes, the number of plane waves required to describe the core wavefunction reduces, hence decreasing the computation time significantly. Thus, using pseudopotential, we could truncate the number of electrons from 3000 to 1200 for a 100-atom Zn system; hence, there is substantial reduction in the number of plane-waves and consequently the computation time.

Ideally, for an element, the pseudopotential is developed by considering the isolated atom of an element. The resulting pseudopotential can be used directly without modification in any chemical environment. Hamann et al. presented the norm-conserving pseudopotential from ab-initio calculations.[77] The proposed pseudopotential gives exact eigenfunction and eigenvalue with atomic wavefunction beyond cutoff radius r_c. Also, the logarithmic derivative of the radial wavefunction and their first energy derivative agree well at the r_c. Another most commonly used pseudopotential is the ultrasoft pseudopotential by Vanderbilt.[78] These pseudopotentials are constructed with low energy cutoffs, and the pseudowavefunction is very smooth within the core region. Softening of the wavefunction is achieved by introducing the generalized orthonormality condition. Ultrasoft pseudopotential shows much better transferability than the norm-conserving pseudopotential. The construction of ultrasoft pseudopotential requires a lot of defined empirical parameters. Another pseudopotential approach is the projector-augmented-wave (PAW) method. It was initially introduced by Bloch[79] and later adapted by Kresse and Joubert.[80] This method introduces a linear transformation from a pseudo wavefunction to an all-electron wavefunction. The rapidly oscillating valence wavefunctions transformed into smooth wavefunctions, making them computationally more efficient. Valence electron wavefunctions are kept orthogonal to the core region. We have employed PAW pseudopotential in this work.

2.2.3 Brillouin zone and plane-wave basis set

Bloch's theorem needs to be satisfied for solving Schrödinger equation for periodic system. The Bloch theorem states that the solution for Schrödinger equation can be expressed as a plane-wave regulated by the Bloch function. The Bloch function is expressed as,

$$\Phi_k(r) = exp(ik.r)u_k(r) \tag{2.12}$$

where u_k(r) is periodic in space and the function exp(ik.r) are called as plane-waves. The space of r is called a real space while the space of k is called reciprocal space (k space). For a simple periodic system with lattice vectors a_1, a_2, and a_3, the three vectors defined in reciprocal space known as reciprocal lattice vectors are,

$$b_1 = 2\pi\frac{a_2\times a_3}{a_1\cdot(a_2\times a_3)}; b_2 = 2\pi\frac{a_3\times a_1}{a_2\cdot(a_3\times a_1)}; b_3 = 2\pi\frac{a_1\times a_2}{a_3\cdot(a_1\times a_2)} \tag{2.13}$$

The length of the reciprocal lattice vectors is inversely related to the length of vectors in real space. Hence, the larger the system in real space, it needs smaller representation in the k-space.

As shown in eq.2.12, the u_k(r) is periodic in space and can be expanded in terms of a set of plane-waves as,

$$u_k(r) = \sum_G c_G exp\,[iG.r] \tag{2.14}$$

A basis set is a set of functions representing electronic wavefunction in DFT. The basis set consists of either atomic orbitals, (linear combination of atomic orbitals) or plane-waves (applied for periodic systems). For periodic system, the wavefunction needs to expand in discrete plane-wave basis set which can be expressed by combining eq.2.12 and 2.14,

$$\Phi_{k,i}(r) = \sum_G c_{i,k+G} exp\,[i(k+G).r] \tag{2.15}$$

Here, G represents the reciprocal lattice vectors, and k is supposed to lie within the first Brillouin zone.

2.3 DFT calculations on surfaces

Until now, we have learned about the theoretical formalism of DFT and the essential approximations used for employing DFT. Now, in this section, we will discuss the choice of model and procedure to set up a DFT calculation for computation of various properties of surfaces.

2.3.1 Setting up the system

For heterogeneous catalysis, surfaces are more important than their bulk counterpart because of the presence of undercoordinated atoms. The nanoparticles synthesized in experiments are generally of the order of a few nanometers, which can be represented as a slab in computational modeling. In this work, we have used slab model to understand their interaction with methanol. We will begin by discussing the generation of the slab and setting up the system for computation as follows:

- To begin with, the bulk structure is required for surface generation. Several open-source databases such as materials project,[81] crystallography open database,[82] etc., are available to obtain the bulk structure of desired material. Once the bulk structure is found, we optimize the bulk with all degrees of freedom, including the position of atoms, cell shape and cell volume. The lattice parameters of the optimized bulk structure are compared with the experimentally reported lattice parameters. The computed lattice parameters are in 2-3% of the experimentally measured value for the work presented in the thesis.

- Upon optimization of the bulk structure, the surface is generated by cleaving the bulk in specific planes using atomic simulation environment (ASE)[83] or Quantumwise-VNL.[84] The

plane of interest is selected based on the XRD of the bulk material used. Generally, the nanoparticles synthesized in the experiments are polycrystalline. However, the XRD represents the most dominant planes (facets) of the material exposed to the adsorbates. For example, in the case of $ZnAl_2O_4$ catalyst, the XRD plot shows dominant peaks of (311) and (220). Hence, we have investigated these two facets for their interaction with methanol.

- **Slab model and periodic boundary conditions** Once the facet is finalized, the surface is cleaved in such a way that it is periodic in the x and y directions but non-periodic in the z-direction. Further, a few parameters, like box size, k-mesh, etc., should be selected appropriately, which otherwise may result in numerical errors in the energy of the system. The errors can be minimized by carefully setting up the system. We perform a few convergences for the cleaved surface. The cell box is carefully chosen to avoid the interaction of atoms in the non-periodic region with their image. We do vacuum convergence to determine the sufficient amount of vacuum so that the atoms in the z direction do not interact with its image. The choice of k-mesh should be made meticulously so that there can be an optimum balance between the accuracy and the computation time. Very dense k-mesh will be computationally costly and may not improve the accuracy significantly.

2.3.2 Surface relaxation

As discussed above, the slab model is cleaved from the bulk structure. The atoms take the same position in this structure as in their bulk counterpart. However, due to under-coordinated atoms at the surface layer, the inter-layer spacing between the atoms in the surface region alters from the spacing in their bulk region. The phenomenon of changing the inter-layer distance between surface layers is called surface relaxation. Depending upon the type of surface termination, there may be substantial changes in the coordination and energy of the surface. Generally, relaxation leads to a decrease in the distance between the first and second layers. It is also observed that the interlayer spacing change for open surfaces is more significant compared to the close-packed surface.

2.3.3 Surface reconstruction

As discussed in the previous section, the surface atoms relax during optimization; hence, they differ from their atomic positions in their bulk structure. Along with relaxation, some surfaces undergo reconstruction. Reconstruction of the surface can be an outcome of the stress on the surface atoms[85] or can be associated with the attainment of minimum energy configuration.[86] Apart from internal factors, surface reconstruction could be induced due to adsorbate atomic or molecular species. There are ways to determine whether a surface has a tendency to reconstruct: imaginary

modes in surface phonon dispersion indicate a driving force for stress-driven reconstruction and an excess of dangling bonds or unsatisfied atomic orbitals can indicate an electronically-driven surface reconstruction.[87]

Limitations of our work:

Although the DFT results are accurate and reliable, there are a few limitations to our work, as mentioned below:

- The slabs modelled for the DFT calculations differs from the catalyst used in experiments. For example, generally, the catalyst used in experiments is polycrystalline, and different facets may have a synergistic effect on the activity of the catalyst, however, we deal with individual facet and the synergy between different facets is not considered. Also, the model used in DFT is very structured which is not true with the real catalyst.
- Due to compute intensive calculation, the number of atoms used for our DFT calculations are restricted to hundreds of atoms, whereas size of the real catalyst ranges to few nanometers.
- As we will discuss in the following chapters, the orientation of methanol does play a crucial role in its interaction with the facet. However, to scan all possible orientations of MeOH molecule wrt to a specific site is a formidable task.
- All our calculations are performed at 0K and zero atmospheric pressure; however, the reaction operates at substantially higher temperatures and pressure which are crucial parameters for the activity of the catalyst. Thus, one-to-one mapping of DFT results to experiments is not easy. Although, we could validate our DFT results of methanol to formaldehyde production at the ZnO surface by experiments will be discussed in detail in chapter 6.

Chapter 3

Interaction of MeOH with pristine and oxygen-preadsorbed Zn surfaces

3.1 Motivation

Considering the importance of MeOH in the chemical industry as feedstock or fuel, its interaction with various catalysts is studied extensively. For the conversion of methanol to any desired product, dissociation of its O-H and/or C-H bond is the primary step. A thorough study of the interaction of methanol with metal surfaces using experimental and theoretical methods is available in the literature.[32–35,58,88–94]

Among transition metals, coinage metals have attracted significant attention due to their usage as feedstock in methanol steam reforming, DMFC, and formaldehyde production. Due to the availability and affordability of copper, its interaction with MeOH is studied extensively.[38,60,61,95,96] The decomposition of methanol on Cu surfaces is initiated by dissociating the O-H bond followed by dehydrogenation of the methoxy group. The rate-limiting step for methanol decomposition on Cu surfaces is the abstraction of hydrogen from the methoxy group. Also, the interaction of methanol with Cu surfaces is structure-sensitive, and the kinetics is facet dependent. In a recent study, David et al. investigated low-index Cu surfaces for methanol decomposition at ambient pressure and temperature conditions.[96] They demonstrated that the kinetics of methanol decomposition is surface sensitive and has faster kinetics on the (110) surface of Cu as compared to its (100) and (111) facets. They observed that the O-H bond of methanol dissociates at all Cu surfaces at ambient conditions. Silver, another coinage metal, is studied extensively for its interaction with MeOH owing to its industrial usage for producing formaldehyde from MeOH. Methanol weakly adsorbs at the Ag surface, making desorption easier. Methanol decomposition on the silver surface starts with the formation of methoxy, followed by dehydrogenation to produce formaldehyde. The dehydrogenation of methoxy is the rate-limiting step on Ag catalysts. The activation barrier for dissociating the

O-H bond on Ag is very high, $\sim$ 1.5 eV.[94]

Pt is also one of the vastly explored metals for methanol interaction because of its usage as an anode in DMFC, where methanol completely oxidizes to CO_2. Sexton investigated Pt (111) surface for its interaction with methanol using high-resolution electron loss spectroscopy and temperature-programmed desorption.[97] They observed that methanol is dehydrogenated to carbon monoxide and hydrogen at as low a temperature as 140 K. The methoxy species is unstable at 170 K and dissociates to CO and hydrogen, which contrasts with the Cu surfaces where methoxy species dehydrogenates to formaldehyde. Mavrikakis and his group predicted the reaction pathway for the decomposition of methanol to CO and hydrogen using periodic DFT and a microkinetics model.[98,99] They suggested that the decomposition of methanol begins with the breaking of two successive C-H bonds to yield hydroxymethylene (HCOH), which is then further dehydrogenated to produce CO and H_2. Further, the production of H_2 increases with the reactor's temperature and methanol concentration. Another precious metal, palladium, has also been of interest due to its application in methanol steam reforming. In an experimental study on methanol reaction with Pd (100), Christmann and Demuth reported that methanol spontaneously decomposes under ultra-high vacuum conditions.[100] However, most dissociated methoxy and hydrogen recombine to desorb as methanol. Further increasing the temperature to $\sim$ 300 K, the methoxy group dehydrogenates to CO and H_2. There are contradictory results for the same Pd surface for methanol decomposition pathways. For example, Schennach et al.[101] suggests that C-H bond dissociation is thermodynamically more favourable on Pd (111) surface, whereas, in another study, Zhang and Hu[29] suggested that O-H bond dissociation is most favourable for the dissociation of methanol on Pd (111) surface.

Adsorption of oxygen at metal surfaces affects their reactivity by altering the surface and associated electronic properties.[102–105] Oxygen binds strongly with almost all metals and triggers surface reconstruction. This reconstruction either facilitates adsorption or blocks the catalyst's active site. Further, the difference in the electronegativity of oxygen and metal atoms leads to a redistribution of charge density, affecting the reactivity of the facet.[106] These observations motivated the investigation of methanol interaction with oxygen-preadsorbed metal surfaces.[27,107–109] Xu et al. investigated the interaction of methanol on oxygen preadsorbed Au(111) surface by employing DFT[27] and reported a substantial reduction in the activation barrier for dissociation of the O-H bond of methanol (0.41 eV, which is one-fourth of the barrier for bare Au(111) surface (1.58 eV)) Similarly, Aljama et al. studied the conversion of methanol to formaldehyde at Ag(111) surface using DFT and microkinetic modelling.[109] They predicted that preadsorbed oxygen enhances the reactivity of the Ag surface by reducing the activation barrier to 0.81 eV which is significantly lower than the clean surface (2.85 eV). This demonstrates the effect of preadsorbed oxygen on metal surfaces in enhancing MeOH decomposition. The activation barrier for inert metals such as Au and Ag is very high, almost of the order of 1.5 eV, while for Pd and Pt, it reduces to $\sim$ 0.80 eV. However, using

precious metals as a catalyst has its own limitations. This motivates us to investigate non-precious metals for the decomposition of methanol. In this chapter, we have investigated the interaction of methanol with different flat and step facets of pure Zn and oxygen-preadsorbed Zn surfaces. The availability and affordability of the Zn metal has motivated us to delve into various facets of Zn and oxygen-preadsorbed Zn facets. The chapter is organized as follows. In section 3.2, we discuss the computational details. In section 3.3 we discuss the results of the interaction of methanol on metallic and oxygen-preadsorbed Zn surfaces followed by conclusion in section 3.4.

3.2 Computational details

All the calculations performed within the Kohn-Sham formalism of density functional theory. Projector Augmented Wave potential[110] is used, with Perdew Burke Ernzerhof (PBE) approximation for the exchange-correlation and generalized gradient approximation,[112] as implemented in plane-wave, pseudopotential-based code, Vienna Ab initio Simulation Package (*VASP*).[113] We obtained the bulk unit cell from the Materials Project.[81] The bulk lattice parameters upon optimization are a = 2.62 Å and c = 5.02 Å which are in excellent agreement with the experimentally measured (a = 2.66 Å, c = 4.95 Å) lattice parameters.[116] Two flat facets ($10\bar{1}0$) and ($10\bar{1}1$) of Zn are modelled as slabs by cleaving a surface with 3x3 periodicity in the x and y direction with four layers using Quantumwise-VNL-2017.1.[84] The step facet ($10\bar{1}3$) is cleaved using 4x1 periodicity in the x and y direction with four layers. We fixed the bottom layer, and all the remaining layers and adsorbate are allowed to relax for all surface calculations. Van der Waals corrections are applied to account for dynamic correlations between fluctuating charge distribution by employing the Grimme method (DFT-D2).[117] It is observed that 20 Å of vacuum is sufficient to avoid interaction between adjacent images of planes along the z-direction. Geometry optimization is carried out with a force cutoff of 0.01 eV/Å on the unfixed atoms, and the total energies converged below 10^{-4} eV for each SCF cycle. A Monkhorst-Pack grid of 3x2x1, 4x2x1, and 2x2x1 is used for ($10\bar{1}0$), ($10\bar{1}1$), and ($10\bar{1}3$) slabs respectively. The energy difference is less than 4 meV/atom upon using finer mesh. The entire surface is scanned by placing the MeOH molecule at various unique sites. The interaction energy is calculated using the formula: $E_{MeOH/Zn} = E_{MeOH+Zn} - (E_{Zn} + E_{MeOH})$ where $E_{MeOH+Zn}$ is the energy of the system when MeOH is placed on the Zn surface, E_{Zn} is the energy of the bare surface and E_{MeOH} is the energy of the MeOH molecule. Further, we placed one oxygen atom on all the facets to investigate the effect of oxygen adsorption on the reactivity of Zn surfaces. The adsorption energy is calculated using the following formula: $E_{O/Zn} = E_{O+Zn} - (E_{Zn} + 1/2\ E_{O2})$ Where E_{O+Zn} is the energy of the system when the oxygen atom is placed on the surface, E_{Zn} is the energy of the bare surface and E_{O2} is the energy of the isolated O_2 molecule. Also, the interaction energy of methanol adsorption on oxygen preadsorbed Zn surface is calculated using the formula:

$E_{MeOH/O-Zn} = E_{MeOH+O-Zn} - (E_{O+Zn} + E_{MeOH})$ Here, $E_{MeOH+O-Zn}$ is the energy of the system with methanol adsorbed on the oxygen-preadsorbed Zn surface. The site-dependent projected Density of States (*pDOS*) are calculated with denser k-mesh using LOBSTER.[118] The activation barrier for O-H bond dissociation of methanol is computed using the climbing image-nudged elastic band (CI-NEB) method for both clean and oxygen preadsorbed surfaces.[122] Three images are considered for transition state calculations using a force convergence of 0.1 eV/Å.

3.3 Results and discussion

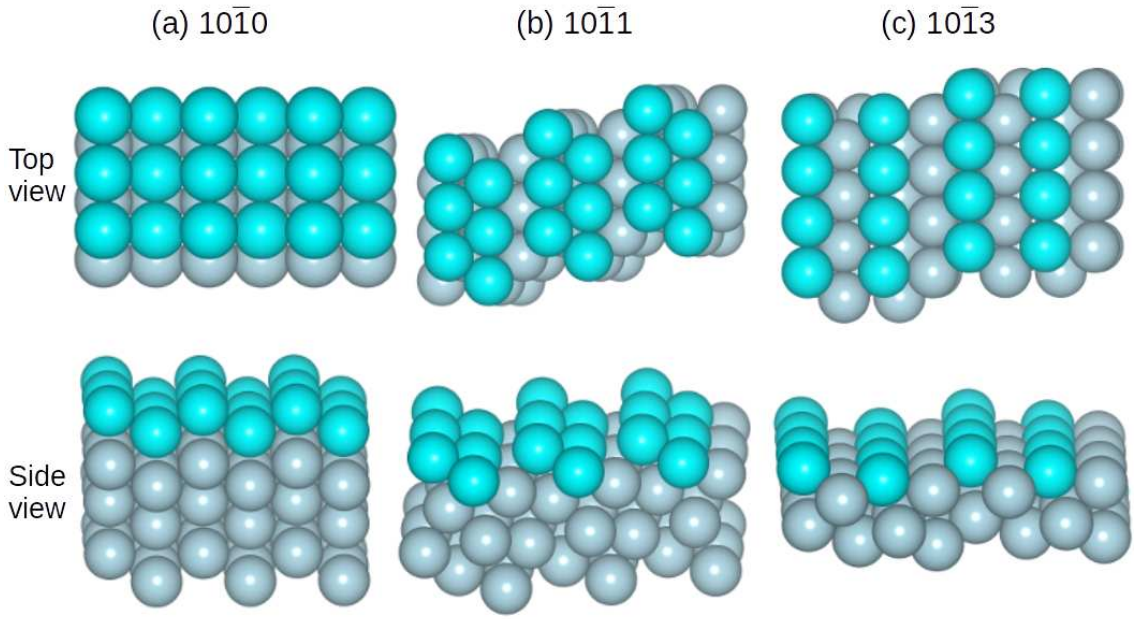

Figure 3.1: *Bare facets of pristine zinc are shown. (a) (10$\bar{1}$0) facet, (b) (10$\bar{1}$1) facet, and (c) shows (10$\bar{1}$3) facet. The upper and lower panels represent the facets' top and side views. The topmost surface layer is in dark colours, while the bottom bulk layers are in light colours.*

Zn-based catalysts are extensively used in many reactions[123–126] because apart from its catalytic properties, Zn is abundant (24^{th} in the earth's crust), cheap, and safe to handle. In its metallic form, Zn exhibits only one oxidation state (+2). Bulk Zn crystallizes in the hexagonal structure with the six nearest neighbours coordinating the Zn atoms in their plane and six Zn atoms in alternate planes. (10$\bar{1}$1), (0002), (10$\bar{1}$0),(10$\bar{1}$3), and (10$\bar{1}$2) facets have prominent peaks in XRD.[127] In this work, we have studied the interaction of methanol with two flat ((10$\bar{1}$0), (10$\bar{1}$1)) and one stepped (10$\bar{1}$3) facets of metallic Zn and oxygen-preadsorbed Zn. Top and side views of metallic Zn facets are shown in Fig. 3.1.

Interaction of MeOH with Zn surfaces

Methanol is a three-dimensional molecule with four different types of atoms, viz. oxygen (O_{MeOH}),

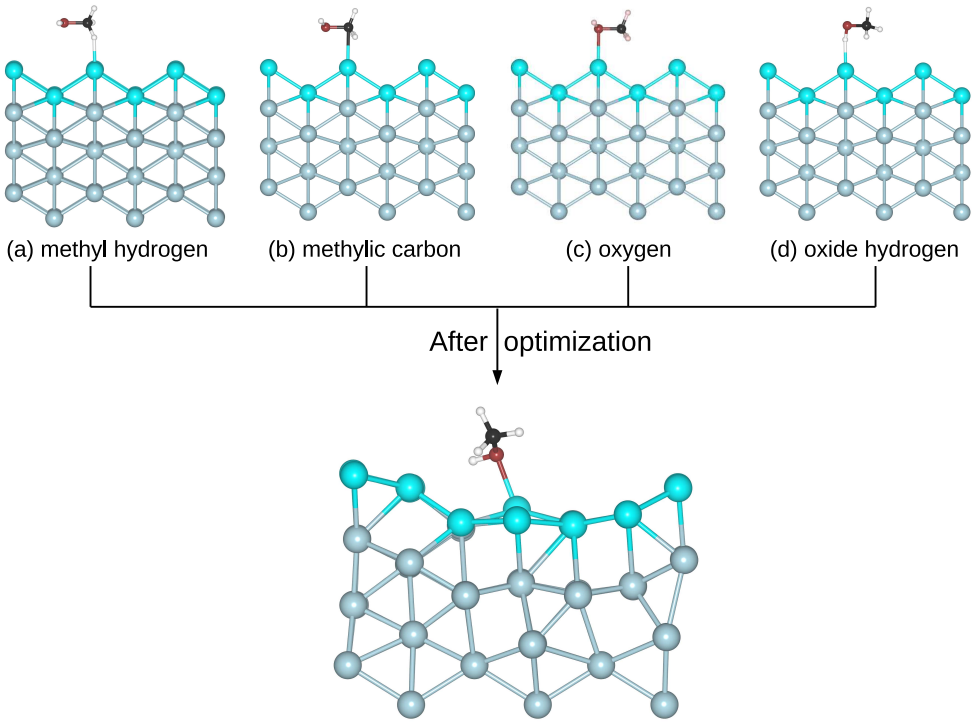

Figure 3.2: *Methanol can approach the zinc surface by any of its four inequivalent atoms. The upper panel represents all those configurations of methanol. We observed that irrespective of its initial configuration, MeOH orients itself upon optimization and adsorbs via its oxygen on the surface Zn atom, as demonstrated in the lower panel.*

hydrogen bonded to oxygen (H_{MeOH}), carbon (C_{MeOH}), and three methylic hydrogen atoms bonded to carbon (H_{Mt}). We observed that irrespective of its initial configuration, upon optimization, MeOH orients itself on the surface and adsorbs through O_{MeOH}, as shown in Fig. 3.2. This information was utilized while constructing the initial state of MeOH at various unique sites on all facets.

We begin by discussing the interaction of methanol with different $(10\bar{1}0)$, $(10\bar{1}1)$, and $(10\bar{1}3)$ facets of Zn. All these facets are scanned by placing methanol at various inequivalent sites. Thermodynamically the most stable cases of methanol adsorption on all the investigated metallic Zn facets are shown in Fig.3.3. Fig.3.3-(a) represents the thermodynamically most stable configuration of MeOH adsorption at $(10\bar{1}0)$ facet. Methanol adsorption results in substantial reconstruction at the surface. The bare facet of $(10\bar{1}0)$ is shown in Fig.3.1-(a). Surface atoms of this facet rearrange themself, and the atomic arrangement resembles that of $(10\bar{1}1)$ facet. Fig.3.3-(b) depicts the adsorption of MeOH at $(10\bar{1}1)$ facet. The extent of reconstruction upon MeOH adsorption is much less

Table 3.1: *Interaction energy (eV), O-H bond-length (Å) of MeOH at various inequivalent sites of (10$\bar{1}$0), (10$\bar{1}$1), and (10$\bar{1}$3) facets of pristine Zn. In all the cases, irrespective of its initial position, MeOH always diffuses on the surface and adsorbs with its oxygen on top of Zn. However, variations in the relative orientation of MeOH wrt surface results into observed variation in E_{int}. The bold numbers represent the thermodynamically most stable cases at each facet.*

Initial Positions	(10$\bar{1}$0)		(10$\bar{1}$1)		(10$\bar{1}$3)	
	E_{int} (eV)	O-H BL (Å)	E_{int} (eV)	O-H BL(Å)	E_{int} (eV)	O-H BL (Å)
Top	-3.37	0.98	-1.31	0.98	**-0.67**	**0.99**
Bridge	—	—	-1.26	0.98	—	—
SB	**-4.09**	**0.99**	—	—	-0.57	0.98
LB	-3.36	0.98	—	—	-0.64	0.99
4FH/3FH	-3.23	0.99	**-1.35**	**0.98**	-0.64	0.99
Top_s	—	—	-1.32	0.98	—	—

than (10$\bar{1}$0). Fig.3.3-(c) shows adsorption of MeOH at (10$\bar{1}$3) facet. No reconstruction is observed at this facet upon MeOH adsorption. Before detailed discussions, we note that the physisorption and chemisorption of methanol are explained based on the O-H bond length of methanol upon adsorption. Physisorption of MeOH is accompanied by surface reconstruction of the flat facets, whereas the step facet does not show any rearrangement of surface atoms. This rearrangement of surface atoms also reflects in the lowering of interaction energy of MeOH (refer to Tab.3.1). In Tab.3.1, we have noted the interaction energy and O-H bond length of methanol on all three facets of metallic Zn. In all cases, upon optimization, irrespective of the initial position, methanol diffuses on the surface and adsorbs on top of Zn. However, in Tab.3.1, we have noted the initial positions to distinguish each configuration. Thermodynamically the most stable configuration for each facet is shown in bold numbers. The interaction energies for (10$\bar{1}$0) facets are significantly larger because the reconstruction energies are buried in them. The extent of reconstruction is significant for the (10$\bar{1}$0) facet because of its open structure and is minimal or absent for the other two facets [(10$\bar{1}$1), (10$\bar{1}$3)] respectively. The reconstruction on (10$\bar{1}$0) causes the rearrangement of atoms on the surface, which resembles that of the (10$\bar{1}$1) facet.

Interaction of methanol with O-preadsorbed Zn surfaces

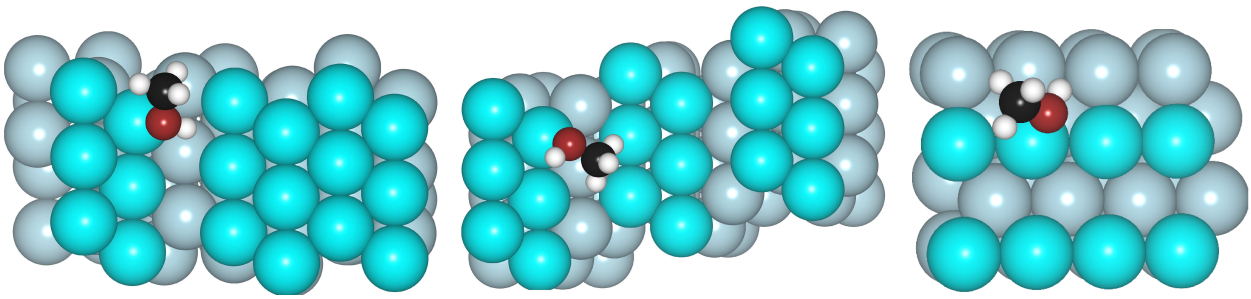

Figure 3.3: *(a) represents the thermodynamically most stable configuration of MeOH adsorption at (10$\bar{1}$0) facet. Methanol adsorption results in substantial reconstruction at the surface. The bare facet of (10$\bar{1}$0) is shown in Fig.3.1-(a). Surface atoms of this facet rearrange themself, and the atomic arrangement resembles that of (10$\bar{1}$1) facet. (b) depicts the adsorption of MeOH at (10$\bar{1}$1) facet. The extent of reconstruction upon MeOH adsorption is much less than (10$\bar{1}$0). (c) Adsorption of MeOH at (10$\bar{1}$3) facet. No reconstruction is observed at this facet upon MeOH adsorption.*

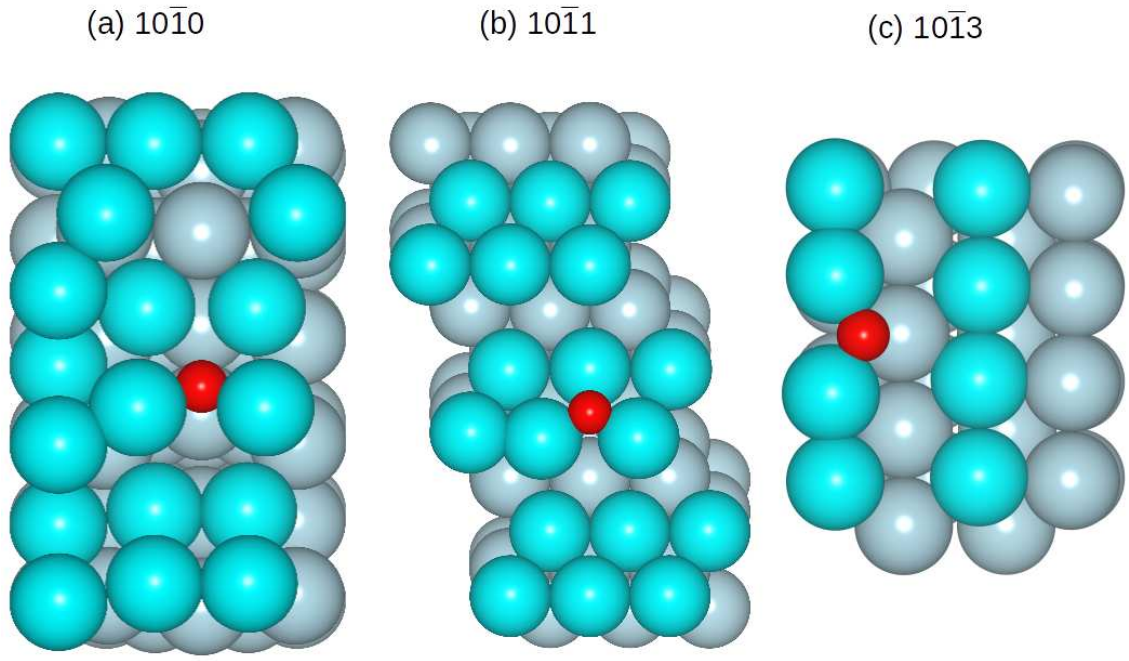

Figure 3.4: *Depicts the adsorption of an oxygen atom on the Zn surfaces. (a) The oxygen atom adsorbs at the subsurface of (10$\bar{1}$0) and triggers substantial reconstruction, whereas the oxygen atom adsorbs at the surface of (b) (10$\bar{1}$1) and (c) (10$\bar{1}$3) facet. The open structure of (10$\bar{1}$0) facet allows oxygen diffusion to the subsurface layer.*

As discussed earlier, exposing a metal surface to oxygen alters its reactivity considerably. To understand the effect of oxygen adsorption on the reactivity of zinc facets, we have adsorbed atomic oxygen on all these facets, as shown in Fig.3.4. The oxygen on the (10$\bar{1}$0) surface diffuses to the subsurface layer, while on the other two facets [(10$\bar{1}$1) and (10$\bar{1}$3)], it adsorbs on the surface. Closed packing of atoms on the (10$\bar{1}$1) and (10$\bar{1}$3) facets do not favour oxygen diffusion in the subsurface layer. The interaction energy of oxygen adsorption on various Zn facets and the bond

Table 3.2: *Interaction energy ($E_{O/Zn}$) (eV) and O-Zn bond-length (Å) of oxygen adsorption at various inequivalent sites of ($10\bar{1}0$), ($10\bar{1}1$), and ($10\bar{1}3$) facets of zinc. It is observed that oxygen diffuses on the zinc surface and hollow sites are thermodynamically most stable for oxygen atom adsorption, represented in bold numbers.* [a] *Upon optimization, the O atom moves to the hollow position.* [b] *O atom moves to the bridge position.* [c] *O atom move to subsurface layer*

Initial Positions	($10\bar{1}0$)		($10\bar{1}1$)		($10\bar{1}3$)	
	$E_{O/Zn}$ (eV)	O-Zn BL (Å)	$E_{O/Zn}$ (eV)	O-Zn BL(Å)	$E_{O/Zn}$ (eV)	O-Zn BL (Å)
Top	-3.30[a]	1.85	-2.31[b]	1.89	-2.76[a]	1.90
Bridge	—	—	-3.19[a]	1.89	-2.75[a]	1.90
SB	-3.22	1.82	-3.17[a]	1.89	—	—
LB	-3.37[c]	1.97	—	—	—	—
4FH/3FH	**-4.06**	**1.96**	**-3.20**	**1.89**	**-2.93**	**1.88**

length of O-Zn are reported in Tab.3.2. The numbers in bold represent thermodynamically the most stable cases.

Table 3.3: *Interaction energy (eV), O-H bond-length (Å) of MeOH at various inequivalent sites of ($10\bar{1}0$), ($10\bar{1}1$), and ($10\bar{1}3$) facets of oxygen-preadsorbed Zn. The numbers in the bracket represent the distance between O_{surf} and H_{MeOH}. Numbers in bold signify the thermodynamically most stable cases.*

Initial Positions	($10\bar{1}0$)		($10\bar{1}1$)		($10\bar{1}3$)	
	E_{int} (eV)	O-H BL (Å)	E_{int} (eV)	O-H BL(Å)	E_{int} (eV)	O-H BL (Å)
Top	-1.66	0.98(3.28)	-0.59	0.99(1.87)	**-1.01**	**1.05 (1.49)**
Bridge	—	—	-0.63	0.99(1.76)	—	—
SB	**-3.26**	**0.99(3.48)**	—	—	-0.93	1.05(1.51)
LB	-1.57	0.98(6.47)	—	—	-1.01	1.06(1.49)
4FH/3FH	-1.98	0.99(3.44)	**-0.72**	**0.99(1.86)**	-0.64	0.99(6.96)
Top_s	—	—	-0.61	0.99(1.87)	—	—

We placed MeOH at various unique sites of oxygen-preadsorbed Zn surfaces. For pristine metallic surfaces, the MeOH physisorbed on the surface with no elongation in the O-H bond. However, oxygen adsorption causes activation of the methanol on the step facet of O-Zn. Ther-

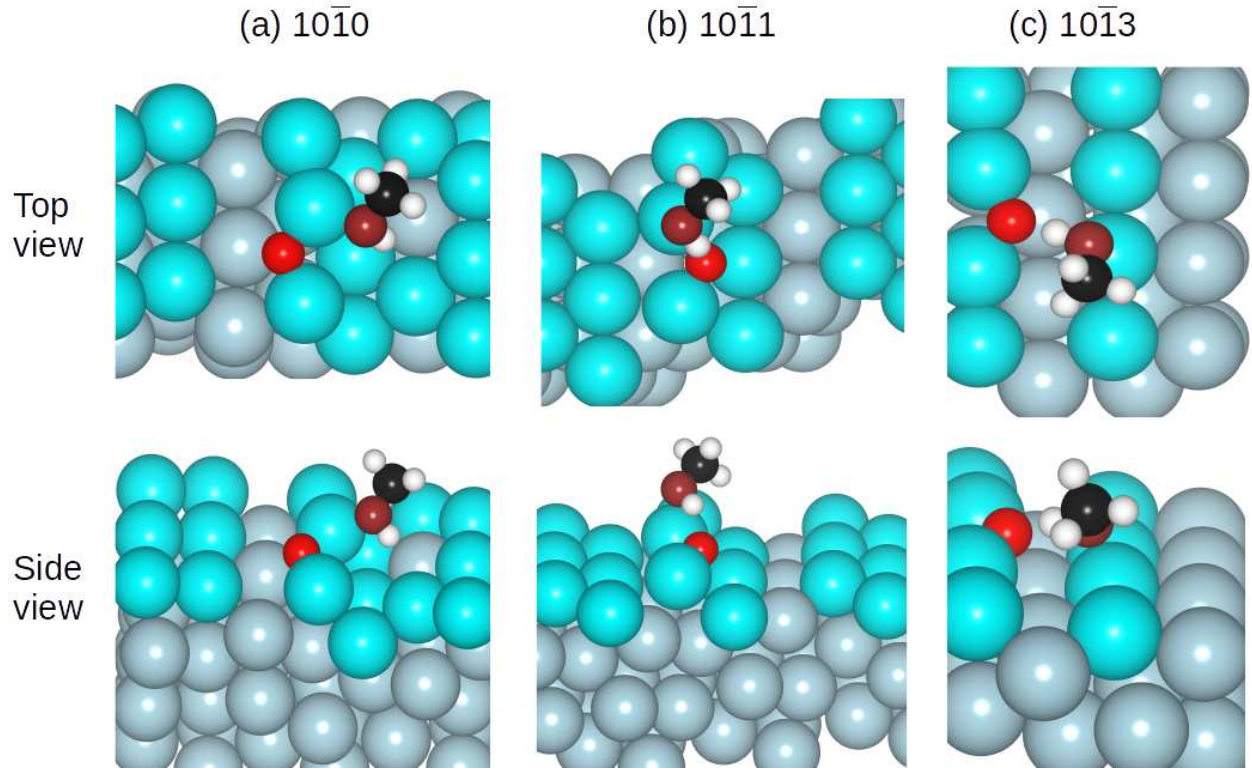

Figure 3.5: *Demonstrate the adsorption of methanol on oxygen-preadsorbed Zn surfaces. (a) shows (10$\bar{1}$0) facet. (b) shows adsorption of MeOH at (10$\bar{1}$1) facet. (c) Adsorption of MeOH at (10$\bar{1}$3) facet. The upper panel represents the top view, and the lower panel shows the side view of all the facets.*

modynamically most favourable cases of MeOH adsorption on oxygen-preadsorbed Zn are shown in Fig.3.5 The interaction energy of methanol adsorption on oxygen-preadsorbed Zn surface and O-H bond length is noted in Tab.3.3. The numbers in the bracket represent the distance between the O_{surf} and H_{MeOH}. Numbers in bold represent the thermodynamically most favourable cases. Although preadsorbed oxygen enhances the catalytic activity of metal surfaces, the reactivity depends on several other factors, such as the structural arrangement of atoms, coordination numbers, and effective charge on surface atoms. As evident from Tab.3.3, the O-H bond does not elongate on the (10$\bar{1}$0) facet of O-Zn because oxygen adsorption below the surface layer results in indirect interaction with adsorbed methanol. In the case of (10$\bar{1}$1) and (10$\bar{1}$3), oxygen is present on the surface and hence favours the adsorption of methanol on the surface by forming hydrogen bonds. The strength of the hydrogen bond between O_{surf}-H_{MeOH} determines the activation of methanol on the O-Zn systems. The proximity of surface oxygen and hydrogen of MeOH results in higher activation of the O-H bond of methanol with 9% elongation on the step (10$\bar{1}$3) facet.

We also computed the activation barrier for dissociation of the O-H bond on all Zn surfaces and oxygen-preadsorbed Zn surfaces. The results are depicted in Fig.3.6. The energy profile shows that the activation barrier decreases for all three facets upon oxygen adsorption. The barrier for (10$\bar{1}$0)

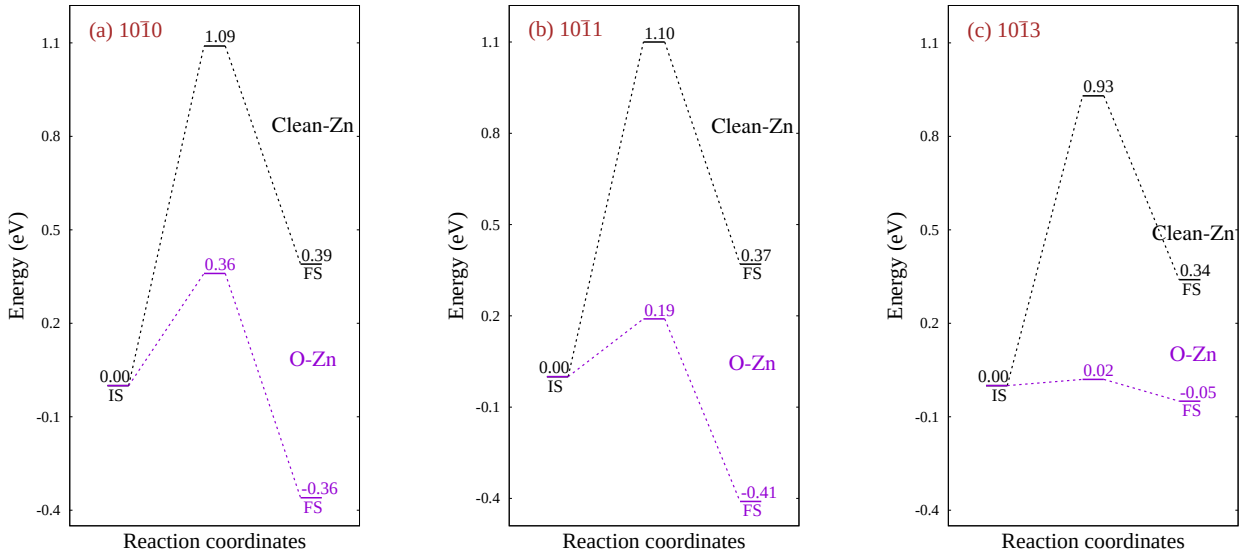

Figure 3.6: *The activation barrier for O-H bond of MeOH at (a) (10$\bar{1}$0), (b) (10$\bar{1}$1), and (10$\bar{1}$3) facets are shown. In the case of flat facets, the activation barrier significantly reduces from clean Zn to an O-assisted Zn surface, and it becomes negligible for the step facet. Also, the thermodynamics of the reaction become favourable upon oxygen adsorption.*

and (10$\bar{1}$1) reduces to one-third and one-fifth, respectively, while for the step facet, it becomes almost negligible. Change in reaction energy from positive to negative upon oxygen adsorption makes the reaction exothermic. The presence of oxygen on the surface also helps stabilize the hydrogen dissociated from methanol by forming the hydroxide.

The change in the underlying electronic structure upon oxygen adsorption provides a rationale for the observed variation in the reactivity of Zn facets upon oxygen adsorption. Fig. 3.7-(a) displays the *p*DOS for Zn-3*d* of all the bare surfaces of clean and oxygen-adsorbed Zn surfaces. Zn has a filled 3*d* level that is substantially below the Fermi level. Fig.3.7-(a): (ii) clearly shows that the *p*DOS of 3*d* has sharpened and is perfectly overlapping for all three facets after oxygen have been adsorbed on the surfaces.

In contrast to 3*d*, the 4*s* levels for Zn metal are close to Fermi and participate in reactivity. Fig.3.7-(b): (i) and (ii) illustrate the site-specific *p*DOS of Zn-4s for bare facets of pristine and oxygen-adsorbed surfaces, respectively. The 4s near Fermi, marked in Fig.3.7-(b), is enlarged and displayed in Fig.3.7-(c). The magnified plot clearly shows that for the step facet, the intensity of 4s states increases near and at the Fermi level in the oxygen-adsorbed facet compared to the pristine one. In contrast, the 4s intensity decreases near the Fermi level for both the flat facets. The presence of 4s states near the Fermi level facilitates the activation of methanol at the step facet. However, non-zero states at Fermi is not the only criteria for MeOH activation. Another crucial factor is the presence of surface oxygen in the vicinity of H_{MeOH}. Thus, although the 4s-*p*DOS are non-zero at Fermi for (10$\bar{1}$0), the absence of surface oxygen near H_{MeOH} results in barely activated MeOH. In

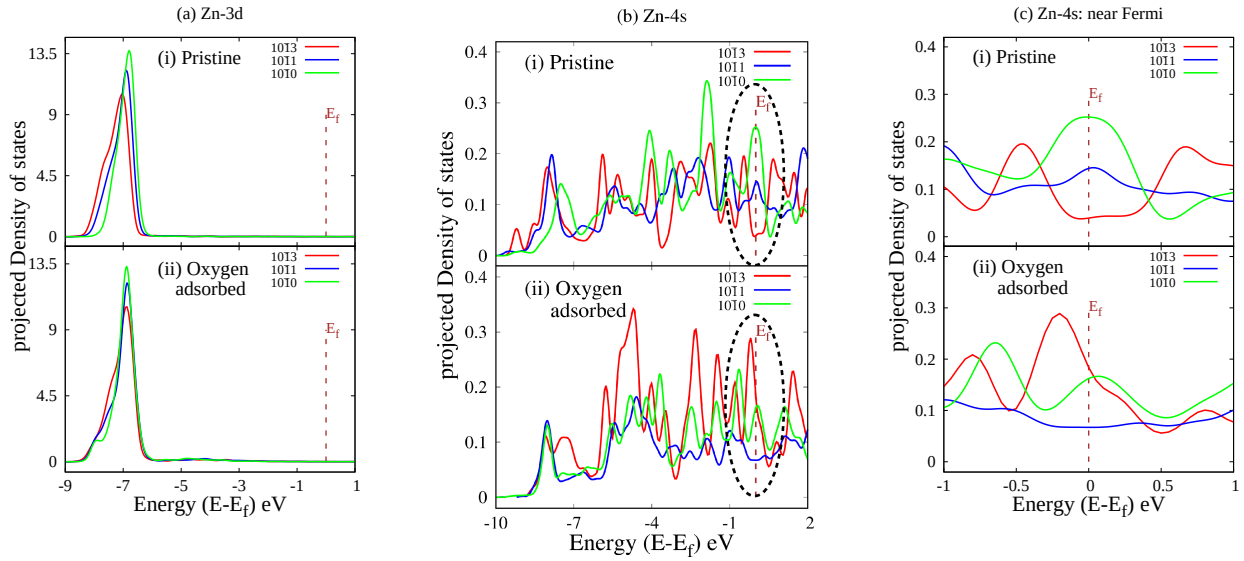

Figure 3.7: *(a) represents pDOS of Zn-3d of pristine zinc and oxygen adsorbed zinc surfaces. It is clear from the pDOS that 3d peaks sharpen and perfectly overlap for all three facets upon oxygen adsorption. (b) represents pDOS of 4s levels of metallic Zn surfaces and oxygen-adsorbed Zn surfaces. Significant variation in the nature of 4s is observed upon oxygen adsorption on Zn surfaces. (c) shows the magnified 4s level near Fermi, marked in (b). It is clear from the figure that for stepped facets (red curve), the peak intensity increases near Fermi, while for both flat facets (blue and green curve) the peak intensity reduces near Fermi as compared to the pristine surfaces.*

the case of (10$\bar{1}$1), although the activation of MeOH is comparable to that of (10$\bar{1}$0), the activation barrier is considerably lower as compared to (10$\bar{1}$0) because of the presence of surface oxygen in the vicinity of H_{MeOH}. On the other hand, in the case of metallic surfaces, the presence of 4s states near Fermi for flat facets does not favour the activation of methanol in the absence of oxygen. Thus, variation in the activity of facets of Zn and O-Zn can be correlated with the electronic structure of the bare facets.

3.4 Conclusions

We have studied the interaction of methanol with zinc and oxygen-preadsorbed zinc surfaces. The most prominent facets in the XRD of bulk Zn viz. (10$\bar{1}$0), (10$\bar{1}$1), and (10$\bar{1}$3) are investigated for their interaction with methanol. Physisorption of MeOH is a common outcome on all the facets of pristine Zn with a substantial reconstruction of (10$\bar{1}$0) surface. Upon adsorption of oxygen, MeOH was chemisorbed on the step facet. Adsorption of methanol in the vicinity of oxygen favours activation of MeOH. The NEB calculations show a significantly low activation barrier for O-H bond dissociation upon oxygen adsorption, with a negligible barrier on the step facet. The dissociation of the O-H bond also changes from being endothermic on pristine Zn surfaces to exothermic on

oxygen-preadsorbed surfaces. Thus, oxygen adsorption enhances the reactivity of the surface with methanol. Finally, the change in reactivity is explained based on the electronic structure of the bare facets.

Chapter 4

Interaction of MeOH with different ZnO surfaces

4.1 Motivation

Metal oxides exhibit better catalytic activity than pure metal surfaces due to various acidic and basic sites on the oxide surface. These different sites act as active sites for adsorbates and various intermediates formed during the reaction. Along with the active site, the oxygen of metal oxides directly participates in the reaction making the reaction more feasible on these surfaces. Numerous studies in the literature discuss the conversion of methanol to value-added products using metal oxide catalysts.[23,49–55,128–131]

The industrial catalyst used to synthesize methanol from syn gas is Cu-ZnO/Al_2O_3. In a recent computational study, Elnabawy et al. demonstrated the role of ZnO in the industrial catalyst for methanol synthesis.[132] They reported that the strong metal support interaction between Cu and ZnO favours higher activity towards methanol synthesis. ZnO reduces and partially covers the Cu surface, which causes modification in the surface. However, the active Cu sites remain unaffected, leading to the higher activity of the catalyst. ZnO is extensively used as a catalyst for many reactions because of its mixed covalent and ionic bonding.[133] Industrially, methanol is partially oxidized to formaldehyde using two different catalysts, silver or iron-molybdenum oxides. However, the reaction takes place at elevated temperatures in both cases. It is as high as 600^{o}C when silver is used as a catalyst, whereas it drops to $\sim$ 250-400^{o}C for a molybdenum catalyst. Clearly, there is room for improvement of the catalyst, which could further bring down the reaction temperature. In an experimental study, Boisen et al. demonstrated that the optimal ammonia synthesis catalyst is not the optimal ammonia decomposition catalyst.[134] Contrary to that, ZnO, an optimal methanol synthesis catalyst, exhibits excellent activity for methanol decomposition. Vo et al. investigated the adsorption and decomposition of methanol on ZnO($10\overline{1}0$) by employing DFT and concluded

that methanol strongly adsorbed on ZnO($10\bar{1}0$) surface as compared to CuCl(111), Cu(111), and Au(111) surfaces. Their results showed that the decomposition of MeOH to CH_2O molecule has a barrier of 1.20 eV.[66] In another interesting study, Abedi et al. employed DFT to understand the conditions leading to the monolayer formation of methanol on the ZnO($10\bar{1}0$) surface. They reported breaking the O−H bond, with a barrier of 0.5 eV, as the preferred mechanism over cleavage of the C−O bond.[135] In a combined experimental and theoretical work, Ruan et al. used high-resolution scanning tunnelling microscopy in combination with density functional theory to identify both the physi- and chemisorbed methanol species on the non-polar ZnO($10\bar{1}0$) surface. The physisorption of methanol dominates at liquid nitrogen temperature, which transforms into chemisorption upon either thermal annealing or electron injection. Moreover, the chemisorbed methanol mostly retains an undissociated state and tends to form a one-dimensional chain structure along the (0001) direction mediated by the intermolecular hydrogen bonding interactions.[136] A DFT study carried out by Smith et al. demonstrated a significantly lower reaction barrier (0.39 eV) towards methanol dissociation on ZnO (0001) compared to PdZn surfaces (0.54 eV).[137] Recently, Jin et al. studied the adsorption and reactions of CH_3OH on non-polar mixed-terminated ZnO($10\bar{1}0$), polar O terminated ZnO($000\bar{1}$) and Zn terminated ZnO(0001) surfaces using high-resolution electron energy loss spectroscopy (HREELS) in conjunction with temperature-programmed desorption (TPD). They found that methanol adsorbs dissociatively at room temperature for all three ZnO surfaces, leading to the formation of hydroxyl and methoxy species. Upon heating to higher temperatures (370K and 440K), the dissociated and intact methanol species on ZnO($10\bar{1}0$) predominantly undergo molecular desorption releasing CH_3OH. While on both polar surfaces, the thermal decomposition of CH_3OH occurs to produce CH_2O, H_2, CO, CO_2, and H_2O at temperatures higher than 500K.[138]

Although ZnO is used extensively as a catalyst in many reactions, its potential has yet to be truly realized. In this chapter, we have investigated the interaction of methanol with several unexplored facets of ZnO. The chapter is organized as follows. In section 4.2, we discuss the computational details. In section 4.3 we discuss the results of the interaction of methanol on ZnO surfaces followed by conclusion in section 4.4.

4.2 Computational details

Before discussing the results, let us briefly go through the computational details. All the calculations are performed within the Kohn-Sham formalism of Density Functional Theory. Projector Augmented Wave potential[110,111] is used, with Perdew Burke Ernzerhof (PBE)[139] approximation for the exchange-correlation and generalized gradient approximation,[112] as implemented in plane-wave, pseudopotential-based code, Vienna Ab initio Simulation Package (*VASP*).[113–115] We obtained the bulk unit cell from the materials project.[81] The bulk lattice parameters upon optimization

are a = 3.28 Å and c = 5.30 Å demonstrate excellent agreement with the experimentally measured (a = 3.24 Å, c = 5.20 Å) lattice parameters.[140,141] Two flat facets, $(10\bar{1}0)$ and $(11\bar{2}0)$ of ZnO are modelled as slabs by cleaving a surface with 3x3 periodicity in the x and y direction with four layers using Quantumwise-VNL-2017.1.[84] Two stepped facets, $(10\bar{1}3)$ and $(11\bar{2}2)$ are also cleaved by taking 3x1 and 2x2 periodicity, respectively, in the x and y direction with six layers. In every model, the bottom layer is fixed, and the rest of the layers and adsorbate are fully relaxed. Van der Waals corrections are applied to account for dynamic correlations between fluctuating charge distribution by employing the Grimme method (DFT-D2).[117] It is observed that 20 Å of vacuum is sufficient to avoid interaction between adjacent images of planes along the z-direction. Geometry optimization is carried out with a force cutoff of 0.01 eV/Å on the unfixed atoms, and the total energies are converged below 10^{-4} eV for each SCF cycle. A Monkhorst-Pack grid of 3x2x1 for $(10\bar{1}0)$ and 3x3x1 for $(11\bar{2}0)$ slabs are used. For both stepped surfaces, a Monkhorst-Pack grid of 2x2x1 is used. The energy difference is less than 4meV/atom for every system upon further refining the K mesh. The entire surface is scanned by placing MeOH molecule at all available unique sites. The interaction energy is calculated using the formula: $E_{int} = E_{system} - (E_{surface} + E_{molecule})$ where E_{system} is the energy of the system when MeOH is placed on the surface, $E_{surface}$ is the energy of the bare surface and $E_{molecule}$ is energy of the MeOH molecule. To understand the electronic structure of these facets, the total Density of States (*tDOS*) are calculated with denser k-mesh using LOBSTER.[118–121] Mulliken charges are computed for all the atoms on the surface.

4.3 Results and discussion

Bulk ZnO crystallizes in the hexagonal wurtzite structure consisting of hexagonal Zn and O planes stacked alternately. Both oxygen and zinc atoms are coordinated by four zinc and oxygen atoms, respectively. Polar ((0001) and $(000\bar{1})$) and non-polar ($(10\bar{1}0)$, $(10\bar{1}1)$, $(11\bar{2}0)$), $(10\bar{1}3)$, and $(11\bar{2}2)$) facets have prominent peaks in XRD.[142,143] In this work, we have studied the interaction of methanol with two flat ($(10\bar{1}0)$, $(11\bar{2}0)$) and two stepped ($(10\bar{1}3)$, $(11\bar{2}2)$) facets of ZnO. The top and side views of all these facets are shown in Fig.4.1.

Each layer of $(10\bar{1}0)$ is divided into two sub-layers leading to various unique sites for methanol adsorption. All these unique sites, such as the top of Zn, bridge of Zn-Zn, O-O, Zn-O, and bridge positions of atoms of two sub-layers, are scanned for methanol interaction. All the sites where MeOH is placed are shown schematically in Fig.4.2. The numbers in Fig.4.2-(a) represent the initial positions where MeOH is placed, and the final position of adsorbed methanol or dissociated methoxy group are shown in Fig.4.2-(b). The black numbers indicate molecular adsorption, while the red numbers denote dissociated methoxy group.

Before discussing the results in detail, we would like to elaborate on the criteria adopted for

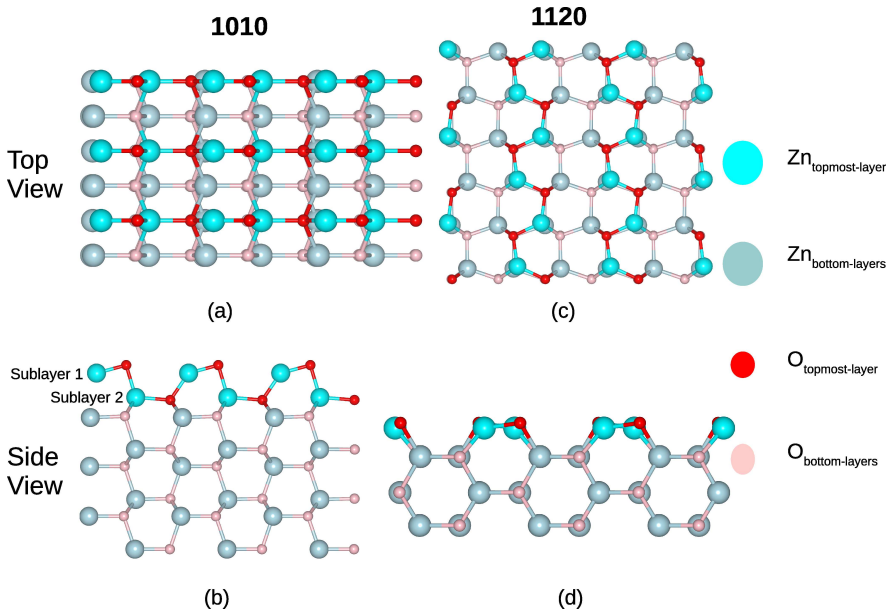

Figure 4.1: *Structural geometry of (10$\bar{1}$0), (11$\bar{2}$0), (10$\bar{1}$3) and (11$\bar{2}$2) facets of ZnO respectively. The upper panel shows the top view, and the lower panel shows the side view of the slabs.*

labeling the interaction of methanol at various ZnO surfaces. For all the configurations reported in this study, we described molecular adsorption or dissociation of MeOH based on its O-H bond length, which is 0.97 Å in the MeOH molecule. The physisorption also referred to as barely activated, is defined as slight elongation of the O-H bond from 0.97 Å to 0.98 Å. On the other hand, O-H bond elongation of more than 0.99 Å is associated with the chemisorption of MeOH on the facet. In all cases of O-H bond dissociation, the distance between O_{MeOH} and H is more than 1.45 Å ($>$ 50% of O-H bond length). Also, the dissociated H atom binds to the surface oxygen atom with a distance of 0.98-1.06 Å, which infers bond formation between them. Although interaction energy is used to define the thermodynamic stability of the resulting complex, it is not a measure of observed bond activation. As will be discussed later, complexes with maximum activation or even dissociation are not always the ones with the highest thermodynamic stability.

Methanol adsorbs either molecularly or dissociatively at different sites on the (10$\bar{1}$0) facet. The interaction energy, O-H bond-length, and Zn-O_{MeOH} bond-length are tabulated in Tab. 4.1. Molecular adsorption of MeOH is thermodynamically the most probable outcome at this facet. However, as seen from the Tab. 4.1, dissociation of MeOH into methoxy is also a viable product at elevated temperatures considering the small energy difference between these two outcomes. We report strong chemisorption and spontaneous dissociation of the O-H bond of MeOH. A weak chemisorption is also observed, consistent with previously reported work,[65] though it is not the thermodynamically most favourable outcome. At this point, it is pertinent to note that a molecule like MeOH could be placed at the symmetry-driven unique points on the surface in various ways.

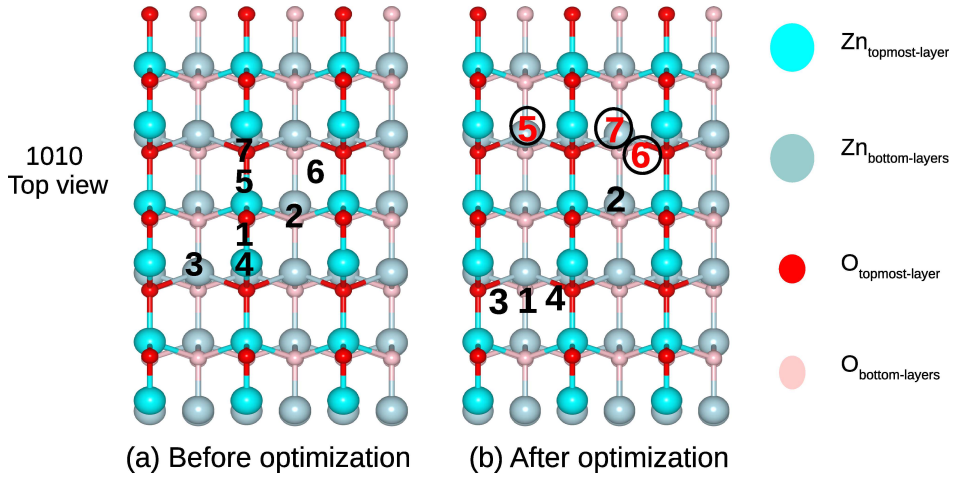

Figure 4.2: *(a) schematic representation of initial positions where MeOH is placed on $(10\bar{1}0)$ facet and (b) the positions where it adsorbed/dissociated after optimization. The numbers in black denote molecular adsorption, while dissociation is shown in red-coloured numbers enclosed in the black circle.*

Table 4.1: *Interaction energy (eV), O-H bond-length (Å), C-O bond-length (Å), and Zn-O_{MeOH} bond-length (Å) for various sites on ZnO $(10\bar{1}0)$ facet. All these positions are indicated in Fig. SI3-(b). Dissociation is indicated in red, while molecular adsorption is shown in black.*

Positions	E_{int} (eV)	O-H BL (Å)	C-O BL (Å)	Zn-O_{MeOH} BL (Å)
4	-1.58	1.04	1.44	2.05
3	-1.52	1.03	1.44	2.06
7	-1.36	3.09	1.43	1.96
6	-1.35	4.37	1.41	1.96
5	-1.25	1.61	1.41	1.93
1	-1.08	0.98	1.45	2.11
2	-0.69	1.00	1.39	3.54

A detailed account of which can be found in our following chapter. A slight change in MeOH orientation wrt the surface leads to a completely different result regarding the extent of O-H bond elongation or even O-H bond dissociation. Considering this, any study of MeOH interaction is always limited by the initial configurations one investigates. There is a dire need to formalize a methodology for accounting for all possibilities.

Fig. 4.3 shows representative conformations of MeOH upon adsorption/dissociation on this facet. A closer look at the adsorbed conformations reveals specific patterns in MeOH interaction with the facet. For example, highly chemisorbed methanol always gets adsorbed through oxygen (refer Fig. 4.3-(b)), whereas in the case of physisorbed MeOH, sometimes it gets adsorb through methylic H (refer Fig. 4.3-(c)). This adsorption through methylic H atom results in the activation of

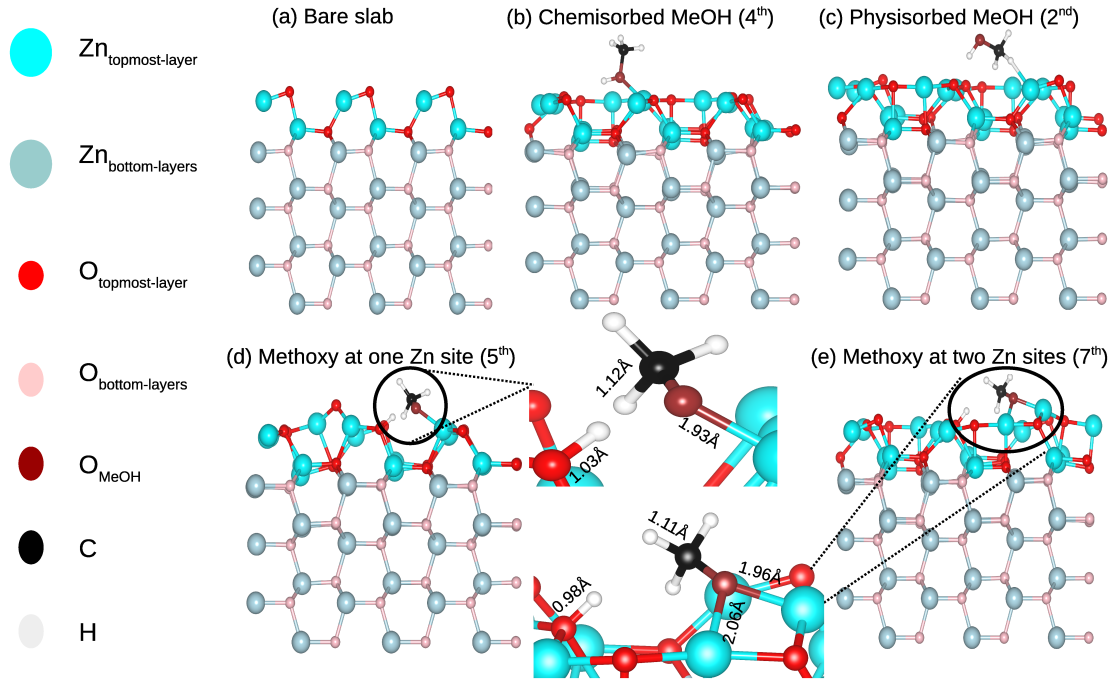

Figure 4.3: *(a) side view of bare the (10$\bar{1}$0) facet, (b) The chemisorbed MeOH with ∼7% elongation of the O-H bond, (c) chemisorbed MeOH with ∼3% elongation of O-H bond, (d) dissociated MeOH with methoxy group attached to the Zn atom, and (e) dissociated MeOH with methoxy group at bridge of two Zn atoms. For clear view of adsorption of methoxy on the surface (d) and (e) figures are enlarged. The numbers in the bracket indicates configuration with other details listed in Tab. 4.1*

the C-H bond of MeOH. The C-H bond elongates to 4%. Consequently, the C-O bond strengthens (as shown in Tab. 4.1) and reduces to 1.39 Å , indicating partial oxidation of methanol. Another interesting observation is that MeOH adsorption also leads to surface reconstruction, which results in the formation of voids, as evident in all the cases. However, the extent of reconstruction depends on the outcome, i.e. chemisorption (Fig. 4.3-(b) and (c)) or dissociation (Fig. 4.3-(d) and (e)). It was also observed that the dissociated methoxy group could adsorb at a Zn site or bridge of two Zn sites.

Another flat facet that we studied is (11$\bar{2}$0). This is a highly symmetric facet with fewer inequivalent sites on the surface, as shown in Fig. 4.4-(a). Interestingly, when MeOH is placed on any sites except 4^{th}, upon optimization, it gets chemisorbed at one specific site as schematically represented in Fig. 4.4-(b). The orientation of methanol on this site is shown in Fig. 4.4-(c). E_{ads} for methanol at this site is -1.24 eV, and the O-H bond of MeOH elongates to 1.02 Å. Further adsorbing the second MeOH molecule on the surface results in the chemisorption of a molecule with elongation in the O-H bond up to 1.03 Å. This shows that the (11$\bar{2}$0) facet does not favour the dissociation of methanol due to uniformity on the surface. Comparing the adsorption of MeOH on flat facets underlines the fact that nonuniform facet provides multiple possibilities.

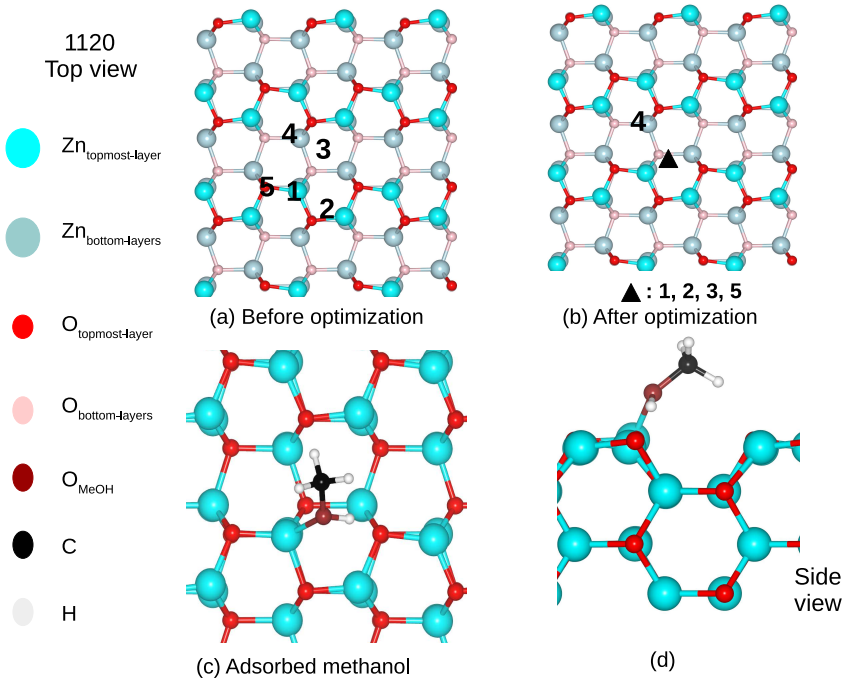

Figure 4.4: *(a) schematic representation of initial positions where MeOH is placed on $(11\bar{2}0)$ facet and (b) the positions where it adsorbed/dissociated after optimization. In most cases, MeOH prefers to adsorb at one position only, as marked in a black triangle. (c) Top view and (d) side view of the orientation of MeOH adsorbed at the facet.*

Table 4.2: *Interaction energy (eV), O-H bond-length (Å), C-O bond-length (Å), and Zn-O_{MeOH} bond-length (Å) for various sites on ZnO $(10\bar{1}3)$ facet. All these position are indicated in Fig. SI5-(b). Dissociation of MeOH is shown in red color while molecular adsorption is shown in black color.*

Positions	E_{int} (eV)	O-H BL (Å)	C-O BL (Å)	Zn-O_{MeOH} BL (Å)
2,7	-3.88	1.57	1.44	1.88
10	-3.70	1.73	1.39	1.89
6,8	-2.87	1.46	1.43	1.90
4,5,9	-1.71	1.03	1.37	3.49
1	-1.54	0.99	1.45	2.17
3	-1.42	0.99	1.45	2.21

Next, we investigate a stepped facet $(10\bar{1}3)$. Various available unique sites where MeOH is placed are shown in Fig. 4.5-(a). Those sites where methanol/methoxy adsorb upon optimization are shown in Fig. 4.5-(b). Interaction energy, O-H bond-length and Zn-O_{MeOH} are tabulated in Tab. 4.2. As evident from the interaction energy, dissociation of methanol is thermodynamically the most favourable outcome on this facet. Fig. 4.6 shows the representative cases of chemisorption

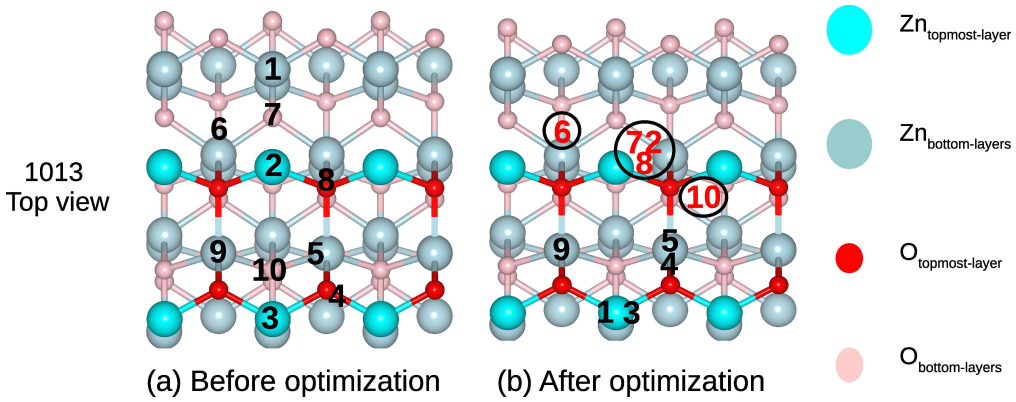

Figure 4.5: *(a) schematic representation of initial positions where MeOH is placed on (10$\bar{1}$3) facet and (b) the positions where it adsorbed/dissociated after optimization. The numbers in black denote molecular adsorption, while dissociation is shown in red-coloured numbers enclosed in the black circle.*

as well as dissociation of methanol on (10$\bar{1}$3) facet. It is observed that generally, MeOH/methoxy group adsorb via its O at the Zn site, but in a few cases, it adsorbs through its methylic H (refer Fig. 4.6-(b)). Contrary to (10$\bar{1}$0) facet, this methylic adsorption shows higher activation of the O-H bond. Adsorption through this methylic H leads to activation of the C-H bond, which elongates by 7% and also, the C-O bond reduces to 1.37 Å (as shown in Tab. 4.2. Elongation in C-H bond length and the reduction in C-O bond length is evidence of partial oxidation of methanol at this stepped facet. The dissociated methoxy group adsorbs on the surface in two different ways, either through O_{MeOH} (monodentate as shown in Fig. 4.6-(c)) or via two atoms, i.e. O_{MeOH} and methylic H (bidentate as shown in Fig. 4.6-(d)). Interestingly, the coordination number of surface sites where the MeOH/methoxy group adsorbs governs the stability of any configuration. Due to the presence of the step, the extent of reconstruction upon methanol adsorption is less on this facet as compared to (10$\bar{1}$0) facet.

Next, we discuss another stepped facet (11$\bar{2}$2) which is more symmetric than (10$\bar{1}$3) facet. Methanol is placed at all available unique sites as shown schematically in Fig. 4.7-(a), and its interaction with the ZnO surface has been studied. In most cases, irrespective of the initial positions of methanol, it diffuses to a single position upon optimization, as indicated by the red triangle in Fig. 4.7-(b). Similar to the previously stepped facet, this facet also shows two outcomes of MeOH interaction: dissociation and chemisorption. However, dissociation is highly favoured over its molecular adsorption, as evident from Tab. 4.3. Distinct conformations of adsorption and dissociation of methanol on this facet are shown in Fig. 4.8. A careful look at the adsorbed conformations reveals that depending on the sites of adsorption viz. bridge (refer Fig. 4.8-(a)) or on-top site (refer Fig. 4.8-(b)), elongation of O-H bond of methanol differs. The dissociated cases have methoxy adsorbed at the Zn site with Zn-O_{MeOH} bond length (1.98 Å) comparable to bulk Zn-O bond length. Further, the second molecule also chemisorbs on the surface with O-H bond elongation up to 1.01

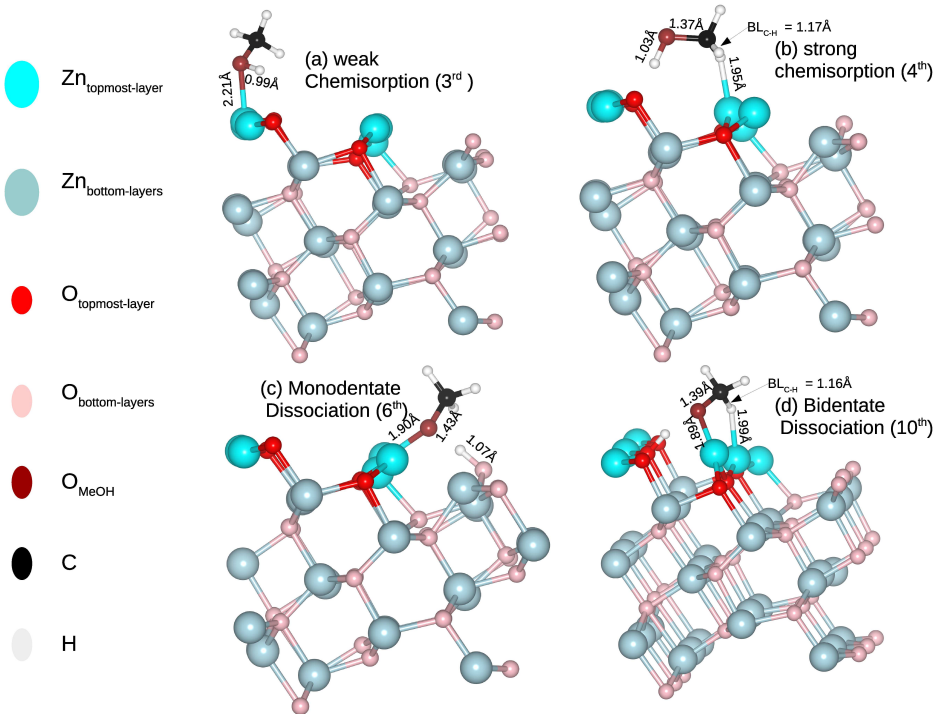

Figure 4.6: *Various conformers of MeOH interaction with $(10\bar{1}3)$ facet. The upper panel shows the chemisorption of MeOH, and the lower panel shows the dissociation of MeOH at the facet. (a) weak chemisorption, (b) strong chemisorption, (c) monodentate adsorption of the methoxy group, and (d) bidentate adsorption of the methoxy group. The numbers in the bracket indicate a configuration. The details are listed in Tab. 4.2.*

Table 4.3: *Interaction energy (eV), O-H bond-length (Å), C-O bond-length (Å), and Zn-O_{MeOH} bond-length (Å) for various sites on ZnO $(11\bar{2}2)$ facet. All these position are indicated in Fig. SI6-(b). Dissociation is indicated in red color while molecular adsorption is shown in black color.*

Positions	E_{int} (eV)	O-H BL (Å)	C-O BL (Å)	Zn-O_{MeOH} BL (Å)
3,9	-6.24	2.25	1.44	1.98
1,2,7,11,12	-3.10	2.04	1.44	1.98
6,8	-2.95	2.01	1.45	1.99
13	-2.86	1.94	1.45	1.98
5	-1.78	1.00	1.45	2.04
10	-1.77	0.98	1.47	2.26
4	-1.56	0.98	1.46	2.08

Å. In short, dissociation of MeOH is thermodynamically the most favourable outcome on stepped facets, while molecular adsorption is favourable on the flat facets.

So far, we have observed that different facets of ZnO interact differently with methanol result-

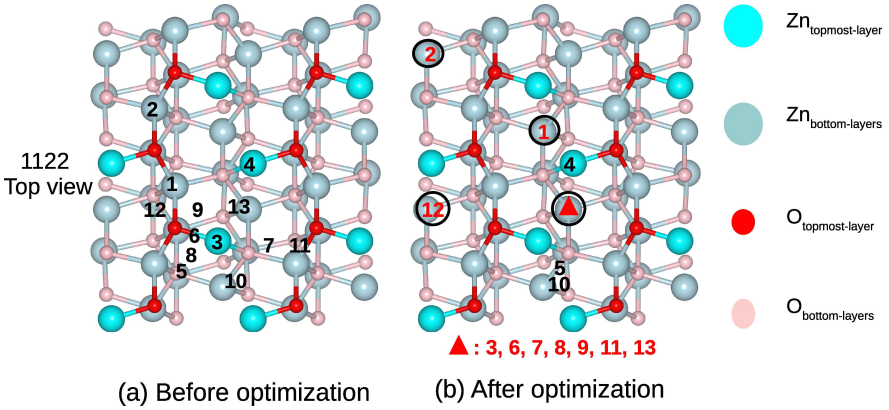

Figure 4.7: *(a) schematic representation of initial positions where MeOH is placed on (11$\bar{2}$2) facet and (b) the positions where it adsorbed/dissociated after optimization. The numbers in black denote molecular adsorption, while dissociation is shown in red-coloured numbers enclosed in the black circle. In most cases, dissociated methoxy group adsorb at one site, as shown in the red triangle.*

Table 4.4: *Coordination number, Mulliken charges of Zn and O atom of top most layer at each facet are shown.*

Surface	Co. no. of Zn	Mulliken charge on Zn	Co. no. of O	Mulliken charge on O
10$\bar{1}$0	2	0.85	2	-0.79
11$\bar{2}$0	3	0.96	3	-0.89
10$\bar{1}$3	3(2)	0.96(0.64)	3	-0.89(-0.82)
11$\bar{2}$2	2	0.81	3	-0.85

ing in molecular adsorption and/or activation and/or dissociation of the O-H bond. This behaviour difference is correlated with these facets' underlying electronic structure. The coordination number and Mulliken charges of surface Zn and O atoms of all the facets are noted in Tab. 4.4. For all facets but (10$\bar{1}$3), all the surface Zn or O atoms are identical. (10$\bar{1}$3) facet has two types of Zn and O atoms on the surface experiencing the difference in their neighbouring environment; hence Mulliken charges. It is also evident that higher coordination of surface atoms leads to higher effective charges and hence reduced reactivity. For example, in the case of (11$\bar{2}$0) facet, Zn and O atoms with the highest coordination and Mulliken charges do not show the dissociation of methanol. The inhibition of O-H bond breaking of MeOH at (11$\bar{2}$0) facet could be explained by analyzing the total density of states (*tDOS*) plot as shown in Fig. 4.9. The *tDOS* plot for (11$\bar{2}$0) facet clearly shows the non-availability of energy states near the Fermi level, which makes it the least reactive. Remaining all facets with energy states available near the Fermi level enhance the reactivity of the facet and explain the observed dissociation of methanol on these facets. Next, we plot the projected density of states (*pDOS*) of surface atoms for all facets. 3*d* and 4*s* states of surface Zn atoms are shown in

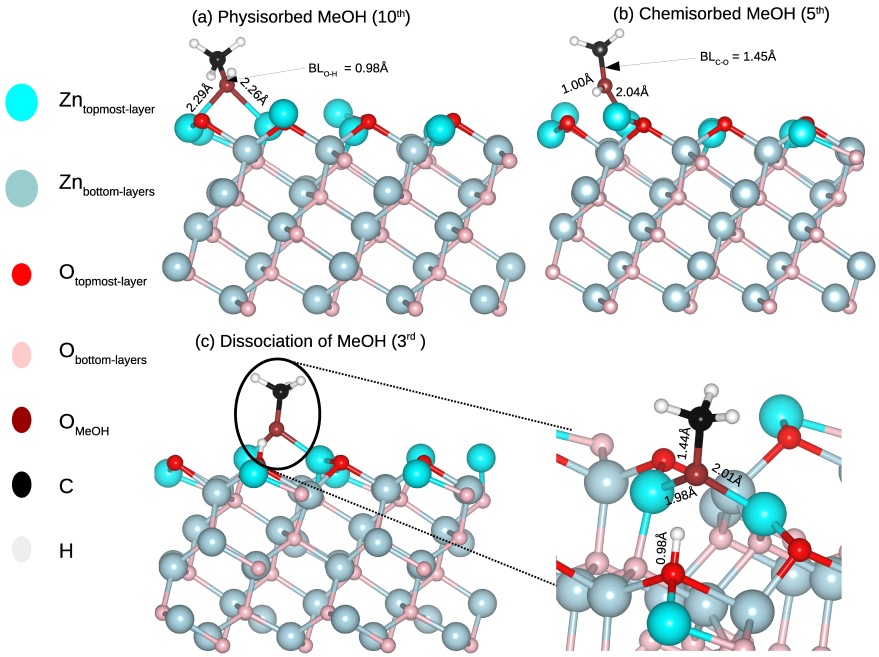

Figure 4.8: *Upper panel shows adsorption of MeOH at (11$\bar{2}$2) facet, and the lower panel shows the dissociation of MeOH. (a) physisorbed MeOH (b) chemisorbed MeOH (c) adsorption of a methoxy group at the bridge of two Zn atoms. The enlarged figure provides a clear view of methoxy group adsorption on the Zn site. The numbers in the bracket indicate configuration, and the details are listed in Tab. 4.3*

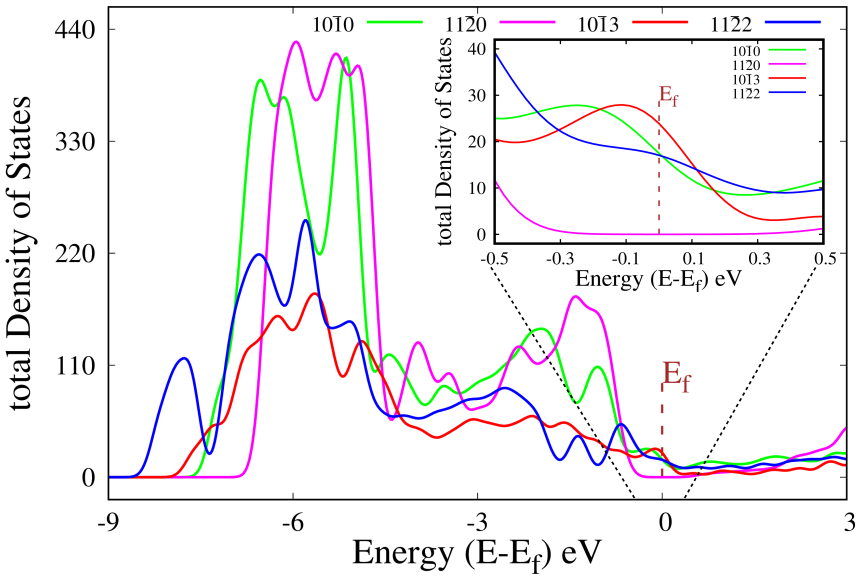

Figure 4.9: *The tDOS of four facets are plotted. The inset figure shows the enlarged tDOS near the Fermi level. Only for (11$\bar{2}$0) facet tDOS is zero at Fermi.*

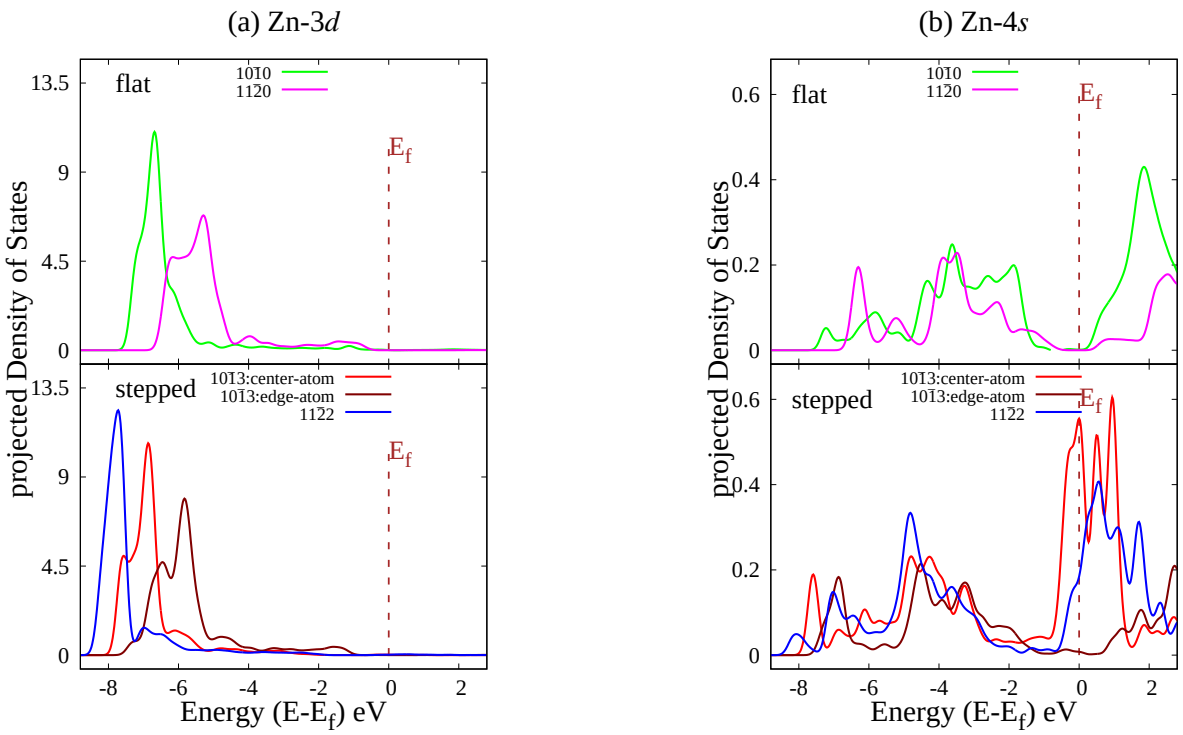

Figure 4.10: *(a) pDOS of Zn-3d orbitals of flat and stepped facets. As expected, 3d in Zn being completely filled are much away from the Fermi level. (b) Zn-4s of flat and stepped facets. It is interesting to note that for flat facets pDOS of surface Zn atoms show unavailability of states near Fermi as opposed to the case of stepped facet*

Fig. 4.10. Zn, being a late transition metal with filled 3*d* states lying much below the Fermi level (refer Fig. 4.10-a), does not participate in reactivity. While its 4*s* states, lying near the Fermi level, participate in the reactivity of the surface. It is seen in Fig. 4.10-b that for flat facets, 4*s* states of surface Zn atoms are zero near Fermi level while it is non-zero for stepped facets. The presence of non-zero 4*s* states near Fermi for stepped facets favours dissociation of MeOH, which is most favourable on these facets.

4.4 Conclusions

ZnO is considered a very active catalyst for many reactions because of its mixed covalent and ionic bonding. Also, it has been shown that the optimal catalyst for synthesizing methanol is an optimal catalyst for dissociating methanol. As evident from XRD, there are various prominent facets in ZnO, and only a few facets have been studied for methanol adsorption. We have carried out a systematic study of methanol adsorption on various facets of ZnO, which includes two flat [$(10\bar{1}0)$ and $(11\bar{2}0)$] and two stepped [$(10\bar{1}3)$ and $(11\bar{2}2)$] surfaces. O-H bond dissociation is thermodynamically

the most favourable outcome on stepped facets where chemisorption of MeOH with 7-10% O-H bond activation is observed on the flat facets. We also report considerable surface reconstruction upon MeOH adsorption. However, the reconstruction is less on the stepped surfaces than on the flat facets. Further, partial oxidation of MeOH is favoured on ZnO facets. Our detailed electronic structure analysis brings out the rationale behind the surface-dependent interaction of MeOH. Analysis of pDOS, tDOS, along with Mulliken charges on surface atoms explain the facet-dependent reactivity observed in the case of ZnO. Facets with available empty states near Fermi lead to O-H bond dissociation, whereas the absence of empty states near Fermi leads to O-H bond activation. Considering the role of ZnO in various reactions and the importance of MeOH in the current energy scenario, we believe our study shade light on some crucial aspects of the interaction of ZnO with MeOH. Finally, ZnO is a known catalyst for synthesis of MeOH. Our work opens up a possibility of ZnO as a catalyst for MeOH dissociation as well which awaits experimental verification.

Chapter 5

Interaction of MeOH with different $ZnAl_2O_4$ surfaces

5.1 Motivation

In the previous chapters, we presented the interaction of MeOH with metallic Zn, oxygen-preadsorbed Zn, and ZnO surfaces. As oxygen concentration on the Zn surface increases, we observed spontaneous dissociation of methanol on the catalyst surface. Metal alloys and metal oxides show better catalytic activity than monometal due to availability of multiple unique sites with varying strengths because of the added complexity of the facet. In this study, we investigate the interaction of methanol with a mixed metal oxide, $ZnAl_2O_4$.

There are few experimental studies demonstrating the decomposition of methanol on the mixed metal oxides like, $Fe_xCe_{1-x}O_2$,[144] $Cu/ZnAl_2O_4$.[145] However, there are no theoretical studies available providing insights for the interaction of methanol with mixed metal oxides. ZnO and Al_2O_3 are the industrially used catalyst for producing methanol from the syn gas mixture.[146] In this chapter, we have investigated the interaction of methanol with $ZnAl_2O_4$ which is a mixture of ZnO and Al_2O_3. The chapter is organized as follows. In section 5.2, we discuss the computational details. In section 5.3 we discuss the results of the interaction of methanol with $ZnAl_2O_4$ surfaces followed by conclusion in section 5.4.

5.2 Computational details

All the calculations were carried out within the Kohn-Sham formalism of density functional theory (DFT). Projector Augmented Wave potential[110] was used, with Perdew Burke Ehrzenhof (PBE) approximation for the exchange-correlation and generalized gradient approximation,[112] as imple-

mented in plane-wave, pseudopotential-based code, Vienna Ab initio Simulation Package (*VASP*).[113] We obtained the bulk unit cell from the materials project.[81] The bulk lattice parameter upon optimization is a = 8.06Å, which is in excellent agreement with the experimentally measured (a = 8.08Å) lattice parameter.[147] Two different facets (220) and (311) are modelled as slabs by cleaving a surface with 2x1 periodicity in the x and y direction with four layers using Quantumwise-VNL-2017.1.[84] The bottom layer is fixed, and all the remaining layers and adsorbate are allowed to relax for all the surface calculations. Van der Waals corrections are applied to account for dynamic correlations between fluctuating charge distribution by employing the Grimme method (DFT-D2).[117] It is observed that 20Å of vacuum is sufficient to avoid interaction between adjacent images of planes along the z-direction. Geometry optimization is carried out with a force cutoff of 0.05 eV/Å on the unfixed atoms, and the total energies converged below 10^{-4} eV for each SCF cycle. A Monkhorst-Pack grid of 6x4x1 is used for both slabs. The energy difference is less than 1meV/atom upon using finer mesh. The entire surface is scanned by placing the MeOH molecule at all available unique sites. The interaction energy is calculated using the formula: E_{int} = E_{system} - ($E_{surface}$ + $E_{molecule}$) where E_{system} is the energy of the system when MeOH is placed on the $ZnAl_2O_4$ surface, $E_{surface}$ is the energy of the bare $ZnAl_2O_4$ surface and $E_{molecule}$ is the energy of the MeOH molecule. The site-dependent projected Density of States (*pDOS*) are calculated with denser k-mesh using LOBSTER.[118] Mulliken charges are calculated for all the atoms on the surface, which provide the quantitative charge transfer.

5.3 Results and discussion

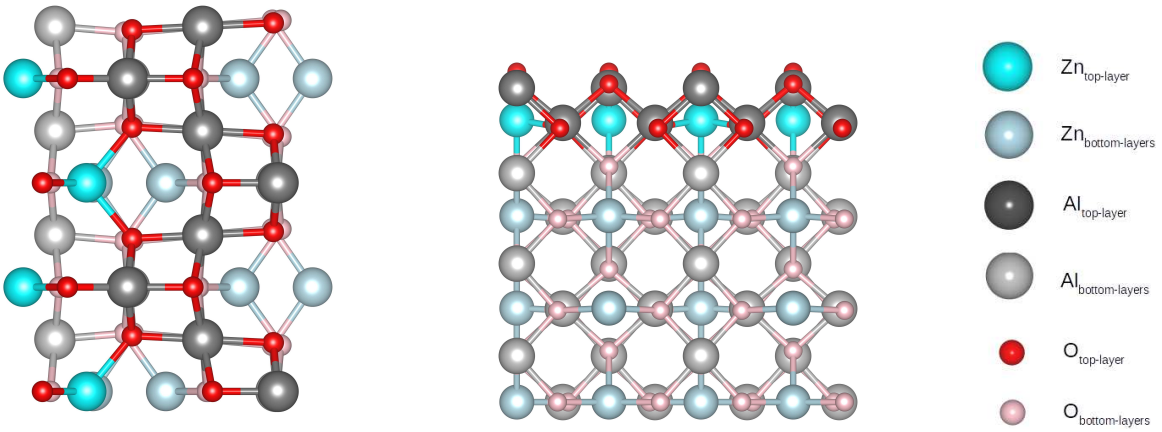

Figure 5.1: *The (220) surface of $ZnAl_2O_4$ with the top view and the side view. The topmost layer of (220) surface consist of Al, and O atoms. Zn atoms are present in the subsurface layers. The Zn, Al, and O atoms are represented in cyan, grey, and red colour respectively. Apart from the top layer, atoms in all the remaining layers are shown in light colours.*

$ZnAl_2O_4$ is a spinel metal oxide with a cubic lattice and $Fd\bar{3}m$ space group.[148] In this spinel compound, oxide ions occupy the Wyckoff position and form a face-centred cubic sublattice where Zn^{+2} ions occupy tetrahedral sites while Al^{+3} occupy octahedral sites. These Zn^{+2} ions are coordinated with four nearest neighbour oxygens, whereas the Al^{+3} ions have six oxygen atoms as their nearest neighbours in the bulk structure. $ZnAl_2O_4$ surface is polar and can be terminated in two different ways. It has been demonstrated that AlO_2 terminated surface is favoured over $ZnAlO_2$ termination.[149] We have investigated the (220) and (311) facets of the $ZnAl_2O_4$ for methanol interaction and these facets are the most prominent peaks in the XRD.[147,150–153]

Interaction of MeOH with $ZnAl_2O_4$ (220) surface

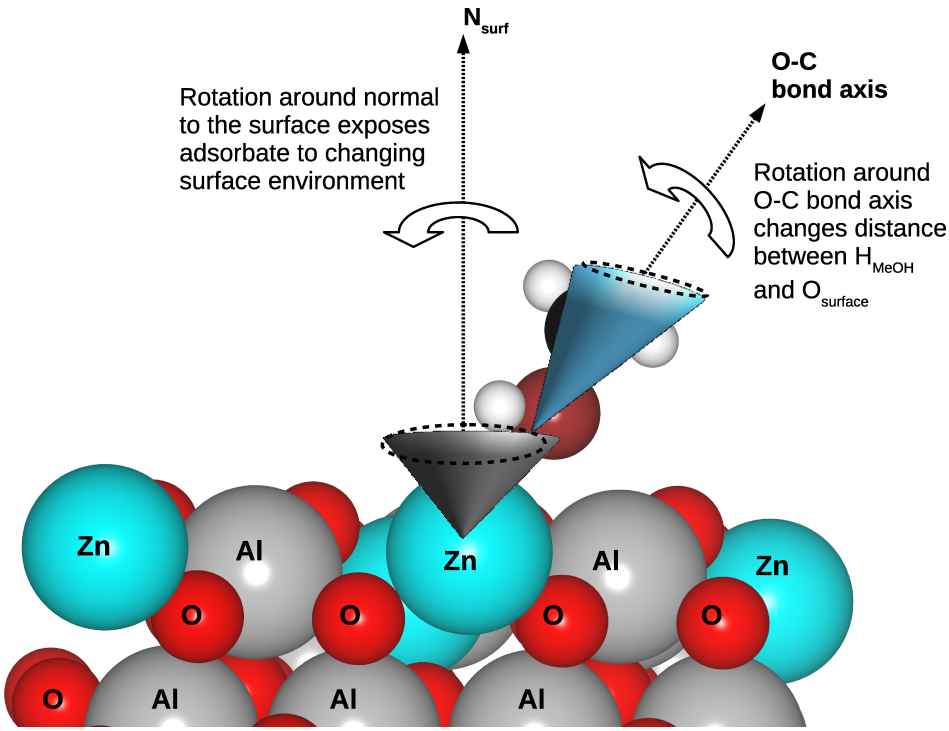

Figure 5.2: *The figure explains the large number of possibilities due to relative orientation of MeOH wrt the surface. Rotation around the normal to the surface, varying angle between N_{surf} and OC axis of MeOH and rotation around OC axis of the MeOH results into large number of possibilities in which molecule can interact with the surface when placed at a specific site.*

The (220) is a flat and symmetric surface shown in Fig.5.1. We model the AlO_2 termination in which the topmost layer of the surface is rich in Al and O atoms. Zn atoms are present in the subsurface layer and are not available to act as an active site for the adsorption of an incoming MeOH molecule. The surface is scanned by placing methanol at various inequivalent sites. However, here

we observed that even the favourable position of MeOH can have many relative orientations wrt surface atoms, leading to variations in adsorption energy for the same adsorption site. In all these cases, a change in the relative orientation of MeOH wrt the surface will affect the interaction between the surface and MeOH. The effect of this relative orientation is explained in detail later and turns out to be an essential factor in understanding interaction energy and bond activation trends. Fig.5.2 explains various possibilities that exist due to the relative orientation of MeOH wrt the surface. Rotation around the normal to the surface (N_{surf}), change in the angle between N_{surf} and O-C axis of MeOH, and rotation around the OC axis of the MeOH results in many possibilities in which a molecule can interact with the surface when placed at a specific site.

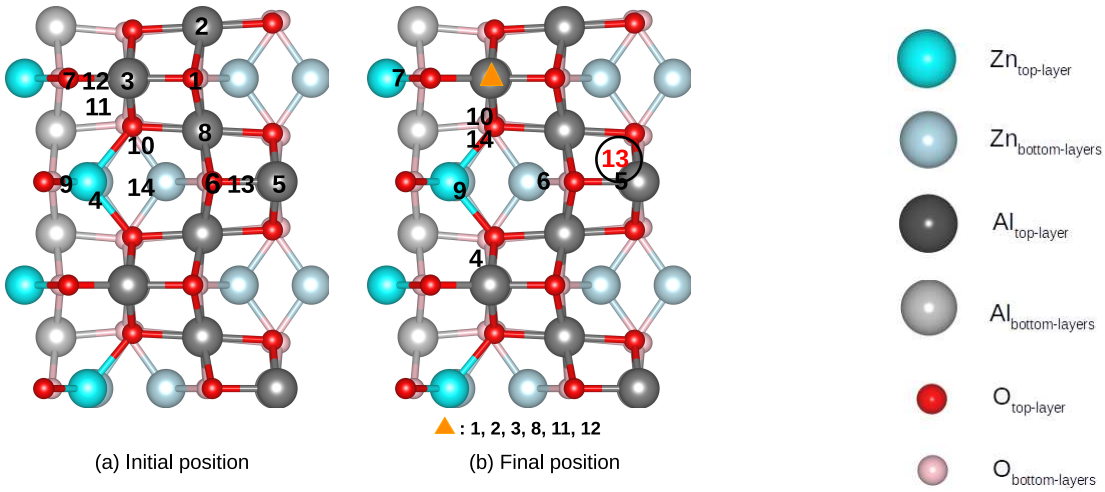

(a) Initial position (b) Final position

Figure 5.3: *(a) schematic representation of initial positions where MeOH is placed on (220) facet and (b) the positions where it adsorbed upon optimization. The numbers in black denote molecular adsorption, while dissociation is shown in red-coloured numbers enclosed in the black circle.*

We scanned all the unique sites of (220) surface by placing MeOH through O, like on top sites of Al and subsurface Zn, various bridge sites between Al-Al, Al-Zn, Al-O, Zn-O, as well as hollow positions. All these sites where MeOH was placed as starting configuration are shown schematically in Fig.5.3-(a), and the final positions of MeOH upon adsorption are shown in Fig.5.3-(b) Methanol prefers to adsorb through its oxygen atom at the metallic site (Zn or Al) at the (220) facet.

In most of the cases, MeOH adsorbs on surface Al in most cases as clear from Fig.5.3-(b). However, there are a few cases where it gets adsorbed on a bridge or at a hollow position. We report the interaction energies E_{int}, O-H bond length, C-O bond length, and shortest distance between metal and O_{MeOH} in Tab.5.1. Dissociation, chemisorption, and physisorption of methanol are shown in red, black, and blue colour respectively. It is evident from Tab.5.1 that the preferential adsorption site of methanol/methoxy adsorption is Al due to its higher affinity for oxygen as com-

Table 5.1: *Interaction energy (eV), O-H bond-length (Å), C-O bond-length (Å), and metal-O_{MeOH} bond-length (Å) with site of adsorption in parenthesis for various sites on $ZnAl_2O_4$ (220) facet. Initial positions are the sites where methanol is placed on the (220) facet as indicated in Fig.5.3-(a). Dissociation, chemisorption, and physisorption are shown in red, black, and blue color respectively.*

Initial positions	E_{int} (eV)	O-H BL (Å)	M-O_{MeOH} BL (Å)	H_{MeOH}-O_{surf} BL (Å)	
13	-1.80	1.72	1.85 (Al)	1.00	dissociation
14	-1.57	1.02	1.96 (Al)	1.66	
10	-1.56	1.02	1.96 (Al)	1.67	
4	-1.55	1.01	1.96 (Al)	1.74	
2	-1.37	1.00	1.92 (Al)	1.76	
12	-1.38	0.98	1.92 (Al)	2.12	chemisorption
8	-1.36	1.00	1.92 (Al)	1.75	
3	-1.36	0.99	1.91 (Al)	1.94	
5	-1.33	1.00	1.90 (Al)	1.79	
11	-1.33	1.00	1.90 (Al)	1.78	
1	-1.26	1.04	1.87 (Al)	1.52	
9	-0.66	1.01	3.62 (Zn)	1.64	
7	-0.61	1.01	3.99 (Zn)	1.69	physisorption
6	-0.50	0.99	4.02 (Al)	1.81	

pared to the Zn and less availability of Zn at the surface. Dissociation of O-H bond of MeOH is the thermodynamically most favourable outcome at the (220) facet. The sites of chemisorption are accompanied with short distance of M-O_{MeOH}, whereas for physisorption, the M-O_{MeOH} distance are considerably large (>3.6Å). However, the physisorption also leads to 3-4% activation in the O-H bond.

The representative cases of interaction of methanol with (220) facets are shown in Fig.5.4. It is clear from Fig.5.4 that irrespective of the outcome of MeOH, the O-H bond would orient itself such that the H_{MeOH} would face the nearest surface oxygen. This observation can also be realized by investigating the H_{OH}-O_{surf} distances in Tab.5.1. For the cases where O-H bond activation is not more than 4-5% (i.e. O-H bond length less than 1.02Å), the distance of O_{surf}-H_{OH} is in the range of 1.74Å to 2.12Å . Whereas the cases where the O-H bond activates by 7-9% (O-H bond length greater than 1.02Å), the distance between H_{OH}-O_{surf} reduces to 1.52Å- 1.67Å. The proximity of the surface oxygen atom and reorientation of the O-H bond explains the trends in bond activation of methanol over the surface. Physisorption is associated with methanol on the hollow sites, wherein the H_{MeOH} interacts with the nearby surface oxygen and shows bond activation;

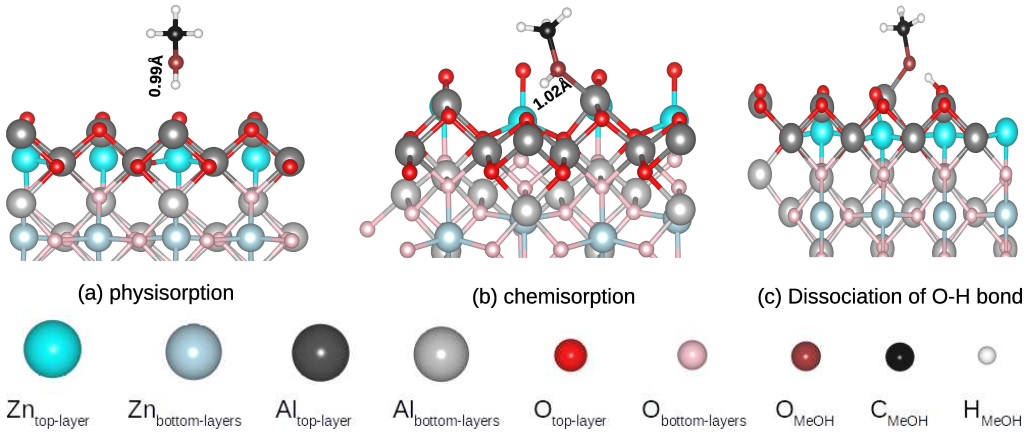

Figure 5.4: *(a) Representation cases of interaction of methanol with (220) facet of $ZnAl_2O_4$. (a) shows the physisorption of methanol on the surface. (b) shows the chemisorption of methanol with 4% elongation in the O-H bond of methanol. (c) shows the dissociation of methanol on the surface. The dissociated methoxy adsorbs at the Al site, and the hydrogen atom adsorbs at the surface oxygen atom.*

however, the O_{MeOH}-metal bond is substantially large. As clear from Tab.5.1, dissociation of the O-H bond of methanol takes place at 13^{th} position. The presence of surface oxygen in the methanol molecule's vicinity favours hydrogen abstraction from the MeOH. Similarly, the 11^{th} position also has the same Al site as that of 13^{th}, but the molecule is oriented in such a way that the H_{OH} is not in the vicinity of surface oxygen. Hence, only moderate activation of the O-H bond occurs, and no dissociation is observed. These observations also bring out an important point here that the rotation or migration of methanol on the (220) facet of $ZnAl_2O_4$ has a substantially high barrier which could not be overcome, which is precisely opposite to what we observed in the case of ZnO.

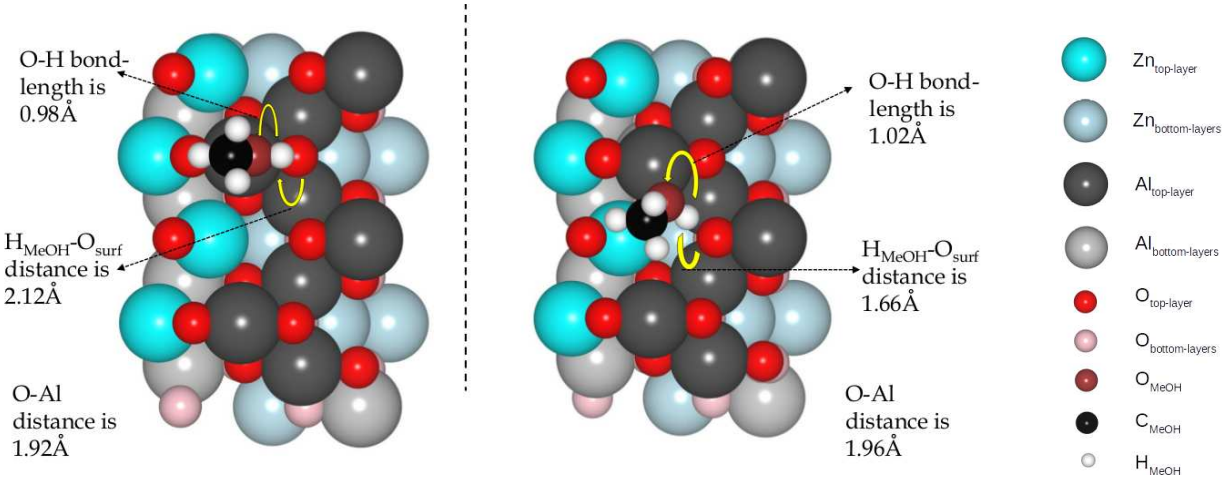

Figure 5.5: *MeOH is adsorbed at the same Al site with different molecule orientations. The O-H bond is barely activated at the 12^{th} position. In contrast, at the 14^{th} position, the O-H bond is moderately activated, bringing out the effect of orientation and hence the resulting MeOH surface interaction.*

Adsorption site and orientation of the molecule affect the interaction of methanol with the

surface. Although we have scanned various unique sites on the surface (taking symmetry into account), scanning all possible orientations of MeOH molecule wrt to a specific site is a formidable task and still needs to be achieved. However, to bring out the effect of 'change in orientation' on the adsorption of MeOH, we have investigated all the cases where the molecule was adsorbed on the surface, which includes cases like MeOH adsorbed at the same site but having different orientations. For example, in Fig.5.5 MeOH is placed at 12^{th} and 14^{th} position on (220) facet at a common adsorption site (refer Fig.5.3-(b)). The Al-O bond distance is nearly the same in both cases, as noted in Fig.5.5. However, the O-H bond activation is 0.98Å (barely activated) in the case of 12^{th} position whereas 1.02Å(moderately activated) in the case of 14^{th} position. And this can be directly understood if we look at the H_{MeOH}-O_{surf} distances. These interaction differences bring out the effect of the molecule's orientation on adsorption. Over the same adsorption site, it could change the surface environment experienced by atoms in the molecule, hence the resultant interaction and activation. A similar phenomenon applies to positions 8 and 3 as well.

It must be noted at this point that activating an adsorbate over any catalyst surface is a complex problem that depends upon a combination of multiple factors like the arrangement of atoms on the surface, the relative orientation of adsorbate, the number of unique sites on the surface to name a few. This picture becomes even more complex for a surface of mixed metal oxides like $ZnAl_2O_4$. The possibilities that are needed to be scanned exhaustively become manifold. Moreover, bringing out a one-to-one correlation between observed activation parameters becomes difficult. Nonetheless, our work illustrates how each parameter contributes to understanding methanol adsorption over $ZnAl_2O_4$. Overall, it is observed that (220) facet of $ZnAl_2O_4$ exhibits excellent catalytic activity towards an incoming methanol molecule. Al atoms on the surface offer activation of O-H bond in the range of 0.98Å to 1.04Å . Spontaneous dissociation of the O-H bond is also observed over the (220) facet of $ZnAl_2O_4$.

Interaction of MeOH with $ZnAl_2O_4$ (311) surface

Unlike (220), (311) is a stepped and highly asymmetric surface as shown in Fig.5.6, and also it has all three elements, viz. Al, Zn, and O on the surface. At (311) facet, MeOH prefers to adsorb through its oxygen atom pointing towards the surface. Because of the absence of symmetry and a step on this (311) facet, the number of adsorption sites increases compared to the (220) facet. All possible unique sites on the (311) surface, like the top, bridge, and hollow sites, are scanned to investigate the interaction of methanol at this surface. The initial and final configurations of methanol on the (311) facet is shown in Fig.5.7. The interaction energy for methanol with a bond length of O-H, O-C and metal-O has been reported in Tab.5.2. It is clear that the active site for methanol adsorption is both Al and Zn; however, Al is more favoured over Zn due to its strong

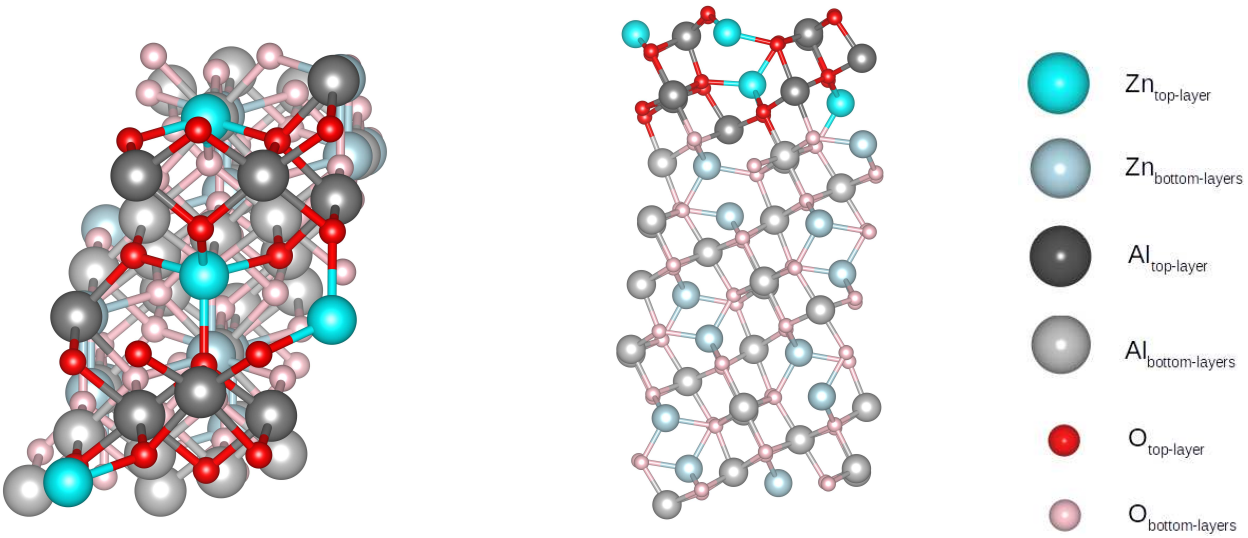

Figure 5.6: *The (311) surface of $ZnAl_2O_4$ with the top view and the side view. The topmost layer of (311) surface consist of all three Al, Zn, and O atoms.*

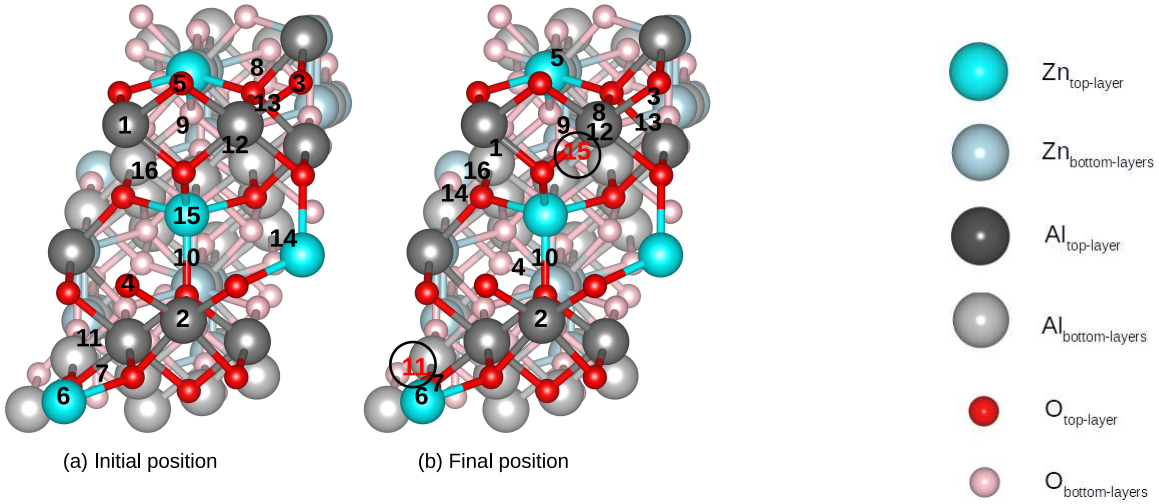

Figure 5.7: *(a) schematic representation of initial positions where MeOH is placed on (311) facet and (b) the positions where it adsorbed/dissociated after optimization. The numbers in black denote molecular adsorption, while dissociation is shown in red-coloured numbers enclosed in the black circle.*

affinity for oxygen. Also, the presence of Zn at the surface provides a more active site at the (311) facet, making it more active for methanol interaction.

At the (311) facet, we observed spontaneous dissociation of O-H and one of the C-H bonds of methanol to produce formaldehyde. Formaldehyde adsorbs at the Al site, and dissociated hydrogen atoms adsorb at surface oxygen to form hydroxyl at the surface as shown in Fig.5.8-(a). Due to the strong affinity of Al for oxygen, the produced formaldehyde does not desorb from the surface. The formation of formaldehyde is the thermodynamically most favourable product at this facet. Apart from formaldehyde, dissociation of the O-H bond to form methoxy is also observed at the

Table 5.2: *Interaction energy (eV), O-H bond-length (Å), C-O bond-length (Å), and metal-O_{MeOH} bond-length (Å) with site of adsorption in parenthesis for various sites on $ZnAl_2O_4$ (311) facet. Initial positions are the sites where methanol is placed on the (311) facet as indicated in Fig.5.7-(a). Dissociation, chemisorption, and physisorption are shown in red, black, and blue color respectively.*

Initial positions	E_{int} (eV)	O-H BL (Å)	M-O_{MeOH} BL (Å)	H_{MeOH}-O_{surf} BL (Å)	
15	-4.14	2.33	2.00 (Al)	0.98	
11	-1.68	1.69	1.97 (Zn)	1.00	Dissociation
16	-1.61	1.04	1.98 (Al)	1.58	
6	-1.46	1.03	2.02 (Zn)	1.58	
7	-1.38	1.10	2.01 (Zn)	1.36	
12	-1.26	0.98	2.02 (Al)	2.36	Chemisorption
8	-1.23	0.99	2.02 (Al)	2.00	
13	-1.16	0.98	2.04 (Al)	2.80	
1	-1.11	0.99	2.03 (Al)	1.96	
14	-0.95	1.02	3.14 (Al)	1.66	Physisorption
2	-0.91	1.03	2.13 (Al)	1.57	Chemisorption
10	-0.83	1.04	3.40 (Al)	1.54	
4	-0.72	1.02	3.74 (Al)	1.60	
9	-0.52	0.99	3.10 (Al)	1.83	Physisorption
5	-0.49	0.99	3.93 (Al)	1.82	
3	-0.48	0.99	3.53 (Al)	1.81	

(311) facet of $ZnAl_2O_4$. As shown in Fig.5.8-(b), upon dissociation, this methoxy group adsorbs at the Zn site, which does not favour further dehydrogenation of methoxy, which is reverse of what is observed at the Al site. The presence of active oxygen near the methanol molecule favours hydrogen abstraction from the methanol leading to the formation of methoxy. Depending upon the site of adsorption of dissociated fragments, further dehydrogenation is determined. It also indicates that Al is the site that would not desorb the products from its surface and favours further dehydrogenation. It is interesting to note here that, at this facet, the orientation of methanol also plays a role in the outcome of the molecule's interaction with the facet. For example, for 6^{th}, 7^{th}, and 11^{th} position, the methanol molecule is adsorbed at the same Zn site with different orientations, but they all result in different outcomes. At 11^{th} position, we observed spontaneous dissociation of the O-H bond to form methoxy, at 7^{th} position, more than 13% elongation of the O-H bond, while at 6^{th} position, only 6% activation of O-H bond of methanol occurs.

Along with dissociation, at various sites, molecular adsorption, i.e. physisorption and chemisorp-

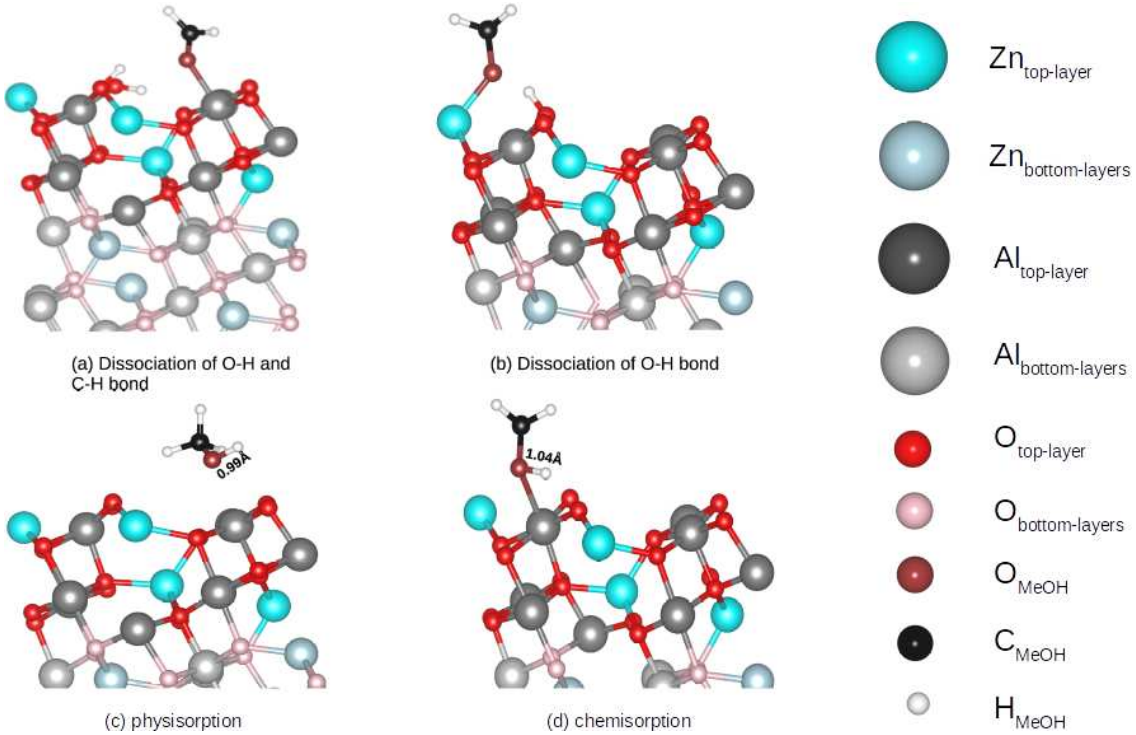

Figure 5.8: *(a) shows the dissociation of O-H and C-H bond of methanol on (311) facet. The formed formaldehyde adsorbs on the Al site of the surface due to the strong affinity of Al with oxygen. Dissociated hydrogens adsorb on the surface to form surface hydroxyl groups. (b) shows the dissociation of methanol to form methoxy on the (311) facet, which adsorb at the Zn site of the surface.(c) shows physisorption and (d) depicts chemisorption with 7% activation in the O-H bond.*

tion, are also observed on the (311) facet. Representative cases of physisorption and chemisorption are shown in Fig.5.8-(c) and (d), respectively. However, as clear from Tab.5.2, the energy difference between the dissociation of methanol to methoxy and molecular adsorption is only 0.07 eV which shows an equal probability of both outcomes at elevated temperatures. There are numerous factors on which the interaction of methanol molecules depends, like the environment of the surface, as experienced by methanol, the orientation of the molecule with respect to the surface, the stepped nature of the surface and the availability of surface oxygen in the vicinity of the molecule.

To understand the variation in interaction of MeOH with (220) and (311) facets, we have investigated the charge distribution, projected Density of States (pDOS) and atomic arrangement of the bare surfaces. We also report the differential Mulliken charges for surface atoms. On the bare (220) surface, four Al and eight O atoms exist on the surface, available for interaction with incoming methanol. All Al atoms on the surface are equivalent in the environment and charge distribution and have an effective positive charge of 1.67e. Every Al atom is surrounded by four O atoms, one Zn atom and three other Al atoms. Interestingly two types of oxygen atoms exist on the surface. Four oxygen atoms on the surface are coordinated with three Al atoms, while the remaining four are

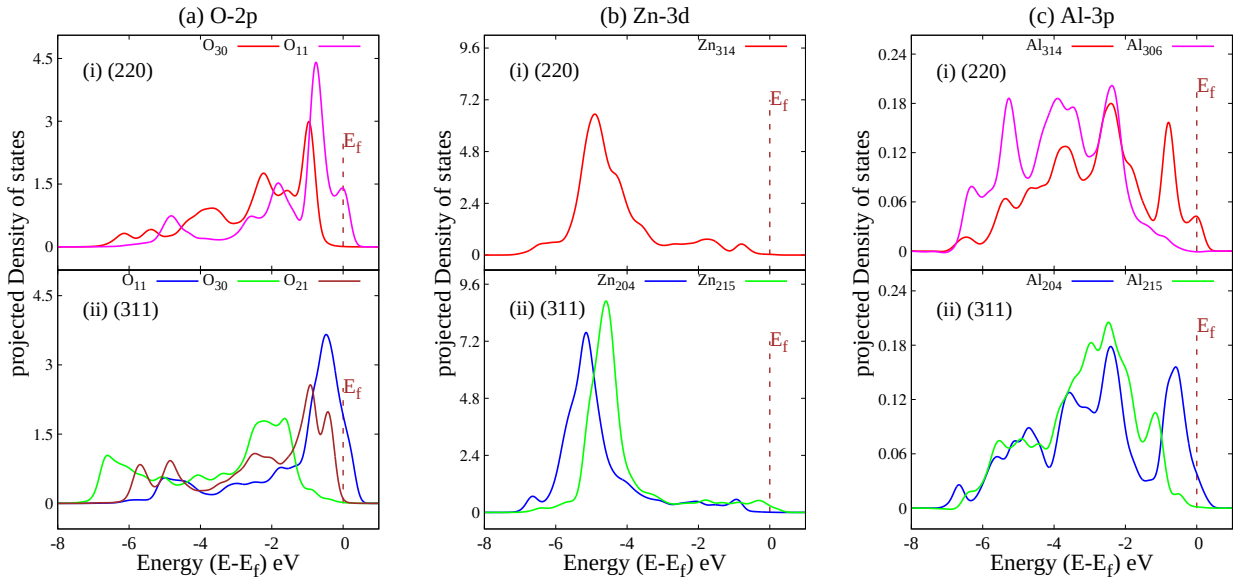

Figure 5.9: *(a) shows the pDOS of 2p orbitals of surface oxygen on (i) 220 and (ii) 311 facets. There are different types of oxygen atoms present on the surface, which have variations in their neighbouring environment. (b) represents the pDOS of 3d of Zn in (i) 220 and (ii) 311 facet. 3d of Zn lies much below Fermi due to a filled orbital. (c) shows the pDOS of 3p of Al in (i) 220 and (ii) 311 facet. Al is the active site of adsorption in both facets and has significant peaks near/at Fermi.*

coordinated with one surface Al atom and one subsurface Zn atom. The oxygens connected with three Al atoms have a higher negative charge, -1.07e. While the ones connected with one Zn and one Al have a negative charge of -1.03e. Thus, though Zn is not exposed on the surface, its coordination with surface oxygen changes the nature of the oxygen atom on the surface. This difference in the surface oxygen can be seen in the corresponding pDOS plots, as shown in Fig.5.9-(a). We denote the coordination of O atoms with Al and Zn atoms as O_{xy}, wherein x and y are the numbers of Al and Zn atoms coordinated with O, respectively. Thus, O_{30} represents an oxygen coordinated with 3 Al and 0 Zn whereas O_{11} represents oxygen coordinated with one Al and one Zn. As shown in Fig.5.9-(a)-(i), on (220) surface, the pDOS plots clearly show a shift in the peaks of the more coordinated oxygen atom (O_{30}) with slightly more negative charge away from the Fermi energy in comparison with the other oxygen, (O_{11}) that is coordinated with lesser number of atoms on the surface. A lesser coordinated O atom is observed to be lesser negative. The presence of different kinds of atoms with varying charge distribution on the surface is desirable as it offers more adsorption sites with varying strengths. On the (311) surface, there are three types of O atoms. The difference in the pDOS signatures can be observed for these O atoms as shown in Fig.5.9-(a)-(ii). The most coordinated, i.e. coordinated with two Al and one Zn atom (O_{21}) shows the maximum shift away from the Fermi energy. The other two oxygen atoms also follow the coordination trends wherein the least coordinated O_{11} is the closest to the Fermi energy, followed by O_{30}. Further, two

kinds of Zn atoms are present on the (311) surface. One is coordinated with 3 oxygen atoms, and the other, Zn, is coordinated with 4 oxygen atoms. These surface Zn atoms act as sites that dissociate the O-H bond of methanol and act as favourable sites for methanol adsorption. These pDOS of Zn atoms in (220) and (311) are shown in Fig.5.9-(b). Zn, being the last transition metal, have a fully filed orbital, and so its peaks are far away from Fermi; however, for (311), one of the Zn has non-zero peaks at Fermi, which explains the dissociation of methanol on the Zn site on (311) facet as discussed above. On both the (220) and (311) facets, two types of Al atoms are present as reflected in their pDOS in Fig.5.9-(c). Both these facets have one type of Al atom, which has a non-zero peak at Fermi, explaining Al being the active site for the dissociation of methanol. All these observations clearly show that not only the active site but the overall surface geometry plays a role in changing the chemical signatures of an atom on the surface.

5.4 Conclusions

Though the adsorption of MeOH is extensively studied on varied classes of catalysts, reports of significantly low activation barrier or spontaneous dissociation of O-H as well as C-H bonds of MeOH are minimal. Therefore, this work on proposed mixed metal oxide as a catalyst becomes even more interesting. It is also interesting to note that the proposed mixed metal oxide is a derivative of two commonly used industrial catalysts, Al_2O_3 and ZnO towards MeOH synthesis. In this work, we illustrate (220) and (311) facets of $ZnAl_2O_4$ as excellent candidates for MeOH activation. These two surfaces offer significant O-H bond activation and exhibit one case each of O-H bond dissociation. The dissociation observed in our studies is crucial as they are spontaneous. Moreover, the (311) surface undergoes subsequent dissociation of one of the C-H bonds. To understand the factors that influence O-H bond activation/dissociation over any catalyst surface, we dwelled deeper into systematically correlating the observed parameters. The availability of surface oxygen in the vicinity of adsorbing methanol is of prime importance. Hence, a surface rich with oxygen atoms of varying charges is desirable for multiple bond activations or dissociation. The atomic arrangement of atoms on the surface turned out to be another essential factor in understanding the adsorption energy trends. The coordination of surface atoms and hence the availability of sites with variation in charges on the surface unravel the trends in bond activations. Lastly, we propose that the (311) surface offers better catalytic activity than (220) due to its stepped geometry and availability of inequivalent adsorption sites for interaction with an incoming MeOH. Through detailed analysis of various factors that govern MeOH activation over these surfaces, we unleash a new chemical space to explore in this direction. Also, the produced formaldehyde on the Al site does not desorb, indicating that Al favours further dehydrogenation; hence, Zn-based material with such active oxygen could be used for methanol to formaldehyde formation.

Chapter 6

Methanol to formaldehyde on ZnO: From computation to experimentation

6.1 Motivation

Aldehydes are industrially important chemicals due to their wide range of applications. Formaldehyde, the simplest aliphatic aldehyde, is of particular interest due to its diverse applications in various fields such as construction, automotive, aviation, pharmaceuticals, and cosmetics.[154] Formaldehyde is an important raw material widely used for synthesizing resins, 1,4-butylene glycol, polyformaldehyde, and pesticides. In recent years, the annual demand for formaldehyde has exceeded 30 megatons.[155] Methanol is the major source of production of formaldehyde. Every year more than 30% of methanol is used for this.[156] Methanol can be converted to formaldehyde by either dehydrogenation process ($CH_3OH \rightarrow CH_2O + H_2$), which is endothermic in nature or by partial oxidation ($CH_3OH + 1/2\ O2 \rightarrow CH_2O + H_2O$), which is an exothermic process. Industrially two catalysts are used for the production of formaldehyde from methanol. In the presence of a silver catalyst, methanol and air mixture are subjected to 600^{o}C for formaldehyde production.[157] Another is iron-molybdenum oxides which work at a relatively lower temperature of 250-400^{o}C.[158] Major limitations of these catalysts are high operational temperature and instability of catalysts at such conditions. Furthermore, there is an acute need to develop a catalyst for the partial oxidation of methanol to formaldehyde which could be operated at low temperatures. Various catalysts based on noble metals, viz. Pt,[159–162] Pd[163,164] have been explored for MeOH oxidation to HCHO, which demonstrate better catalytic activity. In the latest study, Selivanova et al. investigated the mechanism of partial oxidation of methanol on Pt(111) single crystal using X-ray photoelectron spectroscopy (XPS) and polarization-modulation infrared reflection absorption spectroscopy.[162] They observed that the methanol oxidation reaction proceeds with five routes. CO_2, formaldehyde, and methyl formate are the major gas phase products. The reaction starts with breaking the

O-H bond, followed by sequential hydrogen abstraction from the intermediates. Marcinkowski et al., in a combined experiment and theoretical study, examined the Pd single-atom catalyst(SAC) on Fe_2O_3(0001) for partial oxidation of methanol to formaldehyde.[163] They observed that the activation barrier for methanol partial oxidation to formaldehyde reduces to half when Pd SAC is placed on Fe_2O_3 compared to bare Fe_2O_3 surface. Though the formaldehyde desorption was observed at 290K, sintering of Pd takes place at 300K, and hence the yield of formaldehyde reduces greatly. Thus it is observed that the high cost of noble metals and the stability of SAC are the major challenges associated with these noble atom surfaces.

Metal oxides show better catalytic activity due to different sites at the surface. In an experimental study, Wong et al. studied the reaction of methanol on clean TiO_2 (110) and vanadia supported on TiO_2 using temperature-programmed desorption (TPD) and high-resolution electron energy loss spectroscopy (HREELS).[165] Monolayer and submonolayer vanadia films supported on TiO_2(110) in which vanadium cations are in +3 oxidation state are active for the oxidation of methanol to formaldehyde at a temperature higher than 600K. However clean TiO_2(110) and multilayer vanadia films supported on TiO_2(110) are relatively inactive. Similarly, Feng and Vohs carried out a TPD study of the partial oxidation of methanol to formaldehyde on CeO_2 supported vanadium oxide.[166] They observed that during MeOH TPD, formaldehyde was produced at 525, 550, and 610K, on V^{5+}, V^{4+}, and V^{3+} respectively. Furthermore, they concluded that the activation energy for the dehydrogenation of adsorbed methoxides is a function of the oxidation state of the vanadium in the supported layer. Deng et al. compared the activation of methanol on the ZnO(0001) bilayer and bilayer-trilayer step supported on the Au (111) surface using temperature-programmed reaction spectroscopy (TPRS) and DFT study.[67] They observed that the ZnO bilayer is inactive towards the oxidation of methanol and molecular desorption occurs at 220 and 260K in TPRS. Whereas at ZnO bilayer-trilayer, molecular desorption of methanol takes place at 380K and formaldehyde desorption occurs at 580K in TPRS. The activation barrier calculated by the minimum energy pathway with DFT is 19.0 kcal/mol for the ZnO bilayer-trilayer.

ZnO has been studied for methanol oxidation to formaldehyde at high temperatures, but none of the studies reports a reaction at ambient conditions. This chapter discusses the spontaneous conversion of methanol to formaldehyde at the ZnO $(10\bar{1}1)$ facet. Our DFT based investigation of interaction of MeOH with various ZnO facets predicted conversion of MeOH to formaldehyde on ZnO $(10\bar{1}1)$ facet. We have validated our predictions by conducting appropriate experiments. The chapter is organized as follows. In section 6.2, we discuss the computational details and experimental methods used for the current work. In section 6.3 we discuss the theoretical and experimental results of the interaction of methanol with ZnO followed by conclusion in section 6.4.

6.2 Methodology

6.2.1 Computational details

All the calculations were carried out within the Kohn-Sham formalism of density functional theory. Projector Augmented Wave potential[110] was used, with Perdew-Burke-Ernzerhof (PBE) approximation for the exchange-correlation and generalized gradient approximation,[112] as implemented in plane-wave, pseudopotential-based code, Vienna Ab initio Simulation Package (*VASP*).[113] The bulk unit cell was taken from the materials project.[81] The bulk lattice parameters upon optimization were a = 3.28Å and c = 5.30Å which were in excellent agreement with the experimentally measured (a = 3.24Å, c = 5.20Å) lattice parameters.[140,141] The flat facet, $(10\bar{1}1)$ of ZnO, was modelled as a slab by cleaving a surface with 3x3 periodicity in the x and y direction with four layers using Quantumwise-VNL-2017.1.[84] Bottom one layer was fixed, and all the remaining layers and adsorbate were allowed to relax for all the surface calculations. Van der Waals corrections were applied to account for dynamic correlations between fluctuating charge distribution by employing the Grimme method (DFT-D2).[117] It was observed that 20 Å of vacuum was sufficient to avoid interaction between adjacent images of planes along the z-direction. Geometry optimization was carried out with a force cutoff of 0.01 eV/Å on the unfixed atoms, and the total energies converged below 10^{-4} eV for each SCF cycle. A Monkhorst-Pack grid of 3x2x1 for $(10\bar{1}1)$ slabs is used. The energy difference is less than 4meV/atom upon using finer mesh. The entire surface was scanned by placing the MeOH molecule at all available unique sites. The interaction energy is calculated using the formula: $E_{int} = E_{system} - (E_{surface} + E_{molecule})$ where E_{system} is the energy of the system when MeOH was placed on the surface, $E_{surface}$ is the energy of the bare surface and $E_{molecule}$ is the energy of the MeOH molecule. To understand the underlying electronic structure total Density of States (*tDOS*) was calculated with denser k-mesh using LOBSTER.[118]

6.2.2 Experimental methods:

Materials:

All the reagents, such as zinc acetate, sodium hydroxide, methanol, and ethanol of AR-grade quality, were procured from Molychem India, and Thomas Baker Chemicals, India and used as such without further purification.

Preparation of ZnO nanoparticles:

The ZnO nanoparticles were synthesized using the precipitation method.[167] 20 mL of an aqueous solution of 6 mmol $(CH_3COO)_2Zn.2H_2O$ was added to a beaker. Further, 10 mL of 20 mmol

NaOH was added dropwise to the aqueous zinc acetate solution and stirred. Then, the produced precipitate was kept at 70^{o}C for 15 h. The prepared catalyst was cooled at room temperature, filtered and followed by rinsing with a mixture of H_2O:C_2H_5–OH (70:30) and dried at 70^{o}C for 10 h before using it in the experiments.

Catalysts characterization:

X-ray diffraction analysis:

The prepared catalyst was characterized by the X-ray diffraction method using PAN analytical X$^{"}$Pert Pro Dual Goniometer diffractometer. The diffractometer consists of X$^{'}$celerator solid-state detector with CuKα (λ = 1.5406Å, 40kV, 30mA) radiation and a Ni filter. The X-ray diffraction pattern of the sample was collected in the range of 2θ = 20-80^o with a step size of 0.02^o and a scan rate of 4^{o}min^{-1}.

Electron microscopy:

The catalyst morphology was determined using scanning electron microscopy (SEM) on an FEI quanta 200 3D dual beam ESEM instrument with a thermionic emission tungsten filament in the 3 nm range at 30 kV.

Catalytic activity:

The catalytic oxidation of methanol to formaldehyde was carried out in a 5 ml glass vial at room temperature. 2 g methanol and 25 wt% catalysts were added into the vial. After addition, the vial was closed, and the reaction mixture was stirred for 1h.

Fourier transform infrared spectroscopic studies (FTIR):

FTIR spectra of the reaction mixtures were recorded on a Thermo Nicolet Nexus 670 IR instrument using a DTGS detector to analyze the products formed due to methanol oxidation. KBr pellet method was used to prepare samples with a resolution of 4 cm^{-1} in the range of 4000-400 cm^{-1} averaged over 100 scans.

High-performance liquid chromatography (HPLC):

High-performance liquid chromatography (HPLC, Agilent technologies, modal 1250 infinity) was

used to analyze the liquid samples to identify the products. HPLC equipped with an RI detector (at 40 ^{o}C) and H^+ Aminex column (305 × 7.8 mm^2) fitted with a guard column in series was used. The mobile phase used was 0.05M H_2SO_4 at a flow rate of 0.6 mL/min while maintaining the column temperature at 60^{o}C. Quantitative analysis of the products was carried out with that of the reference samples with known concentrations.

6.3 Results and discussion

6.3.1 Theoretical results

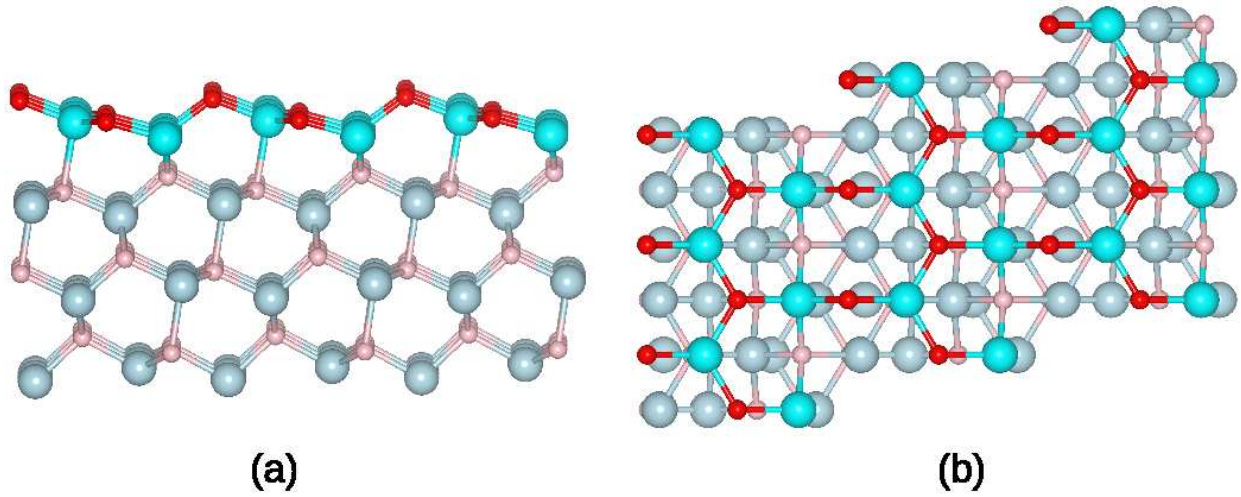

Figure 6.1: *Structural geometry of (10$\bar{1}$1) facet of ZnO. (a) shows the side view. (b) shows the top view.*

Computational studies are pivotal for the rational designing of catalysts and understanding their interaction with adsorbates. Theoretical studies provide evidence for the behaviour of different facets of a material with the interacting adsorbate. Methanol decomposition is of immense importance due to its application in DMFC and the generation of H_2. A more effective catalyst should be capable of breaking the bonds in methanol, allowing further reactivity of the intermediates and eliminating the products. In the previous chapter, we discussed the interaction of methanol with different ZnO surfaces. We observed spontaneous dissociation of methanol on flat (10$\bar{1}$0) and stepped (10$\bar{1}$3), (11$\bar{2}$2) facets of ZnO. Also, on a few sites on (10$\bar{1}$0) and (10$\bar{1}$3) facets, the C-H bond elongates by 6-7%. We also provide a rationale for methanol decomposition at any specific facet by investigating the underlying electronic structure. Apart from all the facets investigated in our previous study, the most dominant peak in ZnO nanoparticle is (10$\bar{1}$1) (as evident from Fig.6.8), which signifies that this facet is greatly exposed and more likely to participate in the reaction with MeOH. This motivated us to investigate the (10$\bar{1}$1) facet in great detail for interaction with methanol. For

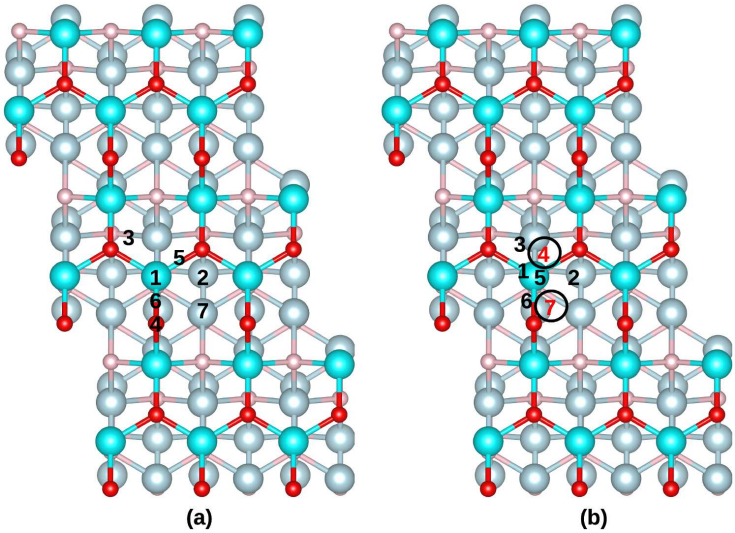

Figure 6.2: *(a) schematic representation of initial positions where MeOH is placed on (10$\bar{1}$1) facet and (b) the positions where it adsorbed/dissociated after optimization. The numbers in black denote molecular adsorption, while dissociation is shown in red-coloured numbers enclosed in the black circle.*

Table 6.1: *Interaction energy (eV), O-H bond-length (Å), C-O bond-length (Å), and Zn-O$_{MeOH}$ bond-length (Å) for various sites on ZnO (10$\bar{1}$1) facet. All these positions are indicated in Fig.6.2-(b). Dissociation is indicated in red colour, while molecular adsorption is shown in black colour.*

Positions	E$_{int}$ (eV)	O-H BL (Å)	C-O BL (Å)	Zn-O$_{MeOH}$ BL (Å)
4	-7.95	3.23	1.23	3.34
1	-4.44	0.98	1.45	2.30
5	-3.17	0.98	1.45	2.27
7	-2.66	1.65	1.41	2.03
3	-1.82	0.98	1.43	2.57
6	-1.75	0.99	1.42	3.55
2	-1.66	0.98	1.42	3.73

this facet, Zn atoms in the bulk layer are coordinated to four oxygen atoms, while the Zn atoms in the surface layers are only coordinated to three oxygen atoms. The top and side view of the (10$\bar{1}$1) facet is shown in Fig.6.1.

Methanol was placed at various unique sites on the facet, viz. on top of Zn, bridge of two Zn, bridge of Zn and O, bridge of two O, etc. All the sites where MeOH was placed are shown schematically in Fig.6.2. The numbers in Fig.6.2-(a) represent the initial positions where MeOH was placed, and the final position of adsorbed methanol or dissociated methoxy group are shown in Fig.6.2-(b). The black numbers indicate molecular adsorption, while the red numbers denote the dissociation of methanol. The interaction energy of MeOH adsorption, O-H bond length, C-O

bond-length, Zn-O_{MeOH} are reported in Tab.6.1.

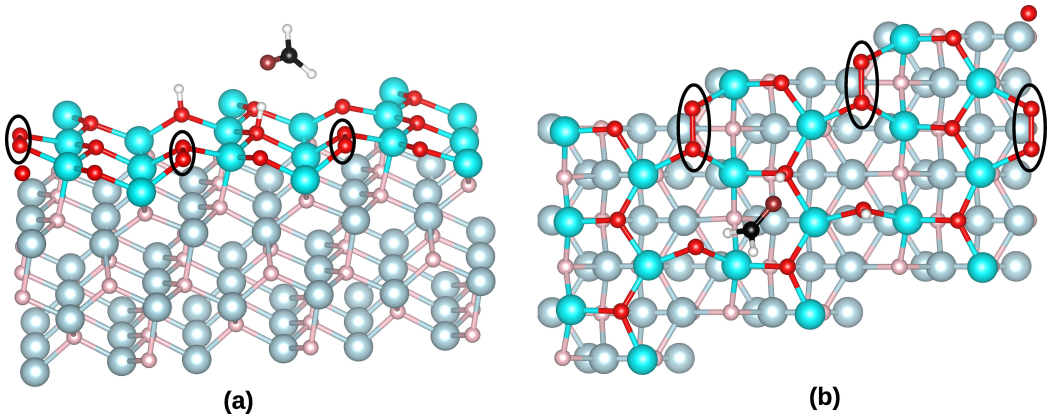

Figure 6.3: *Methanol decomposes to formaldehyde at ZnO (10$\bar{1}$1) facet. (a) depicts the side view, and (b) shows the top view of the slab with formaldehyde formed. The dissociated H atoms adsorb at two O_{surf} atoms. O-O dimers are formed at the ZnO surface.*

We observed the spontaneous decomposition of methanol to formaldehyde at (10$\bar{1}$1) of ZnO. This is thermodynamically the most favourable outcome of the interaction of methanol at this facet, as shown in Tab.6.1. However, as seen from Tab.6.1, the formation of other products from MeOH is very unlikely because of the substantial energy difference (>3.50 eV) for formaldehyde formation and other outcomes. The C-O and C-H bond lengths of the produced formaldehyde were 1.23 Åand 1.11Å, respectively, similar to the bond lengths in isolated formaldehyde molecules (C-O = 1.22 Å; C-H = 1.10 Å). We also computed the vibrational frequency of this produced formaldehyde. The C-O bond vibration frequency was 1713.23 cm^{-1}, which is comparable to that of an isolated formaldehyde molecule (1778.97 cm^{-1}). The vibrational frequency analysis is the evidence for forming formaldehyde on the ZnO surface. The dissociated hydrogen atoms adsorbed at two different surface oxygen atoms as shown in Fig.6.3. Interestingly, surface reconstruction occurred upon the decomposition of methanol which leads to the formation of O-O dimer on the surface as shown in black circles in Fig.6.3. Bond-length of these newly formed O-O dimers vary between 1.43-1.45 Åand are comparable to O-O bond-length in peroxides.

Also, apart from formaldehyde formation, methanol either physisorbs, chemisorbs or dissociates on the surface as shown in Fig.6.4. In the case of physisorption (Fig.6.4-(a)), MeOH is adsorbed at the surface with minimal elongation in O-H bond length (0.98Å). For chemisorption, MeOH adsorbs via its O atom at the surface Zn atom with an O-H bond elongated up to 0.99Å(represented in Fig.6.4-(b)). MeOH dissociates on the surface with methoxy and hydrogen adsorbed at the surface Zn and O atom, respectively (refer Fig.6.4-(c)).

We have also increased the concentration by absorbing two MeOH molecules simultaneously. Both MeOH molecules convert to formaldehydes as shown in Fig.6.5. Here also, O-O dimers form on the surface, which is marked in black. In chapter 4, we discussed the interaction of methanol

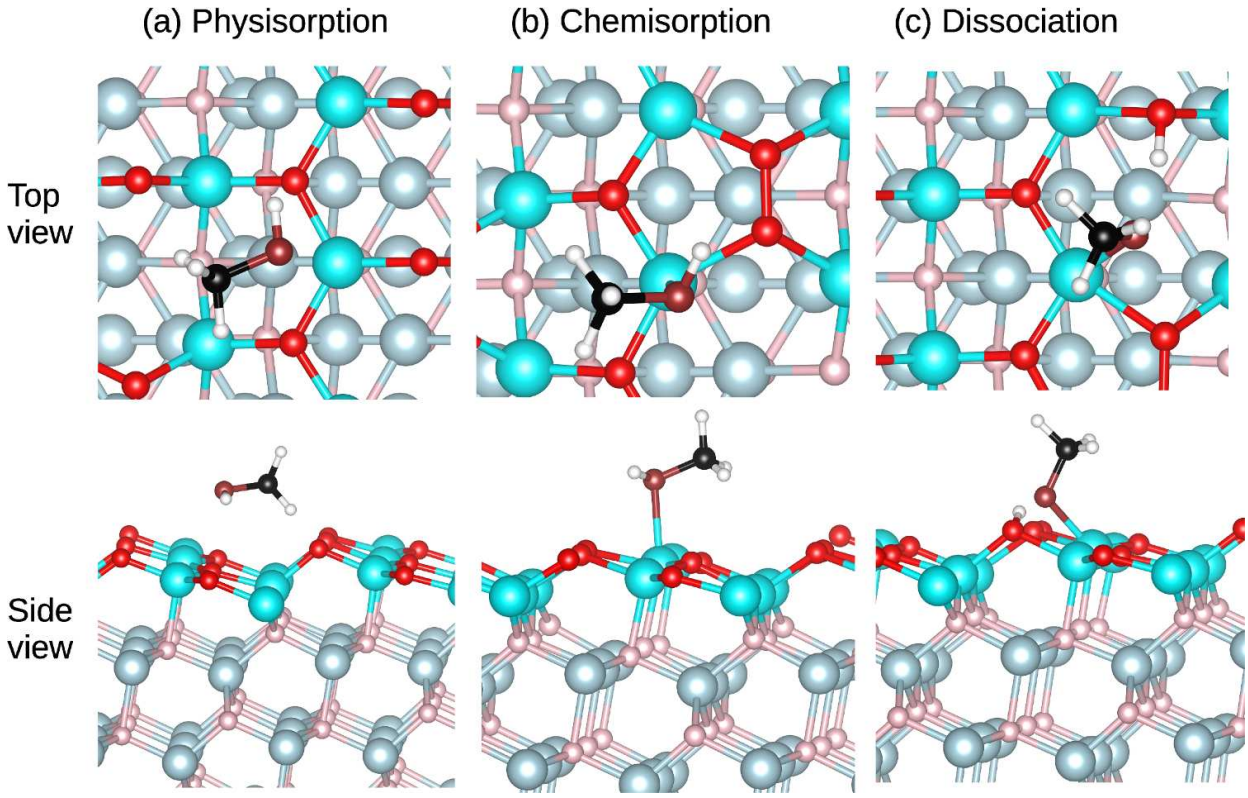

Figure 6.4: *Methanol adsorbed at ZnO (10$\bar{1}$1) facet. (a) represents physisorption of MeOH at the ZnO (10$\bar{1}$1) surface. (b) shows the chemisorption of methanol at the ZnO surface. (c) shows the dissociation of methanol at the ZnO facet. The methoxy group adsorbs at the Zn site while the H adsorbs at O_{surf} site.*

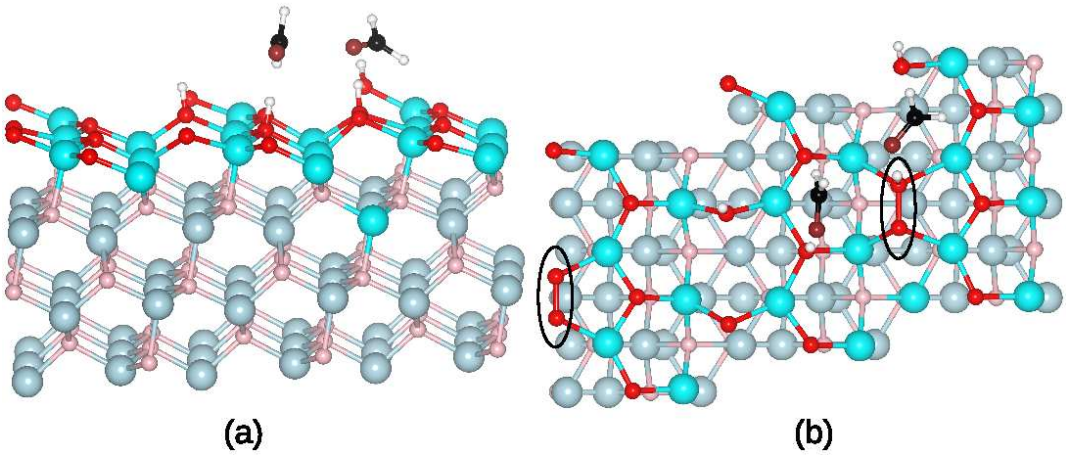

Figure 6.5: *When 2 molecules of methanol are placed at (10$\bar{1}$1) facet. Both of them convert to formaldehyde and desorb from the surface. (a) shows the side view of 2 formaldehyde formed on the surface. (b) shows the top view of the slab. Here also, O-O dimers formed on the surface marked in black circles.*

with four different facets of ZnO. We have explained in detail why a particular facet of ZnO favours the dissociation of methanol by analyzing the underlying electronic structure of this facet. We

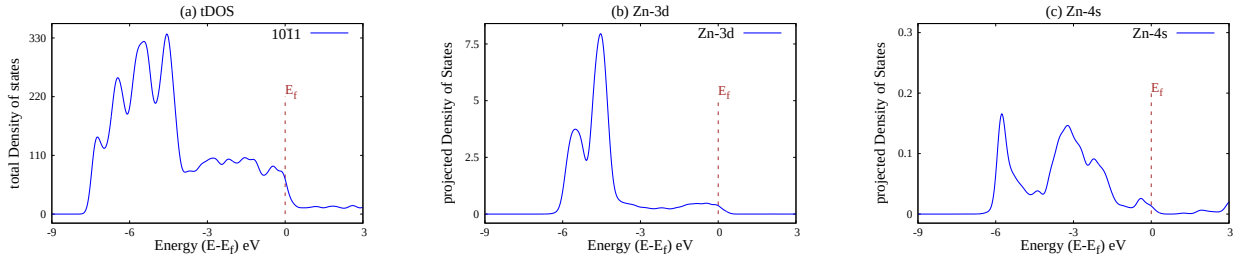

Figure 6.6: *(a) tDOS of (10$\bar{1}$1) facet. There are energy states present at the Fermi level. (b) shows Zn-3d orbitals of the facet. (c) shows Zn-4s orbitals of the facet. For both the orbitals, the energy states are available at the Fermi level.*

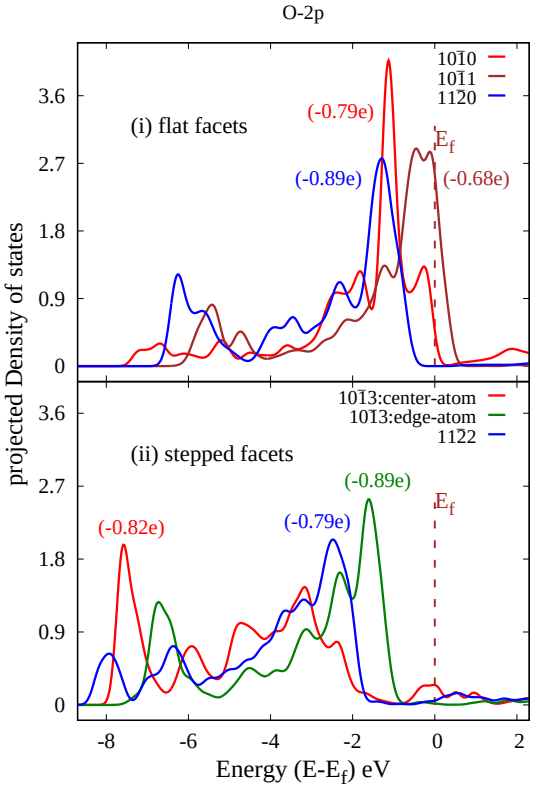

Figure 6.7: *pDOS of 2p of oxygen on all the facets of ZnO investigated in previous and current work (10$\bar{1}$1). It is evident from the plot that oxygen of (10$\bar{1}$1) facet has empty states above the Fermi level. It signifies the unsaturation of oxygen on this facet and their easy availability for abstracting two hydrogens from MeOH.*

report that the availability of non-zero energy states near the Fermi level enhances the reactivity of a facet. Moreover, at stepped facets, dissociation of MeOH was thermodynamically the most stable outcome compared to flat facets, where molecular adsorption was the most favourable. Following our understanding, in the present work, non-zero energy states are available at the Fermi level, enhancing the reactivity of the (10$\bar{1}$1) facet. Fig.6.6 shows the density of states plot for the (10$\bar{1}$)

facet. The tDOS plot is shown in Fig.6.6-(a), where the non-zero energy states are present at the Fermi level. Similarly, Fig.6.6-(b) and (c) show the projected density of states of 3*d* and 4*s* of Zn atom of the surface layer with non-zero energy states at Fermi level. We also compared the nature of oxygen on the surface in all the facets of ZnO investigated in this thesis. We also plotted *pDOS* of 2*p* of oxygen on all facets as shown in Fig.6.7. It is evident from the *pDOS* plot that 2*p* peak of oxygen of $(10\bar{1}1)$ has energy states available at Fermi and after Fermi level, which indicates the presence of empty states.

The formation of formaldehyde at ZnO is particular to this facet. As discussed in chapter 5, Al is the active site in $ZnAl_2O_4$ facet for dissociation of methanol; however, due to its strong affinity with oxygen, the desorption of formaldehyde is not favourable. Zn is the active site where methanol dissociates to formaldehyde in the presence of active oxygen species with desorption of formaldehyde, indicating this as an optimum catalyst that would adsorb not only the reactant but also favour desorption of the product. Taking insights from our theoretical results, we designed an experiment to study the interaction of methanol at ZnO. The following section will discuss the experimental results to validate our predictions.

6.3.2 Experimental results

Catalyst characterization

XRD analysis:

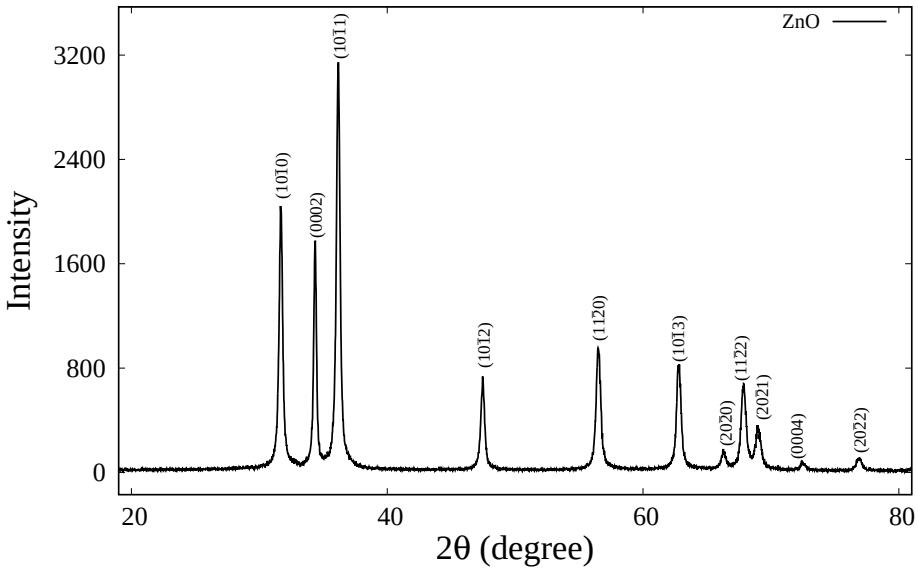

Figure 6.8: *XRD pattern of as-synthesized ZnO. The most prominent peak is $(10\bar{1}1)$.*

The ZnO nanoparticles are prepared by the precipitation method. The XRD pattern for ZnO shows sharp peaks and is shown in Fig.6.8. The sharpness of XRD peaks is ascribed to the synthesized material consisting of nano-scale particles. Sharp peaks at 31.73^o, 34.45^o, 36.16^o, 47.45^o, 56.49^o, 62.84^o, 66.35^o, 68.1^o, 69.2^o, 72.05^o, and 77.13^o corresponding to the following lattice planes (hkl) of wurtzite polycrystalline structure of ZnO are $(10\bar{1}0)$, (0002), $(10\bar{1}1)$, $(10\bar{1}2)$, $(11\bar{2}0)$, $(10\bar{1}3)$, $(20\bar{2}0)$, $(11\bar{2}2)$, $(20\bar{2}1)$, (0004), and $(20\bar{2}2)$, respectively (JCPDS card No. 36-1451). The spectrum does not contain any characteristic peak except ZnO peaks, which corroborates towards purity of the synthesized material. $D = 0.89\lambda / \beta \cos\theta$ where 0.89 is Scherrer's constant, λ is the wavelength of X-rays, θ is Bragg's diffraction angle, and β is the full width at half-maximum (FWHM) of the diffraction peak corresponding to the plane. The calculated particle size is found to be 22 nm, by considering the FWHM of an intense peak located at 36.16^o which attributed to $(10\bar{1}1)$ plane.

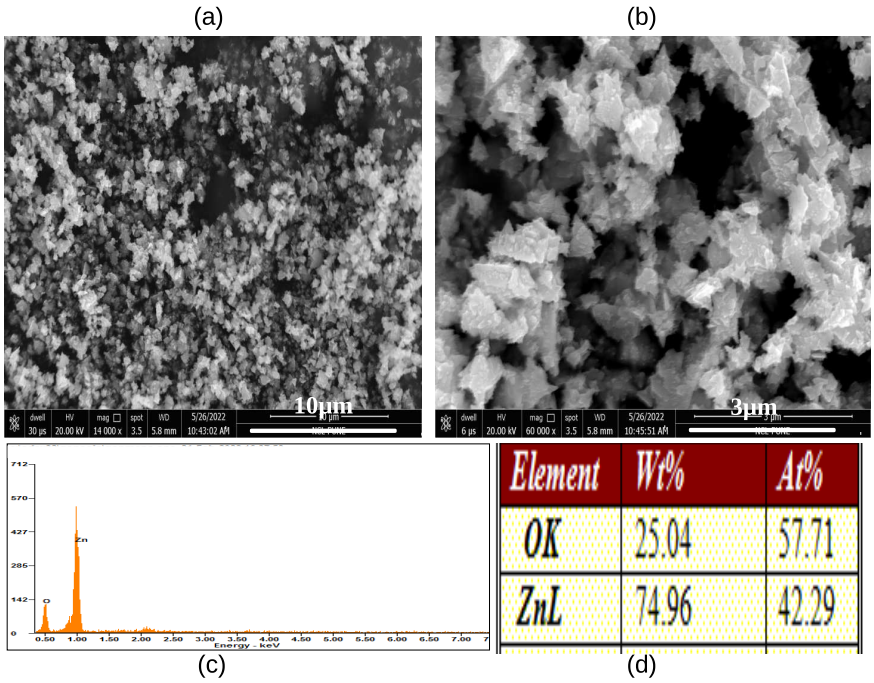

Figure 6.9: *SEM images of ZnO nanoparticles at (a) 10 µm and (b) 3 µm resolution. The image shows irregular and triangular shaped ZnO nanoparticles. (c) and (d) shows EDX analysis of ZnO nanoparticles.*

Scanning electron microscopy (SEM) analysis:

SEM and energy dispersive X-ray (EDX) analysis are carried out to understand the morphology and elemental composition of synthesized ZnO nanoparticles. The SEM images of synthesized ZnO nanoparticles are recorded at 10μm and 3μm resolution, as shown in Fig.6.9-(a) and Fig.6.9-

(b) respectively. The ZnO nanoparticles are found to be irregular in size and triangular-shaped, which is in line with the previous literature.[168] We also observed the formation of clusters in the nanoparticles due to the agglomeration of atoms. EDX analysis represents zinc (74.96%) and oxygen (25.04%) elements. This attributes to the absence of impurity in the synthesized ZnO nanoparticles.

Catalytic activity:

To investigate the interaction of methanol with ZnO nanoparticles, we performed the reaction at ambient conditions (i.e. RT and atmospheric pressure). The reaction mixture is analyzed after an hour using FTIR and HPLC. Our theoretical results show the formation of formaldehyde as a product of MeOH interaction with ZnO. And hence we have compared our reaction mixture with standard formaldehyde in both FTIR and HPLC.(considering our expected outcome as formaldehyde)

FTIR analysis:

To analyze the products formed, we recorded the FTIR spectra of reaction mixtures at 0 min. (after the addition of catalyst in methanol) and 1 h. We have compared this data with pure methanol and formaldehyde spectrum. The FTIR spectra of standard methanol, standard formaldehyde, and reaction mixture at 0 min and 1 h are shown in Fig.6.10. IR spectra of pure methanol show various vibrational peaks such as bending vibrations of Me-O-H at 1447 cm^{-1}, stretching vibrations of Me-O-H at 3338 cm^{-1}, stretching vibration of C-O at 1020-1112 cm^{-1} and stretching vibra-

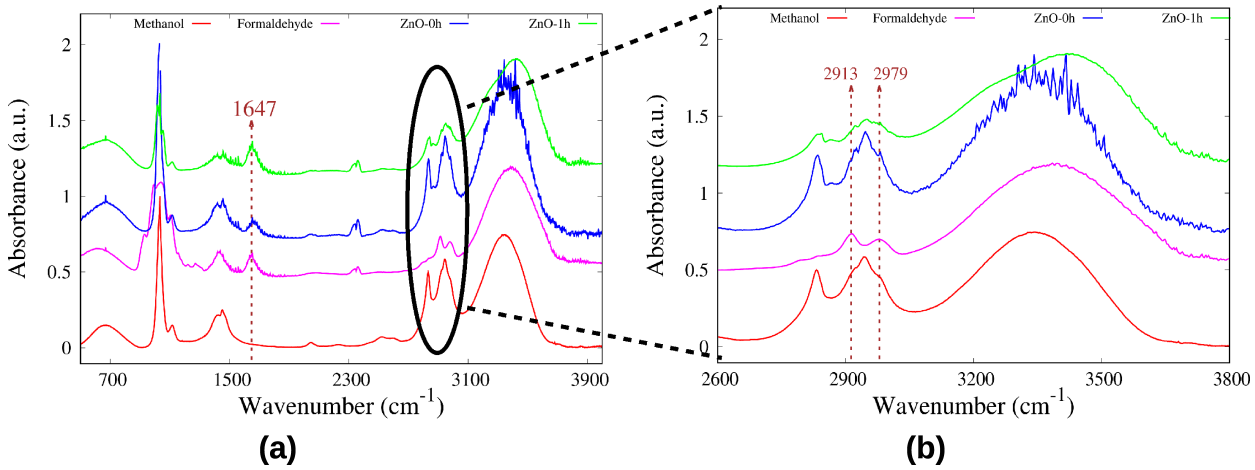

Figure 6.10: *FTIR spectrum of standard methanol, standard formaldehyde, reaction mixture at 0 minute, reaction mixture at 1 h is shown. (a) shows the peak of carbonyl corresponds to 1647 cm^{-1} which coincide with standard formaldehyde. (b) shows two tiny peaks appearing at 2913 and 2973 cm^{-1} in the reaction mixture at 0 min and 1 h. These peaks correspond to C-H vibrations in formaldehyde.*

tions of C-H at 2830 and 2941 cm^{-1} (refer Fig.6.10-(a)). The IR spectra of the reaction mixture at 0 min show the emergence of a peak at 1647 cm^{-1} (blue colour peak in Fig.6.10-(a)), which attributes to carbonyl peak in formaldehyde (pink coloured peak in Fig.6.10-(a)). We also observed the presence of two tiny peaks at 2913 and 2979 cm^{-1}, which corresponds to the C-H peak in formaldehyde.(refer Fig.6.10-(b)) The peaks for C-O and C-H vibrations increase in 1h reaction mixture, which signifies the further conversion of methanol to formaldehyde (as shown in green coloured peak in Fig.6.10-(a)).

HPLC analysis:

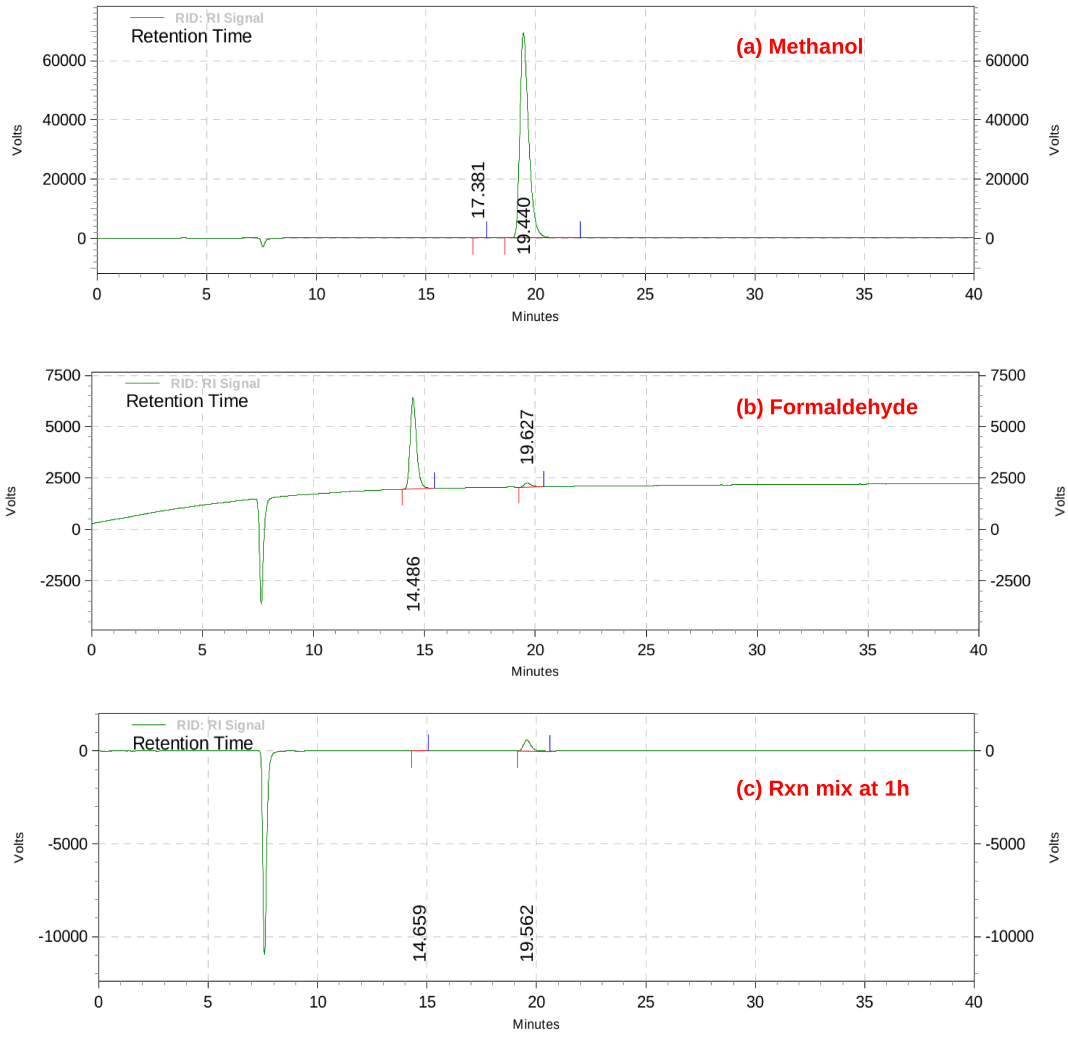

Figure 6.11: *HPLC results for authentic samples with the known concentration of (a) methanol and (b) formaldehyde. (c) HPLC result recorded for reaction mixture with ZnO catalyst at 1 h. The results show that only two peaks of methanol (reactant) and formaldehyde (product) signify 100% selectivity.*

Further, we performed HPLC analysis to validate the presence of formaldehyde as a product

in the reaction mixture. The reactant (methanol) and the expected outcome (formaldehyde) with known concentration and reaction mixture (at 1 h) are subjected to the HPLC set-up at identical conditions. The results are shown in Fig.6.11. It is evident from Fig.6.11 that a new peak appears (apart from methanol) in the reaction mixture at 1 h as shown in Fig.6.11 new peak coincides with the standard formaldehyde peak in Fig.6.11-(b). Interestingly, there are no other peaks for side products which indicate 100% selectivity for formaldehyde.

A fundamental understanding of structures and properties of materials is essential for material design. DFT plays a crucial role in describing the structure-property relationship of a material at the electronic level, which helps understand a catalyst's reactivity. The experimental validation of theoretically predicted results is in trends recently. Designing and discovering catalyst advised by computation is an emerging field of materials science. In this work, we explored the $(10\bar{1}1)$ facet of ZnO for interaction with methanol by employing periodic DFT. We suggested that at this facet, MeOH spontaneously converts to formaldehyde. We further validated our predicted results with experiments and observed formaldehyde formation from methanol at ambient conditions.

6.4 Conclusions

Methanol can be converted to formaldehyde either by partial oxidation or by dehydrogenation. In this work, we investigated the interaction of methanol with ZnO by theoretical and experimental approaches. We observed spontaneous conversion of methanol to formaldehyde on $(10\bar{1}1)$ facet. Not only does formaldehyde form, but it also desorbs from the surface. Formation of formaldehyde is thermodynamically the most favourable outcome at $(10\bar{1}1)$ facet. The presence of non-zero states at the Fermi level explains the greater reactivity of this facet. By carefully understanding our theoretical results, we designed an experiment to study the interaction of methanol with ZnO at RT and atmospheric pressure. The FTIR and HPLC both evident the formation of formaldehyde as a product of this reaction. Also, there is no peak other than formaldehyde in the reaction mixture, which indicates 100% selectivity of formaldehyde at ambient conditions. The theoretical investigation followed by experimental validation paves a very efficient way towards designing of catalyst.

Chapter 7

Electronic fingerprints for various Zn based systems

7.1 Motivation

Continuous efforts are being put in to design more environmentally benign catalysts than the existing ones. The rational designing of a catalyst would demand understanding the interaction of a molecule with different facets and distilling out the essential factors leading to desired products. In all our previous chapters, we have discussed in detail about the interaction of several Zn-based catalytic systems with methanol molecule. We have observed reasonably different interactions of the same Zn and O elements in different environments (Zn, O-Zn, ZnO, and $ZnAl_2O_4$) with methanol molecule. Not only different systems but also different facets in the same system shows significantly different interaction with methanol.

As discussed in Tab.7.1, the two major outcomes of interaction of methanol with these several Zn-based systems observed are, adsorption (physisorption or chemisorption) or spontaneous dissociation. We want to investigate the underlying electronic structure to understand the rationality behind these interactions. In this work, we analyze all the surfaces studied so far to determine the correlation between the electronic structure of bare facets and the outcome of MeOH adsorption. The ultimate goal of any DFT-based computation is to understand the results in terms of underlying electronic structure, derive trends, and gain predictive power. This work is an attempt in that direction.

Table 7.1: *Energetically most stable interaction of MeOH with different Zn based systems are shown. Physisorption is the only outcome for different facets of metallic Zn whereas weak to strong chemisorption is observed for oxygen preadsorbed Zn surfaces. On ZnO and $ZnAl_2O_4$, spontaneous dissociation of methanol is the energetically most stable outcome on every facet except ZnO-(11$\bar{2}$0) facet.*

systems/facets	(10$\bar{1}$0)/(220)	(10$\bar{1}$1)/(311)	(10$\bar{1}$3)	(11$\bar{2}$0)	(11$\bar{2}$2)
Zn	physisorption	physisorption	physisorption		
O-Zn	weak chemisorption	weak chemisorption	strong chemisorption		
ZnO	strong chemisorption	**formation of formaldehyde**	Dissociation of O-H bond	strong chemisorption	Dissociation of O-H bond
$ZnAl_2O_4$	Dissociation of O-H bond	Dissociation of O-H and C-H bond			

Table 7.2: *Interaction energy of methanol on different Zn-based systems are reported in the table. Black numbers depict the energy of metallic Zn and O-Zn systems. Blue and red coloured numbers represent the interaction of methanol at ZnO and $ZnAl_2O_4$ facets, respectively. Adsorption of methanol on these different systems triggers surface reconstruction, which reflects in the interaction energy. WR (with reconstruction) stands for energy with the impact of reconstruction. However, in order to homogenize the energies, we have eliminated the reconstruction effect from the interaction as demonstrated by WOR (without reconstruction).*

systems/facets		(10$\bar{1}$0)/220	(10$\bar{1}$1)/311	(10$\bar{1}$3)	(11$\bar{2}$0)	(11$\bar{2}$2)
Zn	WR	-4.09	-1.36	-0.66		
	WOR	-0.77	-0.69	-0.68		
O-Zn	WR	-3.26	-0.72	-1.01		
	WOR	-0.78	-0.60	-1.13		
ZnO	WR	-1.58	**-7.95**	**-3.88**	-1.24	**-6.24**
	WOR	-1.90	**-4.83**	**-2.91**	-1.40	**-3.38**
$ZnAl_2O_4$	WR	**-1.81**	**-4.14**			
	WOR	**-2.47**	**-4.91**			

7.2 Results and discussion

In previous chapters, we discussed the interaction of methanol with several facets of Zn, O-Zn, ZnO, and $ZnAl_2O_4$. We have investigated different flat and step facets of all the systems for their interaction with methanol. We observed that on the metallic Zn system, only the physisorption of

methanol takes place. On the O-Zn system, we also observed chemisorption at the step surface and physisorption on flat facets. However, as the concentration of oxygen increases, i.e. in the case of ZnO, we observed chemisorption as well as spontaneous dissociation of methanol on the surfaces of ZnO. Also, at $(10\bar{1}1)$ facet, methanol spontaneously converts to formaldehyde. These results were validated by experiments and demonstrated that methanol converts to formaldehyde at ZnO nanoparticles at ambient conditions with 100% selectivity. On other flat facets, molecular adsorption is most favourable, while dissociation of MeOH is thermodynamically the most favourable outcome at step facets. The activity of metal oxides can be altered by modifying their structure. ZnO and Al_2O_3 are both used as industrial catalysts for methanol synthesis. In chapter 5, we discussed the interaction of methanol with (220) and (311) facets of $ZnAl_2O_4$. We observed molecular adsorption and dissociation of methanol on these facets. Depending upon the adsorption site, MeOH interacts differently with $ZnAl_2O_4$. We reported that lesser coordinated surface oxygen atoms actively participate in methanol dissociation.

Table 7.3: *Mulliken charges on surface zinc atoms of Zn, O-Zn, ZnO, and $ZnAl_2O_4$. For Zn and O-Zn, the charges are shown in black, whereas for ZnO and $ZnAl_2O_4$, the charges are represented in blue and red, respectively. Charges for the facets where dissociation of MeOH occurs are shown in bold numbers. Transfer of electron from metal to oxygen is evident from the effective charges on Zn.*

systems/facets	$(10\bar{1}0)$/220	$(10\bar{1}1)$/311	$(10\bar{1}3)$	$(11\bar{2}0)$	$(11\bar{2}2)$
Zn	0.05	0.12	0.19(0.14)		
O-Zn	0.49	0.61	0.50		
ZnO	**0.85**	**1.04**	0.96(**0.64**)	0.96	**0.81**
$ZnAl_2O_4$	**1.52**	**1.53**(1.58)			

We observe that upon changing the environment of Zn and O in a series of different systems (Zn, O-Zn, ZnO, and $ZnAl_2O_4$), the interaction of methanol changes from adsorption to dissociation of O-H as well as C-H bond. To understand this variation, we analyzed different parameters such as interaction energy, Mulliken charges, and distance between MeOH and surface metal and/or oxygen atoms for all the facets of all these systems. The interaction energy of methanol's thermodynamically most stable configuration on various facets of Zn-based systems is noted in Tab.7.2. The interaction energy for each system is computed by including and excluding the surface reconstruction energy and described as WR and WOR, respectively. The black numbers represent methanol's interaction energy with Zn and O-Zn surfaces, while blue and red numbers indicate ZnO and $ZnAl_2O_4$ surfaces, respectively. The numbers in bold signify the dissociation of methanol as the thermodynamically most stable outcome on that facet. It is clear from the interaction energies (computed for both the WR and WOR) of Tab.7.2 that the presence of oxygen facilitates the

Table 7.4: *Mulliken charges on surface oxygen atoms of O-Zn(black color), ZnO(blue color), and $ZnAl_2O_4$(red color). The shortest distance between oxygen and surface atom (BL) is also shown*

systems/facets	property	$(10\bar{1}0)$/220	$(10\bar{1}1)$/311	$(10\bar{1}3)$	$(11\bar{2}0)$	$(11\bar{2}2)$
O-Zn	charge(e)	-0.74	-0.81	-1.38		
	BL(Å)	1.93	1.89	1.88		
ZnO	charge(e)	**-0.79**	**-0.68**	**-0.82**(-0.89)	-0.89	**-0.85**
	BL(Å)	1.77	1.85	1.94(1.87)	1.90	1.82
$ZnAl_2O_4$	charge(e)	**-1.03**(-1.07)	**-1.00**(-1.11; -1.17)			
	BL(Å)	1.82(1.74)	1.77(1.93; 1.85)			

adsorption of MeOH on the step facet of O-Zn. We do not observe any correlation between the interaction energy (WR) and the outcome of the interaction. However, the extent of reconstruction varies from facet to facet. Furthermore, upon normalization of the energies by excluding the impact of reconstruction (WOR), there is a one-to-one correlation between interaction energies (WOR) and the outcome of MeOH. Dissociation is always associated with lower interaction energy than molecular adsorption. Also, irrespective of the outcome, methanol interaction is more favoured on the ZnO and $ZnAl_2O_4$ facets than Zn and O-Zn.

Next, we note effective charges on surface zinc and oxygen atoms for all the facets investigated in Tab.7.3 and Tab.7.4, respectively. The numbers in black depict Zn and O-Zn systems, whereas the blue and red numbers indicate ZnO and $ZnAl_2O_4$ systems. It is clear from Tab.7.3 that with increasing oxygen content, Zn becomes more positive, indicating electron transfer from metal to oxygen. Similarly, as seen from Tab.7.4, charge gained by oxygen atoms varies from -0.68 for ZnO$(10\bar{1}1)$ to -1.38 for O-Zn$(10\bar{1}3)$. However, we do not see any correlation between the charge on surface zinc/oxygen and the outcome of the interaction i.e. adsorption or dissociation of MeOH.

Further, we compare *p*DOS for O-2*p* of O-Zn, ZnO, and $ZnAl_2O_4$ for flat and step facets as shown in Fig.7.1-(a) and (b), respectively. The reference *p*DOS for 2*p* of O_{MeOH} is plotted in each figure as a grey curve. Depending on the environment, the *p*DOS exhibit subtle variation which influences the outcome of the interaction of MeOH with that facet. Two flat facets [$(10\bar{1}0)$ and $(10\bar{1}1)$] and step facets of ZnO with non zero *p*DOS at Fermi favours dissociation of MeOH. Whereas for the $(11\bar{2}0)$ facet, there are no states at the Fermi level, and this is the facet of ZnO with the chemisorption of MeOH as the only outcome. For both step facets of ZnO (see (ii) of Fig.7.1-(b)) significantly low number of O-2*p* states are present near Fermi. However, for both these stepped facets, Zn-4*s* states are present at Fermi (shown in Fig.7.3-(b)-(iii)) and overlaps with 2*p* states of O_{MeOH}, which accounts for the spontaneous dissociation of MeOH on these

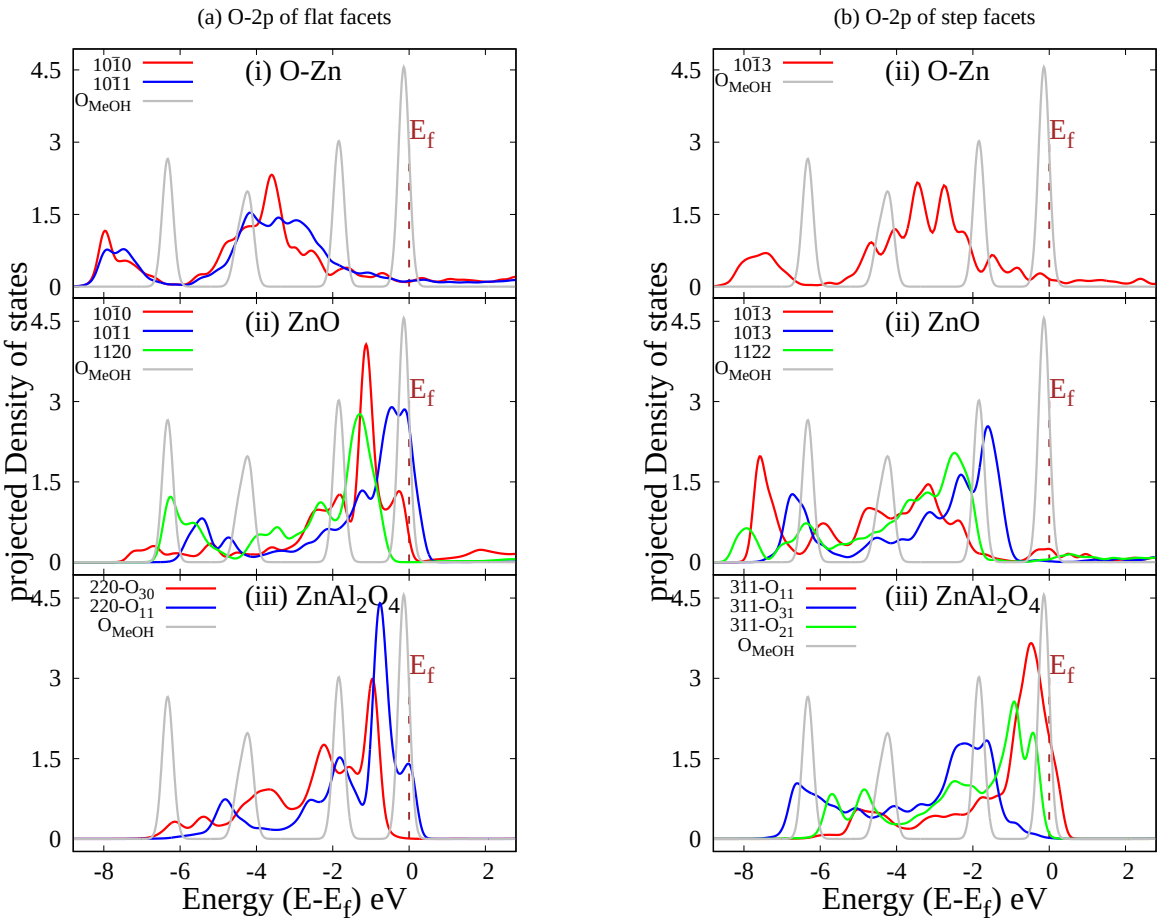

Figure 7.1: *pDOS of 2p of O in different systems (i) oxygen preadsorbed zinc (O-Zn), (ii) metal oxide (ZnO), (iii) mixed metal oxide ($ZnAl_2O_4$). (a) shows flat facets, while (b) represents stepped facets. 2p of oxygen of methanol is plotted in grey colour for reference.*

facets. This site-specific signature of *p*DOS is also observed in the tDOS plot, which reflects the underlying electronic structure of the entire facet. The tDOS plots of flat and step facets of all systems are shown in Fig.7.2-(a) and (b), respectively.

The following system we will discuss is a mixed metal oxide, $ZnAl_2O_4$. For $ZnAl_2O_4$, on (220) and (311) facets dissociation of MeOH is the favoured outcome. Al acts as the active site for methanol adsorption in these cases because of its greater affinity for oxygen than Zn. Surface oxygen atoms have variations in their coordination with Zn and Al atoms. The difference in the coordination of these oxygen atoms also reflects in their *p*DOS plots as seen in Fig.7.1-(a) and (b)-iii. These different 'types' of oxygen atoms on the surface are denoted based on their coordination with Al and Zn atoms, respectively. For example, the label 220-O_{30} in Fig.7.1-a-(iii) represents the *p*DOS of the oxygen atom, which is coordinated with 3 Al atoms. Interestingly, when MeOH is placed near the oxygen atoms having non-zero states at the Fermi, they undergo dissociation. In contrast, if MeOH is placed near oxygen atoms that do not have Fermi states, they are chemisorbed.

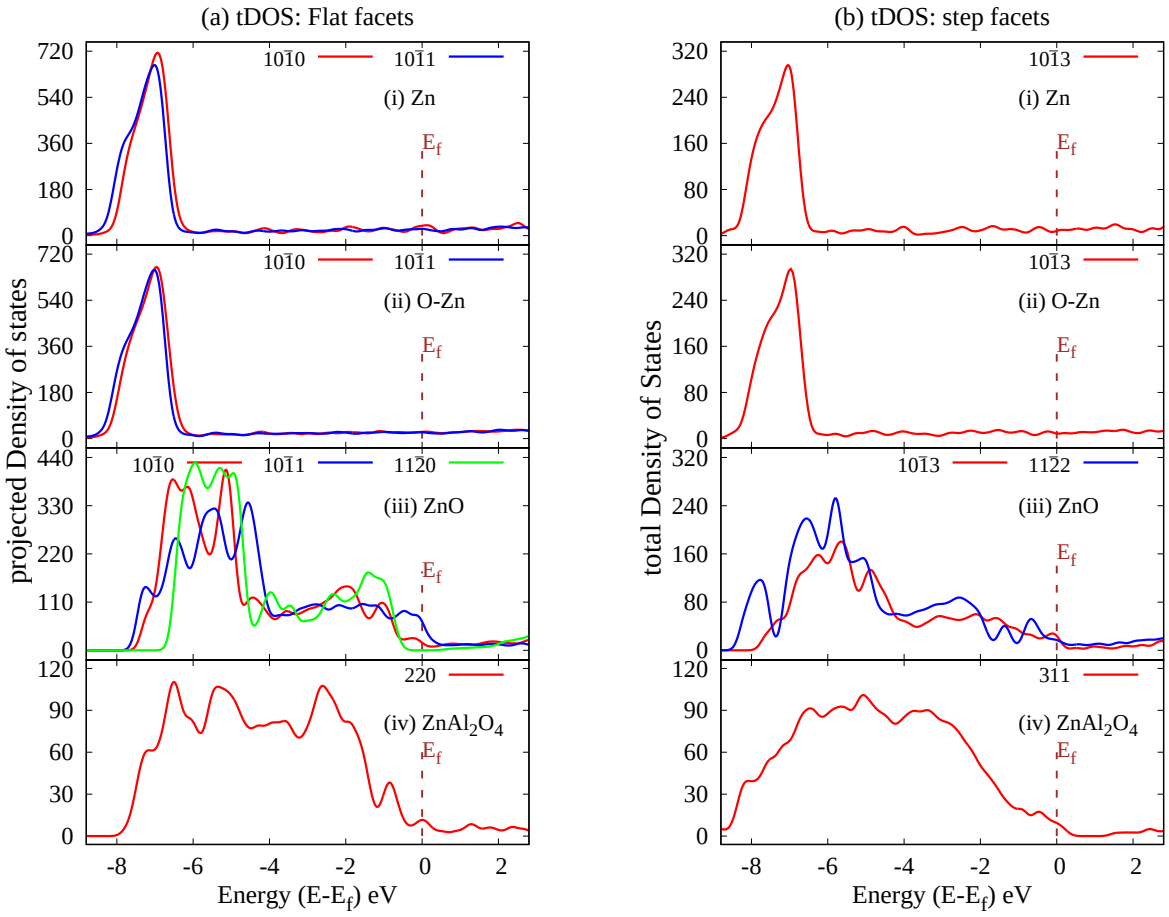

Figure 7.2: *tDOS of different systems (i) metallic Zn, (ii) oxygen preadsorbed zinc (O-Zn), (iii) metal oxide (ZnO), (iv) mixed metal oxide ($ZnAl_2O_4$). (a) shows flat facets, while (b) represents stepped facets.*

Thus, the adsorption of MeOH in the vicinity of oxygen, which has non-zero energy states at Fermi, is essential for dissociating methanol. However, it is not sufficient to have non-zero states at Fermi. The orientation of methanol plays a crucial role in determining the outcome. The preferred orientation is where H_{MeOH} is inclined towards the O_{surf}. Fig.7.4 represents two different orientations of methanol on (220) facet of $ZnAl_2O_4$. The atoms displayed in blue depict those oxygen atoms with non-zero peaks at the Fermi level, and the red ones have zero energy states at the Fermi level. Fig.7.4-(a) and (b) show the adsorption of methanol on the same Al atom in two different orientations, which results in adsorption and dissociation of methanol, respectively. The favoured orientation of methanol (refer Fig.7.4-(b)) for dissociation is the one in which H_{MeOH} is tilted towards the blue-coloured oxygen atom, which has non-zero energy states at Fermi. This observation holds for the (311) facet also. It is interesting to note that this trend is also visible in the *p*DOS plot of each facet, where Al-3*p* is present at Fermi (Fig.7.5) and overlaps with 2*p* of O_{MeOH}, but no Zn-4*s* is seen around Fermi (Fig.7.3). This signature is also clearly seen in the tDOS of $ZnAl_2O_4$ depicted in Fig.7.2-(iv).

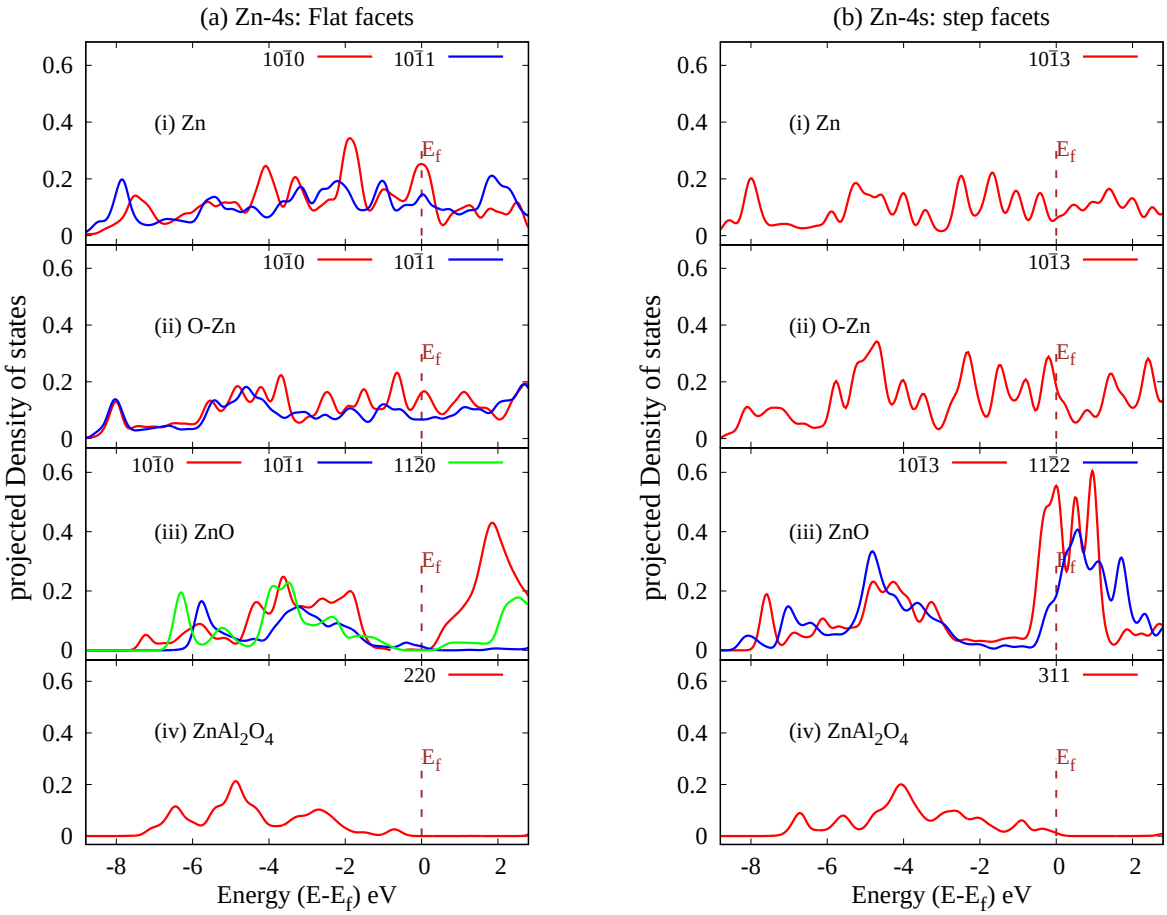

Figure 7.3: *Represents pDOS of Zn-4s in various systems (i) metallic zinc (Zn), (ii) oxygen preadsorbed zinc (O-Zn), (iii) metal oxide (ZnO), (iv) mixed metal oxide ($ZnAl_2O_4$). Figure (a) and (b) shows flat and stepped facets of these systems, respectively.*

7.3 Conclusions

The current study thoroughly examines how methanol interacts with several facets of zinc-based materials. Different arrangement of atoms on any surface creates a unique environment, affecting its reactivity for the incoming adsorbate species. The underlying electronic structure of a surface perfectly captures this pattern of the changing environment. This chapter discusses the underlying electronic structures of different catalytic systems, including Zn, O-Zn, ZnO, and $ZnAl_2O_4$, that have been investigated for interactions with methanol in our study. By carefully analyzing the site-specific *p*DOS plots of these facets, we report that the existence of energy states of oxygen, metal, or both at or near the Fermi level has a substantial influence in the dissociation of MeOH on that particular facet. With this knowledge, we may examine catalytic surfaces for their interactions with incoming adsorbate species from a fresh perspective. The ultimate goal of any DFT-based computation is to understand the results in terms of underlying electronic structure, derive trends

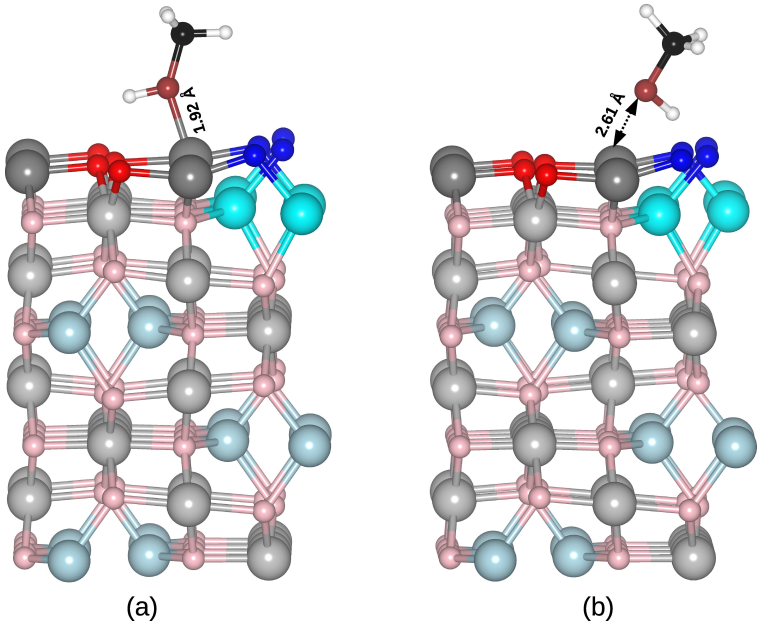

Figure 7.4: *The orientation of methanol on (220) facet of $ZnAl_2O_4$ are shown. The atoms in blue colour correspond to those oxygens which have non-zero energy states at Fermi as shown in Fig.7.1-(a)-(iii) and red are those which have zero energy states at Fermi. (a) shows the initial position of methanol where the H_{MeOH} is inclined towards red oxygen atoms and results in methanol adsorption upon optimization. (b) depicts the initial position of methanol in which H_{MeOH} is tilted towards blue oxygen atoms, resulting in dissociation. It signifies that along with the presence of oxygen with a non-zero peak at Fermi, the orientation of MeOH does play a crucial role in determining the outcome of the interaction of MeOH in a complex system such as $ZnAl_2O_4$.*

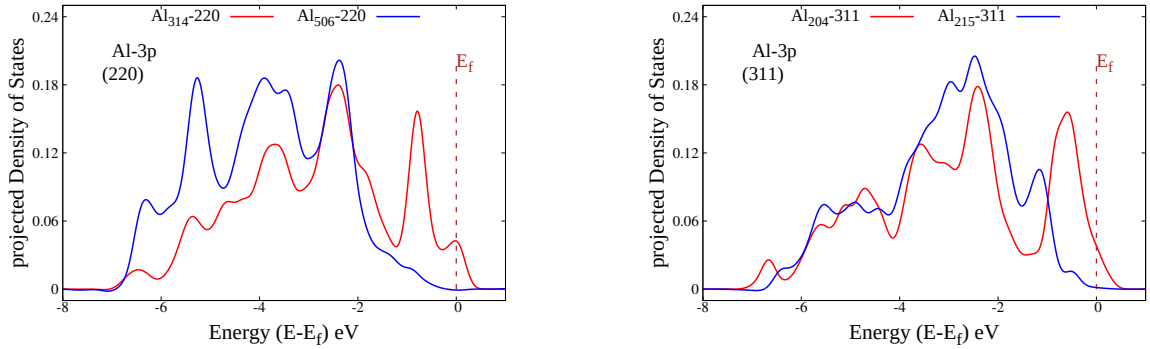

Figure 7.5: *pDOS of Al-3p in different facets of $ZnAl_2O_4$ are shown. (a) represents (220) facet, where two inequivalent Al atoms are present on the surface. These Al atoms are distinguished based on their coordination with the neighbouring atoms. The Al subscript represents a number of Al, Zn, and O atoms to that Al atom. (b) shows (311) facet of $ZnAl_2O_4$. At this facet, two inequivalent Al atoms are present, which differ in their environment. Presence of Al-3p energy states near Fermi favour dissociation of MeOH on this facet.*

and gain predictive power. The work of this thesis is an attempt in that direction.

Chapter 8

Summary and future scope

The rational designing of a catalyst for methanol decomposition demands understanding the interaction of a methanol with different facets and distilling out the essential factors leading to desired products. In this thesis, we have investigated a series of Zn-based catalysts, including pure metallic Zn, oxygen-preadsorbed Zn, ZnO, and $ZnAl_2O_4$ for their interaction with MeOH. We observed that the change of environment of Zn in these different systems affects their catalytic activity. The changing environment is captured in the underlying electronic structure of the catalysts. We demonstrate a one-to-one correlation between the electronic structure of the bare facet and the outcome of that facets interaction with MeOH. By carefully analyzing the site-specific projected density of states of these facets, we report that the existence of energy states of oxygen, metal, or both at or near the Fermi level has a substantial influence on the dissociation of MeOH on that particular facet. The adsorption of MeOH in the vicinity of oxygen, which has non-zero energy states at Fermi, is essential for dissociating methanol. However, it is not sufficient to have non-zero states at Fermi. The orientation of methanol plays a crucial role in determining the outcome. With DFT study, we predicted spontaneous conversion of methanol to formaldehyde, which desorbs from the surface at $(10\bar{1}1)$ facet of ZnO. Later, we validated our DFT results by the experiments and we demonstrated the conversion of methanol to formaldehyde on the ZnO catalyst at ambient conditions.

As discussed earlier, the presence of non-zero energy states at Fermi is necessary but not sufficient condition for the dissociation of methanol. There are several other factors that affect the interaction of methanol which could be explored in detail. We have investigated families of Zn-based catalyst for MeOH interaction and provide a rationale behind the variation in outcome of interaction based on underlying electronic structure. This understanding could be utilized for other classes of metals such as, Cu, Mg, Ti, etc. which are extensively used in industrial catalysts, to investigate the interaction with methanol.

All the DFT results reported in the thesis are at 0K and zero pressure, however, the real reactions takes place conditions are certainly at higher temperature and pressure. Thus, a different theoretical

approach like ReaxFF could be used to investigate the interaction of methanol with these systems at desirable temperature and pressure conditions. ReaxFF is a bond-order based force field tool which finds significant application in exploring the materials properties. ReaxFF can deal with systems as large as 10000 atoms under industrial reaction conditions. Another tool such as microkinetic modelling can be used to understand the reaction mechanism for methanol to formaldehyde at the ZnO. In microkinetic modeling, the microscopic properties of catalyst obtained from DFT are linked to the macroscopic properties of the system like turnover frequency, selectivity towards the desired products.

Numerous factors, like the structural arrangement of surface atoms, environment of the surface exposed to the adsorbate orientation of adsorbate, etc., are important factors that affect interaction of surface-adsorbate. Scanning all the sites on the catalyst surface and orientation of methanol is formidable task using DFT. Machine learning could be used to explore the chemical space and derive trends for the surface-adsorbate interaction.

References

[1] Ali, K. A.; Abdullah, A. Z.; Mohamed, A. R. *Renewable and Sustainable Energy Reviews* **2015**, *44*, 508–518.

[2] SciFinder CAS. https://scifinder-n.cas.org/search/reference/63bbdf6629d8504674dedfdc/1.

[3] SciFinder CAS. https://scifinder-n.cas.org/search/reference/63bbdf8329d8504674dee1c8/1.

[4] Liu, P.; Yang, Y.; White, M. G. *Surface Science Reports* **2013**, *68*, 233–272.

[5] Woods, N. D. *arXiv: Other Condensed Matter* **2018**,

[6] Payne, M. C.; Teter, M. P.; Allan, D. C.; Arias, T. A.; Joannopoulos, J. D. *Rev. Mod. Phys.* **1992**, *64*, 1045–1097.

[7] today in energy. https://www.eia.gov/todayinenergy/detail.php?id=41433, Accessed: 2019-09-24.

[8] Encyclopedia, N. W. Methanol — New World Encyclopedia,. 2022; https://www.newworldencyclopedia.org/p/index.php?title=Methanololdid=1086470.

[9] Olah, G. A. *Angewandte Chemie International Edition* **2005**, *44*, 2636–2639.

[10] Galindo Cifre, P.; Badr, O. *Energy Conversion and Management* **2007**, *48*, 519–527.

[11] Yanju, W.; Shenghua, L.; Hongsong, L.; Rui, Y.; Jie, L.; Ying, W. *Energy & Fuels* **2008**, *22*, 1254–1259.

[12] methanol economy. https://www.niti.gov.in/methanol-economy, Accessed: 2022-13-08.

[13] Thrane, J.; Mentzel, U. V.; Thorhauge, M.; Høj, M.; Jensen, A. D. *Catalysts* **2021**, *11*.

[14] Klissurski, D.; Pesheva, Y. *Reaction Kinetics and Catalysis Letters* **1986**, *32*, 77–82.

[15] Behera, G. C.; Parida, K. *Chemical Engineering Journal* **2012**, *180*, 270–276.

[16] Whiting, G. T.; Bartley, J. K.; Dummer, N. F.; Hutchings, G. J.; Taylor, S. H. *Applied Catalysis A: General* **2014**, *485*, 51–57.

[17] Smith, M. A.; Zoelle, A.; Yang, Y.; Rioux, R. M.; Hamilton, N. G.; Amakawa, K.; Nielsen, P. K.; Trunschke, A. *Journal of Catalysis* **2014**, *312*, 170–178.

[18] Li, Z.; Ivanenko, A.; Meng, X.; Zhang, Z. *Journal of hazardous materials* **2019**, *380*, 120822.

[19] Jenzer, G.; Sueur, D.; Mallat, T.; Baiker, A. *Chemical Communications* **2000**, 2247–2248.

[20] Murphy, L. J.; Hollenhorst, H.; McDonald, R.; Ferguson, M.; Lumsden, M. D.; Turculet, L. *Organometallics* **2017**, *36*, 3709–3720.

[21] Beznis, N. V.; Van Laak, A. N.; Weckhuysen, B. M.; Bitter, J. H. *Microporous and Mesoporous Materials* **2011**, *138*, 176–183.

[22] Honkala, K.; Hellman, A.; Remediakis, I. N.; Logadottir, A.; Carlsson, A.; Dahl, S.; Christensen, C. H.; Nørskov, J. K. *Science* **2005**, *307*, 555–558.

[23] Badlani, M.; Wachs, I. E. *Catalysis Letters* **2001**, *75*, 137–149.

[24] Blanksby, S. J.; Ellison, G. B. *Accounts of chemical research* **2003**, *36*, 255–263.

[25] Ammon, C.; Bayer, A.; Held, G.; Richter, B.; Schmidt, T.; Steinrück, H.-P. *Surface Science* **2002**, *507*, 845–850.

[26] Sun, Q.; Shen, B.; Fan, K.; Deng, J. *Chemical Physics Letters* **2000**, *322*, 1–8.

[27] Xu, B.; Haubrich, J.; Baker, T. A.; Kaxiras, E.; Friend, C. M. *The Journal of Physical Chemistry C* **2011**, *115*, 3703–3708.

[28] Ishikawa, Y.; Liao, M.-S.; Cabrera, C. R. *Surface Science* **2000**, *463*, 66–80.

[29] Zhang, C.; Hu, P. *The Journal of Chemical Physics* **2001**, *115*, 7182–7186.

[30] Wang, G.-C.; Zhou, Y.-H.; Morikawa, Y.; Nakamura, J.; Cai, Z.-S.; Zhao, X.-Z. *The Journal of Physical Chemistry B* **2005**, *109*, 12431–12442.

[31] Neubauer, R.; Whelan, C.; Denecke, R.; Steinrück, H.-P. *Surface science* **2002**, *507*, 832–837.

[32] Sardar, S.; Syed, J.; Tanaka, K.; Netzer, F.; Ramsey, M. *Surface Science* **2002**, *519*, 218–228.

[33] Carbone, M.; Larsson, K. *Journal of Physics: Condensed Matter* **2005**, *17*, 1289–1300.

[34] Kim, D. H.; Bae, S.-S.; Hong, S.; Kim, S. *Surface Science* **2010**, *604*, 129–135.

[35] Yanagisawa, S.; Tsuneda, T.; Hirao, K.; Matsuzaki, Y. *Journal of Molecular Structure: THEOCHEM* **2005**, *716*, 45–60.

[36] Jiang, R.; Guo, W.; Li, M.; Zhu, H.; Zhao, L.; Lu, X.; Shan, H. *Journal of Molecular Catalysis A: Chemical* **2011**, *344*, 99–110.

[37] Bao, X.; Muhler, M.; Pettinger, B.; Schlögl, R.; Ertl, G. *Catalysis Letters* **1993**, *22*, 215–225.

[38] Greeley, J.; Mavrikakis, M. *Journal of Catalysis* **2002**, *208*, 291–300.

[39] de la Fuente, O. R.; Borasio, M.; Galletto, P.; Rupprechter, G.; Freund, H.-J. *Surface Science* **2004**, *566*, 740–745.

[40] Skoplyak, O.; Menning, C. A.; Barteau, M. A.; Chen, J. G. *The Journal of chemical physics* **2007**, *127*, 114707.

[41] Orazi, V.; Bechthold, P.; Jasen, P. V.; Faccio, R.; Pronsato, M. E.; Gonzalez, E. A. *Applied Surface Science* **2017**, *420*, 383–389.

[42] Sein Jr, L. T.; Jansen, S. A. *Journal of Catalysis* **2000**, *196*, 207–211.

[43] Borck, Ø.; Svenum, I.-H.; Borg, A. *Surface science* **2009**, *603*, 2378–2386.

[44] Du, P.; Wu, P.; Cai, C. *The Journal of Physical Chemistry C* **2017**, *121*, 9348–9360.

[45] Mehmood, F.; Greeley, J.; Zapol, P.; Curtiss, L. A. *The Journal of Physical Chemistry B* **2010**, *114*, 14458–14466.

[46] Gasper, R. J.; Ramasubramaniam, A. *The Journal of Physical Chemistry C* **2016**, *120*, 17408–17417.

[47] Zuo, Z.-J.; Wang, L.; Han, P.-D.; Huang, W. *Computational and Theoretical Chemistry* **2014**, *1033*, 14–22.

[48] Ghatak, K.; Sengupta, T.; Krishnamurty, S.; Pal, S. *Theoretical Chemistry Accounts* **2015**, *134*, 1–11.

[49] Petitjean, H.; Tarasov, K.; Delbecq, F.; Sautet, P.; Krafft, J. M.; Bazin, P.; Paganini, M. C.; Giamello, E.; Che, M.; Lauron-Pernot, H., et al. *The Journal of Physical Chemistry C* **2010**, *114*, 3008–3016.

[50] Liu, Z.; Sorrell, C. C.; Koshy, P.; Hart, J. N. *ChemPhysChem* **2019**, *20*, 2074–2081.

[51] Borck, Ø.; Schröder, E. *Journal of Physics: Condensed Matter* **2005**, *18*, 1.

[52] Borck, Ø.; Schröder, E. *Journal of Physics: Condensed Matter* **2006**, *18*, 10751.

[53] Liu, W.; Wang, J.-g.; Guo, X.; Fang, W.; Wei, M.; Lu, X.; Lu, L. *Catalysis today* **2011**, *165*, 32–40.

[54] Choksi, T.; Greeley, J. *ACS Catalysis* **2016**, *6*, 7260–7277.

[55] Kumar, A.; Kumar, R.; Singh, R.; Prasad, B.; Kumar, D.; Kumar, M. *Journal of Coatings Technology and Research* **2021**, 1–13.

[56] Mehta, S.; Agarwal, S.; Kenge, N.; Mekala, S. P.; Patil, V.; Raja, T.; Joshi, K. *Applied Surface Science* **2020**, *534*, 147449.

[57] Andzelm, J.; Govind, N.; Fitzgerald, G.; Maiti, A. *International journal of quantum chemistry* **2003**, *91*, 467–473.

[58] Wang, C.; Chu, Y.; Zheng, A.; Xu, J.; Wang, Q.; Gao, P.; Qi, G.; Gong, Y.; Deng, F. *Chemistry–A European Journal* **2014**, *20*, 12432–12443.

[59] Fellah, M. F.; Onal, I. *The Journal of Physical Chemistry C* **2012**, *116*, 13616–13622.

[60] Ellis, T.; Wang, H. *Langmuir* **1994**, *10*, 4083–4088.

[61] Sakong, S.; Groß, A. *Journal of Catalysis* **2005**, *231*, 420–429.

[62] Garcıa-Muelas, R.; Li, Q.; López, N. *ACS Catalysis* **2015**, *5*, 1027–1036.

[63] Chen, W.-K.; Liu, S.-H.; Cao, M.-J.; Yan, Q.-G.; Lu, C.-H. *Journal of Molecular Structure: THEOCHEM* **2006**, *770*, 87–91.

[64] Xu, B.; Liu, X.; Haubrich, J.; Madix, R. J.; Friend, C. M. *Angewandte Chemie* **2009**, *121*, 4270–4273.

[65] Pala, R. G. S.; Metiu, H. *Journal of Catalysis* **2008**, *254*, 325–331.

[66] Vo, C. T.; Huynh, L. K.; Hung, J.-Y.; Jiang, J.-C. *Applied surface science* **2013**, *280*, 219–224.

[67] Deng, X.; Sorescu, D. C.; Lee, J. *Topics in Catalysis* **2018**, *61*, 499–508.

[68] Yong, S.; Ooi, C.; Chai, S.; Wu, X. *International Journal of Hydrogen Energy* **2013**, *38*, 9541–9552.

[69] Moura, A. S.; Fajín, J. L. C.; Mandado, M.; Cordeiro, M. N. D. S. *Catalysts* **2017**, *7*.

[70] Woolley, R.; Sutcliffe, B. *Chemical Physics Letters* **1977**, *45*, 393–398.

[71] Szabo, A.; Ostlund, N. S. *Modern quantum chemistry: introduction to advanced electronic structure theory*; Courier Corporation, 2012.

[72] Pisani, C.; Dovesi, R.; Roetti, C. *Hartree-Fock ab initio treatment of crystalline systems*; Springer Science & Business Media, 2012; Vol. 48.

[73] Shavitt, I.; Bartlett, R. J. *Many-body methods in chemistry and physics: MBPT and coupled-cluster theory*; Cambridge university press, 2009.

[74] Hohenberg, P.; Kohn, W. *Phys. Rev.* **1964**, *136*, B864–B871.

[75] Probert, M. Electronic Structure: Basic Theory and Practical Methods, by Richard M. Martin: Scope: graduate level textbook. Level: theoretical materials scientists/condensed matter physicists/computational chemists. 2011.

[76] Kohn, W.; Sham, L. J. *Phys. Rev.* **1965**, *140*, A1133–A1138.

[77] Hamann, D. R.; Schlüter, M.; Chiang, C. *Phys. Rev. Lett.* **1979**, *43*, 1494–1497.

[78] Laasonen, K.; Car, R.; Lee, C.; Vanderbilt, D. *Phys. Rev. B* **1991**, *43*, 6796–6799.

[79] Blöchl, P. E. *Phys. Rev. B* **1994**, *50*, 17953–17979.

[80] Kresse, G.; Joubert, D. *Phys. Rev. B* **1999**, *59*, 1758–1775.

[81] Jain, A.; Ong, S. P.; Hautier, G.; Chen, W.; Richards, W. D.; Dacek, S.; Cholia, S.; Gunter, D.; Skinner, D.; Ceder, G., et al. *Applied Materials* **2013**, *1*, 011002.

[82] Vaitkus, A.; Merkys, A.; Gražulis, S. *Journal of Applied Crystallography* **2021**, *54*, 661–672.

[83] Larsen, A. H. et al. *Journal of Physics: Condensed Matter* **2017**, *29*, 273002.

[84] Stradi, D.; Jelver, L.; Smidstrup, S.; Stokbro, K. *Journal of Physics: Condensed Matter* **2017**, *29*, 185901.

[85] Fiorentini, V.; Methfessel, M.; Scheffler, M. *Physical review letters* **1993**, *71*, 1051.

[86] Pandey, K. *Physica B+ C* **1983**, *117*, 761–766.

[87] Jacobsen, K.; Nørskov, J. *Physical review letters* **1988**, *60*, 2496.

[88] Moura, A. S.; Fajín, J. L. C.; Pinto, A. S. S.; Mandado, M.; D. S. Cordeiro, M. N. *The Journal of Physical Chemistry C* **2015**, *119*, 27382–27391.

[89] Yang, X. *ACS Catalysis* **2014**, *4*, 1129–1133.

[90] Kramer, Z. C.; Gu, X.-K.; Zhou, D. D. Y.; Li, W.-X.; Skodje, R. T. *The Journal of Physical Chemistry C* **2014**, *118*, 12364–12383.

[91] Jiang, R.; Guo, W.; Li, M.; Fu, D.; Shan, H. *The Journal of Physical Chemistry C* **2009**, *113*, 4188–4197.

[92] Fang, Y.-H.; Liu, Z.-P. *Surface Science* **2015**, *631*, 42–47.

[93] Gu, X.-K.; Li, W.-X. *The Journal of Physical Chemistry C* **2010**, *114*, 21539–21547.

[94] Montoya, A.; Haynes, B. S. *The Journal of Physical Chemistry C* **2007**, *111*, 9867–9876.

[95] Sexton, B.; Hughes, A.; Avery, N. *Surface Science* **1985**, *155*, 366–386.

[96] Ben David, R.; Ben Yaacov, A.; Head, A. R.; Eren, B. *ACS Catalysis* **0**, *0*, 7709–7718.

[97] Sexton, B. A. *Surface Science* **1981**, *102*, 271–281.

[98] Greeley, J.; Mavrikakis, M. *Journal of the American Chemical Society* **2004**, *126*, 3910–3919, PMID: 15038745.

[99] Kandoi, S.; Greeley, J.; Sanchez-Castillo, M. A.; Evans, S. T.; Gokhale, A. A.; Dumesic, J. A.; Mavrikakis, M. *Topics in catalysis* **2006**, *37*, 17–28.

[100] Christmann, K.; Demuth, J. E. *The Journal of Chemical Physics* **1982**, *76*, 6308–6317.

[101] Schennach, R.; Eichler, A.; Rendulic, K. *The Journal of Physical Chemistry B* **2003**, *107*, 2552–2558.

[102] Xu, Y.; Greeley, J.; Mavrikakis, M. *Journal of the American Chemical Society* **2005**, *127*, 12823–12827, PMID: 16159275.

[103] Wang, G.-C.; Tao, S.-X.; Bu, X.-H. *Journal of Catalysis* **2006**, *244*, 10–16.

[104] Kim, J.; Samano, E.; Koel, B. E. *The Journal of Physical Chemistry B* **2006**, *110*, 17512–17517, PMID: 16942092.

[105] Wang, S.; Zhu, E.; Huang, Y.; Heinz, H. *Science Advances* **2021**, *7*, eabb1435.

[106] Liu, P.; Nørskov, J. K. *Physical Chemistry Chemical Physics* **2001**, *3*, 3814–3818.

[107] Tao, S.-X.; Wang, G.-C.; Bu, X.-H. *The Journal of Physical Chemistry B* **2006**, *110*, 26045–26054, PMID: 17181256.

[108] Cordeiro, M. N. D.; Pinto, A. S.; Gomes, J. A. *Surface Science* **2007**, *601*, 2473–2485.

[109] Aljama, H.; Yoo, J. S.; Nørskov, J. K.; Abild-Pedersen, F.; Studt, F. *ChemCatChem* **2016**, *8*, 3621–3625.

[110] (a) Blöchl, P. E. *Physical Review B* **1994**, *50*, 17953–17979.

[111] Kresse, G.; Joubert, D. *Physical Review B* **1999**, *59*, 1758–1775.

[112] Perdew, J. P.; Burke, K.; Ernzerhof, M. *Physical Review Letters* **1997**, *78*, 1396–1396.

[113] (a) Kresse, G.; Hafner, J. *Physical Review B* **1994**, *49*, 14251–14269.

[114] Kresse, G.; Furthmüller, J. *Physical Review B* **1996**, *54*, 11169–11186.

[115] Kresse, G.; Furthmüller, J. *Computational Material Science* **1996**, *6*, 15–50.

[116] Iokibe, K.; Azumi, K.; Tachikawa, H. *The Journal of Physical Chemistry C* **2007**, *111*, 13510–13516.

[117] Grimme, S. *Journal of computational chemistry* **2006**, *27*, 1787–1799.

[118] (a) Dronskowski, R.; Blöchl, P. E. *The Journal of Physical Chemistry* **1993**, *97*, 8617–8624.

[119] Deringer, V. L.; Tchougréeff, A. L.; Dronskowski, R. *The Journal of Physical Chemistry A* **2011**, *115*, 5461–5466.

[120] Maintz, S.; Deringer, V. L.; Tchougréeff, A. L.; Dronskowski, R. *Journal of Computational Chemistry* **2013**, *34*, 2557–2567.

[121] Maintz, S.; Deringer, V. L.; Tchougréeff, A. L.; Dronskowski, R. *Journal of Computational Chemistry* **2016**, *37*, 1030–1035.

[122] Henkelman, G.; Uberuaga, B. P.; Jónsson, H. *The Journal of Chemical Physics* **2000**, *113*, 9901–9904.

[123] Mostoni, S.; Milana, P.; Di Credico, B.; D'Arienzo, M.; Scotti, R. *Catalysts* **2019**, *9*.

[124] Shamna, S.; Afsina, C. M. A.; Philip, R. M.; Anilkumar, G. *RSC Adv.* **2021**, *11*, 9098–9111.

[125] Sattler, W.; Parkin, G. *Journal of the American Chemical Society* **2012**, *134*, 17462–17465, PMID: 23046174.

[126] Spencer, M. *Topics in Catalysis* **1999**, *8*, 259–266.

[127] Nguyen, D. L. T.; Jee, M. S.; Won, D. H.; Jung, H.; Oh, H.-S.; Min, B. K.; Hwang, Y. J. *ACS Sustainable Chemistry & Engineering* **2017**, *5*, 11377–11386.

[128] Chang, F.-W.; Yu, H.-Y.; Roselin, L. S.; Yang, H.-C. *Applied catalysis A: general* **2005**, *290*, 138–147.

[129] Kapran, A. Y.; Soloviev, S. O.; Orlyk, S. N. *Reaction Kinetics, Mechanisms and Catalysis* **2010**, *101*, 343–353.

[130] Alvarenga, G.; Villullas, H. *Current Opinion in Electrochemistry* **2017**, *4*, 39–44.

[131] Zhou, K.; Ma, W.; Zeng, Z.; Ma, X.; Xu, X.; Guo, Y.; Li, H.; Li, L. *Chemical Engineering Journal* **2019**, *372*, 1122–1133.

[132] Elnabawy, A. O.; Schimmenti, R.; Cao, A.; Nørskov, J. K. *ACS Sustainable Chemistry & Engineering* **2022**, *10*, 1722–1730.

[133] Meyer, B.; Marx, D. *Physical Review B* **2003**, *67*, 035403.

[134] Boisen, A.; Dahl, S.; Nørskov, J. K.; Christensen, C. H. *Journal of Catalysis* **2005**, *230*, 309–312.

[135] Abedi, N.; Herrmann, P.; Heimel, G. *The Journal of Physical Chemistry C* **2015**, *119*, 21574–21584.

[136] Ruan, S.; Li, Z.; Shi, H.; Wang, W.; Ren, X.; Shao, X. *The Journal of Physical Chemistry C* **2019**, *123*, 9105–9111.

[137] Smith, G. K.; Lin, S.; Lai, W.; Datye, A.; Xie, D.; Guo, H. *Surface science* **2011**, *605*, 750–759.

[138] Jin, L.; Wang, Y. *Physical Chemistry Chemical Physics* **2017**, *19*, 12992–13001.

[139] Perdew, J. P.; Burke, K.; Ernzerhof, M. *Physical Review Letters* **1996**, *77*, 3865–3868.

[140] Reeber, R. R. *Journal of applied physics* **1970**, *41*, 5063–5066.

[141] Flores, E. M.; Moreira, M. L.; Piotrowski, M. J. *The Journal of Physical Chemistry A* **2020**, *124*, 3778–3785.

[142] Dulub, O.; Boatner, L. A.; Diebold, U. *Surface Science* **2002**, *519*, 201–217.

[143] Diebold, U.; Koplitz, L. V.; Dulub, O. *Applied Surface Science* **2004**, *237*, 336–342, Proceedings of the Seventh International Symposium on Atomically Controlled Surfaces, Interfaces and Nanostructures.

[144] Neri, G.; Bonavita, A.; Rizzo, G.; Galvagno, S.; Capone, S.; Siciliano, P. *Sensors and Actuators B: Chemical* **2006**, *114*, 687–695.

[145] Chauvin, C.; Saussey, J.; Lavalley, J.-C.; Idriss, H.; Hindermann, J.-P.; Kiennemann, A.; Chaumette, P.; Courty, P. *Journal of Catalysis* **1990**, *121*, 56–69.

[146] Kattel, S.; Ramírez, P. J.; Chen, J. G.; Rodriguez, J. A.; Liu, P. *Science* **2017**, *355*, 1296–1299.

[147] Macedo, H. P. d.; Medeiros, R. L. B. d. A.; Medeiros, A. L. d.; Oliveira, Â. A. S. d.; Figueredo, G. P. d.; Melo, M. A. d. F.; Melo, D. M. d. A. *Materials Research* **2017**, *20*, 29–33.

[148] Seko, A.; Yuge, K.; Oba, F.; Kuwabara, A.; Tanaka, I. *Physical Review B* **2006**, *73*, 184117.

[149] Lahmer, M. *Surface Science* **2018**, *677*, 105–114.

[150] Battiston, S.; Rigo, C.; Severo, E. d. C.; Mazutti, M. A.; Kuhn, R. C.; Gündel, A.; Foletto, E. L. *Materials Research* **2014**, *17*, 734–738.

[151] Bocanegra, S.; Ballarini, A.; Zgolicz, P.; Scelza, O.; De Miguel, S. *Catalysis Today* **2009**, *143*, 334–340.

[152] Okal, J.; Zawadzki, M. *Applied Catalysis B: Environmental* **2011**, *105*, 182–190.

[153] Liu, Q.; Wang, L.; Wang, C.; Qu, W.; Tian, Z.; Ma, H.; Wang, D.; Wang, B.; Xu, Z. *Applied Catalysis B: Environmental* **2013**, *136*, 210–217.

[154] Elvers, B., et al. *Ullmann's encyclopedia of industrial chemistry*; Verlag Chemie, 1991.

[155] Heim, L. E.; Konnerth, H.; Prechtl, M. H. G. *Green Chem.* **2017**, *19*, 2347–2355.

[156] Bahmanpour, A. M.; Hoadley, A.; Tanksale, A. *Reviews in Chemical Engineering* **2014**, *30*, 583–604.

[157] Millar, G. J.; Collins, M. *Industrial & Engineering Chemistry Research* **2017**, *56*, 9247–9265.

[158] Deshmukh, S.; van Sint Annaland, M.; Kuipers, J. *Applied Catalysis A: General* **2005**, *289*, 240–255.

[159] Chen, Z.; Mao, Y.; Chen, J.; Wang, H.; Li, Y.; Hu, P. *ACS Catalysis* **2017**, *7*, 4281–4290.

[160] Tao, L.; Shi, Y.; Huang, Y.-C.; Chen, R.; Zhang, Y.; Huo, J.; Zou, Y.; Yu, G.; Luo, J.; Dong, C.-L.; Wang, S. *Nano Energy* **2018**, *53*, 604–612.

[161] Li, H.; Wu, X.; Tao, X.; Lu, Y.; Wang, Y. *Small* **2020**, *16*, 2001135.

[162] Selivanova, A. V.; Demina, V. G.; Aydakov, E. E.; Saraev, A. A.; Kaichev, V. V.; Bukhtiyarov, V. I. *Applied Surface Science* **2022**, *579*, 152140.

[163] Marcinkowski, M. D.; Yuk, S. F.; Doudin, N.; Smith, R. S.; Nguyen, M.-T.; Kay, B. D.; Glezakou, V.-A.; Rousseau, R.; Dohnálek, Z. *ACS Catalysis* **2019**, *9*, 10977–10982.

[164] Nalajala, N.; Salgaonkar, K. N.; Chauhan, I.; Mekala, S. P.; Gopinath, C. S. *ACS Applied Energy Materials* **2021**, *4*, 13347–13360.

[165] Wong, G. S.; Kragten, D. D.; Vohs, J. M. *The Journal of Physical Chemistry B* **2001**, *105*, 1366–1373.

[166] Feng, T.; Vohs, J. *Journal of Catalysis* **2004**, *221*, 619–629.

[167] Elmorsi, T. M.; Elsayed, M. H.; Bakr, M. F. *Canadian Journal of Chemistry* **2017**, *95*, 590–600.

[168] Venu Gopal, V.; Kamila, S. *Applied Nanoscience* **2017**, *7*, 75–82.

ABSTRACT

Name of the Student: Shweta Mehta **Registration No.:** 10CC16A26016
Faculty of Study: Chemical Science **Year of Submission:** 2023
AcSIR academic centre/CSIR Lab: CSIR-NCL **Name of the Supervisor:** Dr. Kavita Joshi
Title of the thesis: Investigating Interaction of Methanol with Various Surfaces by Employing Periodic Density Functional Theory

---

Continuous efforts are going on to design environmentally benign catalysts than the existing ones. The rational designing of a catalyst would demand understanding the interaction of a molecule with different facets and distilling out the essential factors leading to desired products. Density functional theory (DFT) is a method that describes catalytic reactions at surfaces with the detail and accuracy required for computational results to be meaningfully compared to experiments.

In this thesis, we have investigated various Zn-based catalysts for their interaction with methanol (MeOH). MeOH is one of the most critical molecules being studied extensively, and Zn-based catalysts are widely used in many industrially relevant reactions involving MeOH. We studied the interaction of methanol with different facets of many Zn-based systems, including pure metallic Zn, oxygen-preadsorbed Zn, ZnO, and $ZnAl_2O_4$. We observed that the same element (Zn and O, in the present study) exhibits different catalytic activity in different environments. The changing environment is captured in the underlying electronic structure of the catalysts. We demonstrate the one-to-one correlation between the electronic structure of the bare facet and the outcome of that facets interaction with MeOH. By carefully analyzing the site-specific projected density of states of these facets, we report that the existence of energy states of oxygen, metal, or both at or near the Fermi level has a substantial influence on the dissociation of MeOH on that particular facet. The adsorption of MeOH in the vicinity of oxygen, which has non-zero energy states at Fermi, is essential for dissociating methanol. However, it is not sufficient to have non-zero states at Fermi. The orientation of methanol plays a crucial role in determining the outcome.

The ultimate goal of any DFT-based computation is to deduce trends and gain predictive power by understanding the results in terms of underlying electronic structure. This work presents an attempt in that direction.

Details of the Publications Emanating from the Thesis Work

1) **List of publication(s) in SCI Journal(s) (published & accepted) emanating from the thesis work, with complete bibliographic details.**

(i) **Shweta Mehta,** Sheena Agarwal, Nivedita Kenge, Siva Prasad Mekala, Vipul Patil, T. Raja, and Kavita Joshi. "Mixed metal oxide: A new class of catalyst for methanol activation." *Applied Surface Science* 534 (2020): 147449.

DOI: https://doi.org/10.1016/j.apsusc.2020.147449

(ii) **Shweta Mehta,** and Kavita Joshi. "From molecular adsorption to decomposition of methanol on various ZnO facets: A periodic DFT study." *Applied Surface Science* 602 (2022): 154150.

DOI: https://doi.org/10.1016/j.apsusc.2022.154150

(ii) **Shweta Mehta,** and Kavita Joshi. "Electronic fingerprints for diverse interactions of methanol with various Zn-based systems" Recently Accepted in *Surface Science* (2023).

DOI: https://doi.org/10.1016/j.susc.2023.122350

2) **List of Papers with abstract presented (oral/poster) at national/international conferences/seminars with complete details.**

(i) Presented a poster entitled "*Catching the essence of Hohenberg-Kohn's first theorem while recreating PES for small cluster with machine learning*" at the school on Modelling and Simulations of Materials for Energy and the Environment, during December 2018 at JNCASR Bengaluru.

Abstract: Density functional theory (DFT) is currently one of the most accurate and yet practical theories used to gain insight into the properties of materials. Although successful, the computational cost required is still the main hurdle even today. In recent years, there has been a trend of combining DFT with Machine Learning (ML) to reduce the computational cost without compromising accuracy. Finding the right set of descriptors that are simple to understand in terms of giving insights about the problem at hand, lies at the heart of any ML problem. In this work, we demonstrate the use of nearest neighbor (NN) distances as descriptors to predict the interaction energy between the cluster and an adsorbate. The model is trained over a size range of 5 to 75 atom clusters. When the training and testing is carried out on mutually exclusive cluster sizes, the mean absolute error (MAE) in predicting the interaction energy is ~ 0.24 eV. MAE reduces to 0.1 eV when testing and training sets

include information from the complete range. Furthermore, when the same set of descriptors are tested over individual sizes, the MAE further to ~ 0.05 eV. We bring out the correlation between dispersion in the nearest neighbor distances and variation in MAE for individual sizes. Our detailed and extensive DFT calculations provide a rationale as to why nearest neighbor distances work so well. Finally, we also demonstrate the transferability of the ML model by applying the same recipe of descriptors to systems of different (N_2, O_2, and CO). elements like (Na_{10}), bimetallic systems (Al_6Ga_6, Li_4Sn_6, and $Au_{40}Cu_{40}$) and also different adsorbates.

(**ii**) Presented a poster entitled "*Catching the essence of Hohenberg-Kohn's first theorem while recreating PES for small cluster with machine learning*" during National Science Day Celebrations at CSIR-National Chemical Laboratory, Pune, India, February 2019.

Abstract: See the abstract for entry (**i**).

(**iii**) Presented an oral talk entitled "*Insights from DFT: Interaction of Methanol with Catalysts*" at the Annual Students' Conference 2021, organized by NCL Research Foundation & CSIR-NCL, Pune.

Abstract: Methanol has a potential to replace the existing fuels. It is also a prominent hydrogen source. However, breaking of its O-H and/or C-H bond is required for using it as a fuel or source of hydrogen. The edisonian approach of catalyst improvement or discovery demands humongous lab scale experiments, which are costly and time consuming. Use of computation offers not only flexibility but also accelerate the search by providing a platform to carry out virtual experiments. Since the computation is based on solid foundations of Density Functional Theory (DFT), the underlying electronic structure provides atomistic level insights about functioning of a catalyst. In this talk, I would like to discuss about two investigations where we implemented DFT to unravel interaction of methanol with catalyst. In one of the study, I will be discussing about a mixed metal oxide which has been experimentally synthesized and demonstrated for better activity of methanol. With the help of DFT we provide rationale as to why this mixed metal oxide works better for methanol dissociation. While in another study, we propose interaction of methanol with stepped facets of metal oxide which has not been investigated so far.

(**iv**) Presented an oral talk entitled "Interaction of methanol with metal oxide: from computation to experiments." at the 2nd International Conference on Materials Genome (ICMG-II) at SRM University, Andhra Pradesh in March, 2022.

Abstract: Metal oxides exhibits better catalytic activity than pure metals due to the presence of acidic and basic sites on their surface. Metal oxides are essential catalyst in synthesis of various value added chemicals via oxidation, dehydrogenation, acid-base reactions etc. Methanol, being a prominent hydrogen source, has a potential to replace the existing fuels. However, conversion of methanol to any value added product, requires breaking of its O-H and/or C-H bond. The Edisonian approach of catalyst improvement or discovery demands

humongous lab scale experiments, which are costly and time consuming. Use of computation offers not only flexibility but also accelerate the search by providing a platform to carry out virtual experiments. Since the computation is based on solid foundations of Density Functional Theory (DFT), the underlying electronic structure provides atomistic level insights about functioning of a catalyst. Here, I would like to discuss about employment of DFT to unravel interaction of methanol with metal oxide and mixed metal oxide. Our DFT investigations show spontaneous dissociation of O-H bond of methanol on both the surfaces. Different facets of a catalyst exhibits different activity towards methanol. With the help of electronic structure, we provide rationale as to why these surfaces works better for methanol dissociation. The metal oxide surface presents spontaneous dehydrogenation of methanol to formaldehyde. To validate the DFT results, we designed lab scale experiment on the metal oxide, which also indicates synthesis of formaldehyde at ambient conditions.

Applied Surface Science 596 (2022) 153599

Contents lists available at ScienceDirect

Applied Surface Science

journal homepage: www.elsevier.com/locate/apsusc

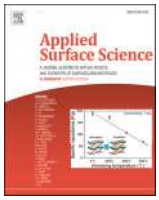

Corrigendum

Corrigendum to "Mixed metal oxide: A new class of catalyst for methanol activation" [Appl. Surf. Sci. 534 (2020) 147449]

Shweta Mehta [a,c,1], Sheena Agarwal [a,c,1], Nivedita Kenge [a,c], Siva Prasad Mekala [b], Vipul Patil [b], T. Raja [b,c], Kavita Joshi [a,c]

[a] Physical and Materials Chemistry Division, CSIR-National Chemical Laboratory, Dr. Homi Bhabha Road, Pashan, Pune 411008, India
[b] Catalysis Division, CSIR-National Chemical Laboratory, Dr. Homi Bhabha Road, Pashan, Pune 411008, India
[c] Academy of Scientific and Innovative Research (AcSIR), Sector 19, Kamla Nehru Nagar, Ghaziabad, Uttar Pradesh 201002, India

The authors regret, Our paper is published in Applied surface science. [https://doi.org/10.1016/j.apsusc.2020.147449]. However by mistake old address of AcSIR appears in published article instead of new. The new address of AcSIR is updated as above.
The authors would like to apologise for any inconvenience caused.

DOI of original article: https://doi.org/10.1016/j.apsusc.2020.147449.
E-mail addresses: t.raja@ncl.res.in (T. Raja), k.joshi@ncl.res.in (K. Joshi).
[1] Shweta Mehta and Sheena Agarwal contributed equally.

https://doi.org/10.1016/j.apsusc.2022.153599

Available online 9 May 2022
0169-4332/© 2020 Elsevier B.V. All rights reserved.

Applied Surface Science 534 (2020) 147449

Contents lists available at ScienceDirect

Applied Surface Science

journal homepage: www.elsevier.com/locate/apsusc

Mixed metal oxide: A new class of catalyst for methanol activation

Shweta Mehta[a,c,1], Sheena Agarwal[a,c,1], Nivedita Kenge[a,c], Siva Prasad Mekala[b], Vipul Patil[b], T. Raja[b,c], Kavita Joshi[a,c]

[a] Physical and Materials Chemistry Division, CSIR-National Chemical Laboratory, Dr. Homi Bhabha Road, Pashan, Pune 411008, India
[b] Catalysis Division, CSIR-National Chemical Laboratory, Dr. Homi Bhabha Road, Pashan, Pune 411008, India
[c] Academy of Scientific and Innovative Research (AcSIR), Anusandhan Bhawan, 2, Rafi Marg, New Delhi 110001, India

ARTICLE INFO

Keywords:
$ZnAl_2O_4$
MeOH
DFT
Spontaneous dissociation

ABSTRACT

In this work, we propose a mixed metal oxide as a catalyst and demonstrate it's ability to not only activate the MeOH molecule upon adsorption but also dissociate O—H and one of it's C—H bonds. MeOH activation is compared on two prominent facets of $ZnAl_2O_4$ viz. (2 2 0) and (3 1 1). While spontaneous O—H bond dissociation is observed on both facets, C—H bond dissociates only on the (3 1 1) surface. Multiple factors like atomic arrangement and steps on the surface, coordination of surface atoms, and their effective charges have a combined effect on MeOH activation. The (3 1 1) surface offers higher catalytic activity in comparison with (2 2 0) surface. Having a stepped surface, availability of multiple sites, and variation in the charge distribution are some of the reasons for better catalytic performance of (3 1 1) facet. Effect of orientation of MeOH with respect to the surface adds both, information and complexity to the problem. Observations pertinent to understanding this effect are also reported. A detailed analysis of atomic arrangement on the two surfaces provides a rationale as to why MeOH gets dissociated spontaneously on the mixed metal oxide. The promising results reported here opens up a new class of catalyst for research.

1. Introduction

Methanol (MeOH), the simplest aliphatic alcohol is a commodity chemical and produced in large quantities. It is used in production of many hydrocarbons like gasoline, olefins, as well as chemicals such as formaldehyde, dimethyl ether to name a few [1,2]. It is also being considered as a source of fuel in direct methanol fuel cells [3,4]. Irrespective of the end product, conversion of MeOH requires one or more of O—H, C—H, and/or C—O bond activation and hence its adsorption and decomposition has been studied extensively by both experimental [5–15] as well as theoretical means [16–29]. Amount of activation in terms of either binding energies or bond lengths, activation barriers for O—H or one of the C—H bond scission along with factors influencing the activation are investigated in these studies. Activation of methanol over different types of materials like transition metal surfaces [30–41], metal clusters [8,34,42,43], binary metal alloys [44,45,43,46–50], metal oxides [20,50–65], and zeolites [28,29] is studied extensively. Among the various studies on transition metal surfaces, enhanced MeOH activation and hence lowered activation barriers are reported on surfaces with preadsorbed oxygen [31,32].

Methanol activation is also investigated theoretically on various binary metal alloys like CoPt [44,45], NiPt [47], NiAl [43,46], PdZn [50] etc. In a combined experimental and theoretical study, Skoplyak et. al. investigates methanol reactivity trends on bimetallic surfaces like NiPt(1 1 1) and CoPt(1 1 1). Their results reveal an interesting correlation between the methanol and methoxy binding energies, and the d-band center of various NiPt(1 1 1) and CoPt(1 1 1) bimetallic surfaces [44]. In an another interesting study, Lawrence et. al. demonstrate the C—O bond weakening over NiAl(1 0 0) facet which leads to ejection of the methyl group from methanol [43]. Du et. al. report that on Pt_3Ni (1 1 1), less electronegative Ni atoms are more favorable for adsorbing radical intermediates and intermediates with lone-pair electrons (such as O-containing species). They also conclude that out of the possible bond scissions, O—H bond scission is the most favorable [47]. In a study by Smith et. al., a detailed analysis of MeOH activation and different pathways through which it can undergo dissociation is reported on various PdZn facets [50]. Their calculations indicate that the dissociation of both methanol and water is highly activated on flat surfaces of PdZn such as (1 1 1) and (1 0 0), while the dissociation barriers can be lowered significantly by surface defects, like (2 2 1), (1 1 0), and (3 2 1) faces of PdZn.

Due to presence of both acidic and basic sites on metal oxide

E-mail addresses: t.raja@ncl.res.in (T. Raja), k.joshi@ncl.res.in (K. Joshi).
[1] Shweta Mehta and Sheena Agarwal contributed equally.

https://doi.org/10.1016/j.apsusc.2020.147449
Received 10 April 2020; Received in revised form 24 June 2020; Accepted 2 August 2020
Available online 13 August 2020
0169-4332/ © 2020 Elsevier B.V. All rights reserved.

surfaces, they are considered to be more efficient for wide variety of catalytic reactions. MeOH adsorption has also been studied on various metal oxide surfaces such as CeO_2 [20], MgO [42,51,64,65], Cr_2O_3 [52], Cu_2O [53], TiO_2 [54,55], Al_2O_3 [18,52,56], ZnO [50,57], β-Ga_2O_3 [58], etc. Riguang et. al. highlight the role of preadsorbed oxygen on Cu_2O (1 1 1) surface in O—H bond dissociation [53]. Their DFT based calculations show that the O—H bond dissociation path has the lowest activation barrier 0.28 eV. Oxygen-precovered Cu_2O (1 1 1) surface exhibits high surface reactivity towards the formation of CH_3O^- by the O—H bond-cleavage, and reduces the activation barrier for O—H bond cleavage. For activation of methanol over MgO surfaces, Branda et. al. explains the important role of coordination numbers for reactivity of adsorbate. They report that oxide surface atoms with different coordination numbers show very different reactivity giving both molecular and dissociated adsorbed species [42,64,65]. Recent study by Liu et. al. reports spontaneous dissociation of methanol over CeO_2 (1 1 0) facet. Further, dissociation on the (1 1 0) surface of CeO_2 is site selective and dissociation does not occur at all on the (1 1 1) surface, where only physisorption was found. Their analysis of surface geometries shows that dominant factors for the dissociation of methanol are under-coordinated surface atoms with their varying charges [61].

Today, ZnO/Al_2O_3 catalysts are the most relevant industrial catalyst for methanol synthesis. DFT based studies in this direction are geared to understand the surface chemistry [18,50,52,56,57]. In a study, Borck et. al. show that while methanol adsorption is not dissociative on α-Al_2O_3 (0 0 0 1) in the absence of co-adsorbed H atoms, their results for methanol adsorption on α-Cr_2O_3 (0 0 0 1) indicate that dissociation may take place to obtain the energetically preferred methoxy adsorption [52]. In another study by the same group, adsorption of methanol on Al_2O_3 surface is shown to have maximum O—H bond elongation up to 1.02 Å. They also studied the decrease in the adsorption energy with increasing monolayer coverage of methanol on the surface [18]. In yet another study catalytic dehydration of methanol to dimethyl ether over modified γ-Al_2O_3 with Nb_2O_5 catalysts were investigated [56]. The conversion of methanol was reported to be enhanced due to Nb_2O_5 modification as it increased the number and reduced the strength of these acidic sites at lower temperatures. Vo et. al. studied the adsorption and decomposition of methanol on ZnO (1 0 1 0) surface. The O—H bond of MeOH elongates up to 1.05 Å. The MeOH dehydrogenation to methoxy has an activation barrier of 0.56 eV and subsequent dehydrogenation of methoxy to formaldehyde has an activation barrier of 1.20 eV [57]. Smith et. al. report an activation barrier of 0.39 eV for dissociation of methanol over defect free polar ZnO(0 0 0 1) surface [50].

As we have discussed, MeOH activation is extensively studied on metals, binary alloys as well as metal oxide surfaces by employing DFT based computation. However, to the best of our knowledge, MeOH activation on a mixed metal oxide is not yet studied. In the present work we investigate the nature of interaction between a methanol molecule and a mixed metal oxide prepared by combining Al_2O_3 and ZnO to form $ZnAl_2O_4$. We demonstrate that activation as well as spontaneous dissociation of O—H and one of it's C—H bonds takes place on this mixed metal oxide catalyst. Study of MeOH activation on (3 1 1) and (2 2 0) surfaces of $ZnAl_2O_4$ were chosen particularly because their stability has been confirmed in XRD peaks [66–70]. Overall, it was observed that both surfaces offer sites that activate as well as dissociate O—H bond in MeOH. Adsorption and activation of O—H bond was observed with varying strengths on both surfaces. (3 1 1) in particular proved to offer greater catalytic activity than (2 2 0). Not only O—H but also C—H bond dissociation was observed on (3 1 1) surface.

2. Computational details

All the calculations were carried out within the Kohn-Sham formalism of density functional theory (DFT). Projector Augmented Wave potential [71,72] was used, with Perdew Burke Ehrzenhof (PBE)[73] approximation for the exchange-correlation and generalized gradient approximation, [74] as implemented in planewave, pseudopotential based code, Vienna Ab initio Simulation Package (*VASP*) [75–77]. The bulk unit cell was taken from the materials project [78] and optimized. The bulk lattice constant without applying DFT + U correction is 8.0640 Å which is in excellent agreement with the experimentally measured lattice parameter 8.0779 Å [70]. Two different facets, (2 2 0) and (3 1 1) of $ZnAl_2O_4$ were modeled as slab by cleaving a surface with 4 layers in 220 (3 1 1) direction with pymatgen [79]. Van der Waals corrections were applied to all the calculations. The vacuum along z-axis which is also adjusted as 220 (3 1 1) direction of the crystal, was varied from 15 Å till 25 Å with the step of 2.5 Å. It was found that 20 Å of vacuum was sufficient to avoid interaction between adjacent images of planes along the z-direction. Geometry optimization was carried out with a force cutoff of 0.05 eV/Å on the unfixed atoms and the total energies were converged below 10^{-4} eV for each SCF cycle. A Monkhorst-Pack grid of 6x4x1 was used which resulted into 12 k-points in IBZ to emulate the solid slab. Entire surface was scanned by placing the MeOH molecule at unique available sites. To compare the adsorption on these sites, adsorption energy was calculated using the formula: $E_{ads} = E_{system} - E_{surface} - E_{molecule}$ where E_{system} is energy of the system when MeOH is placed on the surface, $E_{surface}$ is energy of the bare surface and $E_{molecule}$ is energy of the MeOH molecule. To understand the site specific adsorption pattern, the site-dependent projected Density of States (*pDOS*) were calculated with denser k-mesh using LOBSTER [80–83]. Mulliken charges were calculated for all the atoms on the surface which provided insights about the quantitative charge transfer.

3. Results and discussion

$ZnAl_2O_4$ is a normal spinel metal oxide with a cubic lattice and $Fd\bar{3}m$ space group [84]. In this spinel compound, oxide ions occupy the Wyckoff position and form a face-centered cubic sublattice where Zn^{+2} ions occupy tetrahedral sites while Al^{+3} occupy octahedral sites. These Zn^{+2} ions are coordinated with four nearest neighbor oxygens whereas the Al^{+3} ions have six oxygen atoms as their nearest neighbors in the bulk structure. In case of $ZnAl_2O_4$, since the surface is polar, it could be terminated in two different ways, and it has been demonstrated that AlO_2 terminated surface is favored over $ZnAlO_2$ termination [85]. (2 2 0) and (3 1 1) are the most prominent peaks in the XRD pattern of $ZnAl_2O_4$ and hence we have chosen to study these surfaces for MeOH adsorption [66–70].

3.1. Interaction of MeOH with $ZnAl_2O_4$ (2 2 0) surface

The (2 2 0) is flat and comparatively more symmetric than a stepped surface and is shown in Fig. 1. Since, it is a polar surface, it can be terminated in two different ways, through AlO_2 or $ZnAlO_2$. We model the AlO_2 termination, where the top most layer of the surface is rich in Al and O atoms. Zn atoms are present in the subsurface layer and are not available to act as an active site for adsorption of an incoming MeOH molecule. As will be explained in detail later, the relative arrangement of atoms on the surface changes the environment that an incoming adsorbate experiences. The nature of bonding is hence influenced due to the changing surface catalyst environment.

As a first step towards understanding MeOH adsorption on this facet, most favored orientation of MeOH was investigated by studying it's adsorption through C, O, H_{OH} (H attached to O in MeOH) and H_{CH} (H attached to C in MeOH). When MeOH is placed through carbon or H_{CH} on the surface, the molecule does not adsorb thus indicating that these are the unfavored orientations for adsorption. When MeOH is placed through oxygen or H_{OH} on the surface, the molecule changes its orientation and adsorbs with its oxygen atom pointing towards the surface. Thus, the most favorable orientation of MeOH is when it adsorbs via its oxygen atom and all the initial configurations hence forth have MeOH placed by pointing its oxygen towards the surface.

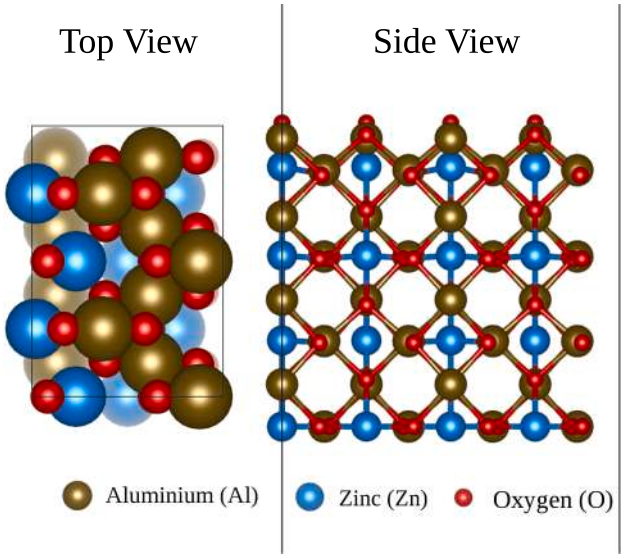

Fig. 1. The (2 2 0) surface of $ZnAl_2O_4$ with the top view and the side view. The top-most layer of (2 2 0) surface consist of Al and O atoms.

However, let's note that even this favorable position of MeOH can have many relative orientations wrt surface atoms as shown in Fig. 2 which leads to the variation in adsorption energy for the same adsorption site. Fig. 2 explains manifold possibilities that exist due to the relative orientation of MeOH wrt the surface. Rotation around the normal to the surface (N_{surf}), change in the angle between N_{surf} and OC axis of MeOH, and rotation around OC axis of the MeOH results into many possibilities in which a molecule can interact with the surface when placed at a specific site. In all these cases, change in the relative orientation of MeOH wrt surface will affect the interaction between surface and MeOH. The effect of this relative orientation is explained in detail later and it turns out to be an important factor in understanding adsorption energy as well as bond activation trends.

All the unique sites are scanned on (2 2 0) surface by placing MeOH through O. This includes on top sites of Al as well as subsurface Zn, various bridge sites between Al—Al, Al—Zn, Al—O, Zn—O as well as hollow positions. All these sites where MeOH was placed as starting configuration are shown schematically in Fig. 3-a and the final positions of MeOH upon adsorption are shown in Fig. 3-b. As Fig. 3-b indicates MeOH adsorbs on surface Al in most of the cases. However, there are few cases where it also gets adsorbed on a bridge or at a hollow position. We report the adsorption energies E_{ads}, O—H bond activation, metal-O_{MeOH} (O of MeOH) distance and H_{OH}-O_{surf} (surface oxygen) distances in Table 1. The observation table is divided in three parts based on the amount of activation O—H bond undergoes and adsorption site. It was observed that the trends in the activation of the O—H bond could be understood if we systematically investigate the nearby environment of the adsorption site. The first class comprises of cases where the O—H bond in methanol was barely activated from 0.97 Å to 0.98–1.00 Å. The second class includes all cases for which the O—H bond activation was greater than 1.00 Å, i.e. between 1.01 Å to 1.04 Å. An important observation made during the adsorption studies was that irrespective of initial orientation of O—H bond, finally the bond would orient itself such that the H_{OH} would face nearest surface oxygen. The entire molecule gets stably adsorbed on top of the nearest Al atom reorienting its H facing the nearby surface oxygen. This observation can also be realized by investigating the H_{OH}-O_{surf} distances in Table 1. For cases where O—H bond activation is not more than 4–5% (class I) the distance of O_{surf} from H_{OH} is in the range of 1.74 Å to 2.12 Å. Whereas for the class II cases, with an activation up to 7–9%, the distance between H_{OH} and O_{surf} reduces to 1.52 Å–1.67 Å. The proximity of surface oxygen atom and reorientation of O—H bond explains the trends in OH bond activation of methanol over the surface.

The adsorption energies for most of the cases in these two classes also follow a trend wherein overall adsorption energies for class II are more than that of class I. The third class of cases, i.e. positions 9, 7, and 6, are the ones that do not adsorb directly on top on any surface atom, but rather adsorb on either a hollow site or a bridge site. As it can be seen from Fig. 3(b), there is no Al atom directly below the adsorbed methanol. But the presence of nearby oxygen atom on surface interacts with the H from methanol leading to the O—H bond activation, as can be seen from Table 1.

Although we have scanned almost all the unique "sites" on the surface (taking into account symmetry), scanning all possible orientations of MeOH molecule wrt to a specific site is a formidable task and

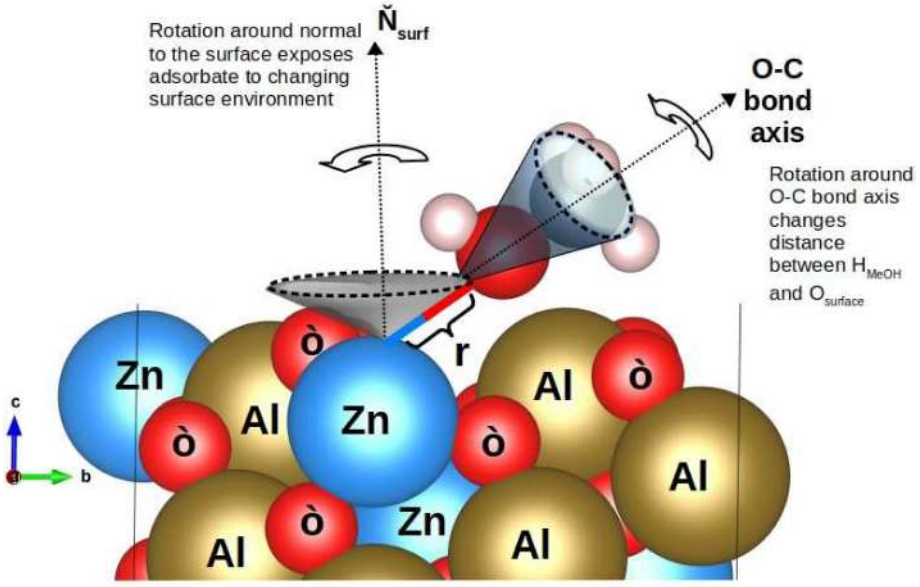

Fig. 2. Figure explains the large number of possibilities due to relative orientation of MeOH wrt the surface. Rotation around the normal to the surface, varying angle between N_{surf} and OC axis of MeOH and rotation around OC axis of the MeOH results into large number of possibilities in which molecule can interact with the surface when placed at a specific site.

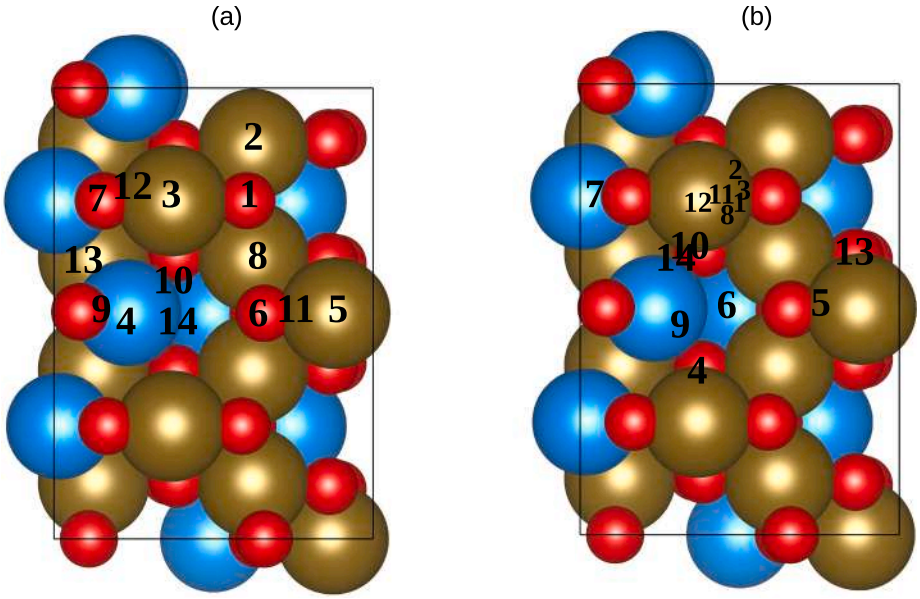

Fig. 3. The (2 2 0) surface of $ZnAl_2O_4$ shows (a) initial positions of adsorbate on the surface (b) final positions of methanol upon relaxation. It could be seen that in most of the cases irrespective of the initial position, MeOH adsorbs on surface Al.

Table 1
Adsorption energies, O—H bond activation, distance between O_{OH} and surface metal (M) atom, and H_{OH}-O_{surf} distance for adsorption studied at various positions as indicated in Column 1 on (2 2 0) (refer to Fig. 3 for site specifications).

Adsorption Site	E_{ads} (eV)	O—H Bondlengths (Å)	O—Al distance (Å)	$H_{(MeOH)} - O_{surface}$ distance (Å)
		Class I - Barely activated		
4	−1.5459	1.01	1.96 -Al	1.74
8	−1.3590	1.00	1.92 -Al	1.75
2	−1.3754	1.00	1.92 -Al	1.76
11	−1.3262	1.00	1.90 -Al	1.78
3	−1.3582	0.99	1.91 -Al	1.94
12	−1.3751	0.98	1.92 -Al	2.12
		Class II - Moderately activated		
1	−1.2636	1.04	1.87 -Al	1.52
14	−1.5687	1.02	1.96 -Al	1.66
10	−1.5590	1.02	1.96 -Al	1.67
		Class III - Adsorbed on bridge/hollow		
9	−0.6603	1.01	3.62 -Zn	1.64
7	−0.6099	1.00	3.99 -Zn	1.69
6	−0.4977	0.99	4.14 -Al	2.04

still not achieved. However, to bring out the effect of "change in orientation" on the adsorption of MeOH, we have added all the distinct cases where molecule was adsorbed on the surface. This includes cases like MeOH adsorbed at same site but having different orientations. For example, in Fig. 4, MeOH is placed at 12^{th} and 14^{th} positions on (2 2 0) surface and share a common adsorption site (refer Fig. 3-b). The Al—O bond distance is nearly same in both the cases as noted in the Fig. 4. Further, the difference in adsorption energies is also less than 1 meV. However, the O—H bond activation is 0.98 Å (barely activated) in case of 12*th* position whereas 1.02 Å (moderately activated) in case of 14^{th} position. And this can be directly understood if we look at the H_{MeOH}-O_{surf} distances. This brings out the effect of orientation of the molecule on adsorption. Over the same adsorption site, it could change the surface environment experienced by atoms in the molecule and hence the resultant interaction and activation. This is applicable to molecule at position 8 and 3 in class I of (2 2 0) surface as well.

Finally, we report the case wherein O—H bond dissociation is observed, i.e. when placed at position 13 and is shown in Fig. 5. This is an important case as it represents spontaneous dissociation of O—H bond in methanol over (2 2 0) facet of $ZnAl_2O_4$. The methanol molecule in this case adsorbs on top of the same Al site on which the adsorbate at position 11 also adsorbs (a case of class I). But, adsorption of methanol on top of same surface atom yields two completely different outcomes. While in one case (position 11) we observe very little O—H bond activation, the other case (position 13) represents complete dissociation of the O—H bond in methanol. The difference lies in the relative orientation of the adsorbate with respect to the surface. The effect of orientation of adsorbate wrt surface can be understood better if we compare 8 cases (position 1, 2, 3, 8, 10, 11, 12 and 14) that adsorb on the same Al atom. All these cases share a common Al as their final adsorption site, as can be seen from Fig. 3(b). But the bond activation and adsorption energies for all these cases are not uniform. This is due to the relative orientation of the methanol molecule with respect to the catalyst surface. It must be noted at this point that the activation of an adsorbate over any catalyst surface is a complex problem which depends upon combination of multiple factors like arrangement of atoms

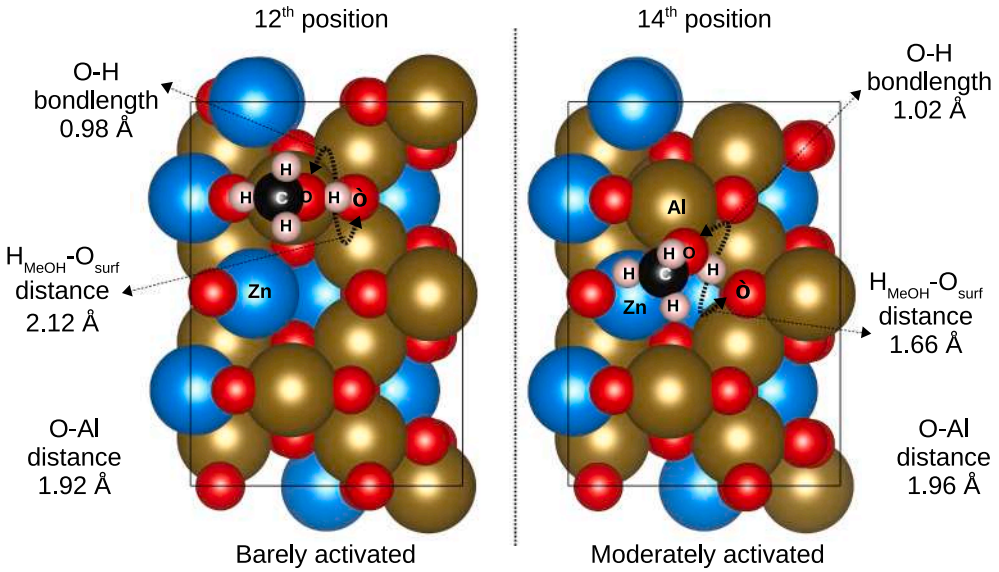

Fig. 4. MeOH is adsorbed at the same site. At 12^{th} position, the OH bond is barely activated whereas at 14^{th} position the OH bond is moderately activated, bringing out the effect of orientation and hence the resulting MeOH surface interaction.

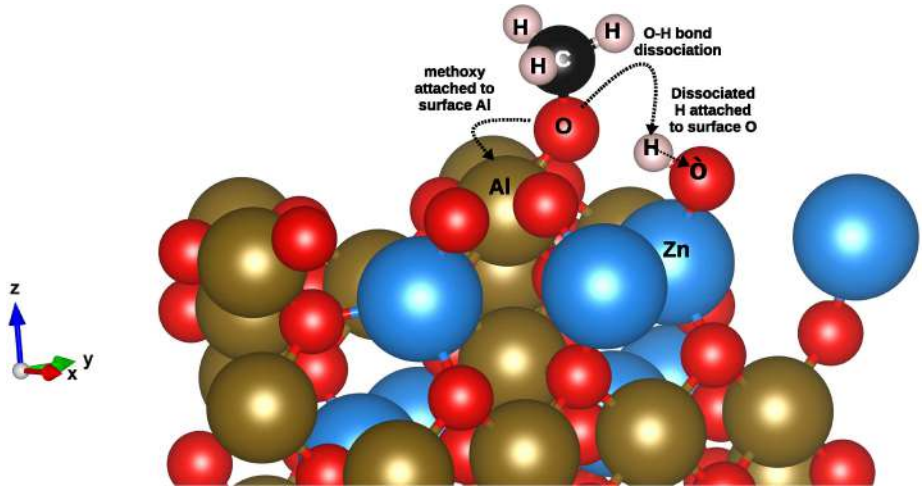

Fig. 5. OH bond dissociation on 220 facet. Surface oxygen atom is marked as Ò. Resultant methoxy group attaches to surface Al atom.

on surface, relative orientation of adsorbate, number of unique sites on surface to name a few. This picture becomes even more complex for a surface of mixed metal oxides like $ZnAl_2O_4$. The possibilities that are needed to be scanned exhaustively become manifold. And hence, bringing out one to one correlation between observed parameters of activation becomes difficult. Nonetheless, our work illustrates the effect that each of these parameters contribute towards understanding adsorption of methanol over $ZnAl_2O_4$. Overall, it is observed that (2 2 0) facet of $ZnAl_2O_4$ exhibits excellent catalytic activity towards an incoming methanol molecule. Al atoms on the surface offer activation of O—H bond in the range of 0.98 Å to 1.04 Å. Complete dissociation of O—H bond indicating spontaneous dissociation over (2 2 0) facet of $ZnAl_2O_4$ was also observed.

3.2. Interaction of MeOH with $ZnAl_2O_4$ (3 1 1) surface

(3 1 1) is a stepped and highly asymmetric surface as shown in Fig. 6. It has all the three elements, viz. Zn, Al, and O on the surface. Like (2 2 0), on (3 1 1) facet also MeOH prefers to be adsorbed via its oxygen pointing towards the surface. Due to asymmetric nature of this stepped surface, it is observed that many more adsorption sites exist as compared to (2 2 0) surface. All possible unique sites on (3 1 1) surface are scanned to study adsorption of methanol. These sites comprise of top, bridge, and hollow sites with different combinations of Al, Zn, and O. All these initial configurations are shown schematically in Fig. 7(a). The numbers indicate position where MeOH is placed for optimization. Upon relaxation, the final position of MeOH is shown schematically in Fig. 7(b). We report the adsorption energies for methanol on (3 1 1) surface along with various bonds lengths in Table 2.

The same scheme for classification, as used for cases on (2 2 0), is employed to analyze the adsorbed cases on (3 1 1) surface. The adsorbed cases based on O—H bond activation are divided into three classes viz. class I - bare minimum activation of O—H bond (0.98 Å–0.99 Å), class II - higher activation (1.03 Å–1.10 Å), and class III - adsorption on bridge/hollow sites. For (3 1 1) surface it was observed that Zn as well as Al atoms acted as active sites for adsorption with varying strengths. The trend between O—H bond activation and presence of a nearby oxygen atom on surface still holds. The distance of O_{surf} atom from H_{OH} in class I ranges between 1.96 Å and 2.36 Å and the corresponding O—H bond activation is in the range of 0.98 Å–0.99 Å (from initial 0.97 Å). When the distance between O_{surf} and reoriented H_{OH} atom reduces to 1.36 Å–1.58 Å, a greater activation of O—H bond, from 1.03 Å to 1.10 Å, is seen. For the adsorption energies, it is observed that generally the adsorption energies for class II

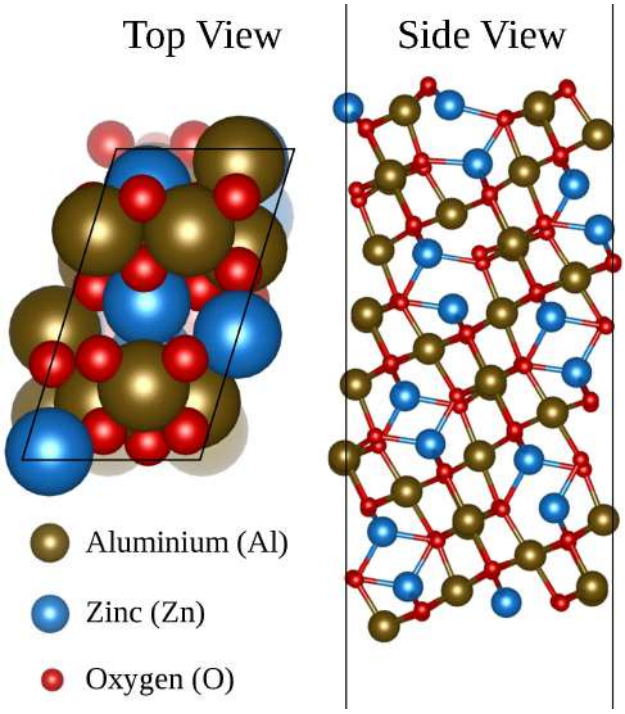

Fig. 6. The (3 1 1) surface of $ZnAl_2O_4$ with the top view and the side view. The (3 1 1) surface has topmost layer composed of Zn, Al and O atoms.

are higher than that of class I. Class III mainly comprises of cases that adsorb at either a bridge or a hollow site and interact mainly via the H_{OH} atom of methanol molecule. The presence of surface oxygen in vicinity explains the bond activation in these cases. However, the adsorption energies for this class are observed to be the least, within 1 eV, when compared with that of other classes.

Interestingly, on (3 1 1) two cases of dissociation are observed viz. one of O—H and other of both O—H and C—H bond dissociation and are shown in Fig. 8-a and b respectively. When the methanol molecule is placed in the vicinity of a surface Zn atom (as seen in 11*th* position), it dissociated to give away it's H atom to a nearby surface oxygen atom as shown in Fig. 8-a. The methoxy group after loosing it's H adsorbs on Zn atom. Again the effect that orientation of molecule plays in governing the adsorption can be seen if we compare the cases of 6, 7 (from class II) and 11. We see that methanol when adsorbed on top of same Zn atom (as seen from Fig. 7-b) results into different outcomes, with dissociation of O—H bond in one case (position 11) (see Fig. 8-a), very high activation of O—H bond (O—H bond stretches to 1.10 Å) in the other (position 7), and considerable activation up to 1.03 Å in the third case (position 6). The second case of dissociation (see Fig. 8-b) is even more interesting as it undergoes dissociation of not only O—H bond but also one of the C—H bonds in methanol. It was observed that the methanol molecule first loses it's H_{OH} and further another H connected to C. The adsorption of methanol in this case is not directly on top of any surface atom but instead at a hollow site where both the dissociated H atoms had surface oxygen atoms in the vicinity. After dissociation of two H from methanol, the remaining H_2CO group adsorbs on a nearby Al site as shown in Fig. 8-b. This case is particularly very important as it indicates spontaneous dissociation of both O—H and C—H bonds from methanol molecule. We also understand that the observed effect is a combined output of various factors like environment of surface as experienced by methanol, orientation of the adsorbate with respect to the surface, stepped nature of the surface and availability of surface oxygen in the vicinity of the molecule.

3.3. Comparison of (2 2 0) and (3 1 1) bare surfaces

To understand the variation in interaction of MeOH with (2 2 0) and (3 1 1) facets, we have investigated the charge distribution, projected Density of States (pDOS) and atomic arrangement of the bare surfaces. We also report the differential Mulliken charges for surface atoms. On the bare (2 2 0) surface, four Al and eight O atoms exist on the surface, available for interaction with incoming methanol. All Al atoms on the surface are equivalent in terms of environment, charge distribution and have an effective positive charge of 1.67e. Every Al atom is surrounded with four O atoms, one Zn atom and three other Al atoms. Interestingly two types of oxygen atoms exist on the surface. Four out of the eight oxygen atoms on surface are coordinated with three surface Al atoms while the remaining four are coordinated with one surface Al atom and one subsurface Zn atom. The oxygens connected with three Al atoms have a higher negative charge on them, −1.07e. While the ones

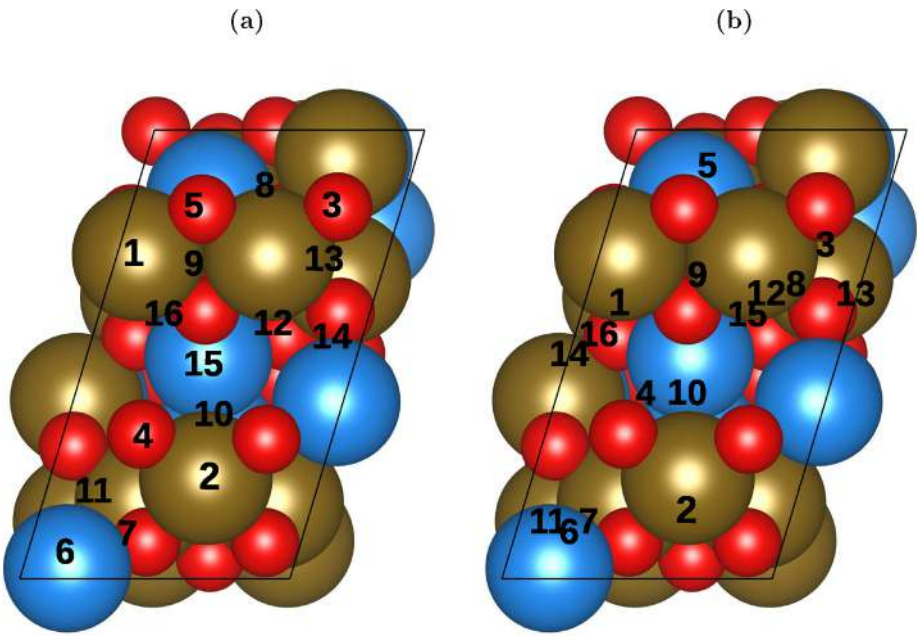

Fig. 7. (a) Initial positions of adsorbate on the surface (b) final positions of methanol upon adsorption on (3 1 1) facet.

Table 2
Adsorption energies, O—H bond activation, distance between O_{OH} and surface metal (M) atom, and H_{OH}-O_{surf} distance for adsorption studied at various positions as indicated in Column 1 on (3 1 1).

Adsorption Site	E_{ads} (eV)	O—H bondlengths (Å)	O—M distance (Å)	H_{OH}-O_{surf} distance (Å)
		Class I - Barely activated		
1	−1.1072	0.99	2.03 -Al	1.96
8	−1.2339	0.99	2.02 -Al	2.00
13	−0.8831	0.98	2.05 -Al	2.28
12	−1.2588	0.98	2.02 -Al	2.36
		Class II - Highly activated		
7	−1.3779	1.10	2.01 -Zn	1.36
16	−1.6118	1.04	1.98 -Al	1.55
6	−1.4647	1.03	2.02 -Zn	1.58
2	−0.9155	1.03	2.13 -Al	1.57
		Class III - Adsorbed on bridge/hollow		
10	−0.8264	1.04	3.40 -Al	1.54
14	−0.9464	1.02	2.97 -Zn	1.66
4	−0.7160	1.02	3.74 -Al	1.60
3	−0.4748	0.99	3.53 -Al	1.81
5	−0.4866	0.99	3.93 -Al	1.82
9	−0.5195	0.99	3.10 -Al	1.83

connected with one Zn and one Al have a negative charge of −1.03e. Thus, though Zn is not exposed on the surface, its coordination with surface oxygen changes the nature of oxygen atom on the surface. This difference in the surface oxygen can be seen in the corresponding pDOS plots, shown in Fig. 9. We denote the coordination of O atoms with Al and Zn atoms as O_{xy}, wherein x and y are the number of Al and Zn atoms coordinated with O respectively. Thus, O_{30} represents an oxygen coordinated with 3 Al and 0 Zn whereas O_{11} represents oxygen coordinated with one Al and one Zn. The pDOS plots clearly shows a shift in the peaks of more coordinated oxygen atom (O_{30} - blue) with slightly more negative charge away from the Fermi energy in comparison with the other O (O_{11} - red) that is coordinated with lesser number of atoms on the surface. Lesser coordinated O atom is observed to be lesser negative. Presence of different kinds of atoms with varying charge distribution on the surface is indeed desirable as it would offer more

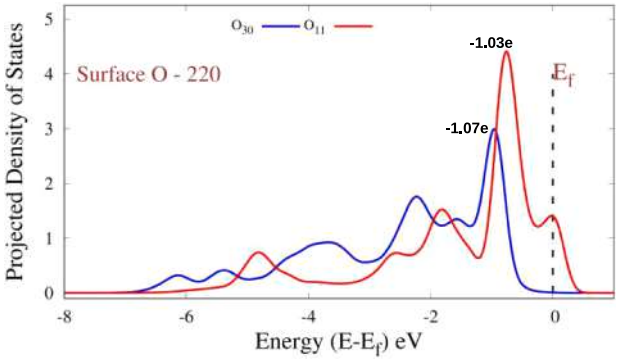

Fig. 9. pDOS plots for two types of surface oxygen atoms on (2 2 0) surface. Charges on each type of oxygen atom is mentioned in the plot. Subscripts on O_{xy} denote the coordination of O atoms, wherein x and y are the number of Al and Zn atoms coordinated with O respectively.

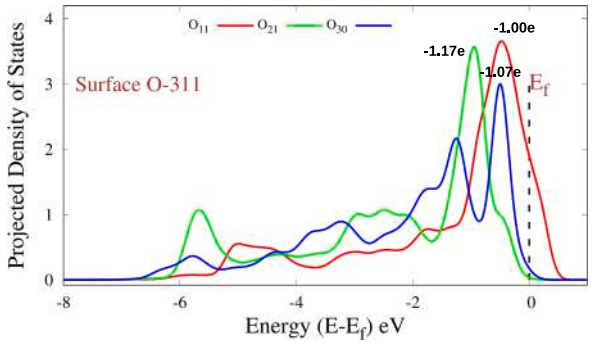

Fig. 10. pDOS plots for three types of surface oxygen atoms on (3 1 1) surface. Charges on each type of oxygen atom is mentioned in the plot. Subscripts on O_{xy} denote the coordination of O atoms, wherein x and y are the number of Al and Zn atoms coordinated with O respectively.

adsorption sites with varying strengths. On (3 1 1) surface, there are four O atoms. Out of these four, two O atoms have differential Mulliken charges of −1.00e and other two with charges −1.07e and −1.17e. Difference in the pDOS signatures can be observed for these O atoms as shown in Fig. 10. The most negatively charged surface oxygen atom

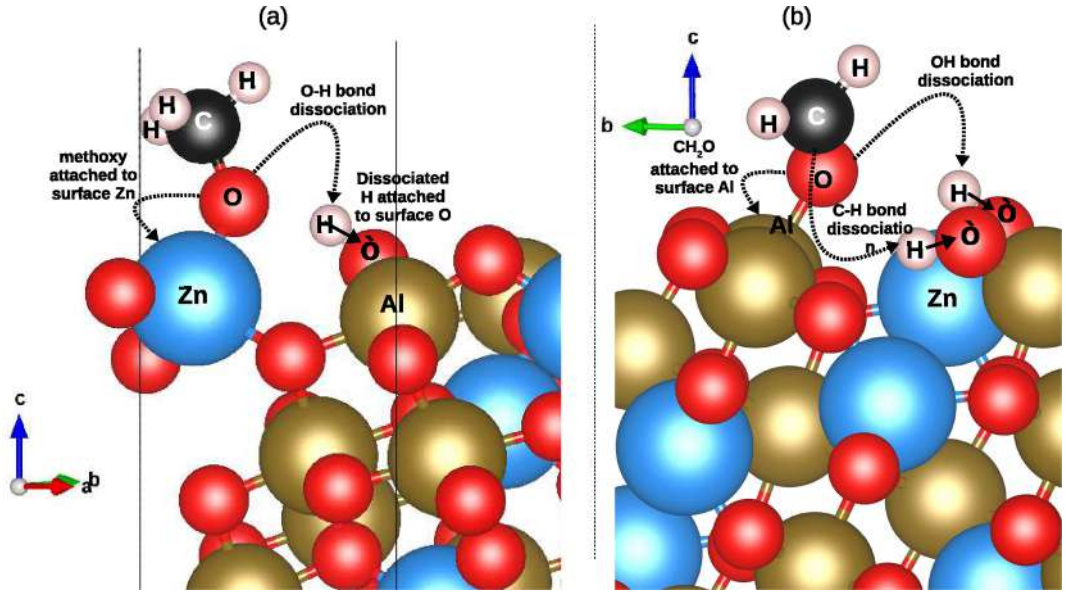

Fig. 8. Spontaneous O—H and C—H bond breaking at 311 facet. Surface oxygen atoms are indicated as Ò. When the active site is Zn(Al), the resultant methoxy group attaches to Zn(Al). The dissociated H atom attaches to surface oxygen atom (Ò).

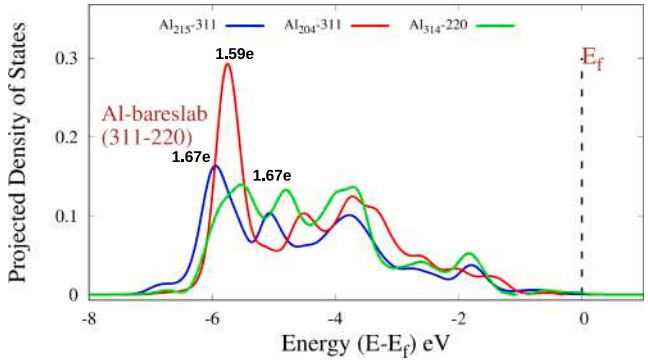

Fig. 11. pDOS plots for Al atoms on (3 1 1) and (2 2 0) surface. Charges on each of the Al atom is mentioned in the plot. Subscripts on Al_{xyz} denote the coordination of Al atoms, wherein x, y, and z are the number of Al, Zn, and O atoms coordinated with Al respectively.

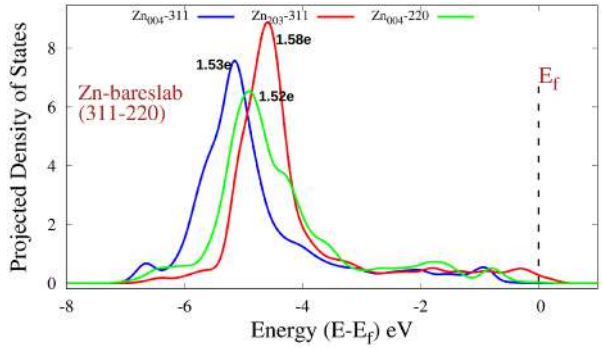

Fig. 12. pDOS plots for Zn atoms on (3 1 1) and (2 2 0) surface. Charge on each of the Zn atom is mentioned in the plot. Subscripts on Zn_{xyz} denote the coordination of Zn atoms, wherein x, y, and z are the number of Al, Zn, and O atoms coordinated with Zn respectively.

also turns out to be the most coordinated i.e. coordinated with two Al and one Zn atom (O_{21}-green) with corresponding maximum shift away from the Fermi energy. The other two oxygen atoms also follow the coordination trends wherein the least coordinated O_{11}(in red) is the closest to the Fermi energy followed by O_{30}. Further, there are two kinds of Zn atoms present on the (3 1 1) surface. One is tri-coordinated with oxygen atoms and has a resultant positive charge of 1.53e while the other Zn is tetra-coordinated with oxygen atoms and contains a charge of 1.58e. These surface Zn atoms act as sites that dissociate the O—H from methanol and also act as one of the favorable site for adsorption of methanol. Out of the three Al sites present on the surface, two have effective positive charge of 1.59e and the remaining one with 1.67e. Corresponding pDOS plots for Al and Zn atoms in (2 2 0) and (3 1 1) surface are shown in Fig. 11 and Fig. 12 respectively. A clear redistribution of energy levels can be seen in case of Al atoms over (2 2 0) vs (3 1 1) surface as shown in Fig. 11. The Al_{314} atom on (2 2 0) surface is surrounded with three Al, one Zn, and four oxygen atoms, and the corresponding pDOS (shown in green) is broad and diffuse. On the other hand, pDOS of Al_{204} (in red) and Al_{215} (in blue) atoms on (3 1 1) surface have sharp peaks at around −6 eV. Further, it is interesting to note that though Zn_{004} (in green) on (2 2 0) and Zn_{004} (in blue) on (3 1 1) have almost same charge and number of atoms in the vicinity, their peaks in Fig. 12 are evidently different. This is due to different charges on coordinated oxygen atoms. Hence, indicating that not only the immediate neighbors of an atom but the overall surface geometry plays a role in changing the chemical signatures of an atom on the surface.

Thus overall, we observe that based on Mulliken charge analysis of (2 2 0) and (3 1 1) surface, more variation in the charge distribution is observed for (3 1 1) surface in comparison with (2 2 0). This variation arises due to the step nature of (3 1 1) surface. Availability of multiple adsorption sites with varying charge distribution is indeed desirable as that allows diffusion of an adsorbate on the catalytic surface. This diffusion is very useful when the adsorbate comes in contact with another reactant. From our adsorption studies for methanol over the two surfaces, we unravel many interesting possibilities of O—H bond activation, O—H bond dissociation and also C—H bond dissociation in methanol. While (2 2 0) demonstrates a case of O—H bond activation, (3 1 1) exhibits its capacity to dissociate both O—H and C—H bonds from methanol. The O—H bond activation on (3 1 1) surface is also observed to be higher in general compared to that of (2 2 0). And hence, we propose that though both surfaces give an excellent catalytic activity towards methanol adsorption, (3 1 1) particularly performs better than (2 2 0). Our work sheds light on various factors that are essential to be considered while studying methanol interaction with mixed metal oxide surface catalysts. Though we do not exhaust all possibilities of methanol adsorption (with respect to changing orientation of methanol over surface), our work points at the immense promise these surfaces hold in terms of not only activating but also dissociating O—H and C—H bonds in methanol without any barrier.

4. Conclusion

Though adsorption of MeOH is extensively studied on varied classes of catalyst, reports of significantly low activation barrier or spontaneous dissociation of O—H as well as C—H bonds of MeOH are very limited. And hence this piece of work on proposed mixed metal oxide as catalyst becomes even more interesting. It is also interesting to note that, proposed mixed metal oxide is in fact a derivative of two commonly used industrial catalyst, Al_2O_3 and ZnO towards MeOH activation. In this work, we illustrate (2 2 0) and (3 1 1) facets of $ZnAl_2O_4$ as excellent candidates for MeOH activation. These two surfaces not only offer significant O—H bond activation but also exhibit one case each of O—H bond dissociation. The dissociation observed in our studies are important as they are spontaneous. To top it, (3 1 1) surface undergoes successive dissociation of one of the C—H bonds as well. In an attempt to understand the factors that influence O—H bond activation/dissociation over any catalyst surface we dwelled deeper into systematically correlating the observed parameters. Availability of surface oxygen in the vicinity of adsorbing methanol is of prime importance. Hence, we can safely say that a surface rich with oxygen atoms of varying charges is desirable for multiple bond activations or even dissociation. Atomic arrangement of atoms on surface turned out to be another important factor in understanding the adsorption energy trends. Coordination of surface atoms and hence availability of sites with variation in charges on the surface unravel the trends in bond activations. Lastly, we propose that (3 1 1) surface offers better catalytic activity than (2 2 0) due to its stepped geometry and availability of inequivalent adsorption sites for interaction with an incoming MeOH. It was observed from the literature that most of the studies were restricted to either (1 1 1) or (1 1 0) planar surfaces. Our work in fact illustrates an upper hand in terms of catalytic activity for stepped surfaces like (3 1 1). Through detailed analysis of various factors that govern MeOH activation over these surface, we unleash a whole new chemical space to be explored in this direction.

CRediT authorship contribution statement

Shweta Mehta: Methodology, Validation, Writing - original draft. **Sheena Agarwal:** Methodology, Validation, Writing - review & editing. **Nivedita Kenge:** Validation. **Siva Prasad Mekala:** Resources. **Vipul Patil:** Resources. **T. Raja:** Funding acquisition. **Kavita Joshi:** Conceptualization, Writing - review & editing, Project administration, Supervision.

Declaration of Competing Interest

The authors declare that they have no known competing financial interests or personal relationships that could have appeared to influence the work reported in this paper.

Acknowledgements

CSIR-4PI is gratefully acknowledged for the computational facility. SM acknowledges UGC for research fellowship. SA acknowledges DST-INSPIRE for research fellowship. Authors also gratefully acknowledge CSIR-HQ and mission mode project "Catalysis for Sustainable Development (HCP0009)".

References

[1] Global methanol market, industry analysis, size, share, growth, trends, and forecast 2019-2026, 2019. https://www.marketwatch.com/press-release/global-methanol-market-industry-analysis-size-share-growth-trends-and-forecast-2019-2026-2019-09-27.
[2] https://www.strategyr.com/market-report-methanol-forecasts-global-industry-analysts-inc.asp, 2020.
[3] A. Hamnett, Mechanism and electrocatalysis in the direct methanol fuel cell, Catal. Today 38 (4) (1997) 445–457.
[4] Hansan Liu, Chaojie Song, Lei Zhang, Jiujun Zhang, Haijiang Wang, David P Wilkinson, A review of anode catalysis in the direct methanol fuel cell, J. Power Sources 155 (2) (2006) 95–110.
[5] Robert Schennach, Andreas Eichler, K.D. Rendulic, Adsorption and desorption of methanol on pd (111) and on a pd/v surface alloy, J. Phys. Chem. B 107 (11) (2003) 2552–2558.
[6] O. Rodrıguez de la Fuente, Marta Borasio, Paolo Galletto, Günther Rupprechter, H.-J. Freund, The influence of surface defects on methanol decomposition on pd (111) studied by xps and pm-iras, Surf. Sci. 566 (2004) 740–745.
[7] Marta Borasio, Oscar Rodríguez de la Fuente, Günther Rupprechter, Hans-Joachim Freund, In situ studies of methanol decomposition and oxidation on pd (111) by pm-iras and xps spectroscopy, J. Phys. Chem. B 109 (38) (2005) 17791–17794.
[8] Janine Lichtenberger, Doohwan Lee, Enrique Iglesia, Catalytic oxidation of methanol on pd metal and oxide clusters at near-ambient temperatures, Phys. Chem. Chem. Phys. 9 (35) (2007) 4902–4906.
[9] B.G. Frederick, G. Apai, T.N. Rhodin, Defect structure of clean and chlorinated aluminum oxide films probed by methanol chemisorption, Surf. Sci. 277 (3) (1992) 337–350.
[10] C.T. Au, W. Hirsch, W. Hirschwald, Adsorption and interaction of methanol with zinc oxide: Single crystal faces and zinc oxide-copper catalyst surfaces studied by photoelectron spectroscopy (xps and ups), Surf. Sci. 221 (1–2) (1989) 113–130.
[11] Samia Ilias, Aditya Bhan, Mechanism of the catalytic conversion of methanol to hydrocarbons, ACS Catal. 3 (1) (2012) 18–31.
[12] Xu. Mingting, Jack H Lunsford, D. Wayne Goodman, Alak Bhattacharyya, Synthesis of dimethyl ether (dme) from methanol over solid-acid catalysts, Appl. Catal. A: Gen. 149 (2) (1997) 289–301.
[13] Siranush S. Akarmazyan, Paraskevi Panagiotopoulou, Anastasios Kambolis, Christina Papadopoulou, Dimitris I. Kondarides, Methanol dehydration to dimethylether over al2o3 catalysts, Appl. Catal. B: Environ. 145 (2014) 136–148.
[14] X. Bao, M. Muhler, B. Pettinger, R. Schlögl, G. Ertl, On the nature of the active state of silver during catalytic oxidation of methanol, Catal. Lett. 22 (3) (1993) 215–225.
[15] Jinlong Gong, David W. Flaherty, Rotimi A. Ojifinni, John M. White, C. Buddie Mullins, Surface chemistry of methanol on clean and atomic oxygen pre-covered au (111), J. Phys. Chem. C 112 (14) (2008) 5501–5509.
[16] Sanket K. Desai, Matthew Neurock, K. Kourtakis, A periodic density functional theory study of the dehydrogenation of methanol over pt (111), J. Phys. Chem. B 106 (10) (2002) 2559–2568.
[17] Sung Sakong, Axel Groß, Density functional theory study of the partial oxidation of methanol on copper surfaces, J. Catal. 231 (2) (2005) 420–429.
[18] Øyvind Borck, Elsebeth Schröder, First-principles study of the adsorption of methanol at the α -al2o3 (0001) surface, J. Phys. Condens. Matter 18 (1) (2005) 1–12.
[19] Alejandro Montoya, Brian S Haynes, Methanol and methoxide decomposition on silver, J. Phys. Chem. C 111 (27) (2007) 9867–9876.
[20] N. Donghai Mei, Aaron Deskins, Michel Dupuis, Qingfeng Ge, Density functional theory study of methanol decomposition on the ceo2 (110) surface, J. Phys. Chem. C 112 (11) (2008) 4257–4266.
[21] Jaime Oviedo, Rocío Sánchez-de Armas, Miguel Angel San Miguel, Javier F. Sanz, Methanol and water dissociation on tio2 (110): the role of surface oxygen, J. Phys. Chem. C 112 (46) (2008) 17737–17740.
[22] Raj Ganesh S. Pala, Horia Metiu, Selective promotion of different modes of methanol adsorption via the cation substitutional doping of a zno (101$\bar{0}$) surface, J. Catal. 254 (2) (2008) 325–331.
[23] Ruibin Jiang, Wenyue Guo, Ming Li, Fu. Dianling, Honghong Shan, Density functional investigation of methanol dehydrogenation on pd (111), J. Phys. Chem. C 113 (10) (2009) 4188–4197.
[24] Sandra Sá, Hugo Silva, Lúcia Brandão, José M. Sousa, Adélio Mendes, Catalysts for methanol steam reforming–a review, Appl. Catal. B: Environ. 99 (1–2) (2010) 43–57.
[25] Solange R. Blaszkowski, Rutger A. van Santen, Theoretical study of c- c bond formation in the methanol-to-gasoline process, J. Am. Chem. Soc. 119 (21) (1997) 5020–5027.
[26] Mehdi D. Esrafili, Leila Dinparast, The selective adsorption of formaldehyde and methanol over al-or si-decorated graphene oxide: A dft study, J. Mol. Graph. Model. 80 (2018) 25–31.
[27] Do Hwan Kim, Sung-Soo Bae, Suklyun Hong, Sehun Kim, Atomic and electronic structure of methanol on ge(100), Surf. Sci. 604 (2) (2010) 129–135.
[28] Jan Andzelm, Niranjan Govind, George Fitzgerald, Amitesh Maiti, Dft study of methanol conversion to hydrocarbons in a zeolite catalyst, Int. J. Quant. Chem. 91 (3) (2003) 467–473.
[29] Rajiv Shah, Julian D. Gale, Michael C. Payne, Methanol adsorption in zeolites a first-principles study, J. Phys. Chem. 100 (28) (1996) 11688–11697.
[30] Ch Ammon, A. Bayer, G. Held, B. Richter, Th. Schmidt, H.-P. Steinrück, Dissociation and oxidation of methanol on cu (110), Surf. Sci. 507 (2002) 845–850.
[31] Qiang Sun, Bairong Shen, Kangnian Fan, Jingfa Deng, Roles of surface and subsurface oxygen in the dehydrogenation of methanol on silver surface, Chem. Phys. Lett. 322 (1–2) (2000) 1–8.
[32] Xu. Bingjun, Jan Haubrich, Thomas A. Baker, Efthimios Kaxiras, Cynthia M. Friend, Theoretical study of o-assisted selective coupling of methanol on au (111), J. Phys. Chem. C 115 (9) (2011) 3703–3708.
[33] Wen-Kai Chen, Shu-Hong Liu, Mei-Juan Cao, Qian-Gu Yan, Lu. Chun-Hai, Adsorption and dissociation of methanol on au (1 1 1) surface: A first-principles periodic density functional study, J. Mol. Struct. THEOCHEM 770 (1–3) (2006) 87–91.
[34] Yasuyuki Ishikawa, Meng-Sheng Liao, Carlos R. Cabrera, Oxidation of methanol on platinum, ruthenium and mixed pt–m metals (m = ru, sn): a theoretical study, Surf. Sci. 463 (1) (2000) 66–80.
[35] C.J. Zhang, P. Hu, A first principles study of methanol decomposition on pd (111): mechanisms for o–h bond scission and c–o bond scission, J. Chem. Phys. 115 (15) (2001) 7182–7186.
[36] Gui-Chang Wang, Yu-Hua Zhou, Yoshitada Morikawa, Junji Nakamura, Zun-Sheng Cai, Xue-Zhuang Zhao, Kinetic mechanism of methanol decomposition on ni (111) surface: a theoretical study, J. Phys. Chem. B 109 (25) (2005) 12431–12442.
[37] Yu-Hua Zhou, Pei-Hong Lv, Gui-Chang Wang, Dft studies of methanol decomposition on ni (1 0 0) surface: compared with ni (1 1 1) surface, J. Mol. Catal. A: Chem. 258 (1–2) (2006) 203–215.
[38] Susumu Yanagisawa, Takao Tsuneda, Kimihiko Hirao, Yoichi Matsuzaki, Theoretical investigation of adsorption of organic molecules onto fe (110) surface, J. Mol. Struct. THEOCHEM 716 (1–3) (2005) 45–60.
[39] Ruibin Jiang, Wenyue Guo, Ming Li, Houyu Zhu, Lianming Zhao, Lu. Xiaqing, Honghong Shan, Methanol dehydrogenation on rh (1 1 1): A density functional and microkinetic modeling study, J. Mol. Catal. A: Chem. 344 (1–2) (2011) 99–110.
[40] Minhua Zhang, Wu. Xingyu, Yu. Yingzhe, A comparative dft study on the dehydrogenation of methanol on rh (100) and rh (110), Appl. Surf. Sci. 436 (2018) 268–276.
[41] Ana S Moura, Jose LC Fajín, Ana SS Pinto, Marcos Mandado, M. Natalia, D.S. Cordeiro, Competitive paths for methanol decomposition on ruthenium: A dft study, J. Phys. Chem. C 119 (49) (2015) 27382–27391.
[42] Maria Marta Branda, Patricia Gabriela Belelli, R.M. Ferullo, Norberto Jorge Castellani, Proton abstraction ability of mgo: a dft cluster model study of the role of surface geometry, Catal. Today 85 (2–4) (2003) 153–165.
[43] Lawrence T. Sein Jr, Susan A. Jansen, Dft study of the adsorption and dissociation of methanol on nial (100), J. Catal. 196 (2) (2000) 207–211.
[44] Orest Skoplyak, Carl A. Menning, Mark A. Barteau, Jingguang G. Chen, Experimental and theoretical study of reactivity trends for methanol on co/ pt (111) and ni/ pt (111) bimetallic surfaces, J. Chem. Phys. 127 (11) (2007) 114707.
[45] Valeria Orazi, P. Bechthold, Paula Verónica Jasen, R. Faccio, Maria Estela Pronsato, Estela Andrea Gonzalez, Dft study of methanol adsorption on ptco (111), Appl. Surf. Sci. 420 (2017) 383–389.
[46] Øyvind Borck, Ingeborg-Helene Svenum, Anne Borg, Adsorption of methanol and methoxy on nial (1 1 0) and ni3al (1 1 1): A dft study, Surf. Sci. 603 (16) (2009) 2378–2386.
[47] Pan Du, Ping Wu, Chenxin Cai, Mechanism of methanol decomposition on the pt3ni (111) surface: Dft study, J. Phys. Chem. C 121 (17) (2017) 9348–9360.
[48] Mehdi D. Esrafili, Roghaye Nurazar, A dft study on the possibility of using boron nitride nanotubes as a dehydrogenation catalyst for methanol, Appl. Surf. Sci. 314 (2014) 90–96.
[49] Carolina Pistonesi, Alfredo Juan, Arnold Péter Farkas, F. Solymosi, Dft study of methanol adsorption and dissociation on β -mo2c (0 0 1), Surface Sci. 602(13) (2008) 2206–2211.
[50] Gregory K. Smith, Sen Lin, Wenzhen Lai, Abhaya Datye, Daiqian Xie, Hua Guo, Initial steps in methanol steam reforming on pdzn and zno surfaces: Density functional theory studies, Surf. Sci. 605 (7–8) (2011) 750–759.
[51] M.M. Branda, J.E. Peralta, N.J. Castellani, R.H. Contreras, Theoretical study of charge transfer interactions in methanol adsorbed on magnesium oxide, Surf. Sci. 504 (2002) 235–243.
[52] Øyvind Borck, Elsebeth Schröder, Adsorption of methanol and methoxy on the α -cr2o3 (0001) surface, J. Phys. Condens. Matter 18 (48) (2006) 10751–10763.
[53] Zhang Riguang, Liu Hongyan, Ling Lixia, Li Zhong, Wang Baojun, A dft study on the formation of ch3o on cu2o (1 1 1) surface by ch3oh decomposition in the absence or presence of oxygen, Appl. Surf. Sci. 257 (9) (2011) 4232–4238.
[54] R. Sanchez de Armas, J. Oviedo, M.A. San Miguel, J.F. Sanz, Methanol adsorption

and dissociation on tio2 (110) from first principles calculations, J. Phys. Chem. C 111 (27) (2007) 10023–10028.
[55] Weijia Liu, Jian-guo Wang, Xiaojing Guo, Wei Fang, Mingjie Wei, Lu. Xiaohua, Lu. Linghong, Dissociation of methanol on hydroxylated tio2-b (1 0 0) surface: Insights from first principle dft calculation, Catal. Today 165 (1) (2011) 32–40.
[56] Dianhua Liu, Chunfeng Yao, Jianqiang Zhang, Dingye Fang, Dasheng Chen, Catalytic dehydration of methanol to dimethyl ether over modified γ -al2o3 catalyst, Fuel 90 (5) (2011) 1738–1742.
[57] Cong T. Vo, Lam K. Huynh, J.-Y. Hung, Jyh-Chaing Jiang, Methanol adsorption and decomposition on zno (10$\bar{1}$0) surface: A density functional theory study, Appl. Surf. Sci. 280 (2013) 219–224.
[58] María M. Branda, Graciela R. Garda, Horacio A. Rodriguez, Norberto J. Castellani, Methanol decomposition on the β-ga2o3 (1 0 0) surface: A dft approach, Appl. Surf. Sci. 254 (1) (2007) 120–124.
[59] Marçal Capdevila-Cortada, Max García-Melchor, Núria López, Unraveling the structure sensitivity in methanol conversion on ceo2: A dft+ u study, J. Catal. 327 (2015) 58–64.
[60] N. Donghai Mei, Aaron Deskins, Michel Dupuis, Qingfeng Ge, Methanol adsorption on the clean ceo2 (111) surface: A density functional theory study, J. Phys. Chem. C 111 (28) (2007) 10514–10522.
[61] Zhao Liu, Charles C. Sorrell, Pramod Koshy, Judy N. Hart, Dft study of methanol adsorption on defect-free ceo2 low-index surfaces, ChemPhysChem 20 (16) (2019) 2074–2081.
[62] Chengwu Yang, Fabian Bebensee, Alexei Nefedov, Christof Wöll, Thomas Kropp, Leonid Komissarov, Christopher Penschke, Robin Moerer, Joachim Paier, Joachim Sauer, Methanol adsorption on monocrystalline ceria surfaces, J. Catal. 336 (2016) 116–125.
[63] Walter G. Reimers, Maria M. Branda, Methanol decomposition on low index and stepped ceo2 surfaces from gga+ u, Appl. Surf. Sci. 394 (2017) 509–518.
[64] Maria Marta Branda, R.M. Ferullo, Patricia Gabriela Belelli, Norberto Jorge Castellani, Methanol adsorption on magnesium oxide surface with defects: a dft study, Surf. Sci. 527 (1–3) (2003) 89–99.
[65] Hugo Petitjean, Konstantin Tarasov, Francoise Delbecq, Philippe Sautet, Jean Marc Krafft, Philippe Bazin, Maria Cristina Paganini, Elio Giamello, Michel Che, Helene Lauron-Pernot, et al., Quantitative investigation of mgo brønsted basicity: Dft, ir, and calorimetry study of methanol adsorption, J. Phys. Chem. C, 114(7) (2010) 3008–3016.
[66] S. Bocanegra, A. Ballarini, P. Zgolicz, O. Scelza, S. De Miguel, Highly selective and stable bimetallic catalysts supported on different materials for n-butane dehydrogenation, Catal. Today 143 (3–4) (2009) 334–340.
[67] Janina Okal, Mirosław Zawadzki, Combustion of propane over novel zinc aluminate-supported ruthenium catalysts, Appl. Catal. B: Environ. 105 (1–2) (2011) 182–190.
[68] Qianhe Liu, Lei Wang, Congxin Wang, Qu. Wei, Zhijian Tian, Huaijun Ma, Donge Wang, Bingchun Wang, Xu. Zhusheng, The effect of lanthanum doping on activity of zn-al spinel for transesterification, Appl. Catal. B: Environ. 136 (2013) 210–217.
[69] Suellen Battiston, Caroline Rigo, Eric da Cruz Severo, Marcio Antonio Mazutti, Raquel Cristine Kuhn, André Gündel, Edson Luiz Foletto, Synthesis of zinc aluminate (znal2o4) spinel and its application as photocatalyst, Mater. Res. 17(3) (2014) 734–738.
[70] H.P. de Macedo, R.L.B. de A. Medeiros, A.L. de Medeiros, A.A.S. de Oliveira, G.P. de Figueredo, M.A. de F. Melo, and D.M. de A. Melo, Characterization of ZnAl2O4 spinel obtained by hydrothermal and microwave assisted combustion method: a comparative study, Mater. Res. 20 (2017) 29–33.
[71] P.E. Blöchl, Projector augmented-wave method, Phys. Rev. B 50 (24) (1994) 17953–17979.
[72] G. Kresse, D. Joubert, From ultrasoft pseudopotentials to the projector augmented-wave method, Phys. Rev. B 59 (3) (1999) 1758–1775.
[73] John P. Perdew, Kieron Burke, Matthias Ernzerhof, Generalized gradient approximation made simple, Phys. Rev. Lett. 77 (18) (1996) 3865–3868.
[74] John P. Perdew, Kieron Burke, Matthias Ernzerhof, Generalized gradient approximation made simple [phys. rev. lett. 77, 3865 (1996)], Phys. Rev. Lett. 78(7) (1997) 1396–1396.
[75] G. Kresse, J. Hafner, *Ab initio* molecular-dynamics simulation of the liquid-metal–amorphous-semiconductor transition in germanium, Phys. Rev. B 49 (20) (1994) 14251–14269.
[76] G. Kresse, J. Furthmüller, Efficient iterative schemes for *ab initio* total-energy calculations using a plane-wave basis set, Phys. Rev. B 54 (16) (1996) 11169–11186.
[77] G. Kresse, J. Furthmüller, Efficiency of ab-initio total energy calculations for metals and semiconductors using a plane-wave basis set, Comput. Mater. Sci. 6 (1) (1996) 15–50.
[78] Anubhav Jain, Shyue Ping Ong, Geoffroy Hautier, Wei Chen, William Davidson Richards, Stephen Dacek, Shreyas Cholia, Dan Gunter, David Skinner, Gerbrand Ceder, et al., Commentary: The materials project: A materials genome approach to accelerating materials innovation, Appl. Materi. 1(1) (2013) 011002.
[79] Shyue Ping Ong, William Davidson Richards, Anubhav Jain, Geoffroy Hautier, Michael Kocher, Shreyas Cholia, Dan Gunter, Vincent L. Chevrier, Kristin A. Persson, Gerbrand Ceder, Python materials genomics (pymatgen): A robust, open-source python library for materials analysis, Comput. Mater. Sci. 68 (2013) 314–319.
[80] Richard Dronskowski, Peter E Blöchl, Crystal orbital hamilton populations (cohp): energy-resolved visualization of chemical bonding in solids based on density-functional calculations, J. Phys. Chem. 97 (33) (1993) 8617–8624.
[81] Volker L. Deringer, Andrei L. Tchougréeff, Richard Dronskowski, Crystal orbital Hamilton population (cohp) analysis as projected from plane-wave basis sets, J. Phys. Chem. A 115 (21) (2011) 5461–5466.
[82] Stefan Maintz, Volker L. Deringer, Andrei L. Tchougréeff, Richard Dronskowski, Analytic projection from plane-wave and paw wavefunctions and application to chemical-bonding analysis in solids, J. Comput. Chem. 34 (29) (2013) 2557–2567.
[83] Stefan Maintz, Volker L. Deringer, Andrei L. Tchougréeff, Richard Dronskowski, Lobster: A tool to extract chemical bonding from plane-wave based dft, J. Comput. Chem. 37 (11) (2016) 1030–1035.
[84] Atsuto Seko, Koretaka Yuge, Fumiyasu Oba, Akihide Kuwabara, Isao Tanaka, Prediction of ground-state structures and order-disorder phase transitions in ii–iii spinel oxides: A combined cluster-expansion method and first-principles study, Phys. Rev. B 73 (18) (2006) 184117.
[85] M.A. Lahmer, First-principles study of the structural, electronic, and optical properties of the clean and o-deficient znal2o4 (110) surfaces, Surf. Sci. 677 (2018) 105–114.

Applied Surface Science 602 (2022) 154150

Contents lists available at ScienceDirect

Applied Surface Science

journal homepage: www.elsevier.com/locate/apsusc

Full length article

From molecular adsorption to decomposition of methanol on various ZnO facets: A periodic DFT study

Shweta Mehta, Kavita Joshi *

Physical and Materials Chemistry Division, CSIR-National Chemical Laboratory, Dr. Homi Bhabha Road, Pashan, Pune 411008, India
Academy of Scientific and Innovative Research (AcSIR), Sector 19, Kamla Nehru Nagar, Ghaziabad, Uttar Pradesh 201002, India

ARTICLE INFO

Keywords:
DFT
Surface interactions
ZnO
MeOH

ABSTRACT

Methanol is an interesting and important molecule to study because of its potential to replace existing fuels. It is also a prominent hydrogen source which can be used to generate hydrogen in-situ. ZnO is widely used as catalyst in synthesis of methanol from CO_2 at industrial scale. In this work, we demonstrate that the same catalyst could be used for MeOH decomposition. We have investigated interaction of methanol with various flat and stepped facets of ZnO by employing Density Functional Theory (DFT). Two flat [$(10\bar{1}0)$ and $(11\bar{2}0)$] and two stepped [$(10\bar{1}3)$ and $(11\bar{2}2)$] facets are studied in detail for methanol adsorption. Chemisorption of MeOH with varying strength is common to all four facets. Most importantly spontaneous dissociation of O-H bond of methanol is observed on all facets except $(11\bar{2}0)$. Our DFT calculations reveal that molecular adsorption is favored on flat facets, while dissociation is favored on step facets. Also, $(10\bar{1}0)$ facet undergoes substantial reconstruction upon MeOH adsorption. Activation of C-H bond along with strengthening of C-O bond on ZnO facets suggest partial oxidation of methanol. With our DFT investigations, we dig deeper into the underlying electronic structure of various facets of ZnO and provide rationale for the observed facet dependent interaction of ZnO with MeOH.

1. Introduction

Methanol is one of the most important chemical for industrial reactions and a primary feed-stock for energy production. Due to easier transportation and compatibility with the existing infrastructure, methanol attracts considerable attention. Methanol emerges as an efficient means to store energy and it can also be used as a convenient fuel [1]. It is also used in the direct methanol fuel cell (DMFC). Methanol can also be converted to various hydrocarbons like formaldehyde, dimethyl ether, etc. Methanol is also a promising hydrogen source because of its high hydrogen content [2,3]. However, use of methanol as a source of hydrogen requires breaking of its O-H and C-H bonds with substantial bond dissociation energies, viz. 96.1 kcal/mol and 104.6 kcal/mol respectively [4]. Over the past two decades, extensive studies of activation and decomposition of methanol on various metal surfaces [5–15], metal alloys [16–21], metal clusters [22–25], metal oxides [26–32], mixed metal oxides [33], and zeolites [34–36] have been carried out. In general metal oxides turn out to be better catalyst for activation of methanol due to the presence of oxygen on the surface, which acts as an active site.

As discussed above, breaking bond of methanol is primary step to convert it to any value added product. The industrial catalyst used for synthesis of methanol from syn gas is Cu-ZnO/Al_2O_3. In a recent computational study, Elnabawy et al. demonstrated the role of ZnO in industrial catalyst for methanol synthesis [37]. They reported that the strong metal support interaction between Cu and ZnO favors higher activity towards methanol synthesis. ZnO reduces and partially covers the Cu surface which causes modification in the surface. However, the active Cu sites remain unaffected leading to higher activity of catalyst. ZnO is considered as a very active catalyst for many reactions because of its mixed covalent and ionic bonding [38]. Industrially methanol is partially oxidized to formaldehyde using two different catalyst, silver or iron-molybdenum oxides. However, the reaction takes place at elevated temperatures in both the cases. It is as high as 600°C when silver is used as catalyst whereas it drops down to ~ 250–400°C for molybdenum catalyst. Clearly there is a room for improvement of the catalyst which could bring down the reaction temperature further. In an experimental study, Boisen et al. demonstrated that optimal ammonia synthesis catalyst is not the optimal ammonia decomposition catalyst [39]. Contrary to that, ZnO, which is an optimal methanol synthesis catalyst exhibits excellent activity for methanol decomposition. Vo et al. investigated the adsorption

* Corresponding author at: Physical and Materials Chemistry Division, CSIR-National Chemical Laboratory, Dr. Homi Bhabha Road, Pashan, Pune 411008, India.
E-mail addresses: sk.mehta@ncl.res.in (S. Mehta), k.joshi@ncl.res.in (K. Joshi).

https://doi.org/10.1016/j.apsusc.2022.154150
Received 1 March 2022; Received in revised form 3 June 2022; Accepted 1 July 2022
Available online 13 July 2022
0169-4332/© 2022 Elsevier B.V. All rights reserved.

and decomposition of methanol on ZnO($10\bar{1}0$) by employing DFT and concluded that methanol strongly adsorbed on ZnO($10\bar{1}0$) surface as compared to CuCl(111), Cu(111), and Au(111) surfaces. Their results showed that decomposition of MeOH to CH_2O molecule has a barrier of 1.20 eV [40]. In another interesting study, Abedi et al. employed DFT to understand the conditions leading to monolayer formation of methanol on ZnO($10\bar{1}0$) surface. They reported breaking of the O-H bond, with a barrier of 0.5 eV, as the preferred mechanism over cleavage of C-O bond [41]. In a combined experimental and theoretical work, Ruan et al. used high-resolution scanning tunneling microscopy in combination with density functional theory to identify both the physi- and chemisorbed methanol species on the non-polar ZnO($10\bar{1}0$) surface. The physisorption of methanol dominates at liquid nitrogen temperature which transform into chemisorption upon either thermal annealing or electron injection. Moreover, the chemisorbed methanol mostly retains an undissociated state and tends to form one-dimensional chain structure along the (0001) direction mediated by the intermolecular hydrogen bonding interactions [42]. A DFT study carried out by Smith et al. demonstrated significantly lower reaction barrier (0.39 eV) towards methanol dissociation on ZnO (0001) compared to PdZn surfaces (0.54 eV) [43]. Recently Jin et al. studied the adsorption and reactions of CH_3OH on non-polar mixed-terminated ZnO($10\bar{1}0$), polar O terminated ZnO($000\bar{1}$) and Zn terminated ZnO(0001) surfaces using high-resolution electron energy loss spectroscopy (HREELS) in conjunction with temperature programmed desorption (TPD). They found that for all three ZnO surfaces, methanol adsorb dissociatively at room temperature which leads to the formation of hydroxyl and methoxy species. Upon heating to higher temperatures (370 K and 440 K), the dissociated and intact methanol species on ZnO($10\bar{1}0$) predominantly undergo molecular desorption releasing CH_3OH. While on both polar surfaces, thermal decomposition of CH_3OH occurs to produce CH_2O, H_2, CO, CO_2, and H_2O at temperatures higher than 500 K [44].

Although ZnO is used extensively as a catalyst in many reactions, its potential is not truly realized. To the best of our knowledge only non-polar ($10\bar{1}0$) and polar (0001) facets of ZnO have been studied for methanol activation. XRD pattern shows that ($11\bar{2}0$), ($10\bar{1}3$), and ($11\bar{2}2$) are also prominent facets. These facets are hardly studied for methanol activation. In the present work, we have systematically studied the interaction of methanol with various flat ($10\bar{1}0$), ($11\bar{2}0$) and stepped surfaces ($10\bar{1}3$), ($11\bar{2}2$) by employing periodic DFT. We report not only molecular adsorption and activation of O-H bond of methanol on these facets but also spontaneous dissociation of its O-H bond leading to formation of methoxy species. The quenched C-O bond-length in methanol along with partial double bond type character indicates onset of oxidation of methanol. We also demonstrate various possibilities regarding interaction of MeOH with ZnO and bring out the rationale behind the reactivity in terms of electronic structure of these facets. Finally we would like to bring out the role of computation in designing catalyst. DFT based computation has played a crucial role in rational design of catalyst while understanding its catalytic activity. To understand why different facets interact differently with MeOH, it is indispensable to investigate the underlying electronic structure. As we will demonstrate in the next section, our work brings out the possibility of ZnO being a suitable catalyst for MeOH decomposition as well. We also demonstrate that with distinguishable trends in the *p*DOS, charge transfer and other computed properties, we could explain variation in the interaction of methanol with different facets.

2. Computational details

All the calculations are carried out within the Kohn–Sham formalism of Density Functional Theory. Projector Augmented Wave potential [45,46] is used, with Perdew Burke Ernzerhof (PBE) [47] approximation for the exchange–correlation and generalized gradient approximation [48], as implemented in planewave, pseudopotential based code, Vienna Ab initio Simulation Package (*VASP*) [49–51]. The bulk unit cell is taken from the materials project [52]. The bulk lattice parameters upon optimization are a = 3.28 Å and c = 5.30 Å demonstrate excellent agreement with the experimentally measured (a = 3.24 Å, c = 5.20 Å) lattice parameters [53,54]. Two flat facets, ($10\bar{1}0$) and ($11\bar{2}0$) of ZnO are modeled as slabs by cleaving a surface with 3×3 periodicity in x and y direction with 4 layers using Quantumwise-VNL-2017.1 [55]. Two stepped facets, ($10\bar{1}3$) and ($11\bar{2}2$) are also cleaved by taking 3×1 and 2×2 periodicity respectively in the x and y direction with 6 layers. In every model, bottom layer is fixed and rest all layers and adsorbate are fully relaxed. Van der Waals corrections are applied to account for dynamic correlations between fluctuating charge distribution by employing Grimme method (DFT-D2) [56]. It is observed that 20 Å of vacuum is sufficient to avoid interaction between adjacent images of planes along the z-direction. Geometry optimization is carried out with a force cutoff of 0.01 eV/Å on the unfixed atoms and the total energies are converged below 10^{-4} eV for each SCF cycle. A Monkhorst–Pack grid of $3 \times 2 \times 1$ for ($10\bar{1}0$) and $3 \times 3 \times 1$ for ($11\bar{2}0$) slabs is used. For both stepped surfaces, Monkhorst–Pack grid of $2 \times 2 \times 1$ is used. The difference in energies is less than 4meV/atom for every system upon refining the K mesh further. Entire surface is scanned by placing MeOH molecule at all available unique sites. To compare the interaction of methanol at these sites, interaction energy is calculated using the formula: $E_{int} = E_{system} - (E_{surface} + E_{molecule})$ where E_{system} is energy of the system when MeOH is placed on the surface, $E_{surface}$ is energy of the bare surface and $E_{molecule}$ is energy of the MeOH molecule. To understand the electronic structure of these facets, total Density of States (*tDOS*) are calculated with denser k-mesh using LOBSTER [57–60]. Mulliken charges are computed for all the atoms on the surface.

3. Results and discussion

Bulk ZnO crystallizes in the hexagonal wurtzite structure consisting of hexagonal Zn and O planes stacked alternately. Both oxygen and zinc atoms are coordinated by four zinc and oxygen atoms respectively. Polar ((0001) and ($000\bar{1}$)) and non-polar (($10\bar{1}0$), ($10\bar{1}1$), ($11\bar{2}0$), ($10\bar{1}3$), and ($11\bar{2}2$)) facets have prominent peaks in XRD [61,62]. In this work, we have studied the interaction of methanol with two flat (($10\bar{1}0$), ($11\bar{2}0$)) and two stepped (($10\bar{1}3$), ($11\bar{2}2$)) facets of ZnO. The top and side view of all these facets are shown in Fig. SI1 and Fig. SI2. Each layer of ($10\bar{1}0$) is divided into two sub-layers leading to various unique sites for methanol adsorption. All these unique sites such as top of Zn, bridge of Zn-Zn, O-O, Zn-O, and bridge positions of atoms of two sub-layers are scanned for methanol interaction. All the sites where MeOH is placed are shown schematically in Fig. SI3. The numbers in Fig. SI3-(a) represent the initial positions where MeOH is placed and final position of adsorbed methanol or dissociated methoxy group are shown in Fig. SI3-(b). The black numbers indicate molecular adsorption while the red numbers denote dissociated methoxy group.

Before discussing the results in detail, we would like to elaborate the criteria adopted for labeling the interaction of methanol at various ZnO surfaces. For all the configurations reported in this study, we described molecular adsorption or dissociation of MeOH based on variation in its O-H bond-length, which is 0.97 Å in MeOH molecule. The physisorption is defined as slight elongation of O-H bond, from 0.97 Å to 0.98 Å. On the other hand, O-H bond elongation more than 0.99 Å is associated with chemisorption of MeOH on the facet. In all cases of O-H bond dissociation, the distance between O_{MeOH} and H is more than 1.45 Å (>50% of O-H bond-length). Also, the dissociated H atom binds to the surface oxygen atom with O-H distance varying between 0.98–1.06 Å, which infers bond formation between them. Although, interaction energy is used to define the thermodynamic stability of the resulting complex, it is not measure of observed bond activation. As will be discussed later, complexes with maximum activation or even dissociation are not always the ones with highest thermodynamic stability.

On the $(10\bar{1}0)$ facet, methanol adsorbs either molecularly or dissociatively at different sites. The interaction energy, O-H bond-length, and Zn-O_{MeOH} bond-length are tabulated in Table 1. Molecular adsorption of MeOH is thermodynamically the most probable outcome at this facet. However as seen from the Table 1, dissociation of MeOH into methoxy is also a likely product at elevated temperatures considering the small energy difference between these two outcomes. We report strong chemisorption and spontaneous dissociation of O-H bond of MeOH. A weak chemisorption is also observed, consistent with previously reported work [63], though it is not thermodynamically most favorable outcome. At this point, it is pertinent to note that a molecule like MeOH could be placed at the symmetry driven unique points on the surface in various different ways. A detail account of which could be found in our previous paper [33]. A small change in MeOH orientation wrt surface leads to completely different result in terms of extent of O-H bond elongation or even O-H bond dissociation. Considering this, any study of MeOH interaction is always limited by initial configurations one investigates and there is a dire need of formalizing a methodology for accounting of all possibilities.

Fig. 1 shows representative conformations of MeOH upon adsorption/dissociation on this facet. A closer look at the adsorbed conformations reveal certain patterns in MeOH interaction with the facet. For example, highly chemisorbed methanol always gets adsorbed through oxygen (refer Fig. 1-(b)) whereas in case of physisorbed MeOH, sometimes it gets adsorb through methylic H (refer Fig. 1-(c)). Adsorption through methylic H atom results in activation of C-H bond of MeOH. The C-H bond elongates to 4%. Consequently, the C-O bond strengthens (as shown in Table 1) and reduces to 1.39 Å which indicates partial oxidation of methanol. Another interesting observation is that MeOH adsorption also leads to the surface reconstruction which results into formation of voids as evident in all the cases. However, the extent of reconstruction depends on the outcome i.e. chemisorption (Fig. 1-(b) and (c)) or dissociation (Fig. 1-(d) and (e)). It was also observed that the dissociated methoxy group can adsorb at a Zn site or at bridge of two Zn sites. Further we investigate the interaction of MeOH with reconstructed surface by introducing second MeOH molecule with the most stable configuration. We placed the second molecule at various sites in the vicinity of previously chemisorbed MeOH. This results into two outcomes, viz. chemisorption and dissociation, depending on availability of oxygen atom near the second molecule for abstraction of proton of MeOH. Dissociation of O-H bond of second MeOH is thermodynamically the most favorable outcome of this interaction (as shown in Tab. SI1).

Another flat facet that we studied is $(11\bar{2}0)$. This is a highly symmetric facet with less number of inequivalent sites on the surface as shown in Fig. SI4-(a). Interestingly, when MeOH is placed on any sites except 4th, upon optimization it gets chemisorbed at one specific site as schematically represented in Fig. SI4-(b). The orientation of methanol on this site is shown in Fig. SI4-(c). E_{int} for methanol at this site is −1.24 eV and O-H bond of MeOH elongates to 1.02 Å. Further adsorbing the second MeOH molecule on the surface, results in chemisorption of molecule with elongation in O-H bond up to 1.03 Å. This shows that $(11\bar{2}0)$ facet does not favor dissociation of methanol due to uniformity on the surface. Comparing adsorption of MeOH on flat facets underlines the fact that nonuniform facet provides multiple possibilities.

Next we investigate a stepped facet $(10\bar{1}3)$. Various available unique sites, where MeOH is placed are shown in Fig. SI5-(a). Those sites where methanol/methoxy adsorb upon optimization are shown in Fig. SI5-(b). Interaction energy, O-H bond-length and Zn-O_{MeOH} bond-length are tabulated in Table 2. As evident from the interaction energy, dissociation of methanol is thermodynamically the most favorable outcome on this facet. Fig. 2 shows the representative cases of chemisorption as well as dissociation of methanol on $(10\bar{1}3)$ facet. It is observed that generally MeOH/methoxy group adsorb via its O at Zn site, but in few cases, it adsorbs through its methylic H (refer Fig. 2-(b)). Contrary to $(10\bar{1}0)$ facet, this methylic adsorption shows higher activation of O-H bond. Adsorption through methylic H leads to elongation of C-H bond by 7% accompanied with reduction in C-O bond to 1.37 Å as shown in Table 2. Elongation in C-H bond-length along with reduction in C-O bond-length is an evidence of partial oxidation of methanol at this stepped facet. The dissociated methoxy group adsorbs on the surface in two different ways, either through O_{MeOH} (monodentate as shown in Fig. 2-(c)) or via two atoms i.e. O_{MeOH} and methylic H (bidentate as shown in Fig. 2-(d)). Interestingly, coordination number of surface sites where MeOH/methoxy group adsorbs governs the stability of any configuration. Due to the presence of step, extent of reconstruction upon methanol adsorption is less on this facet as compared to $(10\bar{1}0)$ facet.

Next, we discuss another stepped facet $(11\bar{2}2)$ which is more symmetric than $(10\bar{1}3)$ facet. Methanol is placed at all available unique sites as shown schematically in Fig. SI6-(a) and its interaction with the ZnO surface has been studied. In majority of the cases, irrespective of initial positions of methanol, it diffuses to a single position upon optimization, as indicated by red triangle in Fig. SI6-(b). Similar to the previous stepped facet, this facet also shows two outcomes of MeOH interaction viz. dissociation as well as chemisorption. However, dissociation is highly favored over its molecular adsorption as evident from Table 3. Distinct conformations of adsorption as well as dissociation of methanol on this facet are shown in Fig. 3. A careful look at the adsorbed conformations reveals that depending on the sites of adsorption viz. bridge (refer Fig. 3-(a)) or on-top site (refer Fig. 3-(b)), elongation of O-H bond

Table 1
Interaction energy (eV), O-H bond-length (Å), C-O bond-length (Å), and Zn-O_{MeOH} bond-length (Å) for various sites on ZnO $(10\bar{1}0)$ facet. All these positions are indicated in Fig. SI3-(b). Dissociation is indicated in red color while molecular adsorption is shown in black color.

Positions	E_{int} (eV)	O-H BL (Å)	C-O BL (Å)	Zn-O_{MeOH} BL (Å)
4	−1.58	1.04	1.44	2.05
3	−1.52	1.03	1.44	2.06
7	−1.36	3.09	1.43	1.96
6	−1.35	4.37	1.41	1.96
5	−1.25	1.61	1.41	1.93
1	−1.08	0.98	1.45	2.11
2	−0.69	1.00	1.39	3.54

Table 2
Interaction energy (eV), O-H bond-length (Å), C-O bond-length (Å), and Zn-O_{MeOH} bond-length (Å) for various sites on ZnO $(10\bar{1}3)$ facet. All these position are indicated in Fig. SI5-(b). Dissociation of MeOH is shown in red color while molecular adsorption is shown in black color.

Positions	E_{int} (eV)	O-H BL (Å)	C-O BL (Å)	Zn-O_{MeOH} BL (Å)
2,7	−3.88	1.57	1.44	1.88
10	−3.70	1.73	1.39	1.89
6,8	−2.87	1.46	1.43	1.90
4,5,9	−1.71	1.03	1.37	3.49
1	−1.54	0.99	1.45	2.17
3	−1.42	0.99	1.45	2.21

Table 3
Interaction energy (eV), O-H bond-length (Å), C-O bond-length (Å), and Zn-O_{MeOH} bond-length (Å) for various sites on ZnO $(11\bar{2}2)$ facet. All these position are indicated in Fig. SI6-(b). Dissociation is indicated in red color while molecular adsorption is shown in black color.

Positions	E_{int} (eV)	O-H BL (Å)	C-O BL (Å)	Zn-O_{MeOH} BL (Å)
3,9	−6.24	2.25	1.44	1.98
1,2,7,11,12	−3.10	2.04	1.44	1.98
6,8	−2.95	2.01	1.45	1.99
13	−2.86	1.94	1.45	1.98
5	−1.78	1.00	1.45	2.04
10	−1.77	0.98	1.47	2.26
4	−1.56	0.98	1.46	2.08

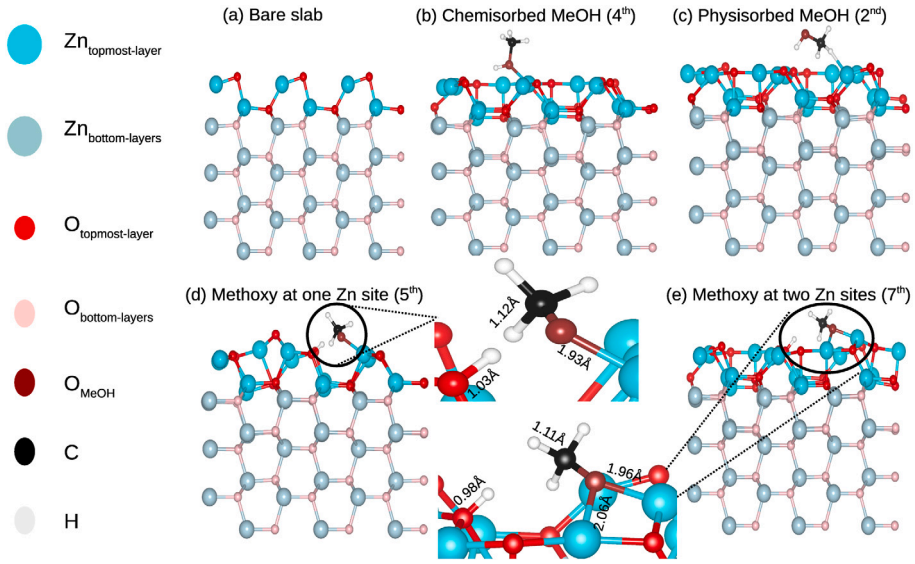

Fig. 1. (a) side view of bare $(10\bar{1}0)$ facet, (b) Chemisorbed MeOH with ~7% elongation of O-H bond, (c) chemisorbed MeOH with ~3% elongation of O-H bond, (d) dissociated MeOH with methoxy group attached to Zn atom, and (e) dissociated MeOH with methoxy group at bridge of two Zn atoms. For clear view of adsorption of methoxy on the surface (d) and (e) figures are enlarged. The numbers in the bracket indicates configuration with other details listed in Table 1.

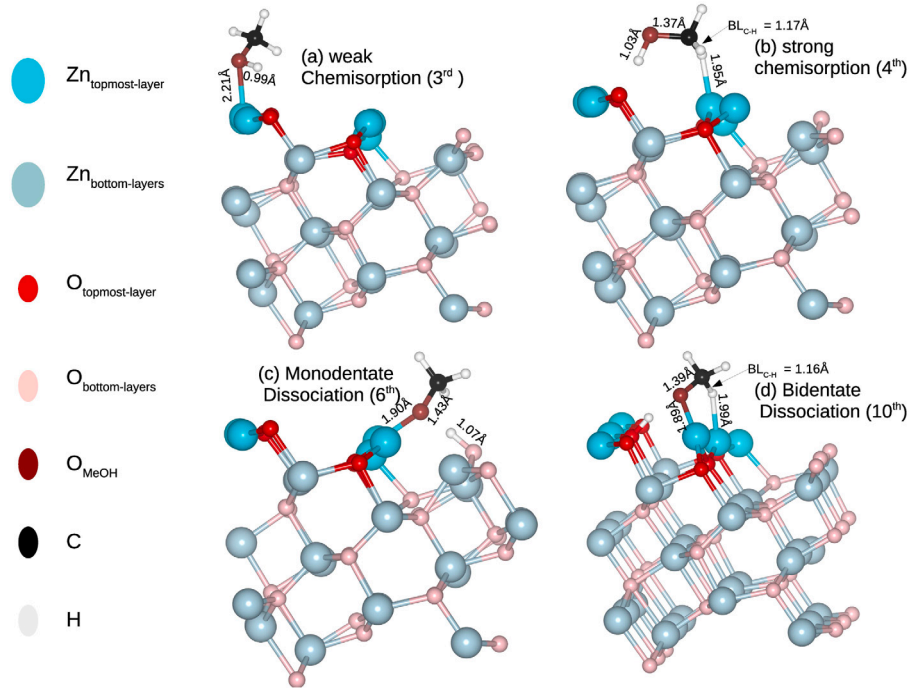

Fig. 2. Various conformers of MeOH interaction with $(10\bar{1}3)$ facet. Upper panel shows chemisorption of MeOH and lower panel shows dissociation of MeOH at the facet. (a) weak chemisorption, (b) strong chemisorption, (c) monodentate adsorption of methoxy group, and (d) bidentate adsorption of methoxy group. The numbers in the bracket indicates configuration and the details are listed in Table 2.

of methanol differs. The dissociated cases have methoxy adsorbed at Zn site with Zn-O_{MeOH} bond-length (1.98 Å) comparable to bulk Zn-O bond-length. Further, second molecule also chemisorbs on the surface with O-H bond elongation up to 1.01 Å. In short, dissociation of MeOH is thermodynamically the most favorable outcome on stepped facets while molecular adsorption is favorable on the flat facets.

So far, we have observed that different facets of ZnO interact differently with methanol resulting into molecular adsorption and/or activation and/or dissociation of O-H bond. This difference in behavior is correlated with underlying electronic structure of these facets. Coordination number and Mulliken charges of surface Zn and O atoms of all the facets are noted in Tab. SI2. For all facets but $(10\bar{1}3)$, all the surface Zn or O atoms are identical. $(10\bar{1}3)$ facet has two types of Zn and O atoms on the surface experiencing the difference in their neighboring environment and hence Mulliken charges. It is also evident that higher coordination of surface atoms leads to higher effective charges and hence reduced reactivity. For example, in the case of $(11\bar{2}0)$ facet, Zn and O atoms with highest coordination and Mulliken charges do not show dissociation of methanol. The inhibition of O-H bond breaking of MeOH at $(11\bar{2}0)$ facet could be explained by analyzing the total density of states (*tDOS*) plot as shown in Fig. 4. The *tDOS* plot for $(11\bar{2}0)$ facet clearly shows non availability of energy states near Fermi level, which makes it least reactive. Remaining all facets with energy states available near Fermi level enhance reactivity of the facet and explain

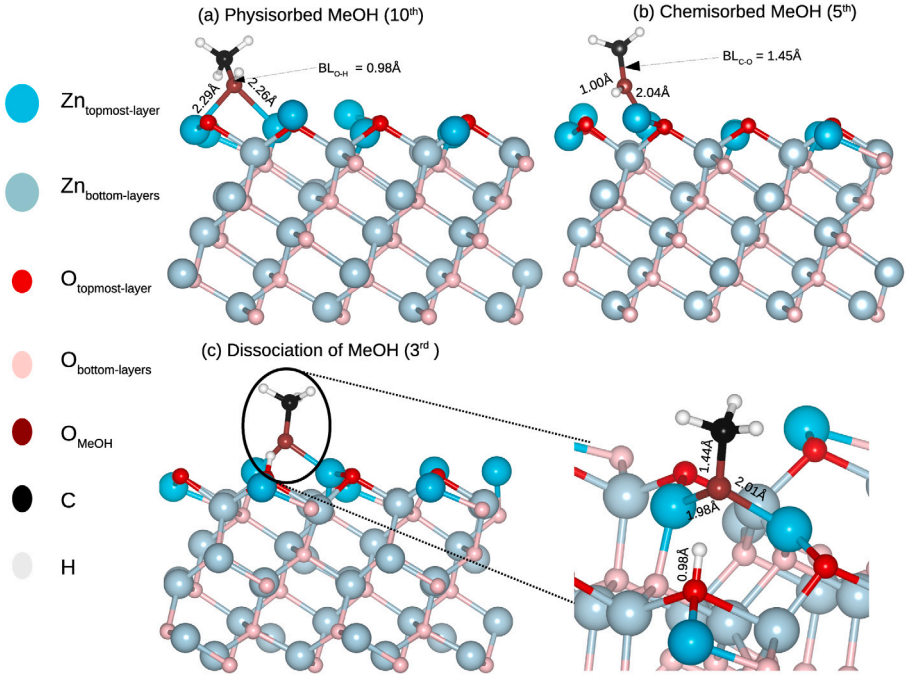

Fig. 3. Upper panel shows adsorption of MeOH at (11$\bar{2}$2) facet and lower panel shows dissociation of MeOH. (a) physisorbed MeOH (b) chemisorbed MeOH (c) adsorption of methoxy group at bridge of two Zn atoms. The enlarged figure is shown to provide a clear view of methoxy group adsorption on Zn site. The numbers in the bracket indicates configuration and the details are listed in Table 3.

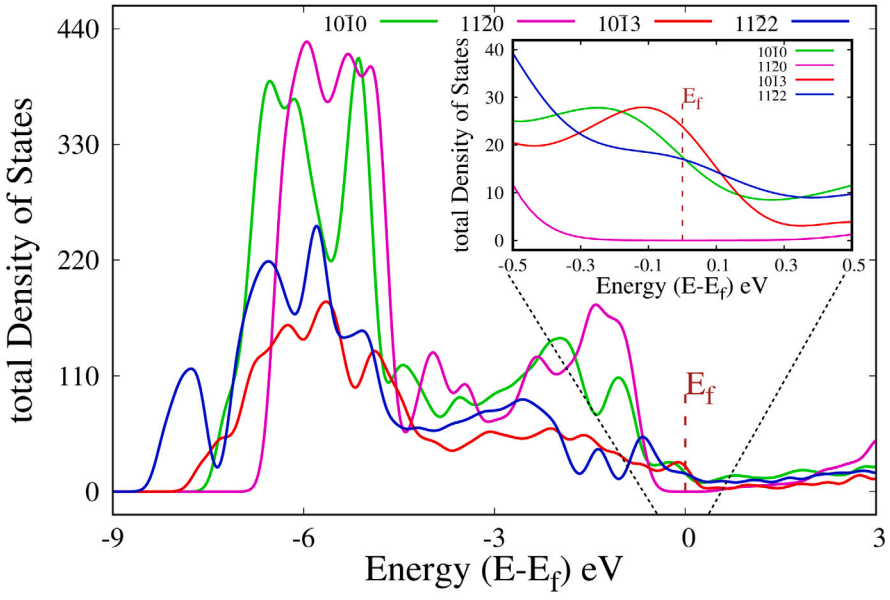

Fig. 4. The *tDOS* of four facets are plotted. The inset figure shows the enlarged *tDOS* near Fermi level. Only for (11$\bar{2}$0) facet *tDOS* is zero at Fermi.

the observed dissociation of methanol on these facets. Next we plot projected density of states (*pDOS*) of surface atoms for all facets. 3*d* and 4*s* states of surface Zn atoms are shown in Fig. 5. Zn, being a late transition metal with fully filled 3*d* states lying much below the Fermi level (refer Fig. 5-a), does not participate in reactivity. While its 4*s* states, lying near the Fermi level, participate in reactivity of the surface. It is clearly seen in Fig. 5-b that for flat facets, 4*s* states of surface Zn atoms are zero near Fermi level while it is non-zero for stepped facets. The presence of non-zero 4*s* states near Fermi for stepped facets favors dissociation of MeOH, which is most favorable on these facets.

4. Conclusion

ZnO is considered as a very active catalyst for many reactions because of its mixed covalent and ionic bonding. As evident from XRD, there are various prominent facets in ZnO and only few facets have been studied for methanol adsorption. We have carried out a systematic study of methanol adsorption on various facets of ZnO which includes two flat [(10$\bar{1}$0) and (11$\bar{2}$0)] and two stepped [(10$\bar{1}$3) and (11$\bar{2}$2)] surfaces. O-H bond dissociation is thermodynamically the most favorable outcome on stepped facets where on chemisorption of MeOH with 7%–10% O-H bond activation is observed on the flat facets. We also report considerable surface reconstruction upon MeOH adsorption. However,

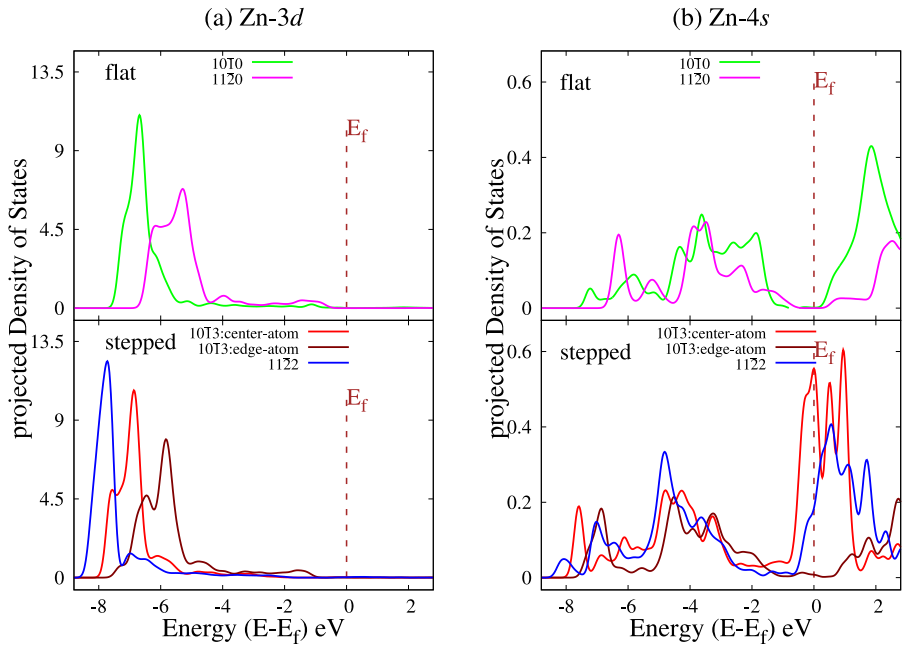

Fig. 5. (a) *pDOS* of Zn-3*d* orbitals of flat and stepped facets. As expected, 3*d* in Zn being completely filled are much away from Fermi level. (b) Zn-4*s* of flat and stepped facets. It is interesting to note that for flat facets *pDOS* of surface Zn atoms show unavailability of states near Fermi as opposed to case of stepped facet.

the reconstruction is lesser on the stepped surfaces compared to the flat facets. Further, partial oxidation of MeOH is favored on ZnO facets. Our detailed electronic structure analysis brings out the rationale behind the surface dependent interaction of MeOH. Analysis of pDOS, tDOS along with Mulliken charges on surface atoms explains the facet dependent reactivity observed in case of ZnO. Facets with available empty states near Fermi leads to O-H bond dissociation whereas absence of empty states near Fermi leads to O-H bond activation. Considering the role of ZnO in various reactions and importance of MeOH in the current energy scenario we believe our study shade light on some important aspects of interaction of ZnO with MeOH. Finally, ZnO is a known catalyst for synthesis of MeOH. Our work opens up a possibility of ZnO as a catalyst for MeOH dissociation as well which awaits experimental verification.

CRediT authorship contribution statement

Shweta Mehta: Methodology, Validation, Analysis, Writing – original draft. **Kavita Joshi:** Conceptualization, Writing – review & editing, Project administration, Supervision.

Declaration of competing interest

The authors declare that they have no known competing financial interests or personal relationships that could have appeared to influence the work reported in this paper.

Acknowledgments

CSIR-4PI is gratefully acknowledged for the computational facility. SM acknowledges UGC for research fellowship.

Appendix A. Supplementary data

Supplementary material related to this article can be found online at https://doi.org/10.1016/j.apsusc.2022.154150.

References

[1] G.A. Olah, Beyond oil and gas: The methanol economy, Angew. Chem. Int. Ed. 44 (18) (2005) 2636–2639, http://dx.doi.org/10.1002/anie.200462121, arXiv:https://onlinelibrary.wiley.com/doi/pdf/10.1002/anie.200462121. URL https://onlinelibrary.wiley.com/doi/abs/10.1002/anie.200462121.

[2] J. Kothandaraman, A. Goeppert, M. Czaun, G.A. Olah, G.S. Prakash, Conversion of CO_2 from air into methanol using a polyamine and a homogeneous ruthenium catalyst, J. Am. Chem. Soc. 138 (3) (2016) 778–781.

[3] L.-N. Chen, K.-P. Hou, Y.-S. Liu, Z.-Y. Qi, Q. Zheng, Y.-H. Lu, J.-Y. Chen, J.-L. Chen, C.-W. Pao, S.-B. Wang, Y.-B. Li, S.-H. Xie, F.-D. Liu, D. Prendergast, L.E. Klebanoff, V. Stavila, M.D. Allendorf, J. Guo, L.-S. Zheng, J. Su, G.A. Somorjai, Efficient hydrogen production from methanol using a single-site Pt1/CeO_2 catalyst, J. Am. Chem. Soc. 141 (45) (2019) 17995–17999, http://dx.doi.org/10.1021/jacs.9b09431, PMID: 31647653. arXiv:https://doi.org/10.1021/jacs.9b09431.

[4] S.J. Blanksby, G.B. Ellison, Bond dissociation energies of organic molecules, Acc. Chem. Res. 36 (4) (2003) 255–263.

[5] C. Ammon, A. Bayer, G. Held, B. Richter, T. Schmidt, H.-P. Steinrück, Dissociation and oxidation of methanol on Cu (110), Surf. Sci. 507 (2002) 845–850.

[6] Q. Sun, B. Shen, K. Fan, J. Deng, Roles of surface and subsurface oxygen in the dehydrogenation of methanol on silver surface, Chem. Phys. Lett. 322 (1–2) (2000) 1–8.

[7] B. Xu, J. Haubrich, T.A. Baker, E. Kaxiras, C.M. Friend, Theoretical study of O-assisted selective coupling of methanol on Au (111), J. Phys. Chem. C 115 (9) (2011) 3703–3708.

[8] Y. Ishikawa, M.-S. Liao, C.R. Cabrera, Oxidation of methanol on platinum, ruthenium and mixed Pt–M metals (M=Ru, Sn): a theoretical study, Surf. Sci. 463 (1) (2000) 66–80.

[9] C. Zhang, P. Hu, A first principles study of methanol decomposition on Pd (111): mechanisms for O–H bond scission and C–O bond scission, J. Chem. Phys. 115 (15) (2001) 7182–7186.

[10] G.-C. Wang, Y.-H. Zhou, Y. Morikawa, J. Nakamura, Z.-S. Cai, X.-Z. Zhao, Kinetic mechanism of methanol decomposition on Ni (111) surface: a theoretical study, J. Phys. Chem. B 109 (25) (2005) 12431–12442.

[11] S. Yanagisawa, T. Tsuneda, K. Hirao, Y. Matsuzaki, Theoretical investigation of adsorption of organic molecules onto Fe (110) surface, J. Mol. Struct.: Theochem. 716 (1–3) (2005) 45–60.

[12] R. Jiang, W. Guo, M. Li, H. Zhu, L. Zhao, X. Lu, H. Shan, Methanol dehydrogenation on Rh (1 1 1): A density functional and microkinetic modeling study, J. Mol. Catal. A 344 (1–2) (2011) 99–110.

[13] X. Bao, M. Muhler, B. Pettinger, R. Schlögl, G. Ertl, On the nature of the active state of silver during catalytic oxidation of methanol, Catal. Lett. 22 (3) (1993) 215–225.

[14] J. Greeley, M. Mavrikakis, Methanol decomposition on Cu (111): a DFT study, J. Catal. 208 (2) (2002) 291–300.

[15] O.R. de la Fuente, M. Borasio, P. Galletto, G. Rupprechter, H.-J. Freund, The influence of surface defects on methanol decomposition on Pd (111) studied by XPS and PM-IRAS, Surf. Sci. 566 (2004) 740–745.

[16] O. Skoplyak, C.A. Menning, M.A. Barteau, J.G. Chen, Experimental and theoretical study of reactivity trends for methanol on Co/ Pt (111) and Ni/ Pt (111) bimetallic surfaces, J. Chem. Phys. 127 (11) (2007) 114707.

[17] V. Orazi, P. Bechthold, P.V. Jasen, R. Faccio, M.E. Pronsato, E.A. Gonzalez, DFT study of methanol adsorption on PtCo (111), Appl. Surf. Sci. 420 (2017) 383–389.

[18] L.T. Sein Jr., S.A. Jansen, DFT study of the adsorption and dissociation of methanol on NiAl (100), J. Catal. 196 (2) (2000) 207–211.

[19] Ø. Borck, I.-H. Svenum, A. Borg, Adsorption of methanol and methoxy on NiAl (110) and Ni_3Al (111): A DFT study, Surf. Sci. 603 (16) (2009) 2378–2386.

[20] P. Du, P. Wu, C. Cai, Mechanism of methanol decomposition on the Pt_3Ni (111) surface: DFT study, J. Phys. Chem. C 121 (17) (2017) 9348–9360.

[21] S.B. Dalavi, S. Agarwal, P. Deshpande, K. Joshi, B.L.V. Prasad, Disordered but efficient: Understanding the role of structure and composition of the Co–Pt alloy on the electrocatalytic methanol oxidation reaction, J. Phys. Chem. C 125 (14) (2021) 7611–7624, http://dx.doi.org/10.1021/acs.jpcc.0c10165, arXiv:https://doi.org/10.1021/acs.jpcc.0c10165.

[22] F. Mehmood, J. Greeley, P. Zapol, L.A. Curtiss, Comparative density functional study of methanol decomposition on Cu_4 and Co_4 clusters, J. Phys. Chem. B 114 (45) (2010) 14458–14466.

[23] R.J. Gasper, A. Ramasubramaniam, Density functional theory studies of the methanol decomposition reaction on graphene-supported Pt_{13} nanoclusters, J. Phys. Chem. C 120 (31) (2016) 17408–17417.

[24] Z.-J. Zuo, L. Wang, P.-D. Han, W. Huang, Insight into the size effect on methanol decomposition over Cu-based catalysts based on density functional theory, Comput. Theor. Chem. 1033 (2014) 14–22.

[25] K. Ghatak, T. Sengupta, S. Krishnamurty, S. Pal, Computational investigation on the catalytic activity of Rh_6 and Rh_4 Ru_2 clusters towards methanol activation, Theor. Chem. Account. 134 (1) (2015) 1–11.

[26] H. Petitjean, K. Tarasov, F. Delbecq, P. Sautet, J.M. Krafft, P. Bazin, M.C. Paganini, E. Giamello, M. Che, H. Lauron-Pernot, et al., Quantitative investigation of MgO Brønsted basicity: DFT, IR, and calorimetry study of methanol adsorption, J. Phys. Chem. C 114 (7) (2010) 3008–3016.

[27] Z. Liu, C.C. Sorrell, P. Koshy, J.N. Hart, DFT study of methanol adsorption on defect-free CeO_2 low-index surfaces, ChemPhysChem 20 (16) (2019) 2074–2081.

[28] Ø. Borck, E. Schröder, First-principles study of the adsorption of methanol at the α-Al_2O_3 (0001) surface, J. Phys.: Condens. Matter 18 (1) (2005) 1.

[29] Ø. Borck, E. Schröder, Adsorption of methanol and methoxy on the α-Cr_2O_3 (0001) surface, J. Phys.: Condens. Matter 18 (48) (2006) 10751.

[30] W. Liu, J.-g. Wang, X. Guo, W. Fang, M. Wei, X. Lu, L. Lu, Dissociation of methanol on hydroxylated TiO_2-B (100) surface: Insights from first principle DFT calculation, Catal. Today 165 (1) (2011) 32–40.

[31] T. Choksi, J. Greeley, Partial oxidation of methanol on MoO_3 (010): A DFT and microkinetic study, ACS Catal. 6 (11) (2016) 7260–7277.

[32] A. Kumar, R. Kumar, R. Singh, B. Prasad, D. Kumar, M. Kumar, Biosynthesis of ZnO nanoparticles and effect of silver doping in gas sensing characteristics of volatile organic compounds, J. Coat. Technol. Res. (2021) 1–13.

[33] S. Mehta, S. Agarwal, N. Kenge, S.P. Mekala, V. Patil, T. Raja, K. Joshi, Mixed metal oxide: A new class of catalyst for methanol activation, Appl. Surf. Sci. 534 (2020) 147449.

[34] J. Andzelm, N. Govind, G. Fitzgerald, A. Maiti, DFT study of methanol conversion to hydrocarbons in a zeolite catalyst, Int. J. Quantum Chem. 91 (3) (2003) 467–473.

[35] C. Wang, Y. Chu, A. Zheng, J. Xu, Q. Wang, P. Gao, G. Qi, Y. Gong, F. Deng, New insight into the hydrocarbon-pool chemistry of the methanol-to-olefins conversion over zeolite H-ZSM-5 from GC-MS, solid-state NMR spectroscopy, and DFT calculations, Chem. Eur. J. 20 (39) (2014) 12432–12443.

[36] M.F. Fellah, I. Onal, DFT study of direct methanol oxidation to formaldehyde by N_2O on the $[Fe]^{2+}$–ZSM-5 zeolite cluster, J. Phys. Chem. C 116 (25) (2012) 13616–13622.

[37] A.O. Elnabawy, R. Schimmenti, A. Cao, J.K. Nørskov, Why ZnO is the support for cu in methanol synthesis? A systematic study of the strong metal support interactions, ACS Sustain. Chem. Eng. 10 (4) (2022) 1722–1730, http://dx.doi.org/10.1021/acssuschemeng.1c07980, arXiv:https://doi.org/10.1021/acssuschemeng.1c07980.

[38] B. Meyer, D. Marx, Density-functional study of the structure and stability of ZnO surfaces, Phys. Rev. B 67 (3) (2003) 035403.

[39] A. Boisen, S. Dahl, J.K. Nørskov, C.H. Christensen, Why the optimal ammonia synthesis catalyst is not the optimal ammonia decomposition catalyst, J. Catal. 230 (2) (2005) 309–312, http://dx.doi.org/10.1016/j.jcat.2004.12.013, URL https://www.sciencedirect.com/science/article/pii/S0021951704006013.

[40] C.T. Vo, L.K. Huynh, J.-Y. Hung, J.-C. Jiang, Methanol adsorption and decomposition on ZnO $(10\bar{1}0)$ surface: A density functional theory study, Appl. Surf. Sci. 280 (2013) 219–224.

[41] N. Abedi, P. Herrmann, G. Heimel, Methanol on ZnO $(10\bar{1}0)$: From adsorption over initial dehydrogenation to monolayer formation, J. Phys. Chem. C 119 (37) (2015) 21574–21584, http://dx.doi.org/10.1021/acs.jpcc.5b07154, arXiv:https://doi.org/10.1021/acs.jpcc.5b07154.

[42] S. Ruan, Z. Li, H. Shi, W. Wang, X. Ren, X. Shao, Identifying different adsorption states of methanol on ZnO$(10\bar{1}0)$: A scanning tunneling microscopy and density functional theory study, J. Phys. Chem. C 123 (14) (2019) 9105–9111, http://dx.doi.org/10.1021/acs.jpcc.9b00576, arXiv:https://doi.org/10.1021/acs.jpcc.9b00576.

[43] G.K. Smith, S. Lin, W. Lai, A. Datye, D. Xie, H. Guo, Initial steps in methanol steam reforming on PdZn and ZnO surfaces: Density functional theory studies, Surf. Sci. 605 (7–8) (2011) 750–759.

[44] L. Jin, Y. Wang, Surface chemistry of methanol on different ZnO surfaces studied by vibrational spectroscopy, Phys. Chem. Chem. Phys. 19 (20) (2017) 12992–13001.

[45] P.E. Blöchl, Projector augmented-wave method, Phys. Rev. B 50 (24) (1994) 17953–17979.

[46] G. Kresse, D. Joubert, From ultrasoft pseudopotentials to the projector augmented-wave method, Phys. Rev. B 59 (3) (1999) 1758–1775.

[47] J.P. Perdew, K. Burke, M. Ernzerhof, Generalized gradient approximation made simple, Phys. Rev. Lett. 77 (18) (1996) 3865–3868.

[48] J.P. Perdew, K. Burke, M. Ernzerhof, Generalized gradient approximation made simple, Phys. Rev. Lett. 78 (7) (1997) 1396; Phys. Rev. Lett. 77 (1996) 3865.

[49] G. Kresse, J. Hafner, *Ab initio* molecular-dynamics simulation of the liquid-metal–amorphous-semiconductor transition in germanium, Phys. Rev. B 49 (20) (1994) 14251–14269.

[50] G. Kresse, J. Furthmüller, Efficient iterative schemes for *ab initio* total-energy calculations using a plane-wave basis set, Phys. Rev. B 54 (16) (1996) 11169–11186.

[51] G. Kresse, J. Furthmüller, Efficiency of ab-initio total energy calculations for metals and semiconductors using a plane-wave basis set, Comput. Mater. Sci. 6 (1) (1996) 15–50.

[52] A. Jain, S.P. Ong, G. Hautier, W. Chen, W.D. Richards, S. Dacek, S. Cholia, D. Gunter, D. Skinner, G. Ceder, et al., Commentary: The materials project: A materials genome approach to accelerating materials innovation, Appl. Mater. 1 (1) (2013) 011002.

[53] R.R. Reeber, Lattice parameters of ZnO from 4.2 to 296 K, J. Appl. Phys. 41 (13) (1970) 5063–5066.

[54] E.M. Flores, M.L. Moreira, M.J. Piotrowski, Structural and electronic properties of bulk ZnX (X=O, S, Se, Te), ZnF_2, and ZnO/ZnF_2: A DFT investigation within PBE, PBE+ U, and hybrid HSE functionals, J. Phys. Chem. A 124 (19) (2020) 3778–3785.

[55] D. Stradi, L. Jelver, S. Smidstrup, K. Stokbro, Method for determining optimal supercell representation of interfaces, J. Phys.: Condens. Matter 29 (18) (2017) 185901.

[56] S. Grimme, Semiempirical GGA-type density functional constructed with a long-range dispersion correction, J. Comput. Chem. 27 (15) (2006) 1787–1799.

[57] R. Dronskowski, P.E. Blöchl, Crystal orbital Hamilton populations (COHP): energy-resolved visualization of chemical bonding in solids based on density-functional calculations, J. Phys. Chem. 97 (33) (1993) 8617–8624.

[58] V.L. Deringer, A.L. Tchougréeff, R. Dronskowski, Crystal orbital Hamilton population (COHP) analysis as projected from plane-wave basis sets, J. Phys. Chem. A 115 (21) (2011) 5461–5466.

[59] S. Maintz, V.L. Deringer, A.L. Tchougréeff, R. Dronskowski, Analytic projection from plane-wave and PAW wavefunctions and application to chemical-bonding analysis in solids, J. Comput. Chem. 34 (29) (2013) 2557–2567.

[60] S. Maintz, V.L. Deringer, A.L. Tchougréeff, R. Dronskowski, LOBSTER: A tool to extract chemical bonding from plane-wave based DFT, J. Comput. Chem. 37 (11) (2016) 1030–1035.

[61] O. Dulub, L.A. Boatner, U. Diebold, STM study of the geometric and electronic structure of ZnO (0001)-Zn,(0001)-o,$(10\bar{1}0)$, and $(11\bar{2}0)$ surfaces, Surf. Sci. 519 (3) (2002) 201–217.

[62] U. Diebold, L.V. Koplitz, O. Dulub, Atomic-scale properties of low-index ZnO surfaces, Appl. Surf. Sci. 237 (1) (2004) 336–342, http://dx.doi.org/10.1016/j.apsusc.2004.06.040, Proceedings of the Seventh International Symposium on Atomically Controlled Surfaces, Interfaces and Nanostructures. URL https://www.sciencedirect.com/science/article/pii/S0169433204009857.

[63] R.G.S. Pala, H. Metiu, Selective promotion of different modes of methanol adsorption via the cation substitutional doping of a ZnO$(10\bar{1}0)$ surface, J. Catal. 254 (2) (2008) 325–331, http://dx.doi.org/10.1016/j.jcat.2008.01.014, URL https://www.sciencedirect.com/science/article/pii/S0021951708000158.

Journal Pre-proof

Electronic fingerprints for diverse interactions of methanol with various Zn-based systems

Shweta Mehta, Kavita Joshi

PII: S0039-6028(23)00103-6
DOI: https://doi.org/10.1016/j.susc.2023.122350
Reference: SUSC 122350

To appear in: *Surface Science*

Received date : 14 February 2023
Revised date : 30 May 2023
Accepted date : 16 June 2023

Please cite this article as: S. Mehta and K. Joshi, Electronic fingerprints for diverse interactions of methanol with various Zn-based systems, *Surface Science* (2023), doi: https://doi.org/10.1016/j.susc.2023.122350.

This is a PDF file of an article that has undergone enhancements after acceptance, such as the addition of a cover page and metadata, and formatting for readability, but it is not yet the definitive version of record. This version will undergo additional copyediting, typesetting and review before it is published in its final form, but we are providing this version to give early visibility of the article. Please note that, during the production process, errors may be discovered which could affect the content, and all legal disclaimers that apply to the journal pertain.

© 2023 Published by Elsevier B.V.

Journal Pre-proof

Electronic fingerprints for diverse interactions of methanol with various Zn-based systems

Shweta Mehta and Kavita Joshi*

Physical and Materials Chemistry Division,

CSIR-National Chemical Laboratory,

Dr. Homi Bhabha Road, Pashan, Pune 411008, India and

Academy of Scientific and Innovative Research (AcSIR), Sector 19,

Kamla Nehru Nagar, Ghaziabad, Uttar Pradesh- 201002, India.

(Dated: May 30, 2023)

Abstract

We have investigated various Zn-based catalysts for their interaction with methanol (MeOH). MeOH is one of the most critical molecules being studied extensively, and Zn-based catalysts are widely used in many industrially relevant reactions involving MeOH. We note that the same element (Zn and O, in the present study) exhibits different catalytic activity in different environments. The changing environment is captured in the underlying electronic structure of the catalysts. In the present work, we compared the electronic structure of Zn-based systems, i.e., $ZnAl_2O_4$ and ZnO along with oxygen preadsorbed Zn (O-Zn) and metallic Zn. We demonstrate the one-to-one correlation between the pDOS of the bare facet and the outcome of that facet's interaction (i.e. either adsorption or dissociation of MeOH) with MeOH. These findings would pave the way towards the in-silico design of catalysts.

* k.joshi@ncl.res.in

Journal Pre-proof

Journal Pre-proof

I. INTRODUCTION

For conversion of methanol to any value added product dissociation of its O-H and/or C-H bond is the primary step. Considering the importance of MeOH in the chemical industry as feedstock or fuel, its interaction with various catalysts is studied extensively. The interaction of methanol with metal surfaces like Al[1], Si[2], Ge[3], Fe[4], Ru[5], Rh[6], Ni[7], Pd[8], Pt[9], Cu[10], Ag[11], Au[12] has been extensively investigated using both experimental and theoretical methods. The activation barrier for inert metals such as Au and Ag is very high, almost of the order of 1.5 eV, while for Pd and Pt, it reduces to $\approx$ 0.80 eV. However one would like to replace precious metals by other earth abundant metals for the economical viability. This encourages further investigations into non-precious metals for methanol dissociation. Cu surfaces have also been studied in detail for MeOH interaction.[10, 13, 14] The activation barrier for O-H bond dissociation of MeOH on Cu surfaces is as low as 0.38 eV. In a recent experimental study, Roey et al. demonstrated the methanol decomposition on various Cu surfaces such as (100), (110), and (111) at ambient conditions.[15] They observed that methanol readily decomposes to methoxy on all these surfaces at atmospheric pressure and room temperature. They also report that the kinetics of conversion of methanol to carbon monoxide is structure sensitive and depends on the surface environment. Adsorption of oxygen on metal surfaces affects their reactivity by altering geometric and electronic properties.[16–19] Oxygen binds strongly with almost all metals and triggers surface reconstruction. This reconstruction either facilitates adsorption or blocks the active sites of catalyst. Also, the higher electronegativity of oxygen as compared to metals leads to redistribution of charge density on metal surfaces and hence affect their chemical reactivity.[20] Methanol decomposition has also been investigated in the presence of preadsorbed oxygen atoms on various metal surfaces.[21–24] Xu et al. investigated the interaction of methanol on oxygen-preadsorbed Au(111) surface by employing DFT.[23] They report that the

Journal Pre-proof

activation barrier for dissociation of the O-H bond of methanol reduces to 0.41 eV, which is one-fourth of the barrier for bare Au(111) surface (1.58 eV). Similarly, Aljama et al. demonstrated the conversion of methanol to formaldehyde at Ag(111) surface using DFT and microkinetic modeling.[24] They observed that preadsorbed oxygen enhances the reactivity of the Ag surface by reducing the activation barrier to 0.81 eV, which is significantly lower than the clean surface (2.85 eV). This manifests effect of preadsorbed oxygen on metal surfaces in enhancing the MeOH decomposition. To our knowledge, no studies report the interaction of methanol with zinc surfaces. In the present work, we have examined the interaction of MeOH on various Zn surfaces viz. $(10\bar{1}0)$, $(10\bar{1}1)$, and $(10\bar{1}3)$ to demonstrate the structure-activity relationship. Effect of oxygen adsorption on the interaction of MeOH with Zn surfaces has also been explored in detail. The activation barrier of O-H bond dissociation significantly reduces on preadsorbed oxygen compared to the pure metallic surface.

On the other hand, it is very well established that the metal oxides exhibit higher catalytic activity than pure metallic surfaces due to presence of various acidic and basic sites. Various metal oxides like MgO,[25] Al_2O_3,[26] Ga_2O_3,[27] TiO_2,[28] CeO_2,[29] and ZnO[30] have been extensively investigated for their interaction with methanol. It is common to all metal oxides, that, anionic oxygen atoms favor the dehydrogenation of MeOH by forming hydroxide with H_{MeOH}, while the dissociated fragments are stabilized over cationic metal atoms. Spontaneous dissociation of methanol is reported by Liu et al. on low index CeO2 surfaces.[29] They investigated the interaction of methanol with (100), (110), and (111) facets of CeO_2 by employing DFT. They report that the interaction of methanol with the facet is highly dependent on the arrangement of atoms on the facet. Spontaneous dissociation of O-H bond of methanol takes place on the (100) and (110) facet while only molecular adsorption at (111) facet. In our previous study, we have also discussed in detail the interaction of methanol with ZnO [31, 32] We elaborate on the site-dependent interaction of methanol (molecular adsorption or dissociation) on various ZnO surfaces. Further,

Journal Pre-proof

we have also investigated interaction of MeOH with $ZnAl_2O_4$.[33] Our periodic DFT calculations demonstrated that the dissociation of methanol is energetically favorable outcome at the $ZnAl_2O_4$ facets.

Our previous work demonstrated that the composition as well as facets play a crucial role in determining the outcome of the interaction. First, we investigated interaction of MeOH with a mixed metal oxide like $ZnAl_2O_4$ followed by metal oxide like ZnO. In the present work, we investigate the interaction of methanol with various Zn metal surfaces as well as oxygen adsorbed Zn facets by exploiting periodic DFT. Thus, we are reducing the complexity to understand factors associated with a particular outcome. In these series of virtual experiments the outcomes are either adsorption of MeOH (physisorption or chemisorption) or spontaneous dissociation of O-H bond. It is indispensable to investigate the underlying electronic structure to understand the rationality behind these interactions. Our group's work over the years shows a clear-cut trend in the interaction of MeOH with Zn-based facets. In this work, we analyze all the surfaces studied so far to determine the correlation between the electronic structure of bare facets and the outcome of MeOH adsorption. The ultimate goal of any DFT based computation is to understand the results in terms of underlying electronic structure, derive trends, and gain predictive power. This work is an attempt in that direction.

II. COMPUTATIONAL DETAILS:

All the calculations are carried out within the Kohn-Sham formalism of DFT. Projector Augmented Wave potential[34] is used, with Perdew Burke Ernzerhof (PBE) approximation for the exchange-correlation and generalized gradient approximation,[35] as implemented in planewave, pseudopotential based code, Vienna Ab initio Simulation Package (*VASP*).[36] The bulk unit cell is taken from the materials project.[37] The bulk lattice parameters upon optimization are a = 2.62 Å and c = 5.02 Å which

Journal Pre-proof

are in agreement with the experimentally measured (a = 2.66 Å, c = 4.95 Å).[38] Two flat facets ($10\bar{1}0$) and ($10\bar{1}1$) of Zn are modeled as slab by cleaving a surface with 3x3 periodicity in x and y direction with 4 layers using Quantumwise-VNL-2017.1.[39] The step facet ($10\bar{1}3$) is cleaved using 4x1 periodicity in x and y direction with 4 layers. Bottom layer is fixed and rest all layers and adsorbate are fully relaxed for all surface calculations. Van der Waals corrections are applied to account dynamic correlations between fluctuating charge distribution by employing Grimme method (DFT-D2).[40] It is observed that 20 Å of vacuum is sufficient to avoid interaction between adjacent images of planes along the z-direction. Geometry optimization is carried out with a force cutoff of 0.01 eV/Å on the unfixed atoms and the total energies are converged below 10^{-4} eV for each SCF cycle. A Monkhorst-Pack grid of 3x2x1, 4x2x1, and 2x2x1 is used for ($10\bar{1}0$), ($10\bar{1}1$), and ($10\bar{1}3$) slabs respectively. The difference in energies is less than 4 meV/atom upon using finer mesh. Entire surface is scanned by placing the MeOH molecule at various available unique sites. To compare the interaction of methanol at these sites, interaction energy is calculated using the formula: $E_{MeOH/Zn} = E_{MeOH+Zn}$ - ($E_{Zn} + E_{MeOH}$) where $E_{MeOH+Zn}$ is energy of the system when MeOH is placed on the Zn surface, E_{Zn} is energy of the bare surface and E_{MeOH} is energy of the MeOH molecule. Further to investigate the effect of oxygen adsorption on reactivity of Zn surfaces, we placed an oxygen atom on all the facets. The interaction energy for oxygen adsorption is calculated using following formula: $E_{O/Zn} = E_{O+Zn}$ - ($E_{Zn} + 1/2\ E_{O2}$) where E_{O+Zn} is energy of the system when oxygen atom is placed on the surface, E_{Zn} is energy of the bare surface and E_{O2} is energy of the isolated O_2 molecule. Also, the interaction energy of methanol adsorption on oxygen preadsorbed Zn surface is calculated using formula: $E_{MeOH/O-Zn}$ = $E_{MeOH+O-Zn}$ - ($E_{O+Zn} + E_{MeOH}$) Here, $E_{MeOH+O-Zn}$ is the energy of system with methanol adsorbed on oxygen preadsorbed Zn surface. To understand the site specific adsorption pattern, the site-dependent projected Density of States (pDOS) are calculated with denser k-mesh using LOBSTER.[41] The activation barrier for O-

Journal Pre-proof

H bond dissociation of methanol is computed using the climbing image-nudged elastic band (CI-NEB) method for both clean and oxygen preadsorbed surfaces.[42] Three images are considered for transition state calculations using a force convergence of 0.1 eV/Å. The computational details of ZnO and $ZnAl_2O_4$ are discussed in detail in our previous papers.[31–33]

III. RESULTS AND DISCUSSION

The rational design of a catalyst for any reaction requires consideration of several parameters like material abundance, cost, the reactivity of the catalyst, reaction conditions, selectivity of products, etc. Some factors, like material abundance and cost, are out of our control. However, the catalytic properties could be altered/improved by understanding its functionality at the atomistic level. Zn-based catalysts are extensively used in many reactions[43–46] because of the abundance of Zn (24^{th} in the earth's crust), inexpensiveness, and safe handling methods. In the present work, we investigate the interaction of MeOH with a series of Zn-based catalysts to understand how the environment changes the properties of a catalyst. We will be comparing the interaction of MeOH with various facets of Zn, oxygen-preadsorbed Zn(O-Zn), ZnO, and finally, with $ZnAl_2O_4$ to understand the reactivity of these catalysts at the electronic level.

We begin by discussing the interaction of methanol with different metallic Zn surfaces. We have modelled $(10\bar{1}0)$, $(10\bar{1}1)$, and $(10\bar{1}3)$ facets of Zn because they exhibit the most prominent peaks in the XRD. Top and side views of all these facets are shown in Fig. SI-1. All these facets are scanned by placing methanol at various inequivalent sites. Before detailed discussions, we note that the physisorption and chemisorption of methanol is explained on the basis of O-H bond-length of methanol upon adsorption. Physisorption of MeOH is accompanied by surface reconstruction of the flat facets, whereas the step facet does not show any rearrangement of surface

Journal Pre-proof

TABLE I: Interaction energy ($E_{MeOH/Zn}$/$E_{MeOH/O-Zn}$) (eV), O-H bond-length (Å) of MeOH at various inequivalent sites of $(10\bar{1}0)$, $(10\bar{1}1)$, and $(10\bar{1}3)$ facets of pristine zinc (in black color) and oxygen preadsorbed Zn (in blue color). For O-Zn, the O_{surf}-H_{MeOH} bond-length is shown in parenthesis. In all the cases, irrespective of its initial position, MeOH always diffuses on the surface and adsorb with its oxygen ontop of Zn. However, variation in the relative orientation of MeOH with respect to surface results into observed variation in E_{int}. The energetically most favorable configuration at each facet is represented by numbers in bold.

Initial positions	$(10\bar{1}0)$		$(10\bar{1}1)$		$(10\bar{1}3)$	
	$E_{MeOH/Zn}$	O-H	$E_{MeOH/Zn}$	O-H	$E_{MeOH/Zn}$	O-H
	$E_{MeOH/O-Zn}$	BL	$E_{MeOH/O-Zn}$	BL	$E_{MeOH/O-Zn}$	BL
	(eV)	(Å)	(eV)	(Å)	(eV)	(Å)
Top	-3.37	0.98	-1.31	0.98	**-0.67**	**0.99**
	-1.66	0.98(3.28)	-0.59	0.99(1.87)	**-1.01**	**1.05(1.49)**
Bridge	—	—	-1.26	0.98	—	—
	—	—	-0.63	0.99(1.76)	—	—
SB	**-4.09**	**0.99**	—	—	-0.57	0.98
	-3.26	**0.99(3.48)**	—	—	-0.93	1.05(1.51)
LB	-3.36	0.98	—	—	-0.64	0.99
	-1.57	0.98(6.47)	—	—	-1.01	1.05(1.49)
4FH/3FH	-3.23	0.99	**-1.35**	**0.98**	-0.64	0.99
	-1.98	0.99(3.44)	**-0.72**	**0.99(1.86)**	-0.64	0.99(6.96)
Top_s	—	—	-1.32	0.98	—	—
	—	—	-0.61	0.99(1.87)	—	—

atoms. We compared the nearest neighbour (NN) distances for all three bare facets before and after methanol adsorption which provides clear evidence of reconstruction in both flat facets as shown in Fig. SI-2. The red line represents the NN distances before MeOH adsorption, and the blue line represents the NN distances after methanol

Journal Pre-proof

adsorption. There is a noticeable variation in NN distances in both flat facets, while the surface reconstruction in the step facet is minimal. This rearrangement of surface atoms also reflects in the lowering of interaction energy of MeOH (refer to Tab.I). In Tab.I, we have noted the interaction energy and O-H bond-length of methanol on all three facets of metallic Zn (in black color) and oxygen preadsorbed Zn (in blue color). The bond-length between O_{surf}-H_{MeOH} are shown in brackets for all facets of O-Zn. In all the cases, irrespective of the initial position, upon optimization, methanol diffuses on the surface and adsorb ontop of Zn. However, in Tab.I, we have noted the initial position where methanol was placed to distinguish each configuration. The energetically most stable configuration for each facet is shown in bold numbers. The interaction energies for $(10\bar{1}0)$ facets are significantly larger because, the reconstruction energies are buried in it. However, to normalize the interaction energy for all systems, we have excluded the reconstruction energy and noted in Tab.II as WOR. The extent of reconstruction is significant for the $(10\bar{1}0)$ facet because of its open structure and is minimal or absent for the other two facets [$(10\bar{1}1)$, $(10\bar{1}3)$]. The reconstruction on $(10\bar{1}0)$ causes the rearrangement of atoms on the surface, which resembles that of the $(10\bar{1}1)$ facet.

As discussed earlier, exposing a metal surface to oxygen alters its reactivity considerably.[16–19] To understand the effect of oxygen adsorption on the reactivity of zinc facets, we have adsorbed atomic oxygen on all these facets, as shown in Fig. SI-3. The oxygen on the $(10\bar{1}0)$ surface diffuses to the subsurface layer, while on the other two facets [$(10\bar{1}1)$ and $(10\bar{1}3)$], it adsorbs on the surface. Closed packing of atoms on the $(10\bar{1}1)$ and $(10\bar{1}3)$ facets doesn't favor oxygen diffusion in the subsurface layer.

We placed MeOH at various unique sites of oxygen-preadsorbed Zn surfaces. For pristine metallic surfaces, the MeOH physisorbed on the surface with no elongation in the O-H bond. Oxygen adsorption causes activation of the methanol on the step facet of O-Zn. Representative cases of MeOH adsorption on Zn and oxygen-preadsorbed

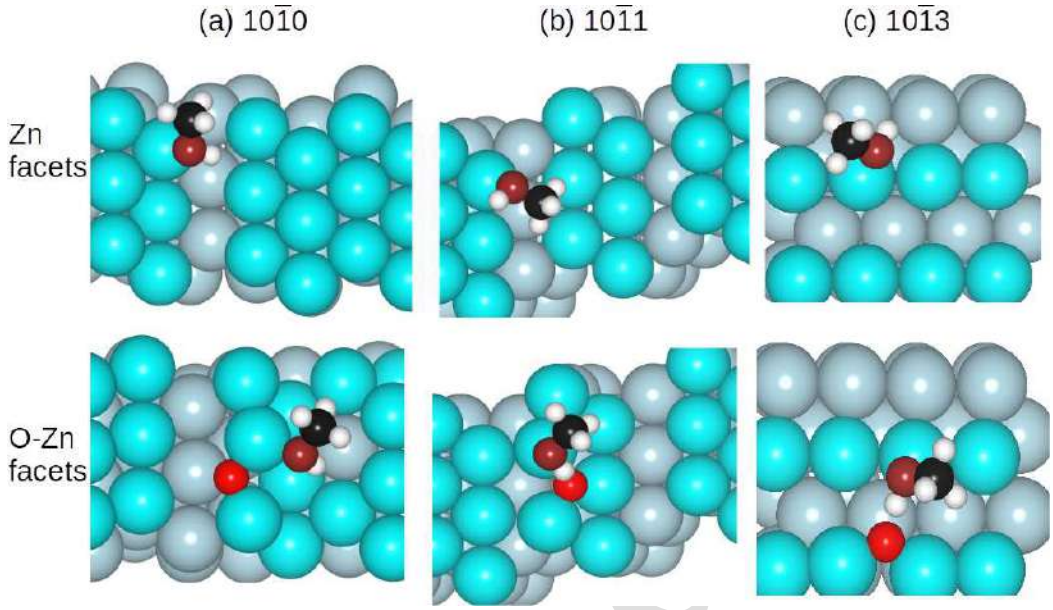

FIG. 1: Interaction of methanol with various facets of pristine Zn (upper panel) and oxygen preadsorbed Zn system (lower panel). (a) represents the energetically most stable configuration of MeOH adsorption at (10$\bar{1}$0) facet. Methanol adsorption results into substantial reconstruction at the surface. The bare facet of (10$\bar{1}$0) is shown in Fig. SI1-(a). Surface atoms of this facet rearrange themselves and the atomic arrangement resembles to that of (10$\bar{1}$1) facet. (b) depicts the adsorption of MeOH at (10$\bar{1}$1) facet. The extent of reconstruction upon MeOH adsorption is much less compared to (10$\bar{1}$0). (c) Adsorption of MeOH at (10$\bar{1}$3) facet. No reconstruction is observed at this facet upon MeOH adsorption.

Zn are shown in Fig.1 (the upper panel and lower panel represent MeOH adsorption at pristine Zn and oxygen-preadsorbed Zn surfaces, respectively). The (10$\bar{1}$0) facet of Zn undergoes substantial reconstruction upon adsorption of methanol as evident from upper panel of Fig.1-(a).

Although preadsorbed oxygen enhances the catalytic activity of metal surfaces, the reactivity depends on several other factors, such as the structural arrangement of atoms, coordination numbers, and effective charge on surface atoms. As evident from Tab.I, the O-H bond does not elongate on the (10$\bar{1}$0) facet of O-Zn because of the adsorption of oxygen below the surface layer resulting into indirect interaction with adsorbed methanol. In the case of (10$\bar{1}$1) and (10$\bar{1}$3), oxygen is present on the sur-

Journal Pre-proof

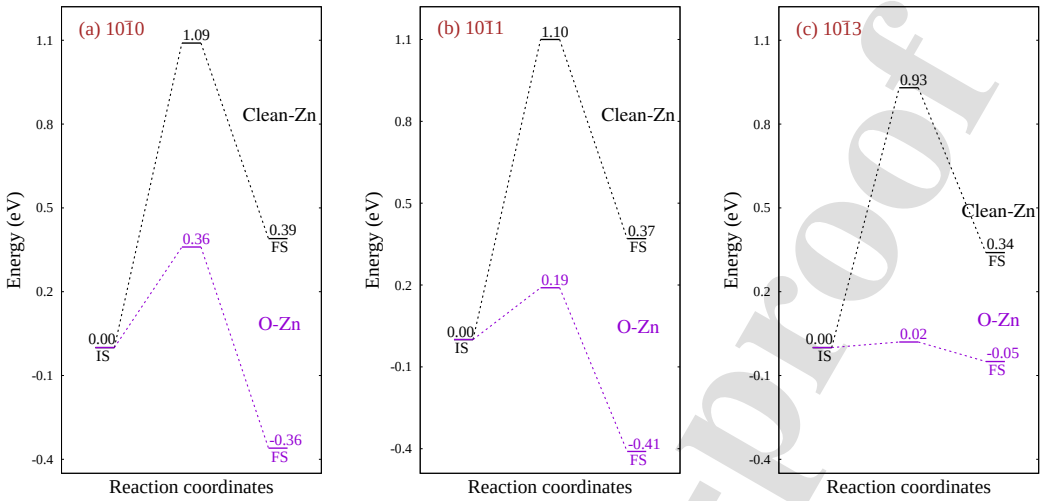

FIG. 2: The activation barrier for O-H bond of MeOH at (a) (10$\bar{1}$0), (b) (10$\bar{1}$1), and (10$\bar{1}$3) facets are shown. In case of flat facets, the activation barrier significantly reduces from clean Zn to O-assisted Zn surface, while for step facet, it becomes negligible. Also, the thermodynamics of reaction become favorable upon oxygen adsorption.

face and hence favors the adsorption of methanol on the surface by forming hydrogen bonds. The strength of the hydrogen bond between O_{surf}-H_{MeOH} determines the activation of methanol on the O-Zn systems. The proximity of surface oxygen and hydrogen of MeOH results in higher activation of the O-H bond of methanol with 9% elongation on the step (10$\bar{1}$3) facet. The O-H bond-length of methanol on the (10$\bar{1}$1) surface of oxygen preadsorbed Zn has little elongation despite interaction with the surface oxygen as shown in Tab.I. This can be explained by the distance between the O_{surf}-H_{MeOH}. The observed activation of O-H in MeOH is directly proportional to the distance between O_{surf}-H_{MeOH}. We computed the activation barrier for dissociation of the O-H bond on all Zn surfaces and oxygen-preadsorbed Zn surfaces. The results are depicted in Fig.2. The energy profile shows that the activation barrier decreases for all three facets upon oxygen adsorption. The barrier for (10$\bar{1}$0) and (10$\bar{1}$1) reduces to one-third and one-fifth respectively, while for the step facet, it becomes almost negligible. Change in reaction energy from positive to negative upon

oxygen adsorption makes the reaction exothermic. The presence of oxygen on the surface also helps in stabilizing the hydrogen dissociated from methanol by forming the hydroxide.

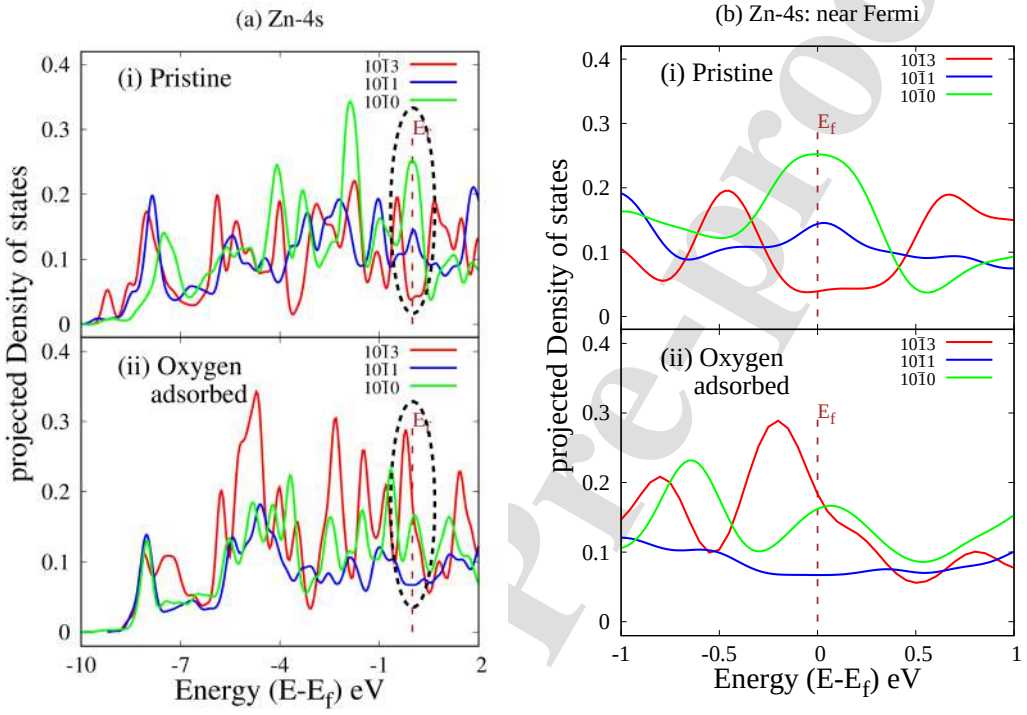

FIG. 3: (a) represents pDOS of 4s levels of pristine Zn surfaces and oxygen adsorbed Zn surfaces. Significant variation in nature of 4s is observed upon oxygen adsorption on Zn surfaces. (b) shows the magnified 4s level near Fermi which are marked in (a). It is clear from the figure that for stepped facets (red curve) the peak intensity increases near Fermi while for both flat facets (blue and green curve) the peak intensity reduces near Fermi as compared to the pristine surfaces.

The change in the underlying electronic structure upon oxygen adsorption provides a rationale for the observed variation in the reactivity of Zn facets. The 4s levels for Zn metal are close to Fermi and participates in reactivity. Fig.3-(a): (i) and (ii) illustrate the site-specific pDOS of Zn-4s for bare facets of pristine and oxygen-adsorbed surfaces, respectively. The 4s near Fermi, marked in Fig.3-(a), is enlarged

Journal Pre-proof

and displayed in Fig.3-(b). The magnified plot clearly shows that for the step facet, the intensity of 4s states increases near and at the Fermi level in the oxygen-adsorbed facet compared to the pristine one. In contrast, the 4s intensity decreases near the Fermi level for both the flat facets. The presence of 4s states near the Fermi level facilitates the activation of methanol at the step facet. The pDOS of O-2p of surface oxygen atoms in all three facets of O-Zn are shown in the Fig. SI-4. The density of energy states near Fermi is substantially higher in the case of the $(10\bar{1}3)$ facet as compared to other two facets. This explains the observed elongation of the O-H bond on $(10\bar{1}3)$ facet and little elongation on $(10\bar{1}1)$ facet. However, non-zero states at Fermi are not the sole criteria for MeOH activation. Another crucial factor is the presence of surface oxygen in the vicinity of H_{MeOH}. Thus, although the 4s-pDOS are non-zero at Fermi for $(10\bar{1}0)$, the absence of surface oxygen near H_{MeOH} results in barely activated MeOH. In the case of $(10\bar{1}1)$, although the activation of MeOH is comparable to that of $(10\bar{1}0)$, the activation barrier is considerably lower as compared to $(10\bar{1}0)$ because of surface oxygen in the vicinity of H_{MeOH}. On the other hand, in the case of metallic surfaces, the presence of 4s states near Fermi for flat facets do not favour the activation of methanol in the absence of oxygen. Thus, variation in the activity of facets of Zn and O-Zn can be correlated with the electronic structure of the bare facets.

In our previous studies, we discussed the interaction of methanol with several facets of ZnO.[31, 32] We have investigated different flat [$(10\bar{1}0)$, $(10\bar{1}1)$, $(11\bar{2}0)$] and step [$(10\bar{1}3)$, $(11\bar{2}2)$] facets of ZnO for their interaction with methanol. We observed at $(10\bar{1}1)$ facet, methanol spontaneously converts to formaldehyde. These results were validated by experiments and demonstrated that methanol converts to formaldehyde at ZnO nanoparticles at ambient conditions with 100% selectivity. On other flat facets, molecular adsorption is most favorable, while dissociation of MeOH is energetically the most favorable outcome at step facets. The activity of metal oxides can be altered by modifying their structure. ZnO and Al_2O_3 are both used

Journal Pre-proof

as industrial catalysts for methanol synthesis.[47] In one of the earlier studies by our group, we investigated the interaction of methanol with (220) and (311) facets of $ZnAl_2O_4$.[33] We observed molecular adsorption as well as dissociation of methanol on these facets. Depending upon the site of adsorption, MeOH interacts differently with $ZnAl_2O_4$. We reported that lesser coordinated surface oxygen atoms actively participate in methanol dissociation.

TABLE II: Interaction energy of methanol on different Zn based systems are reported in the table. Black numbers depict the energy of metallic Zn and O-Zn systems. Blue and red colored numbers represent interaction of methanol at ZnO, and $ZnAl_2O_4$ facets respectively. Adsorption of methanol on these different system triggers surface reconstruction which reflects in the interaction energy. WR (with reconstruction) stands for energy with the impact of reconstruction. However, in order to homogenize the energies, we have eliminated the reconstruction effect from interaction as demonstrated by WOR (without reconstruction).

systems/facets		$(10\bar{1}0)$/220	$(10\bar{1}1)$/311	$(10\bar{1}3)$	$(11\bar{2}0)$	$(11\bar{2}2)$
Zn	WR	-4.09	-1.36	-0.66		
	WOR	-0.77	-0.69	-0.68		
O-Zn	WR	-3.26	-0.72	-1.01		
	WOR	-0.78	-0.60	-1.13		
ZnO	WR	-1.58	**-7.95**	**-3.88**	-1.24	**-6.24**
	WOR	-1.90	**-4.83**	**-2.91**	-1.40	**-3.38**
$ZnAl_2O_4$	WR	**-1.81**	**-4.14**			
	WOR	**-2.47**	**-4.91**			

We observe that upon changing the environment of Zn and O in series of different systems (Zn, O-Zn, ZnO, and $ZnAl_2O_4$), the interaction of methanol changes from adsorption to dissociation of O-H as well as C-H bond. To understand this variation, we analyzed different parameters such as interaction energy, Mulliken charges, distance between MeOH and surface metal and/or oxygen atoms for all the facets of all these systems. The interaction energy of the energetically most stable configuration

Journal Pre-proof

of methanol on various facets of Zn-based systems is noted in Tab.II. The interaction energy for each system is computed by including and excluding the surface reconstruction energy and described as WR and WOR respectively. The numbers in black represent interaction energy of methanol with Zn and O-Zn surfaces, while blue and red numbers indicate ZnO and $ZnAl_2O_4$ surfaces respectively. The numbers in bold signify dissociation of methanol as energetically most stable outcome on that facet. It is clear from the interaction energies (computed for both the WR and WOR) of Tab.II that the presence of oxygen facilitates the adsorption of MeOH on step facet of O-Zn. We do not observe any correlation between the interaction energy (WR) and outcome of the interaction. However, the extent of reconstruction varies from facet to facet. And hence, upon normalization of the energies by excluding the impact of reconstruction (WOR), there is a one-to-one correlation between interaction energies (WOR) and outcome of MeOH. Dissociation is always associated with lower interaction energy than the molecular adsorption. Also, irrespective of the outcome, methanol interaction is more favored on the ZnO and $ZnAl_2O_4$ facets as compared to Zn and O-Zn.

TABLE III: Mulliken charges on surface zinc atoms of Zn, O-Zn, ZnO, and $ZnAl_2O_4$. For Zn, and O-Zn the charges are shown in black color, whereas for ZnO and $ZnAl_2O_4$, the charges are represented in blue and red color respectively. Charges for the facets where dissociation of MeOH occurs, are shown in bold numbers. Transfer of electron from metal to oxygen is evident from the effective charges on Zn.

systems/facets	$(10\bar{1}0)$/220	$(10\bar{1}1)$/311	$(10\bar{1}3)$	$(11\bar{2}0)$	$(11\bar{2}2)$
Zn	0.05	0.12	0.19(0.14)		
O-Zn	0.49	0.61	0.50		
ZnO	**0.85**	**1.04**	0.96(**0.64**)	0.96	**0.81**
$ZnAl_2O_4$	**1.52**	**1.53**(1.58)			

Next, we note effective charges on surface zinc and oxygen atoms for all the facets investigated in Tab.III and Tab.IV, respectively. The numbers in black depict Zn

Journal Pre-proof

TABLE IV: Mulliken charges on surface oxygen atoms of O-Zn(black color), ZnO(blue color), and $ZnAl_2O_4$(red color). The shortest distance between oxygen and surface atom (BL) is also shown

systems/facets	property	$(10\bar{1}0)$/220	$(10\bar{1}1)$/311	$(10\bar{1}3)$	$(11\bar{2}0)$	$(11\bar{2}2)$
O-Zn	charge(e)	-0.74	-0.81	-1.38		
	BL(Å)	1.93	1.89	1.88		
ZnO	charge(e)	**-0.79**	**-0.68**	**-0.82**(-0.89)	-0.89	**-0.85**
	BL(Å)	1.77	1.85	1.94(1.87)	1.90	1.82
$ZnAl_2O_4$	charge(e)	**-1.03**(-1.07)	**-1.00**(-1.11; -1.17)			
	BL(Å)	1.82(1.74)	1.77(1.93; 1.85)			

and O-Zn systems, whereas the blue and red numbers indicate ZnO and $ZnAl_2O_4$ systems. It is clear from Tab.III that with increasing oxygen content Zn becomes more positive, indicating electron transfer from metal to oxygen. Similarly, as seen from Tab.IV, charge gained by oxygen atoms varies from -0.68 for ZnO$(10\bar{1}1)$ to -1.38 for O-Zn$(10\bar{1}3)$. However, we do not see any correlation between the charge on surface zinc/oxygen and the outcome of the interaction i.e. adsorption or dissociation of MeOH.

Next, we compare pDOS for O-2p of O-Zn, ZnO, and $ZnAl_2O_4$ for flat and step facets as shown in Fig.4-(a) and (b), respectively. The reference pDOS for 2p of O_{MeOH} is plotted in each figure as a gray curve. Depending on the environment the pDOS exhibit subtle variation which influences the outcome of the interaction of MeOH with that facet. Two flat facets [$(10\bar{1}0)$ and $(10\bar{1}1)$] and step facets of ZnO with non zero pDOS at Fermi favours dissociation of MeOH. Whereas for $(11\bar{2}0)$ facet, there are no states at Fermi level and this is the facet of ZnO with chemisorption of MeOH as the only outcome. For both step facets of ZnO (see (ii) of Fig.4-(b)) significantly low number of O-2p states are present near Fermi. However, for both these stepped facets,

Journal Pre-proof

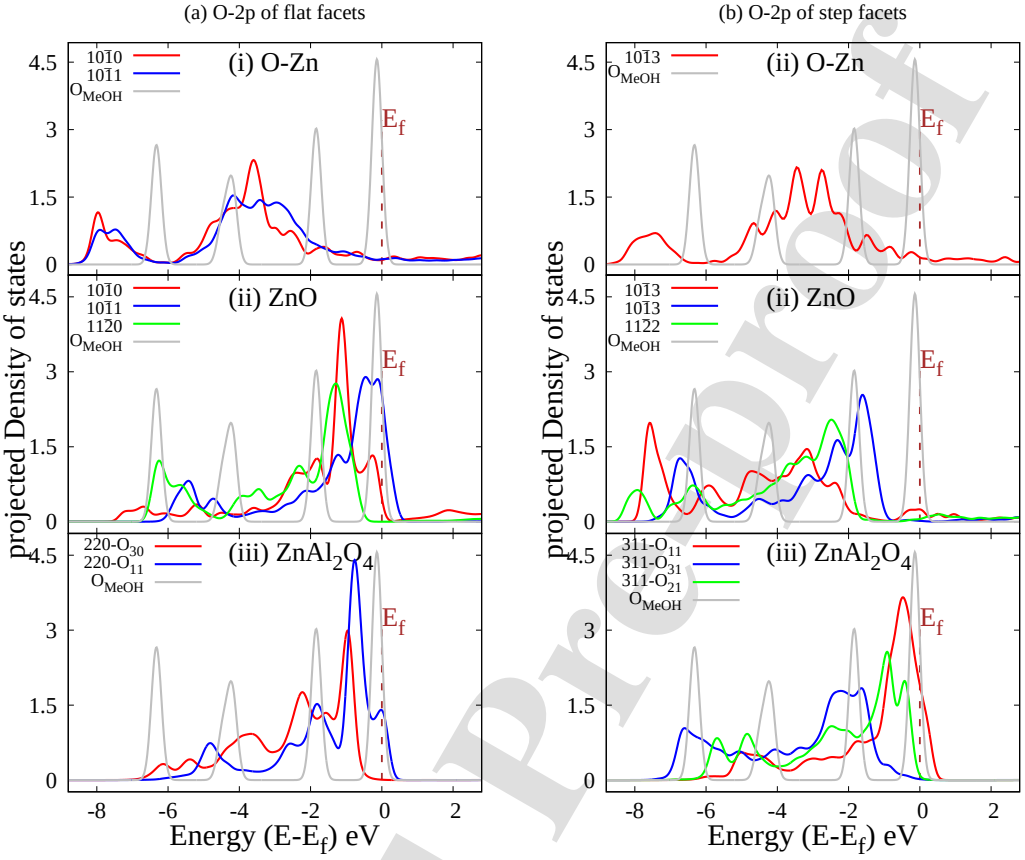

FIG. 4: pDOS of $2p$ of O in different systems (i) oxygen preadsorbed zinc (O-Zn), (ii) metal oxide (ZnO), (iii) mixed metal oxide ($ZnAl_2O_4$). (a) shows flat facets while (b) represents stepped facets. $2p$ of oxygen of methanol is plotted in gray color for reference.

Zn-4s states are present at Fermi (shown in Fig. SI-5-(b)-(iii)) and overlaps with $2p$ states of O_{MeOH}, which accounts for the spontaneous dissociation of MeOH on these facets. This site specific signature of pDOS is also observed in the tDOS plot which reflects the underlying electronic structure of the entire facet. The tDOS plots of flat and step facets of all systems are shown in Fig.5-(a) and (b) respectively. The next system we will discuss is a mixed metal oxide, $ZnAl_2O_4$. For $ZnAl_2O_4$, on (220) and (311) facets dissociation of MeOH is the favoured outcome. Al acts as the active site

Journal Pre-proof

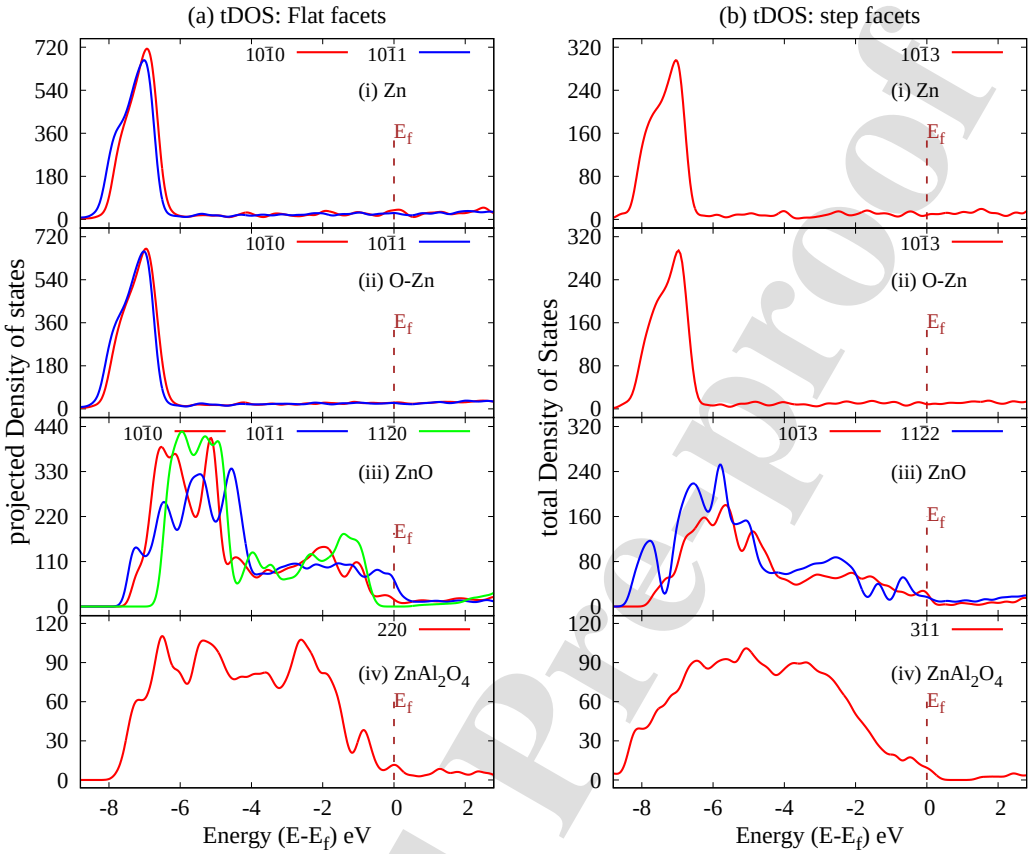

FIG. 5: tDOS of different systems (i) metallic Zn, (ii) oxygen preadsorbed zinc (O-Zn), (iii) metal oxide (ZnO), (iv) mixed metal oxide ($ZnAl_2O_4$). (a) shows flat facets while (b) represents stepped facets.

for methanol adsorption in these cases because of its greater affinity for oxygen than Zn. Surface oxygen atoms have variations in their coordination with Zn and Al atoms. The difference in the coordination of these oxygen atoms also reflects in their *p*DOS plots as seen in Fig.4-(a) and (b)-iii. These different 'types' of oxygen atoms on the surface are denoted based on their coordination with Al and Zn atoms, respectively. For example, the key 220-O_{30} in Fig.4-a-(iii) represents the *p*DOS of the oxygen atom, which is coordinated with 3 Al atoms. Interestingly, when MeOH is placed near the oxygen atoms having non-zero states at the Fermi, they undergo dissociation. In

Journal Pre-proof

contrast, if MeOH is placed near oxygen atoms which do not have states at Fermi, then they are chemisorbed. Thus, the adsorption of MeOH in the vicinity of oxygen, which has non-zero energy states at Fermi, is essential for dissociating methanol. However, it is not sufficient to have non-zero states at Fermi. The orientation of methanol plays a crucial role in determining the outcome. The preferred orientation is where H_{MeOH} is inclined towards the O_{surf}. Fig.6 represents two different orientations of methanol on (220) facet of $ZnAl_2O_4$. The atoms displayed in blue depict those oxygen atoms with non-zero peaks at the Fermi level, and the red ones have zero energy states at the Fermi level. Fig.6-(a) and (b) show the adsorption of methanol on the same Al atom in two different orientations, which results in adsorption and dissociation of methanol, respectively. The favoured orientation of methanol (refer Fig.6-(b)) for dissociation is the one in which H_{MeOH} is tilted towards the blue-coloured oxygen atom, which has non-zero energy states at Fermi. This observation holds for the (311) facet also. It is interesting to note that this trend is also visible in the pDOS plot of each facet, where Al-3p is present at Fermi (Fig. SI-6) and overlaps with 2p of O_{MeOH}, but no Zn-4s is seen around Fermi (Fig. SI-5). This signature is also clearly seen in the tDOS of $ZnAl_2O_4$ depicted in Fig.5-(iv).

IV. CONCLUSION

To conclude, we have demonstrated a one-to-one correlation between the availability of DOS at the Fermi and the dissociation of MeOH by investigating the interaction of MeOH with various Zn-based catalysts. To our knowledge, no studies have been reported on the interaction of methanol with zinc surfaces. The current study thoroughly examines how methanol interacts with zinc and oxygen-preadsorbed zinc surfaces. Since the most prominent facets in the XRD of bulk Zn are $(10\bar{1}0)$, $(10\bar{1}1)$, and $(10\bar{1}3)$, we investigated these facets for interaction with methanol. Physisorption of MeOH is a common outcome on all the facets of pristine Zn with a substantial

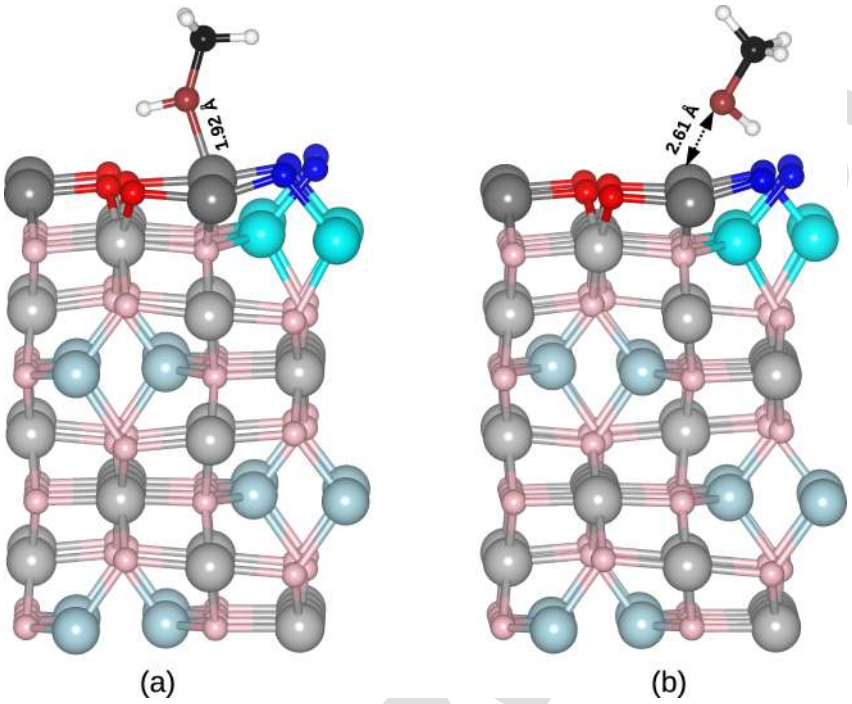

FIG. 6: The orientation of methanol on (220) facet of $ZnAl_2O_4$ are shown. The atoms in blue color corresponds to those oxygens which have non-zero energy states at Fermi as shown in Fig.4-(a)-(iii) and red are those which have zero energy states at Fermi. (a) shows the initial position of methanol where the H_{MeOH} is inclined towards red oxygen atoms and results into adsorption of methanol upon optimization. (b) depicts the initial position of methanol in which H_{MeOH} is tilted towards blue oxygen atoms result into dissociation. This signifies that along with presence of oxygen with non-zero peak at Fermi, orientation of MeOH does play a crucial role in determining the outcome of interaction of MeOH in complex system such as $ZnAl_2O_4$.

reconstruction of $(10\bar{1}0)$ surface. We observed the chemisorption of MeOH on the step facet of oxygen-preadsorbed Zn and physisorption on pristine Zn. Thus, oxygen adsorption enhances the reactivity of the surface with methanol. Oxygen adsorption significantly lowers the activation barrier for O-H bond dissociation, with a negligible barrier on the step facet. The dissociation of the O-H bond also changes from being endothermic on pristine Zn surfaces to exothermic on oxygen-preadsorbed surfaces. Finally, we discuss the underlying electronic structures of different catalytic systems, including Zn, O-Zn, ZnO, and $ZnAl_2O_4$, that have been investigated for interactions

Journal Pre-proof

with methanol in our current and earlier studies. By carefully analyzing the site-specific pDOS plots of these facets, we report that the existence of energy states of oxygen, metal, or both at or near the Fermi level has a substantial influence on the dissociation of MeOH on that particular facet. With this knowledge, we may examine catalytic surfaces for their interactions with incoming adsorbate species from a fresh perspective.

V. ACKNOWLEDGEMENT

CSIR-4PI is gratefully acknowledged for the computational facility.

[1] S.A Sardar, J.A Syed, K Tanaka, F.P Netzer, and M.G Ramsey. The aluminium-alcohol interface: Methanol on clean Al(111) surface. *Surface Science*, 519(3):218–228, 2002.

[2] Marilena Carbone and Karin Larsson. Methanol adsorption on the Si(100)-2x1 surface: a first-principles calculation. *Journal of Physics: Condensed Matter*, 17(8):1289–1300, feb 2005.

[3] Do Hwan Kim, Sung-Soo Bae, Suklyun Hong, and Sehun Kim. Atomic and electronic structure of methanol on Ge(100). *Surface Science*, 604(2):129–135, 2010.

[4] Susumu Yanagisawa, Takao Tsuneda, Kimihiko Hirao, and Yoichi Matsuzaki. Theoretical investigation of adsorption of organic molecules onto Fe (110) surface. *Journal of Molecular Structure: THEOCHEM*, 716(1-3):45–60, 2005.

[5] Ana S. Moura, Jose L. C. Fajín, Ana S. S. Pinto, Marcos Mandado, and M. Natália D. S. Cordeiro. Competitive paths for methanol decomposition on ruthenium: A DFT study. *The Journal of Physical Chemistry C*, 119(49):27382–27391, 2015.

Journal Pre-proof

Journal Pre-proof

[6] Xinzheng Yang. Mechanistic insights into ruthenium-catalyzed production of H_2 and CO_2 from methanol and water: A DFT study. *ACS Catalysis*, 4(4):1129–1133, 2014.

[7] Zeb C. Kramer, Xiang-Kui Gu, Dingyu D. Y. Zhou, Wei-Xue Li, and Rex T. Skodje. Following molecules through reactive networks: Surface catalyzed decomposition of methanol on Pd(111), Pt(111), and Ni(111). *The Journal of Physical Chemistry C*, 118(23):12364–12383, 2014.

[8] Ruibin Jiang, Wenyue Guo, Ming Li, Dianling Fu, and Honghong Shan. Density functional investigation of methanol dehydrogenation on Pd(111). *The Journal of Physical Chemistry C*, 113(10):4188–4197, 2009.

[9] Ya-Hui Fang and Zhi-Pan Liu. First principles tafel kinetics of methanol oxidation on Pt(111). *Surface Science*, 631:42–47, 2015.

[10] Xiang-Kui Gu and Wei-Xue Li. First-principles study on the origin of the different selectivities for methanol steam reforming on Cu(111) and Pd(111). *The Journal of Physical Chemistry C*, 114(49):21539–21547, 2010.

[11] Alejandro Montoya and Brian S. Haynes. Methanol and methoxide decomposition on silver. *The Journal of Physical Chemistry C*, 111(27):9867–9876, 2007.

[12] Lei Wang, Chaozheng He, Wenhua Zhang, Zhenyu Li, and Jinlong Yang. Methanol-selective oxidation pathways on Au surfaces: A first-principles study. *The Journal of Physical Chemistry C*, 118(31):17511–17520, 2014.

[13] Sung Sakong and Axel Gross. Total oxidation of methanol on Cu(110): a density functional theory study. *The Journal of Physical Chemistry A*, 111(36):8814–8822, 2007.

[14] Donghai Mei, Lijun Xu, and Graeme Henkelman. Potential energy surface of methanol decomposition on Cu(110). *The Journal of Physical Chemistry C*, 113(11):4522–4537, 2009.

[15] Roey Ben David, Adva Ben Yaacov, Ashley R. Head, and Baran Eren. Methanol decomposition on copper surfaces under ambient conditions: Mechanism, surface kinetics,

Journal Pre-proof

Journal Pre-proof

and structure sensitivity. *ACS Catalysis*, 12(13):7709–7718, 0.

[16] Ye Xu, Jeff Greeley, and Manos Mavrikakis. Effect of subsurface oxygen on the reactivity of the Ag(111) surface. *Journal of the American Chemical Society*, 127(37):12823–12827, 2005.

[17] Gui-Chang Wang, Shu-Xia Tao, and Xian-He Bu. A systematic theoretical study of water dissociation on clean and oxygen-preadsorbed transition metals. *Journal of Catalysis*, 244(1):10–16, 2006.

[18] Jooho Kim, Enrique Samano, and Bruce E. Koel. CO adsorption and reaction on clean and oxygen-covered Au(211) surfaces. *The Journal of Physical Chemistry B*, 110(35):17512–17517, 2006.

[19] Shiyi Wang, Enbo Zhu, Yu Huang, and Hendrik Heinz. Direct correlation of oxygen adsorption on platinum-electrolyte interfaces with the activity in the oxygen reduction reaction. *Science Advances*, 7(24):eabb1435, 2021.

[20] Ping Liu and Jens Kehlet Nørskov. Ligand and ensemble effects in adsorption on alloy surfaces. *Physical Chemistry Chemical Physics*, 3(17):3814–3818, 2001.

[21] Shu-Xia Tao, Gui-Chang Wang, and Xian-He Bu. Effect of pre-covered oxygen on the dehydrogenation reactions over copper surface: a density functional theory study. *The Journal of Physical Chemistry B*, 110(51):26045–26054, 2006.

[22] M. Natália D.S. Cordeiro, Ana S.S. Pinto, and José A.N.F. Gomes. A DFT study of the chemisorption of methoxy on clean and low oxygen precovered Ru(0001) surfaces. *Surface Science*, 601(12):2473–2485, 2007.

[23] Bingjun Xu, Jan Haubrich, Thomas A Baker, Efthimios Kaxiras, and Cynthia M Friend. Theoretical study of o-assisted selective coupling of methanol on Au (111). *The Journal of Physical Chemistry C*, 115(9):3703–3708, 2011.

[24] Hassan Aljama, Jong Suk Yoo, Jens K. Nørskov, Frank Abild-Pedersen, and Felix Studt. Methanol partial oxidation on Ag(111) from first principles. *ChemCatChem*, 8(23):3621–3625, 2016.

Journal Pre-proof

Journal Pre-proof

[25] Shahin Goodarznia and Kevin J. Smith. Properties of alkali-promoted Cu-MgO catalysts and their activity for methanol decomposition and C2-oxygenate formation. *Journal of Molecular Catalysis A: Chemical*, 320(1):1–13, 2010.

[26] Øyvind Borck and Elsebeth Schröder. First-principles study of the adsorption of methanol at the α-Al_2O_3 (0001) surface. *Journal of Physics: Condensed Matter*, 18(1):1, 2005.

[27] Mariia Merko, G. Wilma Busser, and Martin Muhler. Non-oxidative dehydrogenation of methanol to formaldehyde over bulk β-Ga_2O_3. *ChemCatChem*, 14(13):e202200258, 2022.

[28] Feg-Wen Chang, Hsin-Yin Yu, L Selva Roselin, and Hsien-Chang Yang. Production of hydrogen via partial oxidation of methanol over Au/TiO_2 catalysts. *Applied catalysis A: general*, 290(1-2):138–147, 2005.

[29] Zhao Liu, Charles C Sorrell, Pramod Koshy, and Judy N Hart. Dft study of methanol adsorption on defect-free CeO_2 low-index surfaces. *ChemPhysChem*, 20(16):2074–2081, 2019.

[30] Navid Abedi, Philipp Herrmann, and Georg Heimel. Methanol on ZnO $(10\bar{1}0)$: From adsorption over initial dehydrogenation to monolayer formation. *The Journal of Physical Chemistry C*, 119(37):21574–21584, 2015.

[31] Shweta Mehta and Kavita Joshi. From molecular adsorption to decomposition of methanol on various ZnO facets: A periodic DFT study. *Applied Surface Science*, 602:154150, 2022.

[32] Shweta Mehta, Mirabai Kasabe, Shubhangi Umbarkar, and Kavita Joshi. Methanol to formaldehyde at ambient condition: from computation to experiments. *to be communicated*, 2022.

[33] Shweta Mehta, Sheena Agarwal, Nivedita Kenge, Siva Prasad Mekala, Vipul Patil, T Raja, and Kavita Joshi. Mixed metal oxide: A new class of catalyst for methanol activation. *Applied Surface Science*, 534:147449, 2020.

Journal Pre-proof

Journal Pre-proof

[34] P. E. Blöchl. Projector augmented-wave method. *Physical Review B*, 50(24):17953–17979, 1994.

G. Kresse and D. Joubert. From ultrasoft pseudopotentials to the projector augmented-wave method. *Physical Review B*, 59(3):1758–1775, 1999.

[35] John P. Perdew, Kieron Burke, and Matthias Ernzerhof. Generalized gradient approximation made simple [phys. rev. lett. 77, 3865 (1996)]. *Physical Review Letters*, 78(7):1396–1396, 1997.

[36] G. Kresse and J. Hafner. *Ab initio* molecular-dynamics simulation of the liquid-metal–amorphous-semiconductor transition in germanium. *Physical Review B*, 49(20):14251–14269, 1994.

G. Kresse and J. Furthmüller. Efficient iterative schemes for *ab initio* total-energy calculations using a plane-wave basis set. *Physical Review B*, 54(16):11169–11186, 1996.

G. Kresse and J. Furthmüller. Efficiency of ab-initio total energy calculations for metals and semiconductors using a plane-wave basis set. *Computational Material Science*, 6(1):15–50, 1996.

[37] Anubhav Jain, Shyue Ping Ong, Geoffroy Hautier, Wei Chen, William Davidson Richards, Stephen Dacek, Shreyas Cholia, Dan Gunter, David Skinner, Gerbrand Ceder, et al. Commentary: The materials project: A materials genome approach to accelerating materials innovation. *Applied Materials*, 1(1):011002, 2013.

[38] Kei Iokibe, Kazuhisa Azumi, and Hiroto Tachikawa. Surface diffusion of a Zn adatom on a Zn(001) surface: a DFT study. *The Journal of Physical Chemistry C*, 111(36):13510–13516, 2007.

[39] Daniele Stradi, Line Jelver, Søren Smidstrup, and Kurt Stokbro. Method for determining optimal supercell representation of interfaces. *Journal of Physics: Condensed Matter*, 29(18):185901, 2017.

Journal Pre-proof

Journal Pre-proof

[40] Stefan Grimme. Semiempirical GGA-type density functional constructed with a long-range dispersion correction. *Journal of computational chemistry*, 27(15):1787–1799, 2006.

[41] Richard Dronskowski and Peter E Blöchl. Crystal orbital hamilton populations (COHP): energy-resolved visualization of chemical bonding in solids based on density-functional calculations. *The Journal of Physical Chemistry*, 97(33):8617–8624, 1993.

Volker L Deringer, Andrei L Tchougréeff, and Richard Dronskowski. Crystal orbital hamilton population (COHP) analysis as projected from plane-wave basis sets. *The Journal of Physical Chemistry A*, 115(21):5461–5466, 2011.

Stefan Maintz, Volker L Deringer, Andrei L Tchougréeff, and Richard Dronskowski. Analytic projection from plane-wave and PAW wavefunctions and application to chemical-bonding analysis in solids. *Journal of Computational Chemistry*, 34(29):2557–2567, 2013.

Stefan Maintz, Volker L Deringer, Andrei L Tchougréeff, and Richard Dronskowski. Lobster: A tool to extract chemical bonding from plane-wave based DFT. *Journal of Computational Chemistry*, 37(11):1030–1035, 2016.

[42] Graeme Henkelman, Blas P. Uberuaga, and Hannes Jónsson. A climbing image nudged elastic band method for finding saddle points and minimum energy paths. *The Journal of Chemical Physics*, 113(22):9901–9904, 2000.

[43] Silvia Mostoni, Paola Milana, Barbara Di Credico, Massimiliano D'Arienzo, and Roberto Scotti. Zinc-based curing activators: New trends for reducing zinc content in rubber vulcanization process. *Catalysts*, 9(8), 2019.

[44] Salahudeen Shamna, C. M. A. Afsina, Rose Mary Philip, and Gopinathan Anilkumar. Recent advances and prospects in the Zn-catalysed mannich reaction. *RSC Adv.*, 11:9098–9111, 2021.

[45] Wesley Sattler and Gerard Parkin. Zinc catalysts for on-demand hydrogen generation and carbon dioxide functionalization. *Journal of the American Chemical Society*,

Journal Pre-proof

Journal Pre-proof

134(42):17462–17465, 2012. PMID: 23046174.

[46] MS Spencer. The role of zinc oxide in Cu/ZnO catalysts for methanol synthesis and the water–gas shift reaction. *Topics in Catalysis*, 8(3):259–266, 1999.

[47] Malte Behrens, Felix Studt, Igor Kasatkin, Stefanie Kühl, Michael Hävecker, Frank Abild-Pedersen, Stefan Zander, Frank Girgsdies, Patrick Kurr, Benjamin-Louis Kniep, et al. The active site of methanol synthesis over $Cu/ZnO/Al_2O_3$ industrial catalysts. *Science*, 336(6083):893–897, 2012.

Journal Pre-proof

Journal Pre-proof

- Electronic properties of many Zn-based systems investigated for their reactivity.
- pDOS of bare facets is correlated with the outcome of methanol interaction with a facet.
- Dissociation of MeOH is associated with presence of energy states near the Fermi.
- Adsorption (chemi/physi) is associated with absence of energy states near the Fermi.

Journal Pre-proof

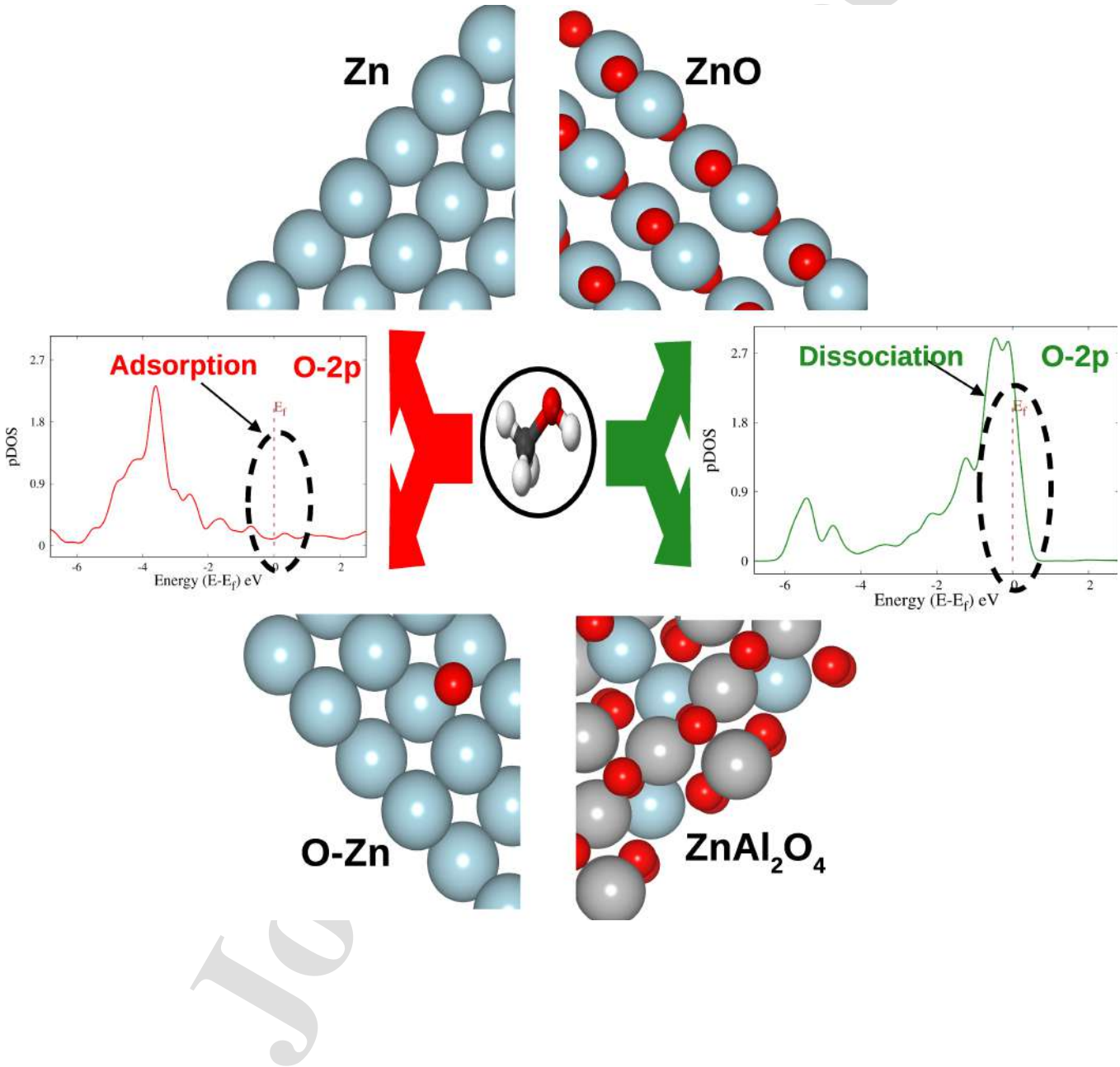

Journal Pre-proof

Journal Pre-proof

Author Statement:

Shweta Mehta: Methodology, Formal Analysis, Investigation, Writing original draft
Kavita Joshi: Conceptualization, Writing -Review& Editing, Supervision

Journal Pre-proof

Journal Pre-proof

Declaration of interests

☒ The authors declare that they have no known competing financial interests or personal relationships that could have appeared to influence the work reported in this paper.

☐ The authors declare the following financial interests/personal relationships which may be considered as potential competing interests:

Journal Pre-proof